373

MITIGATION TECHNIQUES OF POWER-FREQUENCY MAGNETIC FIELDS ORIGINATED FROM ELECTRIC POWER SYSTEMS

Working Group
C4.204

February 2009

WG C4.204

MITIGATION TECHNIQUES OF POWER FREQUENCY MAGNETIC FIELDS ORIGINATED FROM ELECTRIC POWER SYSTEMS

Members of the WG

Ener Salinas (Convener) - United Kingdom
Oriano Bottauscio - Italy
Mario Chiampi - Italy
Renato Conti - Italy
Pedro L. Cruz Romero - Spain
Than Dovan - Australia
Patrick Dular - Belgium
Jean Hoeffelman - Belgium
Rolf Lindgren - Sweden
Paolo Maioli - Italy
Gary Melik - Australia
Michele Tartaglia - Italy

Contributions were also received from

Breda Cestnik (Slovenia), Aldo Canova (Italy), François Deschamps (France), Marc De Wulf (Belgium), Fabrizio Donazzi (Italy), Jarmo Elovaara (Finland), Alessandro Fabbri (Italy), Daniel Goulet (Canada), Jim Hoburg (USA), Bruce Howard (Australia), Marko Istenic (United Kingdom), Anette Larson (Sweden), Giovanni Lucca (Italy), Leena Korpinen (Finland), Alessandra Manzin (Italy), Peeter Muttik (Australia), Robert Olsen (USA), Pieter Pretorius (South Africa), David Renew (United Kingdom), Pauli Vanhala (Finland), György Varju (Hungary), Paul Wong (Canada), Mauro Zucca (Italy), Juan Atalaya (Sweden), Marina Rezinkina (Ukraine) and Robin Hilton (United Kingdom).

ISBN: 978-2-85873-060-5

TABLE OF CONTENTS

INTRODUCTION

In recent years, issues related to power frequency magnetic fields (PFMF) originating from various sources of the electric network have been a significant concern amid customers, utilities and the electromagnetics research community. An important reason for this concern is some alleged health risks due to long-term exposure to these fields that have been associated with them, for example and particularly childhood leukaemia. Another reason is related to electromagnetic compatibility issues in the form of interferences with electron-beam driven devices.

Consequently, after the CIRED 2001 Conference in Amsterdam, where the topic was largely addressed, the special reporter, Jean Hoeffelman, proposed CIGRE to set up a new working group (WG) with the aim to collect (more than 140 papers), discuss and synthesise - in the form of a technical brochure - the available technical data (including some economic aspects) referring to the possible techniques to mitigate ELF (extremely low frequency) magnetic fields.

In order to achieve this goal, the formed WG, convened by Ener Salinas, searched for experts around the world working on the topic, finding several who dynamically participated. In addition, collaboration with CIGRE members of study committees SC B1, B2 and B3 as well as with the IEEE has been very helpful.
The main issues addressed in this document are the field emissions due to HV power installations (i.e. overhead lines, underground cables and substations) and the ways to mitigate them (without reference to exposure limits). LV installations are also dealt with as magnetic fields are in fact not voltage but current related.

The fundamental principles governing the mitigation techniques are described as well as the employed methods. In addition, since this document is intended to be of practical use, examples taken from actual implementations are included.

The main audience for this technical brochure are engineers directly concerned with the generation, transmission and distribution of electricity or working for industries making extensive use of electricity in their process. Yet, any person interested in magnetic field mitigation will certainly find useful information reading this technical brochure.

It is also worth mentioning that this document has in no way the pretension to put an end point to the topic. It is rather an introduction and a general synthesis of the state of the art. In particular, within CIGRE, WG B1.23 dealing with the “Impact of EMF on current ratings and cable systems**”** will continue to analyse in more details the mitigation methods for cable systems. There is also the possibility of formation of new working groups to expand or study in greater detail any of the topics treated in this document.

EXECUTIVE SUMMARY

Background and scope

Electric and magnetic fields (EMF) at extremely low frequency (ELF), and more particularly at power frequency, are an important concern for Power System Operators and for electricity users due to their possible impacts on living organisms. After more than 30 years of research, the scientific community has not yet reached an agreement on whether prolonged exposure to EMF, at levels lower than those of the international recommendations, can have an influence on the human health.

Based on known acute effects, reference levels in the range of 100 μT or more have been proposed by international bodies like ICNIRP[1] or IEEE and by international authorities like the Council of the European Union. On the other hand, possible long-term health effects have been associated to average fields lower than 1 μT in epidemiological studies. Taking into account the absence of any plausible mechanism for explaining the statistical association found between the exposure to ELF magnetic field and childhood leukaemia and the impossibility to confirm it by in vivo or in vitro studies, the International Agency for Research on Cancer (IARC), which is part of the World Health Organisation (WHO), has classified in 2002 the ELF magnetic field among the "possibly carcinogenic" physical agents.

For those reasons, some countries or local authorities have taken the decision to apply the precautionary principle and sometimes to set up much lower exposure limits than the reference levels of ICNIRP and IEEE. On the other hand, the WHO has established in 1996 the International EMF Project aiming to assess the scientific evidence of possible health effects of EMF. Since that time the WHO has published several fact sheets and reports on the topic and, more particularly, in May 2007, its Monograph 238 on ELF field that makes a large synthesis of the available scientific knowledge. In the summary of this important document (445 p), it can be read among other that "*it is not recommended that limits values in exposure guidelines be reduced to some arbitrary level in name of precaution*" and that "*the costs of precautionary measures should be very low*".

Taking all these facts into account and also the very large number of papers dealing with magnetic field mitigation techniques that have been published during the last 15 years, it has been decided to set up in Cigré SC4 a working group aiming at trying to make a synthesis of the main publications under the form of a practical technical brochure.

The purpose of this document is to present a comprehensive set of techniques to mitigate the magnetic fields created by various electrical power systems. The mitigation phenomena are analysed starting from the basic principles. The physical mechanisms leading to efficient mitigation methods are focused and developed. The electric power system is subdivided in its various elements such as overhead lines, underground cables and substations, and the practical methods for achieving optimal mitigation designs are described. The document is complemented with a collection of examples of actual designs and implementation.

In addition to possible health effects, power-frequency magnetic fields are also able to interfere with electron beam driven devices such as VDUs, electron microscopes and oscilloscopes, resulting in image distortion. This influence is sometimes evident at values as low as 1 microtesla, i.e. in the same range of levels as those mentioned in the epidemiological studies, implying that the same techniques used for health motivated mitigation can be used to solve this kind of electromagnetic compatibility problems.

Outline

The document starts with the basic definitions that characterises a magnetic field. The concepts of ***magnetic flux density*** (**B**) and ***magnetic field intensity*** (**H**) are introduced. However, the notation of "magnetic field" or simply "field" is deliberately adopted for **B** – when there is no risk of confusion – and its most suitable unit, in the context of this document, is chosen to be the microtesla (μT). Time-varying magnetic fields (AC)

[1] International Commission on Non-Ionizing Radiation Protection.

are differentiated from static fields (DC) and the field created by the most typical power-frequency (50/60 Hz) sources, namely homopolar, single phase, three phase and dipolar (punctual) are described.

The interaction of magnetic fields with metallic materials, is the most determining mechanism that produces mitigation of power frequency magnetic fields. Among the metallic materials, some are purely conductive, like copper and aluminium and other have ferromagnetic properties, like iron, and steel. Contrary to a well established belief, not only ferromagnetic materials are able to interact with low frequency magnetic fields. Indeed, time varying magnetic fields are also able to induce currents in conductive loops (passive loops, coils) and in non-ferromagnetic metals (eddy currents), leading to fair results in term of field mitigation.

Magnetic field mitigation, as any physical phenomenon, needs to be quantified. Therefore the ***shielding factor*** (SF) is introduced. It is defined as the ratio between the magnetic flux density in a given point (P) in absence (B_0) and in presence (B_s) of the mitigation means: $SF(P) = B_0(P)/B_s(P)$. Sometimes the logarithm of the shielding factor is considered leading to the concept of ***shielding effectiveness*** expressed in dB; this expression, however, is mainly used at higher frequencies when the shielding factor largely exceeds 10. The use of metallic material, whether ferromagnetic or not, are usually referred to as ***shielding methods***, whereas the use of (passive or active) conductive loops are preferably referred to as ***compensation methods***.

Aside from the shielding methods, based on the use of metallic materials or conductive loops, it is often possible to reduce the field at the source by playing on the geometry of the conductors that produce the field. This is called ***conductor management***, a very effective way of reducing magnetic fields. The second chapter describes with more details the different mitigating methods, starting with the conductor management. A detailed analysis of the field produced by various three phase conductor arrangements is presented. It is followed by a description of how the phase currents can be split into several conductors in order to further reduce the field levels.

The next technique described, compensation, is based on the Lenz Law: the currents induced in the compensation conductors are at the origin of a magnetic field that partially cancels the original field. Sometimes it is possible to enhance the shielding effectiveness by tuning with a capacitor the loop in which the current is induced. Another improvement can be obtained by amplifying the induced currents (e.g. adding a capacitor) or by using an external current source electronically controlled and synchronised with the original field. This is called ***active loop*** compensation.

A significant part of chapter 2 is dedicated to shielding by metallic materials starting with pure ***ferromagnetic shields***. The involved shielding mechanism is sometimes called the "***flux-shunting mechanism***" because the material, thanks to its high permeability, has the property to attract and to concentrate the field lines. Hence, this kind of material is able to divert the field lines far from the area of interest, resulting in high shielding factors.

The properties of the main ferromagnetic materials like iron, grain oriented silicon steel, low carbon steel, or µ-metal are presented and discussed but the chapter focuses mainly on the difference in behaviour of closed shields compared to open shields, showing in particular that, contrary to close shields, open ferromagnetic shields are only effective in the direct vicinity of the shield. The next section of the chapter is dedicated to pure ***conductive shields***. The related mitigating mechanism is sometimes called "***induced current shielding mechanism***", and which, contrary to the flux-shunting mechanism, results in a repelling effect on the field lines. Close and open shields are again analysed in detail showing the influence of the main parameters (conductivity, distance to the shield, thickness) and, in particular, of the skin depth that plays an important part in all shielding processes involving eddy currents. One of the conclusions of this section is that open conductive shields can be effective in regions far from the shield. An important section is dedicated to the simultaneous effect of permeability and conductivity because most ferromagnetic materials take largely advantage of their conductivity in achieving good shielding properties. Moreover it is also possible to use multilayer shields with different intrinsic properties. The two last sections of this chapter on shielding deal with corrosion properties of the three basic materials used in mitigation (i.e. steel, copper and aluminium) and with the impact of the different mitigation techniques on the operating conditions.

Chapter 3 concerns the various methods used to design and assess mitigation techniques. ***Analytical*** methods are useful to understand and predict the physical mechanisms, but are generally limited to one- or two-dimensional simple and symmetrical systems. With the increasing power of computers, ***numerical simulations*** have a growing popularity as design tools; yet they are most reliable when complemented by

experimental validation. In this respect a novel validation method based on scaling rules is presented in this document.

After chapter 4 giving some tips about the best strategy to follow, chapter 5 describes, with more details, how the mitigation principles can be applied to the different parts of the electric power system, starting with ***overhead lines***. Clearly, when acting at the source, only conductor management techniques (compact lines, phase transposition, split line) and compensation methods can be applied. illustrates a typical example of passive compensation.

The section dealing with mitigation methods for ***power cables*** starts also with conductor management (e.g. trefoil formation with respect to flat formation, effect of twisting the conductors, phase splitting and compensation loops, to mention a few) and proceeds then with the use of conductive shielding based on aluminium or copper plates. The effectiveness of each solution is analysed in function of the geometrical dimensions (shape, thickness) and the electric continuity. This latter parameter is obviously of utmost importance when dealing with conductive material. Yet, depending of the shape of the shield (flat, U-shape, H-shape) a good continuity is not always required between all of the planar elements.

Shielding with ferromagnetic materials is highlighted in the next section with different examples of closed shields (open ferromagnetic shield being, as already mentioned, ineffective) starting with the classical tubular shield and focusing then on the so called “raceway” shield made of a profiled U shaped base and a cover solidly fastened together in order to avoid any air gaps. The chapter ends with an important section highlighting the advantages and drawbacks of each shielding techniques.

The last chapter, before the practical examples completing this technical brochure, deals with a third important kind of magnetic field source that, contrary to overhead lines and power cables, which are mainly two-dimensional sources, behaves generally as a tri-dimensional source concentrated in a particular location. It concerns ***substations*** involving several individual sources like busbars, transformers with their low voltage connections and cables. The best strategy to mitigate the field from these sources is to consider each of the relevant components as an individual problem, thus the resulting solutions can be composed and interpreted as a global result.

Target Groups

This technical brochure is intended for those who have at least an elementary background in power systems and electromagnetism. Along the various chapters more advanced concepts are sometimes developed and details are given in boxes. This document also targets engineers directly related to the generation, transmission and distribution of electricity or working for industries making extensive use of electricity in their processes (e.g. steel industry, chemical industry using electrolysis, electrical traction systems, etc.). However, any person interested in magnetic field mitigation will certainly find useful information reading this document.

NOTATION AND ABREVIATIONS

The main physical quantity discussed throughout the document is the ***magnetic flux density*** (***B***) which is a vector quantity. For simplicity, further in the text this quantity is referred to as ***magnetic field***.

The units of measurements used throughout the document are MKSA units, which form part of the SI system (for the French "Le Système International d'Unités"). In the SI system the unit for the magnetic flux density is tesla (T), while microtesla (μT) is the most commonly used sub-unit.

When considered as a scalar quantity (e.g. when RMS value is applied), the magnetic flux density will be denoted as *B*.

The magnetic field intensity, ***H***, is another physical quantity which is used for describing the magnetic field strength. Its unit of measurement in SI system is A/m.

The ***B*** is related to ***H*** via permeability of the medium, that is $B = \mu H$.

The word ***mitigation*** is used in these document to represent an operation (or set of operations) that aims to limit the flow of magnetic field from a region containing the *source* to an *area of interest*. In the technical literature related to this document, *reduction* and *attenuation* are used as synonyms of mitigation, as are *screening* and *shielding*. However, the latter two generally entail the application of metallic structures (e.g. plates) acting as barriers. The word *mitigation* is preferable to *reduction*; since the word reduction would not be adequate in many cases when field reduction is desired only in a certain area of interest whilst the increase of the magnetic field in other areas could be acceptable (e.g. the ground). For this reason, the word ***mitigation*** was selected in this document, as the most suitable.

Regarding materials, the term ***pure conductive*** is used for materials having conductivity other than zero, and relative magnetic permeability equal to 1. On the other hand the term ***pure ferromagnetic*** is used for materials that have large relative magnetic permeability and negligibly low conductivity.

Other commonly used unit for describing the magnetic flux density is gauss (G). A useful conversion is 1 microtesla = 10 milligauss. The convention is to write these units in small letters.

Some abbreviations used in this brochure are:

MF: Magnetic field

MT: Mitigation techniques

PF: Power frequency (50/60 Hz)

ELF: Extremely Low Frequency

EMC: Electromagnetic compatibility

***SE*:** Shielding efficiency

***SF*:** Shielding factor

GO: Grain oriented (ferromagnetic material)

NO: Non-oriented (ferromagnetic material)

ICNIRP: International Commission on Non-Ionizing Radiation Protection

A more complete list of physical quantities with units in the S.I. system:

$\boldsymbol{A}$: magnetic vector potential [T/m]

$\boldsymbol{H}$: magnetic field strength vector (or magnetic field intensity) [A/m]

$\boldsymbol{B}$: magnetic flux density vector (or magnetic induction, or simply magnetic field) [T]

$\boldsymbol{E}$: electric field strength vector (or simply electric field) [V/m]

$\boldsymbol{J}$: current density vector [A/m^2]

D : electric induction vector [C/m^2]

Q : electric charge [C]

ρ_V : charge per unit volume [C/m^3]

t : time variable [s]

f : frequency [Hz]

ω: angular frequency or pulsation [s^{-1}]

μ: magnetic permeability [H/m]

μ_r: relative magnetic permeability [no units]

ε: electric permittivity [F/m]

σ : electric conductivity [S/m]

δ : skin depth or penetration depth [m]

The following physical constants are useful:

ε_0 : permittivity of free space » 8.85 10^{-12} [F/m]

μ_0 : magnetic permeability of free space = $4\pi\ 10^{-7}$ [H/m].

1 GENERAL PRINCIPLES

This chapter presents the origin and the characteristics of magnetic fields. Some familiar examples of magnetism are given, followed by a description of time-varying fields. The interaction between these varying fields with some specific materials (i.e. metals and ferromagnetic materials) is fundamental in the design of magnetic field mitigation. Therefore the basics of these interactions are highlighted. Fundamental concepts and definitions related to mitigation techniques are also presented here and expanded in further chapters.

1.1 Physical phenomena

Magnetic fields have two possible origins. The first one is related to materials such as magnetite (the story goes that it was discovered around 900 B.C. in Crete by a shepherd called Magnes when he found his iron-nail shoes and the metal tip of his willow staff sticking to the ground). Nowadays, magnets with much stronger properties are being artificially produced. The second origin relates to a source of current, which produces magnetic field in its vicinity.

Magnetic fields can be static or time varying. In the case of a magnetic field that is produced by a current, it has the same frequency as its source. Magnetic fields have the ability to interact among themselves as well as with materials that are ferromagnetic, conductive or have both properties. These interactions are governed by a set of equations which will be presented here.

1.1.1 Magnetic field and its sources

Bar magnets (Figure 1.1.1) generate a static magnetic field – i.e. do not vary in time. We are familiar with their basic properties through their common usage such as refrigerator magnets. Similar magnets are inside most small motors and many household appliances.

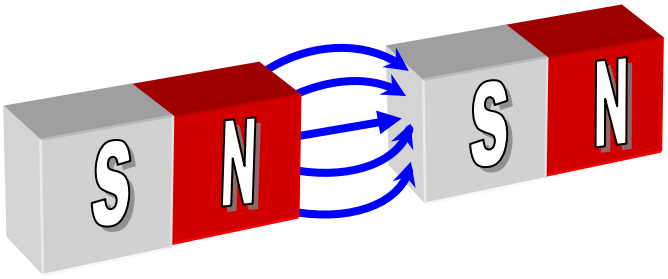

Figure 1.1.1 Bar magnets.

Magnetic field is also produced by the Earth (Figure 1.1.2). This field is nearly permanent and ranges from 30 to 60 μT depending of the location. However the magnetic field of the Earth is not purely static and can have some time variations. Although sometimes it is in the range of frequencies covered by this document, geomagnetic issues will not be addressed here.

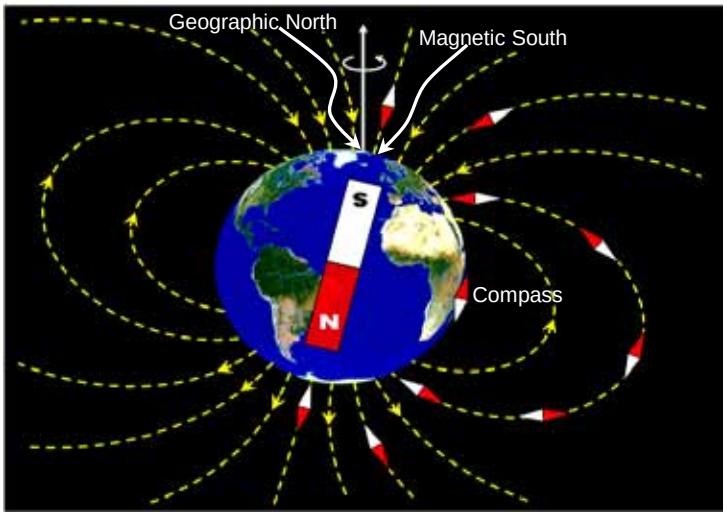

Figure 1.1.2 The magnetic field of the Earth showing its different directions at different locations.

Variations in Earth's Magnetic Field

Geomagnetic Reversals
Earth's magnetic field flips polarity unpredictably on geological time scale due to sudden changes in fluid motions in core.

Secular Variations
Observations of Earth's magnetic field made over 400 years show a gradual change in position of the magnetic pole.

Diurnal Variations
Daily changes in field due to changes in currents of charged particles in ionosphere. These changes are smooth and average around 50 nT.

Geomagnetic Storms
Short term disturbances in magnetic field associated with sun spot activity and streams of charged particles from sun. They can be up to 1000 nT in magnitude and can induce important zero sequence currents in long overhead lines able to cause transformer saturation, tripping and even blackouts.

One of the most significant scientific revolutions – which, later resulted in profound technological developments – started simply as an "accident" during a routine preparation for a physics demonstration by the Danish physicist Hans Christian Oersted in 1820. He observed that after an electric current was switched on, a nearby magnetic compass needle started to move [1]. Although he was not able to explain this phenomenon, he published his observation without realizing that 18 years before, Gian Dominico Romagnosi had already made the very same observation [2, 3]. Unfortunately, two things contributed for this observation to be largely overlooked by the scientific community. Fistly, Romagnosi was not a scientist but a jurist; and secondly, he published his account in a newspaper (*La Gazetta de Trentino*) [3].

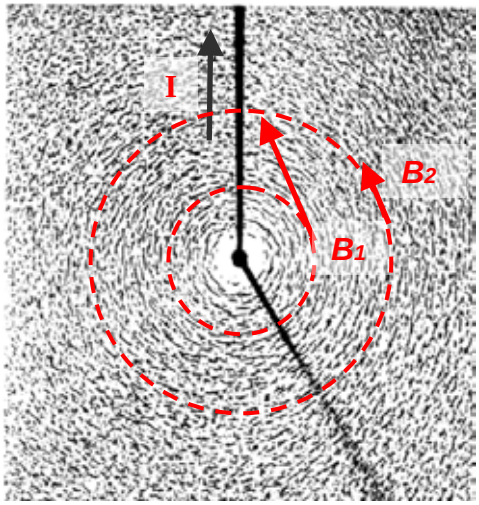

Figure 1.1.3 Experimental verification of the Oersted discovery: when a current passes through a wire, a magnetic field whose value decays with the distance ($B_2 < B_1$) is generated in its vicinity.

1.1.2 Time varying magnetic fields

In fact, the current which Christian Oersted applied was basically constant (DC), since in that time the alternating current (AC) had not yet been invented. In modern times, however, we are surrounded by alternating (50 Hz or 60 Hz depending on the country we are) currents that run through electric wiring systems such as appliances, motors, power lines, substations – to mention only a few. They also produce magnetic fields. Moreover, the variation of the magnetic field strength is exactly the same as the variation of the current, i.e. if the current is sinusoidal, then the magnetic field is sinusoidal too. In addition, the average rms value of the field decays with the distance. To visualize a time-varying field of 50 Hz, a mechanical device can be constructed using a bar magnet (Figure 1.1.4).

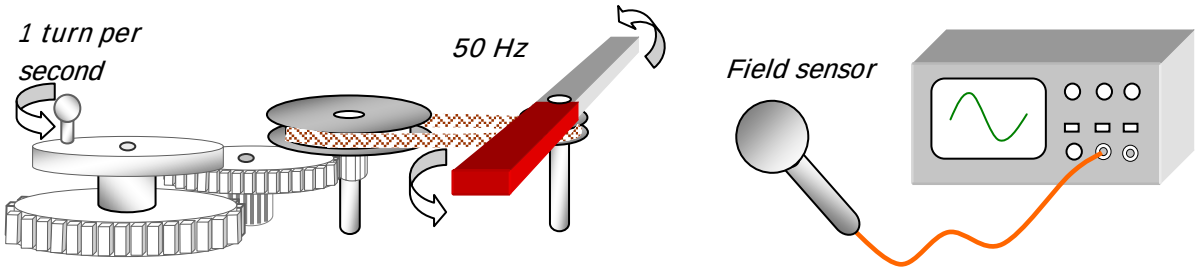

Figure 1.1.4 Mechanical generation and measurement of 50 Hz magnetic fields.

When a manual wheel, at the left, is rotated at a rate of one turn per second, a gear mechanism will make the magnet rotate at 50 cycles per second (50Hz). A magnetic field sensor and an oscilloscope are used to observe this variation.

1.1.3 Magnetic field from an infinite wire

The formula for computing the value of the magnetic field (given the current source) is called Biot-Savart formula. The simplest expression of this formula is obtained for an infinite wire, as is shown in Fig. 1.1.5

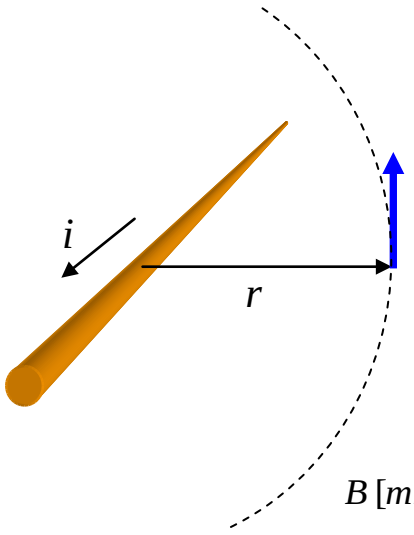

$$B(r) = \frac{m_0 i}{2\pi r} \qquad (1.1.1)$$

$$B\,[microtesla] = \frac{0.2 \cdot i\,[amperes]}{r\,[metres]} \qquad (1.1.2)$$

Figure 1.1.5 Expression to compute the magnetic induction from an infinite long wire; it is valid for DC or AC currents. For example, a current of 5 amperes, at the distance of 1 metre will produce a magnetic field of 1 microtesla.

1.1.4 Magnetic field of wires carrying opposite currents

In electrical systems and wiring installations, there can be several wires. A typical case concerns two wires carrying opposite currents. To compute the total field in a certain point, the direction of each field is relevant. Thus superposition via vector computation is required (see next box). Assuming infinite length, wire separation *a*, and vertical distance *y*, a simple expression for the field dependence on distance can be obtained (Figure 1.1.6). When the vertical distance *y* is much larger than the separation *a* – most usual case – two facts can be deduced: firstly, the magnetic field depends linearly on the separation *a*; and secondly, the magnetic field decays as ~ 1/(*distance*)^2, this is a much faster decay than the case of a single line.

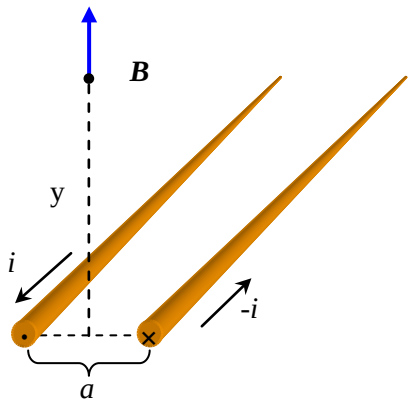

$$B(y)=\frac{\mu_0 i}{2\pi}\left[\frac{a}{(a/2)^2+y^2}\right] \qquad (1.1.3)$$

Figure 1.1.6 Magnetic induction produced by two infinite parallel wires along the vertical distance.

Computation of the magnetic field of two parallel wires

The aim is to compute the magnetic field (and its dependence with the distance) of two parallel wires carrying a single phase current *i* (one wire carrying a current *i* and the other the return current –*i*). The field of one finite wire (segment with length *L*) is first evaluated:

$$\boldsymbol{B}(x,y,z)=\frac{\mu_0 i}{4\pi}(y\boldsymbol{e}_x - x\boldsymbol{e}_y)\,f(x,y,z) \qquad (1.1.4)$$

where,

$$f(x,y,z)=\frac{1}{(x^2+y^2)}\left[\frac{L/2+z}{\sqrt{x^2+y^2+(L/2+z)^2}}+\frac{L/2-z}{\sqrt{x^2+y^2+(L/2-z)^2}}\right] \qquad (1.1.5)$$

For a two-wire configuration with a separation *a* (Figure 1.1.7) both field contributions will superimpose

$$\boldsymbol{B}=\frac{\mu_0 i}{4\pi}\left\{\left[(y_1 f(x_1,y_1,z_1)-y_2 f(x_2,y_2,z_2)\right]\boldsymbol{e}_x+\left[(-x_1 f(x_1,y_1,z_1)+x_2 f(x_2,y_2,z_2)\right]\boldsymbol{e}_y\right\} \qquad (1.1.6)$$

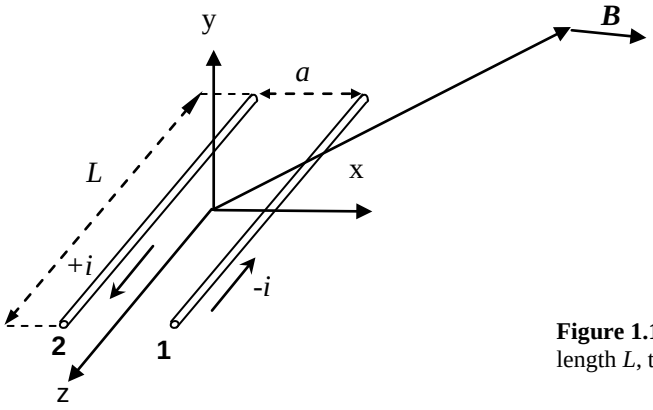

Figure 1.1.7 Magnetic field of two parallel finite wires of length *L*, the instantaneous currents are also shown.

The following relations hold: $x_1=x-a/2;\ x_2=x+a/2;\ y_1=y_2=y;\ z_1=z_2=z$.

In order to study the field decay with distance, e.g. along the y-axis, the calculation is made for $z=0$ and $x=0$. In that case, the field component along the x-axis vanishes, leaving a simple expression for the field of two parallel wires of finite length

$$\boldsymbol{B}(0,y,0)=\frac{\mu_0 i}{4\pi}\left[\frac{aL}{\left[(a/2)^2+y^2\right]\sqrt{(a/2)^2+y^2+(L/2)^2}}\right]\boldsymbol{e}_y \qquad (1.1.7)$$

Furthermore, for long wires $y << L$ the formula reduces to:

$$\boldsymbol{B}(0,y,0)=\frac{\mu_0 i}{2\pi}\left[\frac{a}{(a/2)^2+y^2}\right]\boldsymbol{e}_y \qquad (1.1.8)$$

1.1.5 Magnetic field of a three-phase system of conductors with length *L*

In this case three segments are parallel and carry currents with different phase angles (Fig. 1.1.7). In general the resultant field will be a rotating vector, i.e. an elliptically polarized field. A frequently used measure of the magnitude of B is given by the following expression,

$$B_{result} = \sqrt{B_{\text{major}}{}^2 + B_{\text{minor}}{}^2} \tag{1.1.9}$$

where B_{major} and B_{minor} are the maximum and the minimum magnitudes of **B** in the ellipse. However, under certain conditions (e.g. if the distance between segments is much smaller than the distance to the plane X-Y, used as area of interest) one can sometimes assume that the polarization of the magnetic field in the region of interest (the plane X-Y, at some metres above the system) is approximately linear. The field at the point ***P*** is calculated adding the vector-field contribution of each current of the three-conductor system.

After some lengthy but straightforward calculations, the rms-value of the magnetic field, in mT, acquires the following expression for points in the plane X-Z:

$$\left|\mathbf{B}_{Total}(x,y)\right|_{rms} = \frac{i_{rms}}{10}\cdot\left[\left(A_1 - \frac{A_2}{2} - \frac{A_3}{2}\right)^2 + \left(C_1 - \frac{C_2}{2} - \frac{C_3}{2}\right)^2 + \frac{3}{4}\left[(A_2 - A_3)^2 + (C_2 - C_3)^2\right]\right]^{1/2} \tag{1.1.10}$$

where,

$$A_k(x,y) = \frac{x}{x^2 + Z_k^2}\left[\frac{L/2 + y}{\sqrt{x^2 + (L/2+y)^2 + Z_k^2}} + \frac{L/2 - y}{\sqrt{x^2 + (L/2-y)^2 + Z_k^2}}\right] \tag{1.1.11}$$

$$C_k(x,y) = \frac{Z_k}{x^2 + Z_k^2}\left[\frac{L/2 + y}{\sqrt{x^2 + (L/2+y)^2 + Z_k^2}} + \frac{L/2 - y}{\sqrt{x^2 + (L/2-y)^2 + Z_k^2}}\right] \quad k = 1,2,3$$

The vertical distance of each conductor to the plane of interest is given by Z_k.(where *k:1=R*, 2=*S*, 3=*T*). This equation evaluates the field from a geometrical arrangement of straight conductors in a plane above the system.

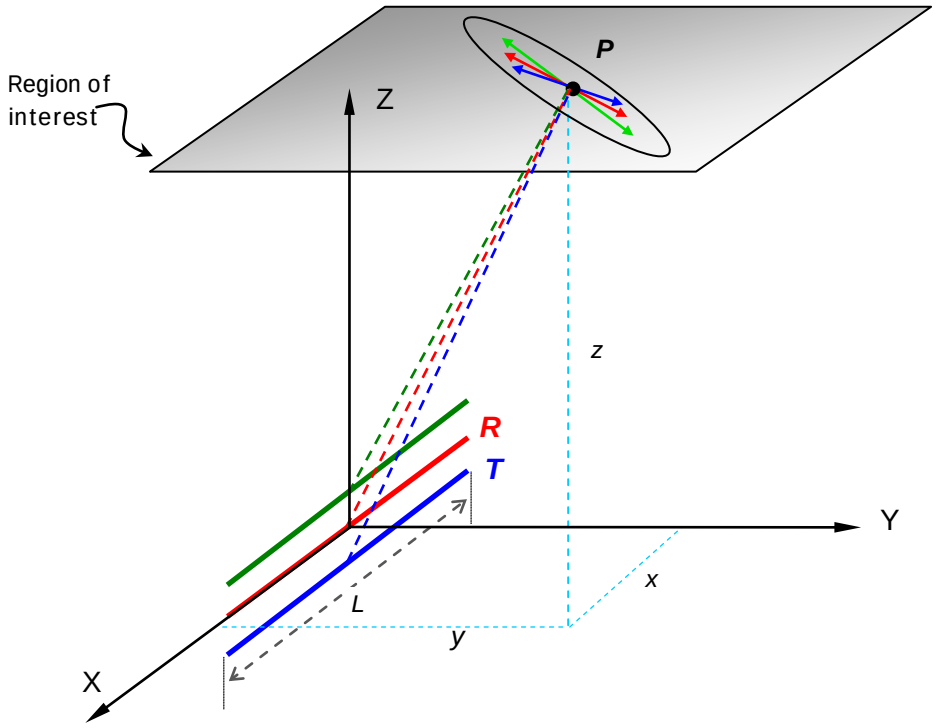

Figure 1.1.8 Magnetic field of a three-phase system of conductors (e.g. busbars) evaluated at the point ***P***. In general, the resulting field, which is a vector superposition, is rotating and elliptically polarized.

When the length of the segments becomes infinite, the dependence along a distance perpendicular to the 3-phase system is ~ 1/(*distance*)^2, similar to the case of 2 wires carrying opposite currents. The analytical expressions for the magnetic field emitted by 3-phase conductor systems are good models for analyzing power lines and busbars. In the case of power lines, an approximation for large length *L* is possible, whereas for busbars systems the expression for finite *L* is preferable. Another way to study a 2-conductor system is to consider it as a dipole and to visualize a 3-phase system as the superposition of two dipoles (see Chapter 2).

1.1.6 Maxwell equations

Just a few days after the receipt of the news of Oersted's discovery, André Marie Ampère presented to the French academy in Paris a list of new results based on Oersted's observations, including the one involving the attraction between conductors. In England, Michael Faraday constructed the first device that could move continuously with electricity, and, not much later, he proved the existence of electromagnetic induction, at the same time inventing the transformer. A flurry of investigations ignited and soon other results were obtained, culminating brilliantly with the synthesis and unification of all electromagnetic phenomena by James C. Maxwell in 1871. Strangely enough, no conservatives opposed to this revolution; neither was there a time of gradual acceptance as for example happened with the Copernican revolution [4]. In fact it seemed the world was prepared and waiting for it.

All the electromagnetic phenomena are governed by the Maxwell equations, which describe the general properties of the electromagnetic field, and by the constitutive equations establish a link between different quantities depending on the material properties. The Maxwell equations are described in the following box:

The Maxwell equations

$$div\,\boldsymbol{B} = 0 \tag{1.1.12}$$

$$div\,\boldsymbol{D} = r_v \tag{1.1.13}$$

$$curl\,\boldsymbol{H} = \boldsymbol{J} + \frac{\partial \boldsymbol{D}}{\partial t} \tag{1.1.14}$$

$$curl\,\boldsymbol{E} = -\frac{\partial \boldsymbol{B}}{\partial t} \tag{1.1.15}$$

- The first equation (1.1.12) describes the nature of magnetic fields such as those produced by permanent magnets. Moreover it also expresses the fact that magnetic monopoles do not exist, meaning that the north and south poles cannot be separated from a magnet, even if we break it in two - in other words, the magnetic field lines always follow closed paths.

- The second equation (1.1.13) is analogous to the first one. It describes the nature of the electric field. Yet there are some fundamental differences; basically the term on the right hand side is responsible for the existence of isolated electrical charges and for currents therefore electric field lines can follow "open" or divergent paths.

- The third equation (1.1.14) describes the creation of magnetic field due to electric phenomena (Ampere Law). The first term of the right hand side represents the currents (sources) and the second is the variation of the displacement. In these guidelines only the first term will be used.

The fourth equation (1.1.15) describes the creation of electric field due to magnetic phenomena. The variation of the magnetic flux across a surface induces an electric field that can drive a current through a conductor loop surrounding that surface. The minus sign represents the Lenz law, i.e. the induced current will have a direction such that the magnetic field generated by it will oppose the cause that produced it (increase or decrease of magnetic flux).

1.2 Interaction of fields with matter and mitigation concepts

So far, the origins of magnetic fields have been highlighted and various sources have been characterized. It is however very important for the goals of these guidelines to address the behaviour of a magnetic field when it encounters a conductive or ferromagnetic material. This material can have various shapes and intrinsic properties, which will be characterized in this section. As an example, Figure 1.2.1 illustrates the behaviour of some typical shapes and materials used to developed mitigation techniques. These materials are in general metals (also ferrites and some ceramics) and are also called shields. Observe the clear differences between ferromagnetic (field lines are “attracted“ and arrive perpendicular to the plate) and pure conductive shields (where the field is “repelled” and, therefore, the field lines are tangential to the shield).

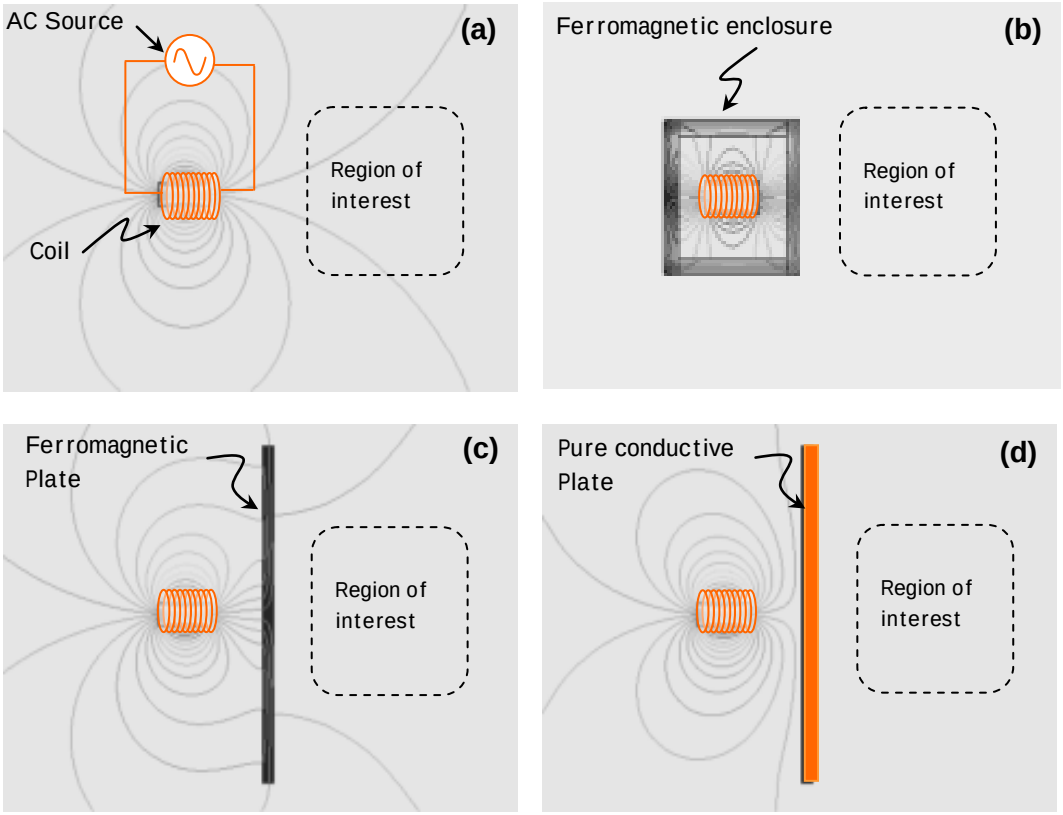

Figure 1.2.1 Interaction of a magnetic field with screens used to achieve field reduction in a given region. Clear differences can be observed between ferromagnetic and pure conductive screens.

1.2.1 The constitutive equations

The constitutive equations provide a link between some electric or magnetic quantities, depending on the characteristics of the material. These equations are:

$$\boldsymbol{B} = \mu \boldsymbol{H} \tag{1.2.1}$$

$$\mathbf{J} = \sigma\, \mathbf{E} \tag{1.2.2}$$

$$\mathbf{D} = \varepsilon\, \mathbf{E} \tag{1.2.3}$$

All these parameters are usually non-constant. In particular, they depend on the temperature. Also, in a ferromagnetic material, μ depends on the magnetic field amplitude. Hence, $\boldsymbol{B} = f(\boldsymbol{H})$ defines a more realistic model.

For mitigating the magnetic field, the interest for the equations involving the electric field quantities is weak, so that only three Maxwell equations and the first two constitutive equations are to be taken into account.

1.2.2 Magnetic material properties

In the presence of a (magnetic) material, the constitutive equation linking magnetic flux density and magnetic field strength is written introducing the magnetisation $\boldsymbol{M}$:

$$\boldsymbol{B} = \mu_0 \boldsymbol{H} + \boldsymbol{M} = \mu_0 \boldsymbol{H} + \chi_M \mu_0 \boldsymbol{H} = (1 + \chi_M)\mu_0 \boldsymbol{H} = \mu_r \mu_0 \boldsymbol{H} = \mu \boldsymbol{H} \qquad (1.2.4)$$

where χ_M is the magnetic susceptibility. From the magnetic point of view, the materials are classified as:

- **diamagnetic**: the value of μ_r is slightly less than 1 (range: $1\text{-}10^{-5}$ to $1\text{-}10^{-6}$)
- **paramagnetic**: the value of μ_r is slightly greater than 1 (range: $1+10^{-4}$ to $1+10^{-2}$)
- **ferromagnetic**: the value of μ_r is sensibly greater than 1 (up to 10^6). If $\sigma = 0$, the material will be denoted in this document as **pure ferromagnetic**.

Even if their behaviour at microscopic level is strongly different, from the applicative point of view, diamagnetic and paramagnetic can be assumed to have the air permeability ($\mu_r = 1$). These materials are also called *amagnetic* materials.

Besides their higher permeability, ferromagnetic materials (iron, cobalt, nickel and their alloys) are characterized by a strongly non-linear relationship between magnetic flux density and magnetic field strength; thus, the definition of a constant permeability represents only a rough approximation of their behaviour. Starting from the demagnetized state, an example of B-H curve is reported in Figure 1.2.2. This curve is the so-called *first magnetization curve* of the material.

The slope of the curve gradually increases in the first part of the characteristic (called the Rayleigh zone) and then it strongly increases up to a given point (*knee* of the characteristic, corresponding to the maximum value of the permeability). The slope then decreases until a relative permeability of one is reached in correspondence of an induction value called saturation flux density ($\boldsymbol{B}_s$). By increasing the magnetic flux density further, the material behaves similar to an amagnetic one.

In presence of a reversing excitation, the B-H relationship presents an hysteretic behaviour, depending on the past history. When the excitation is periodic, the B-H curve becomes a closed loop, characterized by a residual magnetization $\boldsymbol{B}_r$ (when $\boldsymbol{H} = 0$) and by a coercive field $\boldsymbol{H}_C$ (when $\boldsymbol{B} = 0$). An example of symmetric hysteresis loop is reported in Figure 1.2.3. More characteristics of ferromagnetic materials will be presented in section 2.3.1.

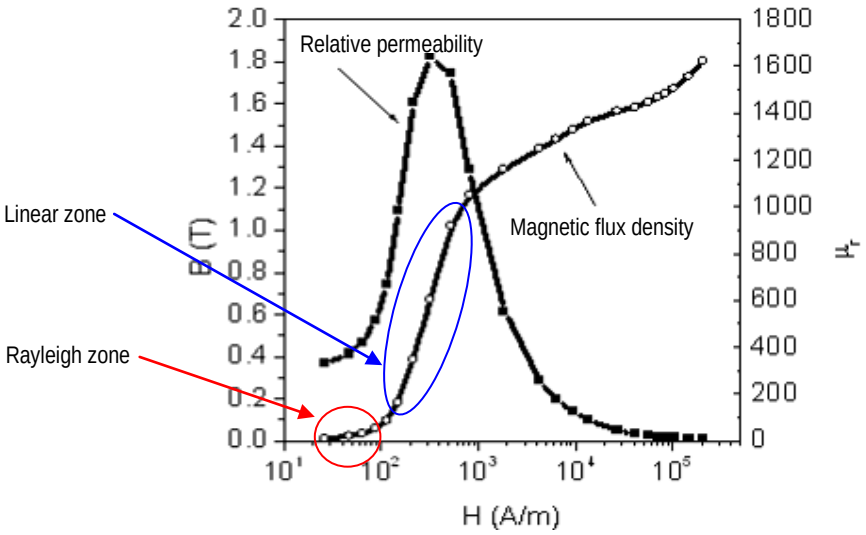

Figure 1.2.2 First magnetization curve of a ferromagnetic material.

With respect to other applications, shielding devices are characterized by low or very low flux density working values, so that the parameter that mainly characterizes the material efficiency is the permeability value in the Rayleigh zone or in the beginning of the linear zone. In addition, hysteresis does not

significantly affect the shielding properties of the materials and, in a first approximation, they can be neglected.

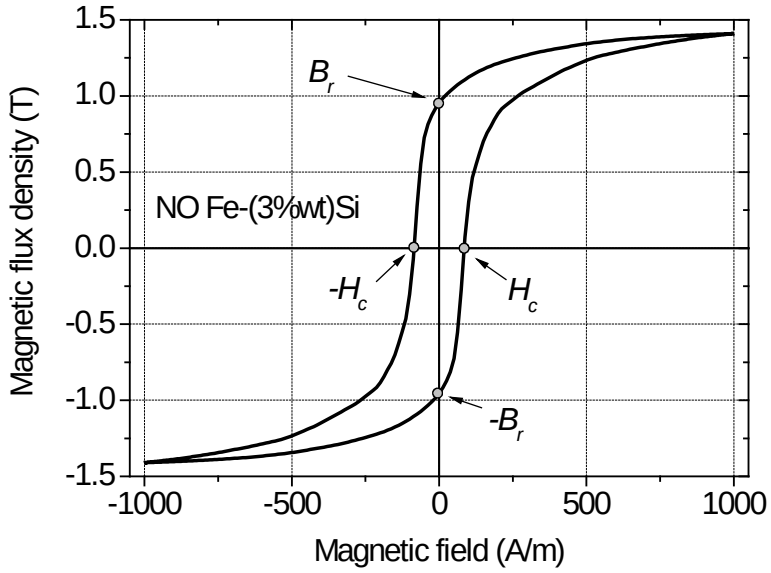

Figure 1.2.3 Hysteresis loop.

1.2.3 Electromagnetic induction and eddy currents

A time-varying magnetic field generates electromotive forces, as stated by the Faraday law. In presence of conductive materials the electromotive forces give rise to electric currents (eddy currents) flowing in the material itself. The circulation of eddy currents produces an additional magnetic field, leading to a global reduction of resultant field. This phenomenon is utilized in pure conductive shields to mitigate time varying magnetic fields.

Electromagnetic induction is also responsible for the skin effect, whose effect is to concentrate magnetic field and current density towards the boundary of the material. As a consequence, skin effect can produce an incomplete penetration of the magnetic flux and current density, which is quantified by the penetration depth δ defined as:

$$\delta = \frac{1}{\sqrt{\pi f \sigma \mu}} \tag{1.2.5}$$

where f is the frequency, μ the permeability and σ the electrical conductivity. The incomplete penetration of the magnetic flux can reduce the efficiency of magnetic or pure conductive shields having large thickness, mainly when the frequency is increased.

1.2.4 Shielding efficiency

The efficiency of magnetic or pure conductive shields can be quantified introducing different parameters. The most usual are the following ones:

Shielding factor (SF) [2]

It is the ratio between the magnetic flux density in a given point (P) in absence (B_0) and in presence (B_s) of the shield,

$$SF(P) = \frac{B_0(P)}{B_s(P)} \tag{1.2.6}$$

The higher the value of *SF*, the more efficient the shield.

[2] Some authors use the inverse of this ratio to qualify the shielding factor. In that case, the lower the *SF* the higher the efficiency.

Shielding effectiveness (SE)

It is the shielding factor expressed in dB,

$$SE(P) = 20 \log \frac{B_0(P)}{B_s(P)} \tag{1.2.7}$$

In fact, shielding effectiveness is used for higher frequencies where mitigation rates could have values with several orders of magnitude. In this document, to measure mitigation, shielding factors will be used. As most mitigation rates will be within the first order of magnitude, a logarithmic expression is not necessary.

1.3 Note on the quantities characterizing the magnetic field

Some aspects of the notation for the magnetic field have been a matter of discussion since Maxwell times [5]-[8]. An example is the following: what is most fundamental, the magnetic flux density ***B*** or the magnetic field intensity ***H*** to be called magnetic field? [1], [8].This has been an unresolved issue since different specializations may demand their own most convenient notation. In this guideline we have adopted the magnetic flux density ***B*** as the fundamental quantity characterizing the magnetic field. This is convenient since the magnetic field intensity and the magnetic flux density are related in the air by: $\boldsymbol{B} = \mu_0 \boldsymbol{H}$.

Yet, in cases in which the simplification is not possible, i.e. when ***B*** and ***H*** are being discussed, it is better to call them by magnetic flux density and magnetic field intensity respectively.

Taking as an example mitigation using a ferromagnetic plate (Figure 1.3.1), the use of ***B*** as the *magnetic field* is more convenient, as it will preserve the units [microtesla] in all locations of the mitigation.

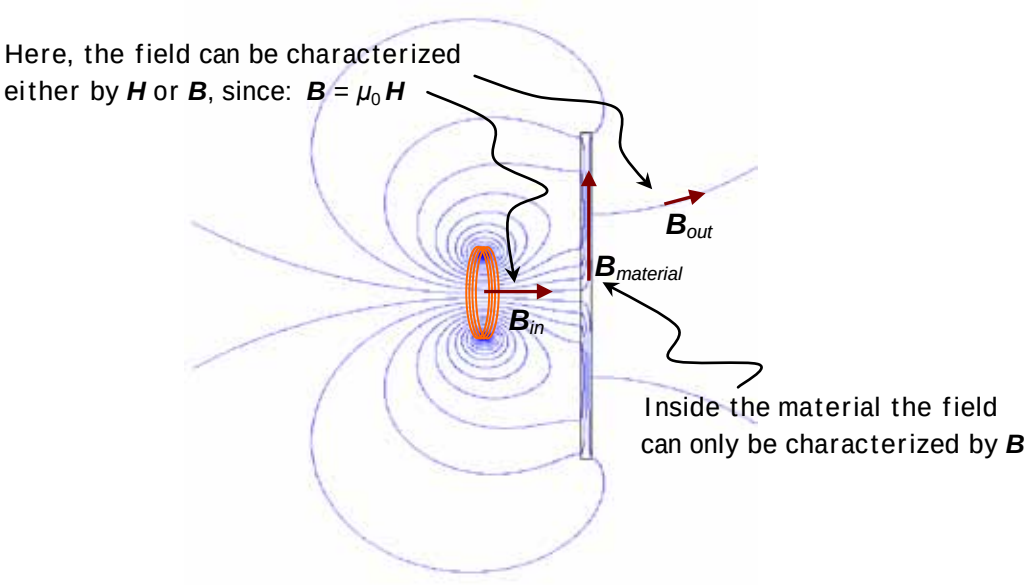

Figure 1.3.1 In this guide the use of ***B*** as the *magnetic field* is more convenient.

1.4 References

[1] E. M. Purcell Electricity and Magnetism, Berkeley Physics Course vol. 2, 2nd Ed. McGraw-Hill Book Company, 1985.

[2] J. F. Keithley *The Story of Electrical and Magnetic Measurements* IEEE Press, New York, 1999.

[3] S. Stringari and R. R. Wilson, *Romagnosi and the discovery of electromagnetism,* Rend. Fis. Acc. Lince s. 9, vol. 11, (2000) pp 115-136.

[4] T. S. Kuhn, *The Structure of Scientific Revolutions*, The University of Chicago Press, 1962.

[5] J. D. Jackson, *Classical Electrodynamics*, Third Edition, John Wiley & Sons, Inc. N.Y. 1999, pp. 175-180.

[6] D. K. Cheng, *Field and Wave Electromagnetics*, Addison-Wesley Massachusetts, 1989, pp. 600-605.

[7] R. P. Feynman, *The Feynman Lectures on Physics. Vol. II*, Redwood City: Addison-Wesley, 1964.

[8] Cloete, J.H. *Is B or H the fundamental magnetic field?* 1996., IEEE AFRICON 4th Volume 1, Issue 24-27, pp. 354-361, Sep 1996.

2 MITIGATION TECHNIQUES

According to the general principles stated in chapter 1, a direct and obvious way to mitigate the magnetic field from a source is by attempting to reduce the current through it. For example, to reduce the field from an overhead line the voltage of the line could be increased and, for the same transmitted active power, the current would decrease. These kinds of solutions are technically feasible, but in general are ruled out on a first stage of the mitigation system design due to the high costs that are general involved. On the contrary it is of more interest looking for solutions that, with minimum impact on the service operation and low cost can reduce the field emissions effectively.

This chapter presents the cost-effective techniques that, in a greater or lesser extent, are being used for the ELF MF mitigation in power installations. It is intended in this chapter to present a general overview of the fundamentals of different techniques, and of the parameters that, for each technique, have a strong influence on the mitigation effectiveness. No real applications are presented in this chapter; they are referred to in chapters V and VI. The content of this chapter demonstrates particular mitigation cases for different installations, shown later, and gives an understanding of the application of some of the techniques in other installations not included in this report.

The techniques have been gathered in three different groups, according to the characteristics of the mitigation elements inserted: **conductor management**, **compensation** and **shielding**. In the first group, there is actually no external element of mitigation. As the name evokes, the techniques are related to the grouping of conductors in a manner that lowers the global field. The second technique is based on the placement of a compensating conductor forming a loop. Parameters of the loop are selected in order to obtain an effective mitigation. In the third group, a shield, usually in sheet form, with particular materials and dimensions, is inserted between the source and the area of interest.

Finally a brief summary of the potential impact of these techniques on the operating conditions of the electrical installations is presented.

2.1 Conductor management

The techniques included in this epigraph are applied to MF sources composed by two or more conductors, normally arranged in parallel (for example overhead lines, underground cables, busbars, etc). As will be seen through this subchapter, these techniques are effective as long as the zero-sequence current of the source is reduced.

2.1.1 Layout and compaction

If the relative positions of the conductors are rearranged, the MF generated by them changes. As an example, Figure 2.1.1 shows the cross sectional view of three long and straight current-carrying conductors composing a three-phase balanced system. If they are aligned the equal-value contour curves are shown in (a). If they form an equilateral triangle, as in (b), the contour curves are closer to the conductors, as the field is decaying faster as the distance to conductors increases.

A further reduction can be obtained by reducing the phase-to-phase clearance (compaction). Figure 2.1.2 shows the same configurations for the current but with distance between conductors is halved.

If there is a net current in the conductor system (zero-sequence current) the field is higher in all the arrangements at certain distances from the conductors, and the effectiveness of both mitigation methods is not so obvious. To illustrate this, contour curves of Figures 2.1.1 and 2.1.2 are repeated in Figures 2.1.3 and 2.1.4, with the addition of a zero-sequence current of 10 %. From Figures 2.1.3 and 2.1.4, it is seen that with delta configuration, there are some points where the field is even higher than with flat configuration. Likewise, if Figures 2.1.3(b) with 2.1.4(b) are compared, the compaction mitigation effect is almost cancelled for values of $y < 0$. The contour curves are quite dependent on the phase of the zero-sequence current, so there is no general rule for field magnitude spatial distribution.

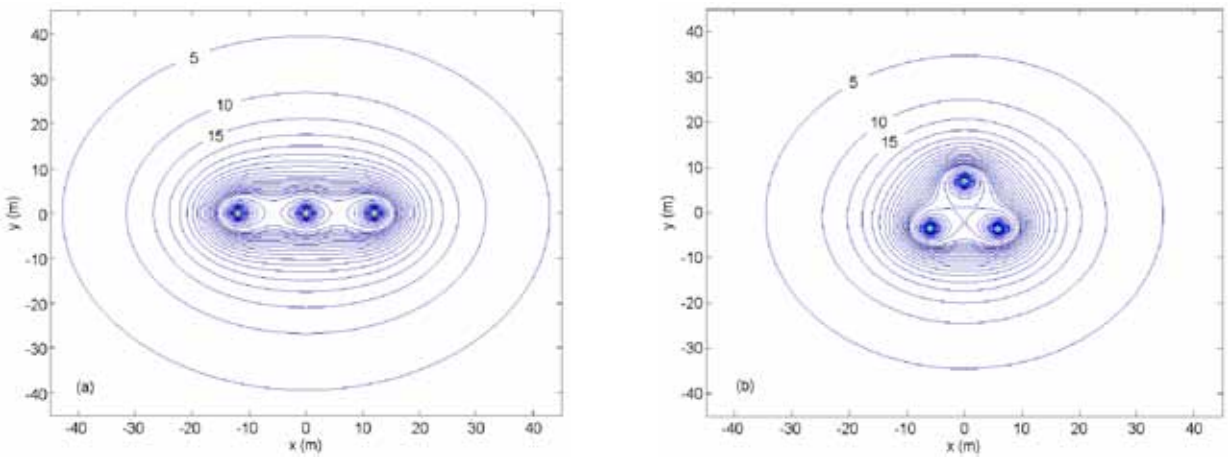

Figure 2.1.1 Contour curves of the magnetic field (in mT) generated by flat (a) and delta (b) three-phase configurations with equal phase-to-phase clearance (12 m) and current (2000 A).

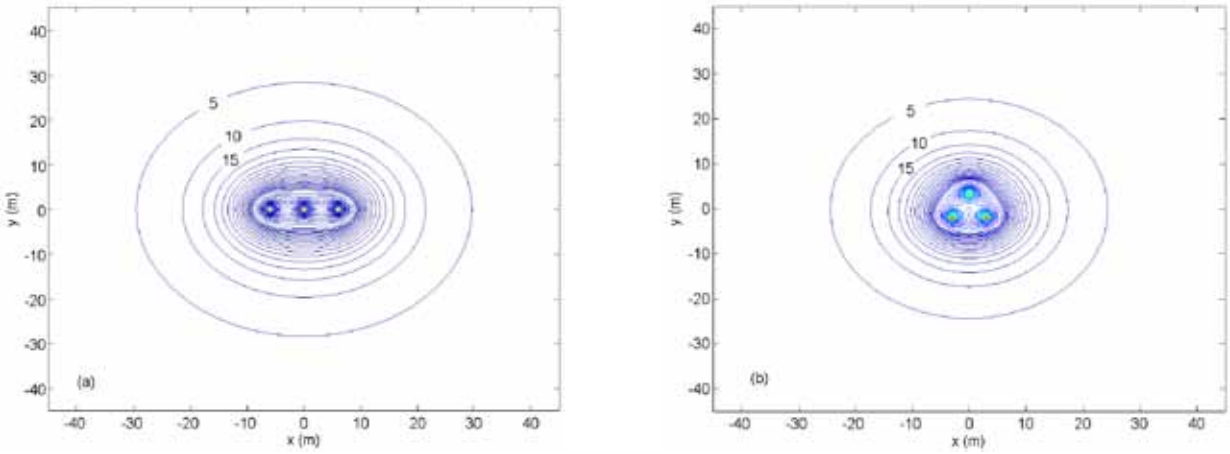

Figure 2.1.2 Contour curves of the magnetic field (in mT) generated by flat (a) and delta (b) three-phase configurations with phase-to-phase clearance halved in relation to Figure 2.1.1 and current. 2000 A.

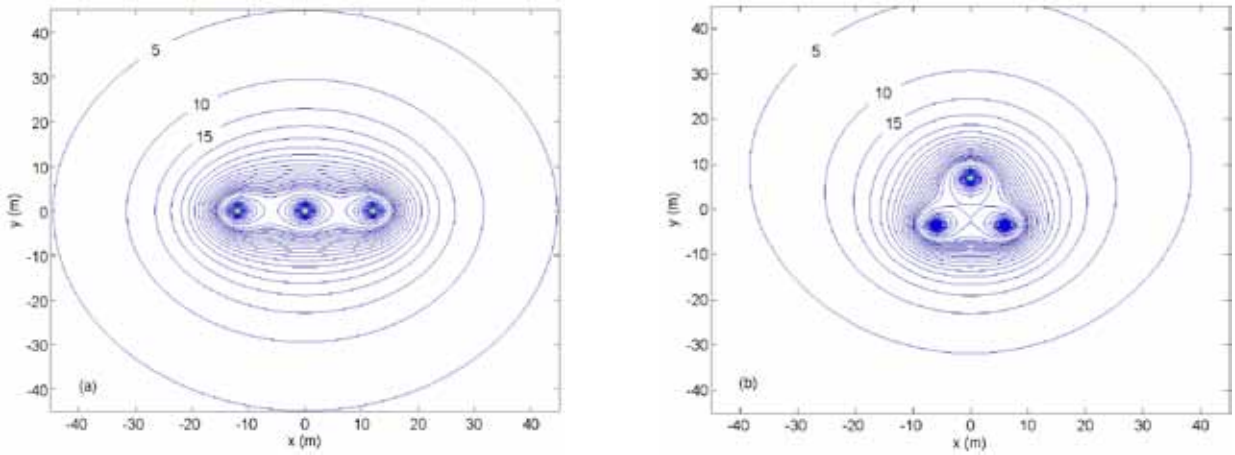

Figure 2.1.3 Contour curves of magnetic field (in mT) generated by the same configurations as in figure 2.1.1 with an addition of 10% of zero-sequence current.

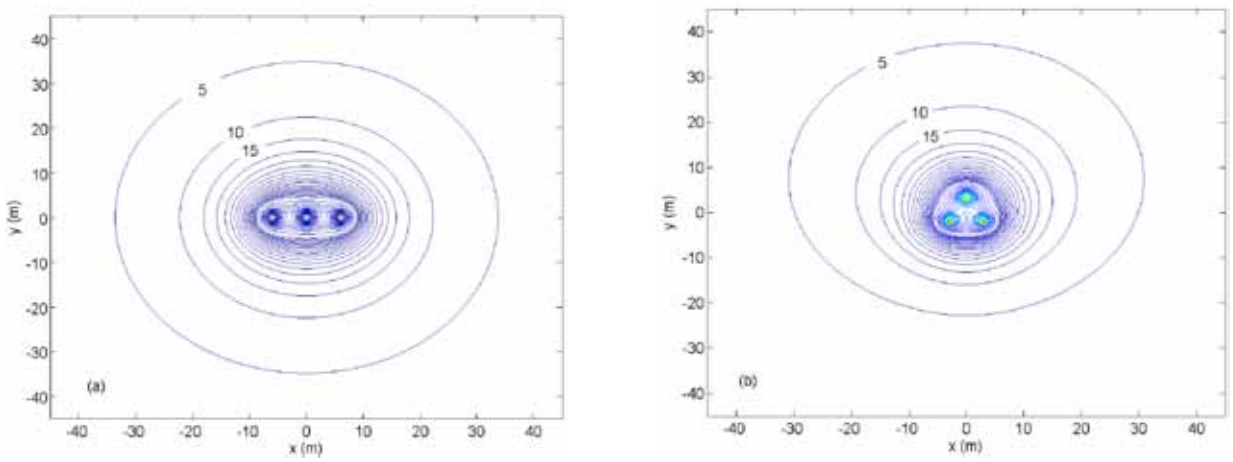

Figure 2.1.4 Contour curves of magnetic field (in mT) generated by the same configurations as in Figure 2.1.2 with an addition of 10% of zero-sequence current.

Simple formulation of the field far from the conductors

Precise expressions for the calculation of the magnetic field for two parallel wires in three-phase systems of conductors were obtained in chapter 1. In many cases it is more convenient to use approximated simple formulae that can provide a clearer understanding of parameters involved. They can be used to calculate the field at points far from the conductors (i.e. at a distance of several times the phase-to-phase clearance distance). They can be deduced by means of series expansion of Biot-Savart Law (seen in chapter 1) applied to every conductor [1] or to pairs of conductors carrying the same but opposite current (current dipoles) [2]. For instance, in the case of balanced three-phase systems, the field at distance r from the conductors can be expressed by the following approximated formula [1]:

$$B(r) = \frac{dI}{5\sqrt{2}r^2} \quad (\mu T)$$

where

$$d = \sqrt{d_{ab}^2 + d_{bc}^2 + d_{ac}^2} \quad \text{(m)} \qquad (2.1.1)$$

d_{ab}, d_{bc}, d_{ac} : phase-to-phase clearances (m)

r : distance between the geometrical centre of line conductors and the calculation point in space ($r >> d$) (m)

I : phase current (A)

With this formulation, it is easy to compare the field for different conductor arrangements, as in flat and equilateral triangular. If minimum phase-to-phase clearance d_{pp} is the same for both arrangements the field yields

$$B_{flat}(r) = \frac{\sqrt{3}d_{pp}I}{5r^2} \quad (\mu T) \qquad (2.1.2)$$

$$B_{triangular}(r) = \frac{\sqrt{6}d_{pp}I}{10r^2} \quad (\mu T) \qquad (2.1.3)$$

As can be seen, compared with flat configuration, the triangular configuration realises a magnetic field reduction by a factor of 1.4. It can be deduced from (2.1.1) that the lowest field-generating configuration is the equilateral one.

Likewise, from (2.1.2) and (2.1.4) it can be seen that the field far from the conductors is proportional to phase-to-phase clearance.

Approximate expression for the field at zero-sequence current

The behaviour of the field from zero-sequence current can be easily understood by means of the approximate formulation (also valid far from the conductors), deduced from series expansion of Biot-Savart law (see chapter 1). The field at distance *r* from the conductors due to zero-sequence current I_0 is given by

$$B = \frac{I_0}{5r} \quad (\mu T)$$

where *r* is the distance between the geometrical centre of conductors and the calculation point in space (in m). It is important to check that this expression is the same as the field from a single wire (see chapter 1). It can be seen that the field does not depend on the layout or the conductor-to-conductor distance. Moreover, it decays only with distance. Therefore, far from the conductors, MF due to zero-sequence current is greater than the field due to the positive-sequence current.

2.1.2 Distance management

From the contour curves in Figures 2.1.1 through 2.1.4, it is clear that the magnetic field decreases with distance to the source. If only positive or negative sequence is present in the current, the field will decrease with the inverse of the square of the distance. If some percentage of zero-sequence current is present the field decay is just proportional to inverse of distance. In the first case the mitigation effectiveness will be higher. In any case, a field reduction is guaranteed.

Normally, this method is more feasible in practice when the source is nearer to the interest area, and a slightly higher clearance source-interest area is enough to reduce the field significantly. This can be clearly seen in Figure 2.1.5. In (a), the interest area is at 30 m from the line (point P). In this location, the magnetic field at P is 4.1 mT. If this point is moved away 10 m (point P'), the field decreases to 2.4 mT. In (b) the configuration is the same but the current is higher. The point of interest P is now at 65 m, and the field at this point is similar to case (a). The same reduction factor than in (a) is desired, but in this case the point has to be moved 20 m (P'). In general, the more clearance required the less feasibility of the solution (increase of cost, practical limitations, etc.).

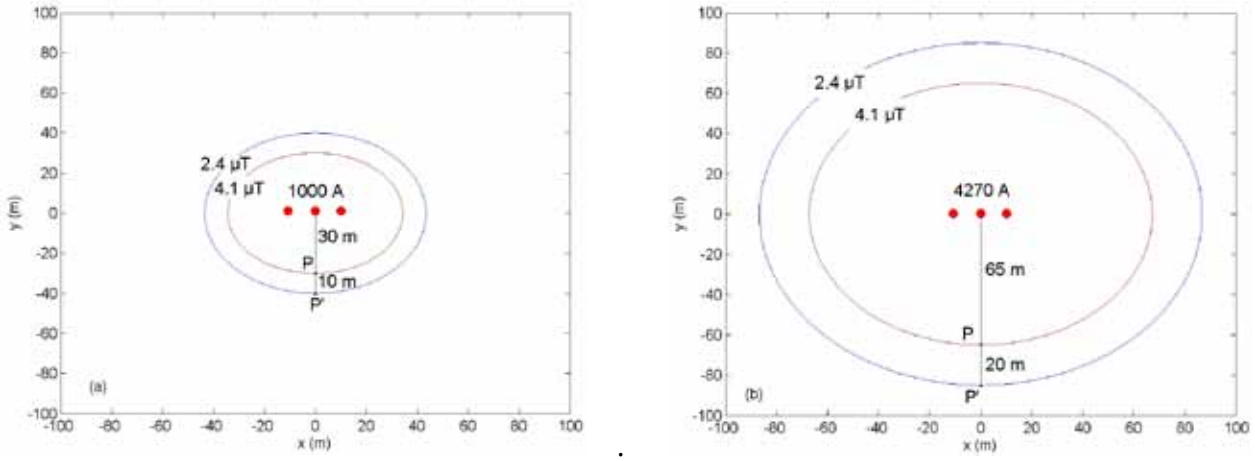

Figure 2.1.5 Example of how the initial clearance interest area-source influences the mitigation effectiveness due to an increase of distance.

2.1.3 Phase splitting

If a single-phase two-conductor circuit is converted into a single-phase four-conductor circuit, a low-field configuration is obtained as the magnetic field decays as the inverse of the cube of distance (Figure 2.1.6). Each phase has been split into two conductors, and the four-conductor set is called a quadrupole. This forms the foundation of phase splitting.

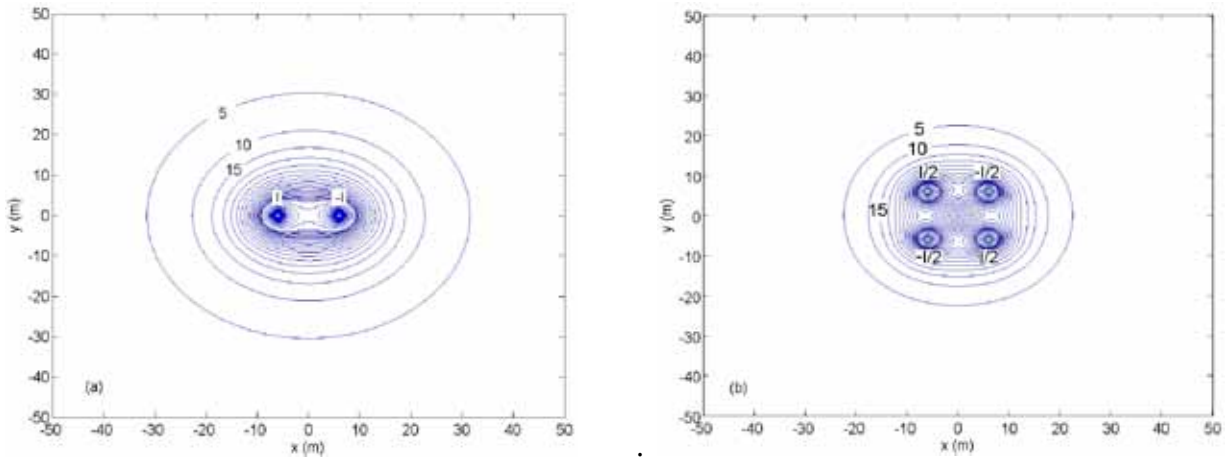

Figure 2.1.6 Contour curves of field (in mT) generated by a single-phase two-conductor circuit (a) and a single-phase four-conductor system (b). The net phase current in each circuit is the same (1000 A), as is the phase-to-phase clearance (12 m).

Formulation of the field from a current quadrupole

There are several aproximative formulations for the field generated by a quadrupole, based on the dipole decomposition [2,4]. The simplest and reasonably accurate formulation to give the distance from the conductors is the following:

$$B = \frac{2Idq}{5r^3} \quad (\mu T) \qquad (2.1.4)$$

where r is the distance between the geometrical centre of conductors and the calculation point in space (in m), and d and q shown in figure 2.1.7. Although the field depends on other parameters like d or q, the dominant term is the distance r cubed.

Not all single-phase four-conductor configurations are quadrupoles, and not all quadrupoles must be composed by four conductors. Figure 2.1.7 shows two quadrupoles, one of four conductors and the other of three.

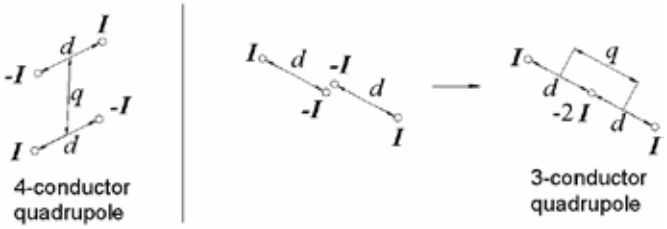

Figure 2.1.7 Examples of a 4-conductor and 3-conductor quadrupoles. This quadrupole can be seen as a 4-conductor quadrupole where two conductors are superimposed.

The concept of quadrupole forms the theoretical basis, as three-phase split-phase configurations can be easily synthesized starting from elemental quadrupoles, and analysed decomposing into quadrupoles. It is important to distinguish clearly if 3 or 4 conductors form a quadrupole. A quadrupole can be decomposed into two current dipoles with the following features:

- Both current dipoles have the same width d and current I
- If a spatial vector is drawn for each dipole, from I-current carrying conductor to $-I$-current conductor, both vectors are in opposite directions.

A formal definition of quadrupole can be seen in [4].

The field generated by three-phase split-phase configurations will be the sum for the fields generated by each quadrupole, so the global field decays with distance cubed. Depending on the type of quadrupole (4-conductor or 3-conductor), it is possible to obtain low field three-phase configurations by splitting two (Figure 2.1.8) or three (Figure 2.1.9) phases.

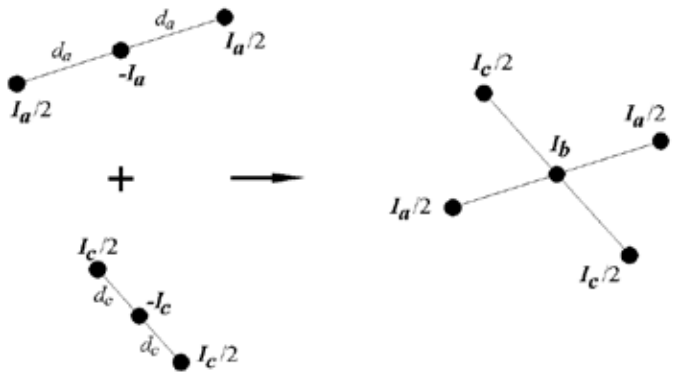

Figure 2.1.8 Examples of synthesis of a three-phase configuration with two split phases, starting from two 3-conductor quadrupoles.

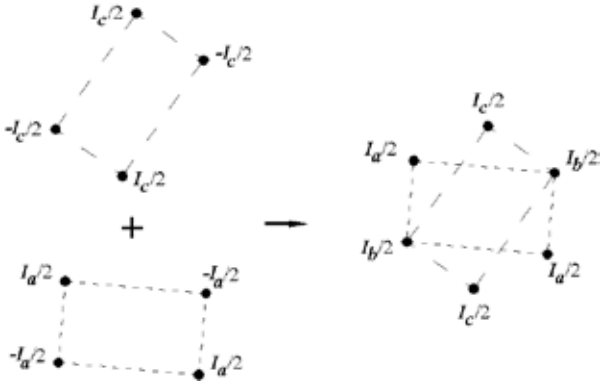

Figure 2.1.9 Example of synthesis of a three-phase configuration with three split phases, starting from two 4-conductor quadrupoles.

There is no advantage, in mitigation terms, for splitting three phases instead of two. This can be seen in Figure 2.1.10. The magnetic field contour curves for the configuration with two split phases are closer to conductors than with three split phases, assuming the same phase-to-phase clearance.

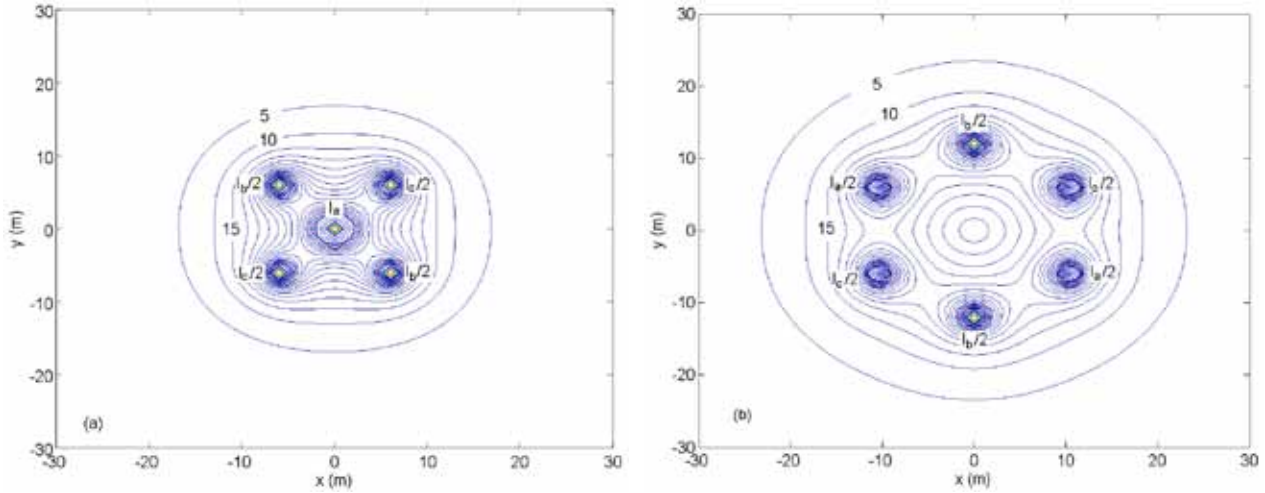

Figure 2.1.10 Magnetic field contour curves (in mT) for two split-phase three-phase configurations: (a) with two split phases; (b) with three. The current in each phase is 1000 A and the phase-to-phase clearance 12 m.

Split-phase configurations: simple formulation for the field at large distance

It is possible to obtain simplified formulations of field distances for split-phase configurations, similar to (2.1.4). Formulae are given here, as examples, for two configurations, each one with two split-phases [1].

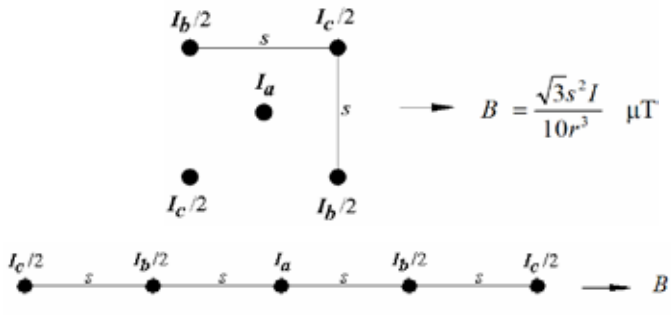

In these formulae, r is the distance between the geometrical centre of conductors and the calculation point, and I is the net phase-current in amperes (all distances in metres).

Higher mitigation rates are obtained if, instead of splitting two or three phases into two conductors, they are split into three or more (Figure 2.1.11). If so, then the field decays with distance to the power to 4. A general formulation for the field generated by a three-phase configuration with n subphases can be seen in [5]. The magnetic field contour curves for this configuration are shown in Figure 2.1.12.

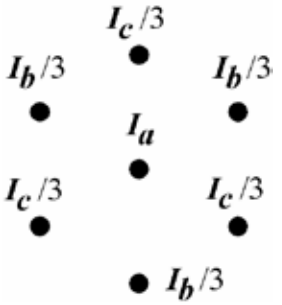

Figure 2.1.11 Configuration with three conductors per phase.

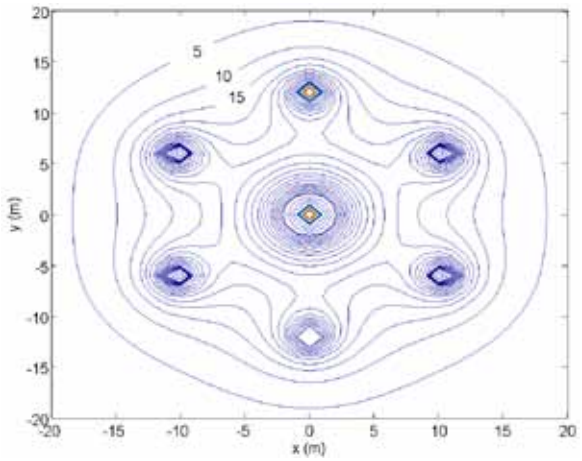

Figure 2.1.12 MF contour curves (in mT) for the configuration shown in figure 2.1.11, with phase current 1000 A and phase-to-phase distance 12 m.

Finally, it is worth to mention that, as in the case of layout and reduction of distance, the presence of zero-sequence current reduces the effectiveness of phase splitting. Indeed, in this case, the effect is even more marked because the field due to zero-sequence current decays with distance, so it cancels partially the major advantage of phase splitting: a fast field decay.

2.1.4 Phase cancellation

The fundamentals of this method are the same as for phase splitting, attempting to obtain low field configuration of conductors, so the field decays at least with distance cubed. The difference is based on practical reasons. In the phase splitting method, two or three phases are split into two or more conductors. In the phase cancellation method there is already a multi-circuit configuration, so the phases are split, and the method consists on just rearranging them accordingly. This method is, therefore, cost effective, because no new material has to be added.

A particular case of phase splitting is the low reactance configuration. If a double circuit configuration can be decomposed into two quadrupoles the field will decay with distance cubed. An example is the super-bundle double circuit vertical configuration (Figure 2.1.13). If phases *a* and *c* are interchanged, the result is a low field low reactance configuration. In this case the mitigation method does not consist on splitting phase conductors, but in rearranging them in order to get a low field design.

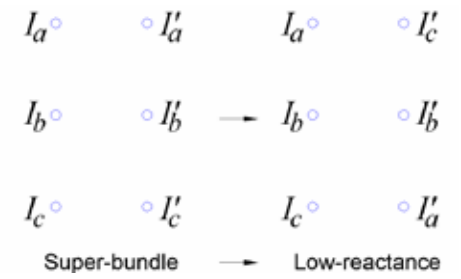

Figure 2.1.13 Rearrangement of phases in order to obtain a low-field configuration.

Simple expressions of the field far from double circuit configurations

There are approximate formulae for the magnetic field generated by double circuit configurations with the same current in both circuits [1]. For example, the furthest magnetic field generated by the balanced double circuit vertical or horizontal super-bundle configuration is given by replacing in (2.3) I by $2I$ (I is the current in each circuit):

$$B(r) = \frac{2\sqrt{3}dI}{5r^2} \qquad (\mu T) \qquad (2.1.5)$$

However, for the low-reactance or "reversed-phase" configuration, the field decays as $1/r^3$:

$$B(r) = \frac{2dI}{5r^3}\sqrt{d^2 + 3s^2} \qquad (\mu T)$$

where s is the distance between both circuits.

If the direction of the current in each circuit is the opposite, the field for the low-reactance configuration is given by (2.1.5), and for the super-bundle by

$$B(r) = \frac{2\sqrt{3}sdI}{5r^3} \qquad (\mu T)$$

Other multi-circuit configurations can be considered, with several conductors per phase. In many cases, it is not always possible to obtain a low field configuration with which the field decays with distance cubed, due to the impossibility to decompose the arrangement into two quadrupoles. However, by correctly arranging the phases, some reduction can be obtained [6]. As an example, Figure 2.1.14 depicts two different arrangements for three-phase triangular configurations with two conductors per phase.

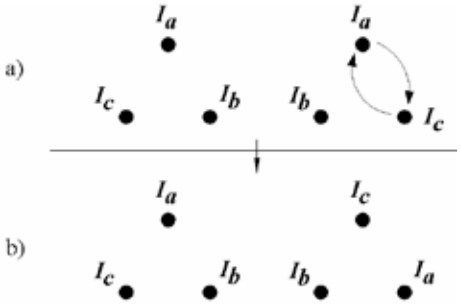

Figure 2.1.14 Two possible phase configurations for three-phase six-conductor triangular arrangements.

The only difference between both arrangements is the exchange of two subphases, as can be seen in the Figure. In Figure 2.1.15 the contour curves of both configurations are shown. In both cases, the field decays with distance squared, because the configuration can not be divided into quadrupoles. However, in case b) the field decays faster through direction $y > 0$. This fact can be exploited in some cases, e.g., to reduce the field over underground transmission cables.

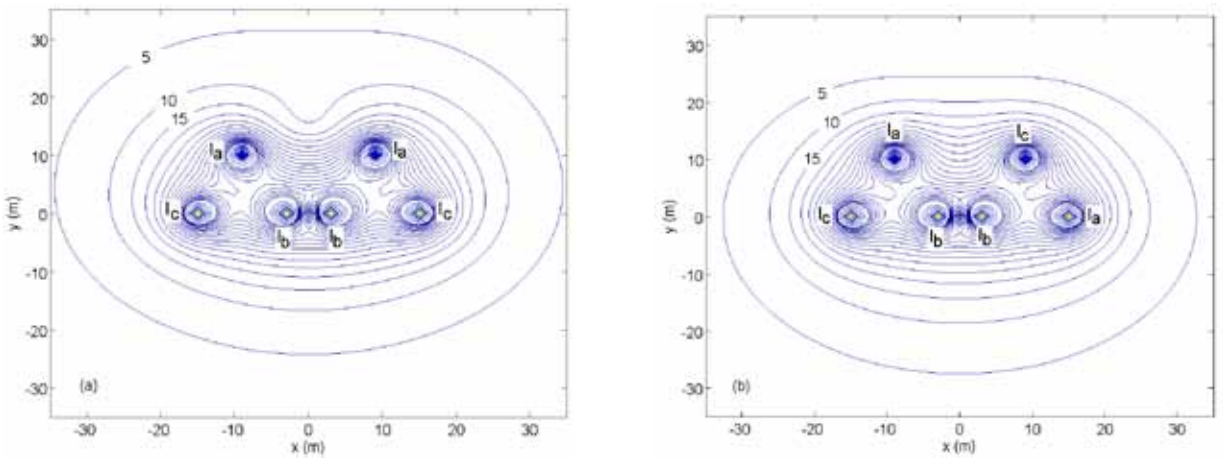

Figure 2.1.15 Magnetic field contour curves (in mT) of configurations shown in Figure 2.1.14 (phase current = 2000 A, phase-to-phase clearance = 12 m).

2.1.5 Neutral management

As demonstrated in previous sections, the presence of a zero-sequence current can negate the mitigation strategies that reduce the field for a system of conductors. In electrical installations, this current, also called ***stray current***, is the result of summing up all the phase and neutral currents, and exists because they can follow some uncontrolled return paths.

Although some percentage of ***zero-sequence current*** can exist in transmission systems, they can become a real concern in distribution systems, mainly when using a multigrounded neutral.

This topic is not addressed extensively in this report. In chapter 5, some procedures to reduce the stray currents are just listed. For those readers interested in pursuing this issue, reference [7] is recommended.

2.1.6 References

[1] W.T. Kaune, L.E. Zaffanella: "Analysis of magnetic fields produced far from electric power lines". *IEEE* Transactions on Power Delivery, Vol. 7, No. 4, pp. 2082-91, oct. 1993.

[2] P. Pettersson: "Simple method for characterization of magnetic fields from balanced three-phase systems". *CIGRE* 1992 Session, paper 36-103.

[3] L. Lindberg: "Reduction of magnetic fields from electric power and installation lines". *IEE* Proceedings-Science, Measurement and Technology, Vol. 145, No. 5, pp. 215-221, Sep. 1998.

[4] P. Cruz, C. Izquierdo, M. Burgos: "Optimal split-phase configurations". *Power Tech* Proceedings, Vol. 3, Porto, Sep. 2001.

[5] P. Pettersson: "Principles in Transmission Line Magnetic Field Reduction", *IEEE* Transactions on Power Delivery, vol. 11, no. 3, pp. 1587-1592, July 1996.

[6] M. M. Dawoud, I.O. Habiballah, A.S. Farag, A. Firoz: "Magnetic field management techniques in transmission underground cables", Electric Power Systems Research No. 48, pp. 177–192.

[7] E.A. Leeper, "Silencing the fields: a practical guide to reducing AC magnetic fields", Symmetry Books, Boulder, Colorado, 2001.

2.2 Compensation

This method relies upon generating an external-to-source current that creates a magnetic field in such a way that compensates the source field. There are two major compensation techniques, passive and active.

2.2.1 Passive compensation

This technique consists of appropriately placing a coil or loop of determined characteristics so that, in accordance with Faraday's Induction Law, the linked-to-coil alternating magnetic flux due to the source creates an induced current in the loop in such a way that the magnetic field produced attempts to compensate the original field (Lenz's Law). The flux from the coil is partially compensating the original source flux. Figure 2.2.1 shows an instant of this interaction, where the field from the source is increasing with time, and the field from the compensating coil has the direction shown.

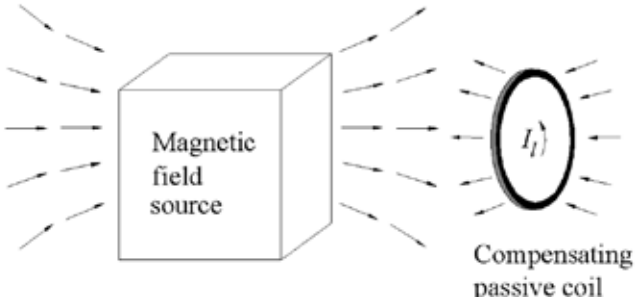

Figure 2.2.5 The field produced by the induced current in the compensating coil opposes the source field.

Several main aspects should be taken into account in the design of a passive coil-based compensating system:

- **Shape of the coil**. This depends strongly on the shape of the source. Common wire shapes are linear (overhead and underground lines, busbars, etc) and circular (reactors, transformers, etc). In order to have an effective mitigating field the compensating coil must realistically have the same shape as that of the source.
- **Location of the coil**. The field reduction is not guaranteed within the vicinity of a compensating coil. A correct location must be adopted. Normally, if the coil is placed concentrically to the source a general reduction can be obtained. However, in many situations this is not practical, and the reduction is more located in a restricted interest area. In this case higher reductions can be obtained with non-concentric coils, closer to the interest area, but at the expense, sometimes, of increasing the field elsewhere.
- **Electrical parameters of the coil**. The amplitude and phase of the induced current in the coil will define the characteristics of the compensating magnetic field. This current is dependent, among other factors, upon the coil resistance and inductance. In general, the lower the resistance the higher the mitigation. Regarding the inductance, there is a value where optimum mitigation is obtained. This value is normally lower than the real inductance of the coil, to obtain the correct value it is possible to add a series capacitor to the coil. To reduce the capacitance required, it is usual to design the coil with several turns.
- **Number of coils**. Higher mitigation is normally obtained with more than one coil, conveniently spaced.
- **Losses of the coil**. If the induced current in the compensated coil is high, Joule losses in this coil can be significant. This fact has two implications: increase of cost and heat, and hence, temperature (in some cases this can be a major restriction).

A first simple example is shown in Figure 2.2.2. The source is composed by two parallel long and straight current-carrying conductors (also called current dipole or coil without having a circular shape), so the problem becomes 2D. The compensating coil is also composed by two infinitely long conductors (resistance = 0.06 W/km) shortcircuited at both ends.

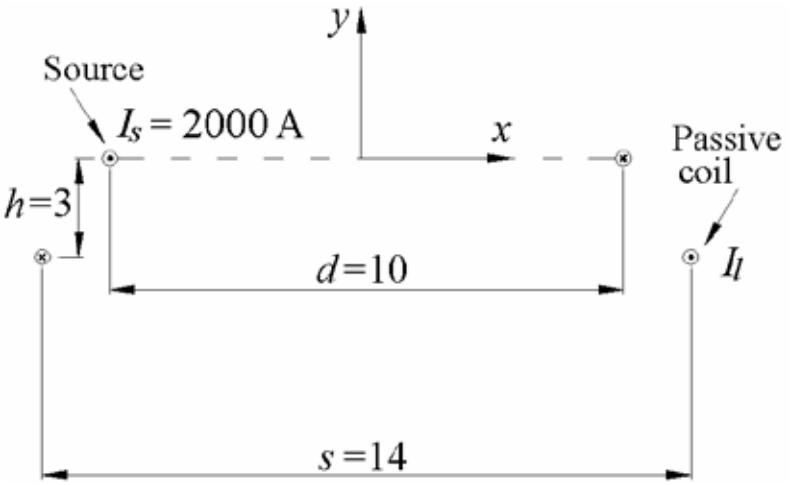

Figure 2.2.6 Cross sectional view of a source constituted by two long conductors and a compensating single-turn coil composed of long conductors shortcircuited at both ends (units in m).

The field created exclusively by the source is shown in Figure 2.2.3(a). If the coil is placed in the location shown in Figure 2.2.2, the induced current is 340 A, and the contour curves are shown in Figure 2.2.3(b). The effect is a global reduction of the field that is greater in the area under the compensating coil.

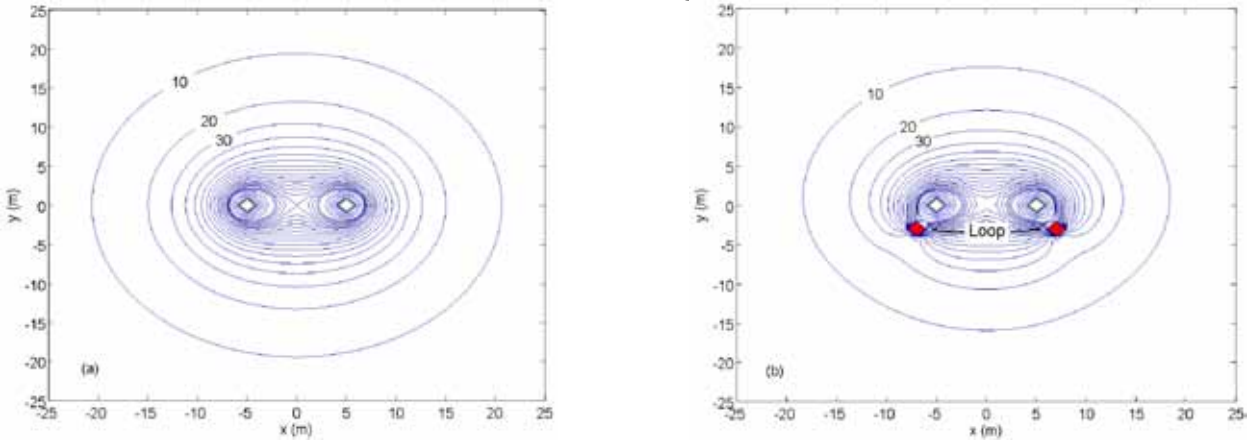

Figure 2.2.7 Contour curves of original magnetic field created by the source shown in Figure 2.2.2(a) and final field after placement of passive coil (b) (values in mT).

If a capacitor is placed in series with the compensating coil, the current induced increases due to resonance, and hence, also, the field mitigation. For a compensation of 60 % of the inductive reactance the induced current value is 840 A. The contour curves are shown in Figure 2.2.4.

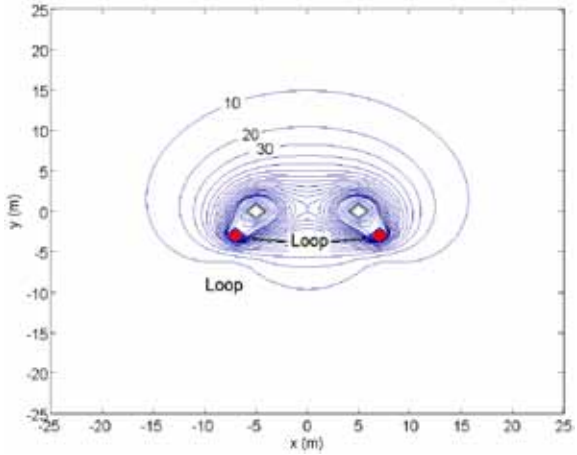

Figure 2.2.8 Contour curves of mitigated field (in mT) when a capacitor is placed in series with the passive coil in Figure 2.2.2.

Expression for the reduction factor at distance from the set generating-compensating coils

It is possible to obtain, for simple configurations, an approximate analytical expression for the reduction factor (ratio between non-mitigated and mitigated field) at distance from the source and passive loop. For example, for the case of figure 2.2.2, the current induced in the passive loop is given by

$$\boldsymbol{I}_l = \frac{-\,j\omega M \boldsymbol{I}_s}{R + j\omega L} \frac{-\,j\omega \frac{\mu_0}{2\pi} \ln \frac{h^2 + (s+d)^2}{h^2 + (s-d)^2}}{R + j\omega \frac{\mu_0}{\pi} \ln \frac{s}{GMR}} \boldsymbol{I}_s \approx \frac{-\ln \frac{h^2 + (s+d)^2}{h^2 + (s-d)^2}}{2 \ln \frac{s}{GMR}} \boldsymbol{I}_s = -K\boldsymbol{I}_s \tag{2.2.1}$$

where:

M: source-passive coil mutual inductance per unit of length
L: passive coil self-inductance per unit of length
R: passive coil resistance per unit of length
ω: current pulsation
μ_0: vacuum permeability
GMR: geometrical mean radius of passive coil conductor

The field generated by the source at points far from conductors is given by [1]

$$\boldsymbol{B}_s = \frac{\mu_0 d \boldsymbol{I}_s}{2\pi r^2} \tag{2.2.2}$$

and the field due to the passive coil has the same direction and its amplitude is similar to (2.2.2)

$$\boldsymbol{B}_l = \frac{\mu_0 s \boldsymbol{I}_l}{2\pi r^2} = -\frac{\mu_0 s K \boldsymbol{I}_s}{2\pi r^2} \tag{2.2.3}$$

The shielding factor will be

$$SF = \frac{|\boldsymbol{B}_s|}{|\boldsymbol{B}_s + \boldsymbol{B}_l|} = \frac{d}{d - Ks} \tag{2.2.4}$$

Another example is depicted in Figure 2.2.5. It shows a source single-turn circular coil and a compensating concentric coil. The RMS value of the induced current in the coil is 229 A. Figure 2.2.6 shows the original and the compensated field. It can be seen that the field level has been reduced approximately 50 %.

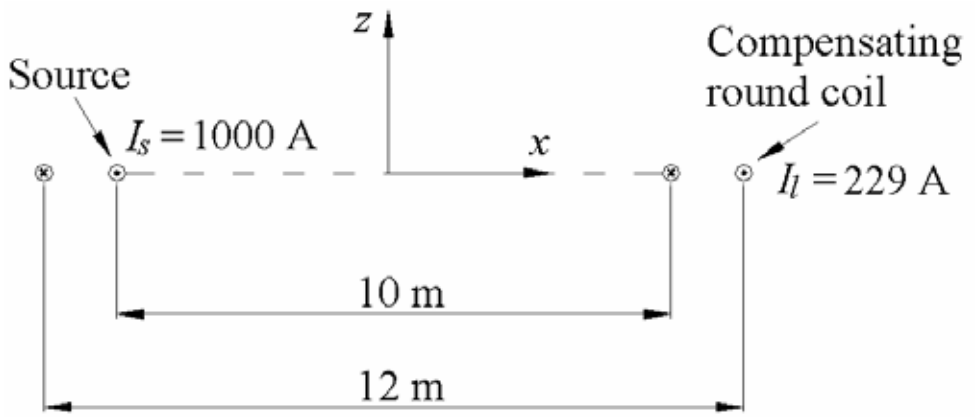

Figure 2.2.9 Cross-sectional view of a single-turn compensating round coil concentric to a source round coil (the current values are RMS).

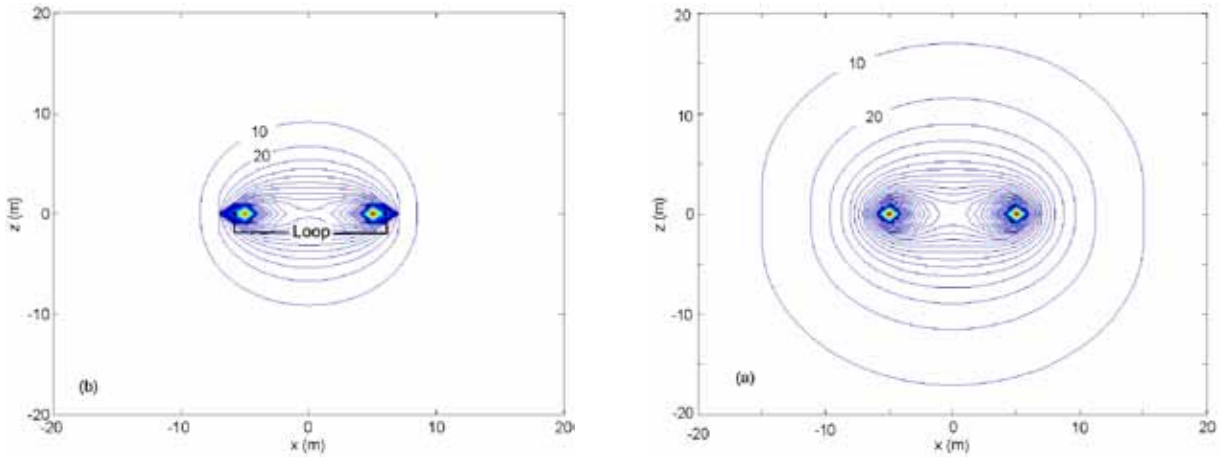

Figure 2.2.10 Contour field curves (values in mT) of: (a) magnetic field generated by a source round coil of Figure 2.2.5; (b) compensated field when a passive coil is in place.

2.2.2 Active compensation

It is possible to increase the mitigation effectiveness if, by means of an external power source, an appropriate current is injected in the compensating coil [1, 2]. The current value in magnitude and phase has to be calculated in order to obtain the highest mitigation in the point or area of interest. It is obvious that this current is dependent directly upon the source current, and as long as this one changes, the compensating loop current must change accordingly. Therefore, some kind of control system is needed to have a correct performance (Figure 2.2.7).

Some differences can be pointed out in relation to passive compensation:

- Additional sophisticated equipment is needed, implying maintenance. In the case of passive loops, only a capacitor with its protective equipment is required.
- The passive loop is a self-regulating system. As long as the source current changes, the loop current varies in a natural way. The active shield needs an additional regulation system.
- The location of an active loop is not as critical as with a passive one.
- The resistance of the active loop does not need to be small to obtain good mitigation.
- Due to the correct injected current, the mitigation is in general higher than with passive loops.
- The need for external equipment makes this solution costly and less reliable than the passive loop.

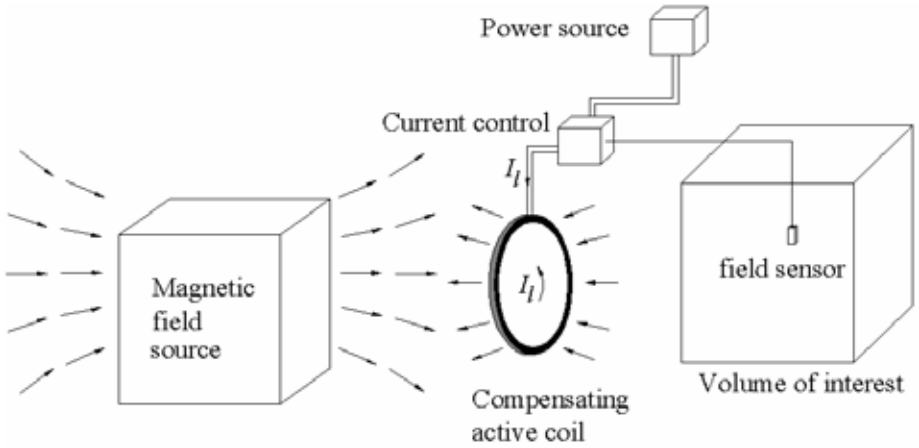

Figure 2.2.11 The current through the active coil is derived from an external source and is regulated by a control system.

As an example of the application, see Figure 2.2.2. The aim is to reduce as much as possible the field level at, for example, point (-10, 10). The current required in the coil can be calculated [1] at 980 A. With a passive compensated loop, the contour curves are shown in Figure 2.2.4, and are repeated with another scale in Figure 2.2.8(a). With active loop the contour curves are shown in Figure 2.2.8(b). The field at point (-10,10) is approximately 5 mT with the passive loop, and 3 mT with the active loop. This shows that

with the active loop higher reductions are obtained. However, if the passive loop resistance is lowered greatly, equivalent reductions can be obtained.

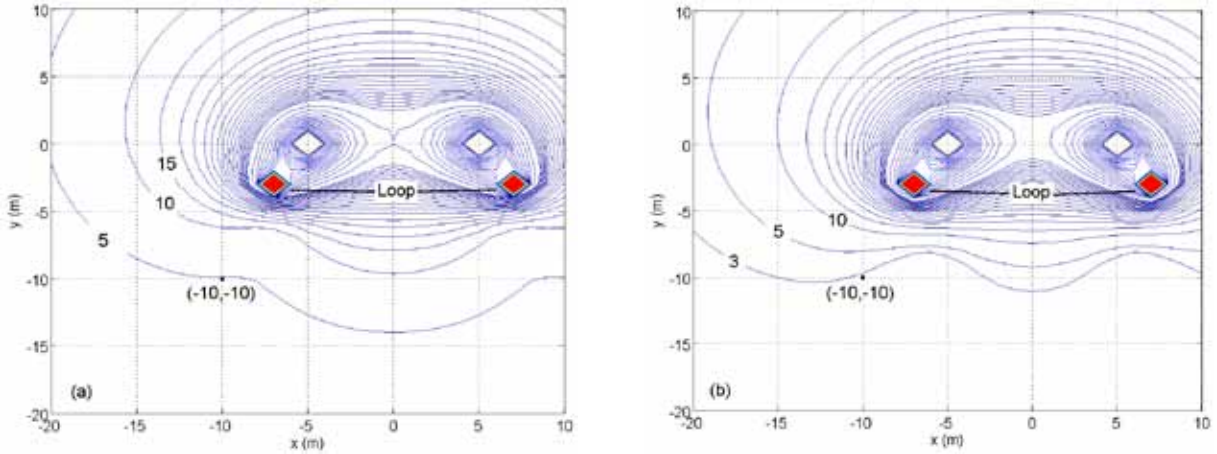

Figure 2.2.12 Contour curves of magnetic field (in mT) with passive loop and capacitor (a) and with active loop (b). The active loop current has been calculated to minimize the field at (-10,-10). Characteristics of the source: see Figure 2.2.2.

2.2.3 References

[1] P. Cruz, C. Izquierdo, M. Burgos: "Optimal design of active shielding for power lines". 14th *Power System Computation Conference* Proc., Session 24, Paper 2, page 1, Sevilla 2002.

[2] L. Hiles, G. Olsen, C. Holte, R. Jensen, L. Griffing, "Power frequency magnetic field management using a combination of active and passive shielding technology". *IEEE* Transactions on Power Delivery, vol.13, no.1, pp. 171-179, January 1998.

2.3 Shielding by metallic materials

This chapter[3] highlights the interactions of the magnetic field with metallic materials, which were introduced in chapter 1 and also contains more detailed information that will give a deeper understanding of the involved mechanisms and the way to quantify them.

As it was mentioned in chapter 1, one strategy for reducing ELF magnetic fields in a specific region is to make use of the properties of metallic materials (i.e. their conductivity[4] and permeability) as a mean for altering the spatial distribution of the magnetic field from a given source. When a shielding material separates the current-carrying conductors that serve as sources for a magnetic field from a region where reduction of field magnitude is desired, the shield causes a change in the structure of the magnetic field, diverting the magnetic flux away from the shielded region.

A quantitative measure of the effectiveness of a magnetic shield in reducing the magnitude of the magnetic field magnitude at a given point is the ***shielding factor*** (*SF*), defined in chapter 1. In general, the shielding factor is a function of the position at which it is measured. If the properties of a shield are independent of the field magnitudes, *SF* is correspondingly independent of the excitation amplitude. However, if the magnetic permeability of the shield material depends significantly upon the flux density within the material, the shielding factor becomes dependent upon excitation amplitude.

Another quantitative measure is the ***shielding effectiveness*** **(***SE***),** also defined in chapter 1. Shielding effectiveness is mainly used at high frequencies where shielding factors can be rather large, but normally not at power frequency.

Metallic shields are usually composed of thin sheets, which can be arranged as an open surface (open shield) or to form a surface enclosing a space volume (closed shield). The closed shields can be disposed in two alternative geometries, as shown in Figure 2.3.1. In Fig. 2.3.1(a), a magnetic field is imposed by distant external conductors, and a shielding material in the form of a cylinder or a sphere encloses the region where the field reduction is desired. In Fig. 2.3.1(b), the shielding material, again in the form of a cylinder or a sphere, encloses the conductors, with a resultant field reduction in the whole region outside the shield.

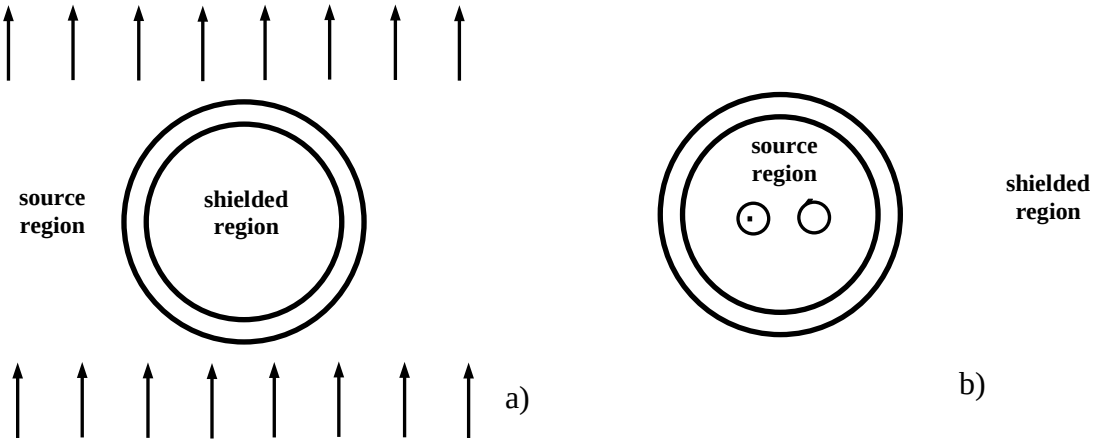

Figure 2.3.1 Two alternative shielding geometries; (a) enclosure of shielded region; the field is imposed by distant external conductors (b) enclosure of source conductors; region outside is shielded.

Two separate physical mechanisms can contribute to material-based ELF magnetic shielding. The physical phenomena involved in the shielding effects are the eddy currents in electrically conducting materials and mainly the ferromagnetic behaviour in high-permeability materials. In the following the two shielding mechanisms will be described and discussed separately.

[3] Mainly based on the work by J.F. Hoburg that was published in 1995 in the IEEE Transaction on Electromagnetic Compatibility [7] and completed with contributions based on [8 - 11] by O. Bottauscio et al.

[4] It has to be noted that there are other non-metallic materials, like ferrites, that have permeability, but very low or even zero conductivity.

2.3.1 (Pure) Ferromagnetic shielding

In this section, the manner in which ferromagnetic materials concentrate the field lines is described and the two shapes of the ferromagnetic shielding are presented and analysed: closed and open geometries. Care must be taken when looking to the calculation results ***that the material is assumed to have zero conductivity***. In most actual ferromagnetic materials[5], this conductivity plays also an important part in the shielding effectiveness.

2.3.1.1 The flux-shunting shielding mechanism

When a material with a magnetic permeability m is immersed in air, two conditions govern the behaviour of the magnetic field strength and magnetic flux density at the surface of the material [1], [2]:

1) Ampère's Law requires that the tangential component of magnetic field strength, $\boldsymbol{H}$, must be continuous across the interface.
2) Gauss' Law for magnetic flux requires that the normal component of magnetic flux density, $\boldsymbol{B}$, must be continuous across the interface.

Since $\boldsymbol{B} = \mu\boldsymbol{H}$ within the material, while $\boldsymbol{B} = \mu_o\boldsymbol{H}$ in the air, the field strength and flux density must abruptly change direction in crossing the interface in order to simultaneously satisfy both conditions. At the interface between a high permeability material and air, the field strength and flux on the air side of the interface are nearly perpendicular to the surface as they enter the material. By contrast, on the material side of the interface, the field strength and flux are nearly tangential to the surface (see Figure 2.3.2).

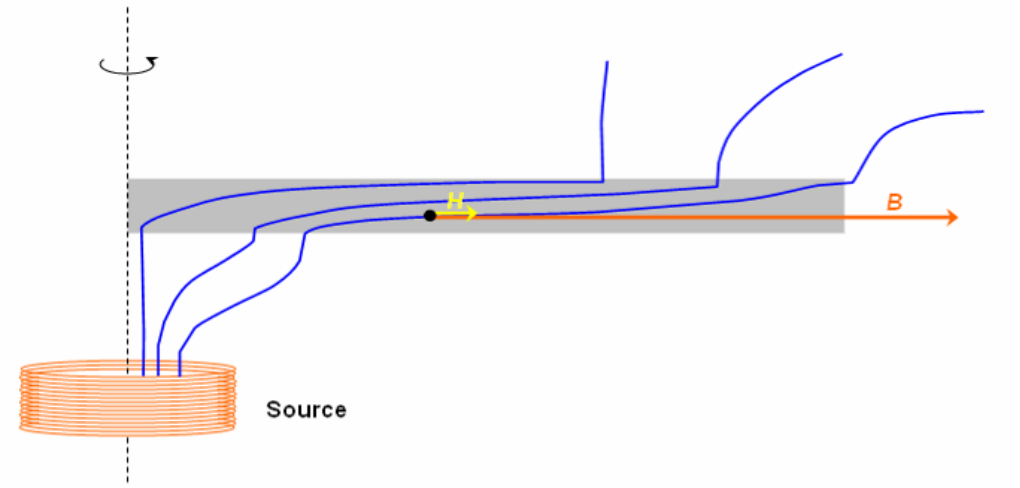

Figure 2.3.2 Plate of magnetic material above a coil - the lines of magnetic flux density change dramatically when they reach the interface air-magnetic material but they keep nearly tangential to the surface inside the material.

In the resulting overall structure, the magnetic flux that is produced by a configuration of source conductors is "pulled" toward a shielding material so as to enter it nearly perpendicular to the surface that faces the source conductors, then "shunted" within the material in a direction nearly parallel to its surface, and finally “released” back into the air, again on the surface that faces the source conductors [3], [4].

This mechanism of magnetic flux shunting, sometimes called ***magnetostatic shielding*** since it is effective even for DC fields, is well evident by the analysis of Figure 2.3.3 where the field lines are modified by the presence of the shield both for a closed (Fig. 2.3.3a taken from [14]) or open (Fig. 2.3.3b) configuration. The magnetostatic mechanism for a source inside the shielded enclosure is illustrated in Figure 2.3.3c.

It is important to note that, for a closed magnetostatic shield, the source needs to be entirely inside or outside the shielded enclosure: if the shield crosses the area bounded by the currents forming the source, e.g. when the return path of some currents is outside the shielded area, the shielding is inefficient, i.e. the shielding factor remains equal to 1 (Figure 2.3.4).

[5] Except ferrites, which are not really metals but hard and brittle ceramic-like materials with good magnetic properties.

The degree to which some flux "leaks" out of the magnetic material at the surface that faces the shielded region is determined by the permeability of the material and by both the large scale dimensions and the thickness of the shield. The shield gathers flux over a region whose size is determined by the large-scale dimension (diameter) of the shield and shunts it through the thickness of the shield. Thus, the flux density within the shield material is amplified from the imposed flux density by a factor determined by the ratio of shield diameter to thickness. The flux that leaks into the shielded region is attenuated from that within the shield material by the ratio of material permeability to air permeability. These effects combine to produce a shielding factor that can be increased (improved shielding) either by increasing the material permeability relative to air or by increasing the material thickness relative to the shield diameter.

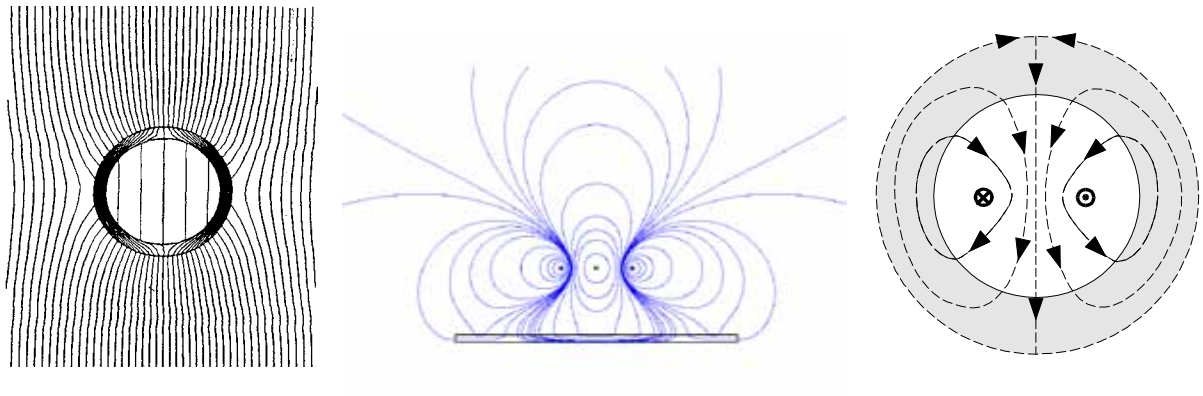

(a) (b) (c)

Figure 2.3.3 "Attracting-like" displacement of the magnetic field lines by a ferromagnetic shield: a) closed shield with external source (homogeneous field), b) open shield (three-phase field) and c) closed shield with internal source (single-phase field).

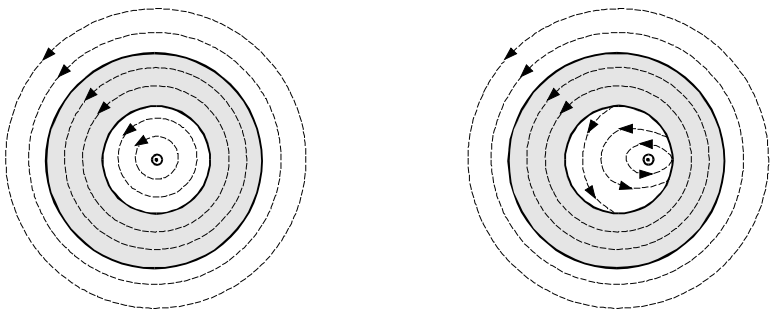

Figure 2.3.4 Totally ineffective magnetic shielding when the source is not completely enclosed by the shield and regardless of the shield position with respect to the source (return path at large distance from the shield and not shown).

When considering shielding applications, ferromagnetic materials (usually alloys) can be divided into low-cost and high-cost materials. The first category mainly includes both iron and magnetic steel structural shapes and laminations for laminated cores of electrical machinery. The materials are: iron, magnetic steel, low-carbon alloys, silicon-iron alloys (oriented and non-oriented grain), amorphous materials and nanocristalline materials. The profiled materials can be plane sheets, tube, U-shaped, etc. with a thickness of millimetres or tens of millimetres. The classical alloys for magnetic cores are available as laminations with a thickness of hundreds of micrometers. Amorphous and nanocristalline alloys are produced as ribbons with a thickness of tens of micrometers.

The high-cost materials, cobalt alloys (mumetal, permalloy), present very high permeabilities. The use of these materials is justified when shielding limited regions, in particular, for applications where

experiments or measurements of high accuracy levels are required. In any case, the nonlinear magnetization curve (see chapter 1) defines the magnetic behaviour of all the ferromagnetic materials. Some typical magnetisation curves of the ferromagnetic materials generally used for shielding applications are shown in Figure 2.3.5.

In closed shields or in the presence of high field levels (e.g. close to the source), *saturation* can occur, significantly reducing the shielding factor. On the contrary, in open shields, ferromagnetic materials usually work at low or very low flux density values. In these cases the efficiency of the shield essentially depends on the initial part of the magnetic characteristic, before the first knee of the magnetization curve (Rayleigh region). Therefore the materials can be classified on the basis of their relative permeability at low flux density values: cobalt alloys ($\mu_r \sim 100{,}000$), amorphous and nanocristalline (μ_r = 10,000 to 100,000), grain oriented silicon-iron alloys ($\mu_r \sim 10{,}000$), iron low-carbon steel alloys, non-oriented silicon-iron alloys (μ_r = 100 to 5,000). The general magnetic behaviour of some ferromagnetic materials are summarized in Table 2.3.1.

Tabel 2.3.1 Magnetic properties of some typical ferromagnetic materials.

Material	Initial Relative Permeability $\mu_{r,ini}$	Maximum Relative Permeability $\mu_{r,max}$	Coercive Field Strength H_c [A/m]
Iron, 99.8% pure	150	5000	80
Iron, 99.95% pure	10,000	200,000	4
Steel, 0.9% C	50	100	5600
Low Carbon Steel (LCS)	300-400	2000	50-100
Ultra Low Carbon Steel (ULC)[6]	250	1100	150
Silicon steel (Si 3%) - Grain oriented (GO)	–	40,000	8
78 Permalloy (μ-material)	8,000	100,000	4
Superpermalloy (μ-material)	100,000	1,000,000	0.16
Cobalt, 99% pure	70	250	800
Nickel, 99% pure	110	600	56

Figure 2.3.6 presents the relative permeability values in the Rayleigh and linear regions for some materials largely employed in shielding applications. In the linear region, most permeabilities are virtually constant, so that a linear simplifying assumption is justified. For calculation purposes, the same assumption can be made for the Rayleigh region, but with lower permeability values.

Finally, some additional considerations have to be taken into account with grain-oriented silicon iron alloys. These materials present different magnetic characteristics depending on the angle between the applied field and the rolling direction: in the rolling direction (easy direction) the material has a high initial permeability, while in the other the initial slope of the magnetization curve is significantly lower. Therefore, a single oriented sheet can be used only if the field to be mitigated is expected to be unidirectional; in other cases a multilayered shield composed of two sheets with orthogonal easy directions has to be employed.

[6] Hot rolled ultra low carbon steel (HR ULC) can have maximum relative permeability up to 2800 at 200 A/m

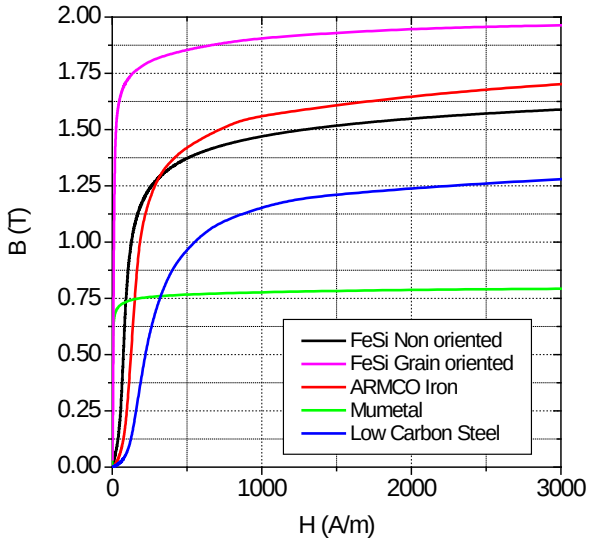

Figure 2.3.5 Magnetisation curve of ferromagnetic materials commonly employed for shielding.

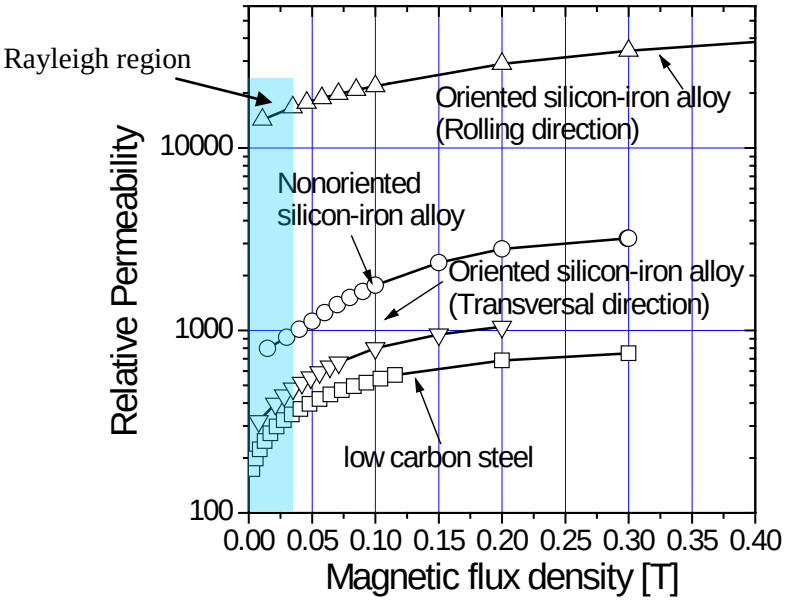

Figure 2.3.6 Relative permeability in the Rayleigh and linear regions for some classes of low cost ferromagnetic materials.

2.3.1.2 Closed ferromagnetic shields (cylindrical or spherical)

For shields that take the form of long cylinders and spheres, the fields in the source, material and shielded regions are calculated analytically by splicing together uniform and dipole field solutions within the bulk of each region and requiring continuity of tangential magnetic field and normal magnetic flux density at each interface [1], [2]. For both long cylindrical and spherical shields, the analytic analysis can be carried out for the two separate source / shielded region configurations:

1) With a uniform magnetic field imposed by a distant source outside the shield, the shielding factor is calculated in the region inside the shield.
2) With a dipole source at the centre of the shield, the shielding factor is calculated in the region outside the shield. "Dipole source" here has different meanings for cylinders and spheres:
    a) For the long cylindrical geometry, a dipole source consists of two long wires, coaxial with the cylinder, that carry currents in opposite directions.

b) For the spherical geometry, a dipole source consists of a circular wire loop at the center of the sphere.

For each of the four cases (long cylindrical or spherical shield with uniform external field or dipole source), the shielding factor is uniform throughout the shielded region - for the uniform external field source, the field in the inner shielded region is also uniform while, for the dipole source, the field in the outer shielded region has a spatial distribution with the same structure as would be produced by the source with the shield absent: the magnitude is reduced by the same factor at each point in space.

In addition, the uniform external field and the dipole source configurations satisfy reciprocity conditions for both the long cylindrical and the spherical geometries - each shield provides the same shielding factor inside from an externally applied uniform field as it does outside from an interior dipole source.

For ***a long cylindrical shield*** with permeability μ inner radius *a* and thickness D the shielding factor for either source configuration is:

$$s = \frac{(\mu/\mu_0 + 1)^2 - \dfrac{(\mu/\mu_0 - 1)^2}{4r^2 + 4r + 1}}{4\mu/\mu_0} \qquad (2.3.1)$$

where $r = \dfrac{D}{2a}$ is the ratio of shield thickness to inner diameter.

When the shield thickness Δ is small in comparison with the inner radius *a*, and when the permeability μ is large enough in comparison with μ_o that the condition $(\mu / \mu_o)\,(\Delta/a) >> 1$ is satisfied, the shielding factor is much higher than 1.0 and (2.3.1) can be approximated by:

$$s = \frac{\mu}{\mu_0}\frac{D}{2a} \qquad (2.3.2)$$

In this form, the effects of large relative permeability and large ratio of thickness to diameter in producing good shielding are apparent.

For ***a spherical shield*** with permeability μ, inner radius *a* and thickness D the shielding factor for either source configuration is:

$$s = \frac{(\mu/\mu_0 + 2)(2\mu/\mu_0 + 1) - \dfrac{2(\mu/\mu_0 - 1)^2}{8r^3 + 12r^2 + 6r + 1}}{9\mu/\mu_0} \qquad (2.3.2)$$

When the shield thickness Δ is small in comparison with the inner radius *a*, and when the permeability μ is large enough in comparison with μ_o that the condition $(\mu / \mu_o)\,(\Delta/a) >> 1$ is satisfied, the shielding factor is much higher than 1 and (2.3.3) can be approximated by:

$$s = 2\frac{\mu}{\mu_0}\frac{D}{3a} \qquad (2.3.4)$$

Again, in this form, the effects of large relative permeability and large ratio of thickness to diameter in producing good shielding are apparent. The spherical shielding factor described by (2.3.4) is higher (better shielding) than the long cylindrical shielding factor described by (2.3.2) by a factor of 4/3.

Figure 2.3.6 shows, for a long cylindrical shield and for a spherical shield respectively, the shielding factor as a function of ratio of shield thickness to inner diameter $\Delta/(2a)$ for various values of relative shield permeability μ/μ_o.

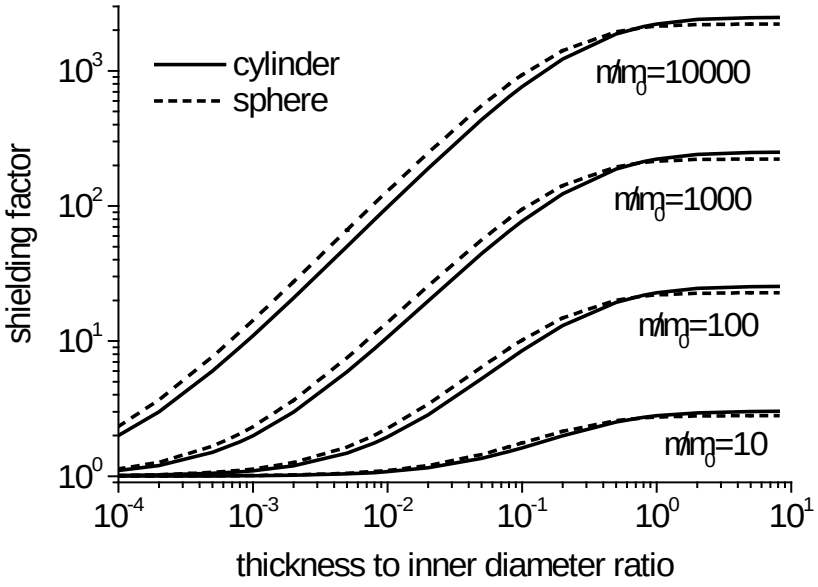

Figure 2.3.6 Shielding factor as a function of the thickness to inner diameter for a long cylinder shield and for a spherical shield.

Degrading effect of saturation in closed ferromagnetic shields

All magnetic materials present a non-linear behaviour due to the slope of the magnetization curve (and hence, the permeability) which greatly reduces when the applied field increases. This phenomenon is negligible in usual shielding applications, but it can become important in some closed arrangements or in the presence of very high currents in the conductors. In these cases the shielding factor significantly decreases with the increase of the source field. A possible solution for a more efficient mitigation is the use of additional shields placed between the source and the region to be protected.

These considerations are highlighted with the curves shown in Figure 2.3.7. In this simulation one or more concentric hollow Armco iron cylinders (axial length: 200 mm; thickness: 5 mm; diameters: 99 mm, 111 mm, 135 mm) are placed inside a uniform magnetic field along the axial directions. The shielding factor is evaluated in the central point of the cylinder.

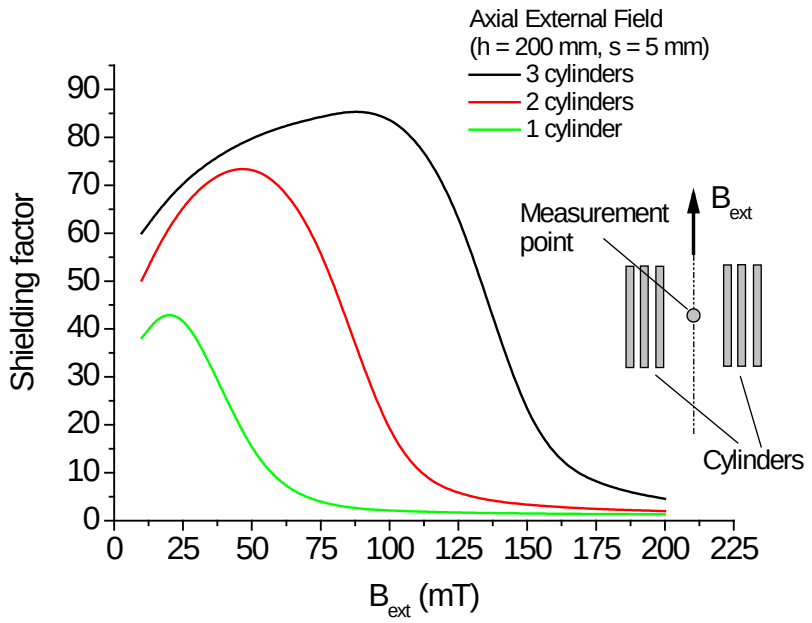

Figure 2.3.7 The shielding factor of concentric hollow Armco iron cylinders as a function of applied external field.

2.3.1.3 Open ferromagnetic shields (flat shields, U shaped shields…)

Open shields are usually employed for large-scale screening or when an easy access to the region to be mitigated must be guaranteed. In these cases, the shields take the form of thin sheets (of the order of millimetres or lower), formed into a partially closed shield. Due to the fact that the magnetic flux lines in the material cannot follow a closed circuit and are always obliged to escape in the air, the reluctance path they follow is always much higher than in a closed magnetic shield and the resultant shielding efficiency is always much poorer.

In addition the prediction of the shielding effects can no longer be performed by simple analytical formulas, and numerical computations, based on the solution of Maxwell equations, are needed (although simple cases can be analytically formulated, as can be seen in chapter 3). The parameters that control the shielding efficiency are numerous and the effect of each one also substantially depends on the values assumed by the other parameters. In particular, the parameters controlling the shielding phenomenon are: the permeability of the material, the shield dimension and thickness, the distance between source and shield, and the shield shape. An exhaustive analysis of their effect cannot be reported here; however some examples of their influence on the shielding performances of ferromagnetic shields are described in the following.

The analysis is developed for simplicity making reference to a two-dimensional source, formed by a lead-and-return conductor. The shield (with thickness D and permeability m) is realized by a planar sheet (having width *L*) or a by a U-shaped sheet, and it is placed at a distance *d* from the source (see Figure 2.3.8).

It must be noted that, in the U-shaped arrangement, each side has the same length *L* as the planar sheet. Hence, the U-shaped shield involves more shielding material than the planar shield.

The shielding factor depends on the position; the value is plotted along the y-axis (at x = 0) and along the x-axis (at y = d + 0.5, that is at 0.5 m from the shield).

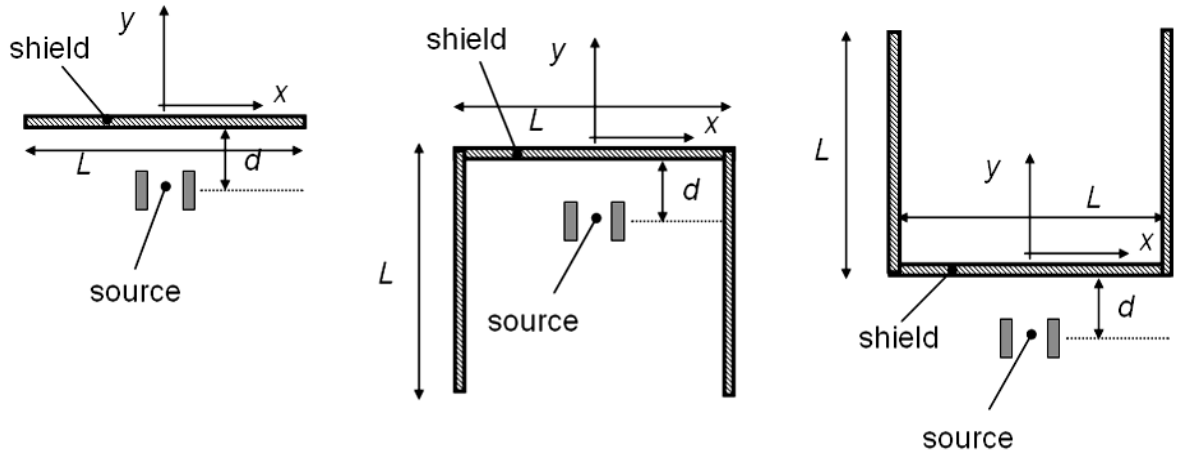

Figure 2.3.8 Different shielding configurations of the field source, (a) planar (flat), (b) U-shaped around the source and (c) U-shaped around the protected area.

The first results, which aimed at evidencing the role of some parameters, are provided by a numerical model considering flat shields. Permeability plays an important role in the shielding efficiency also for open ferromagnetic screens. The greater the permeability, the greater the shielding efficiency (Figure 2.3.9). However the increase of the *SF* is not linear with the increase of permeability and reduces at high permeability values.

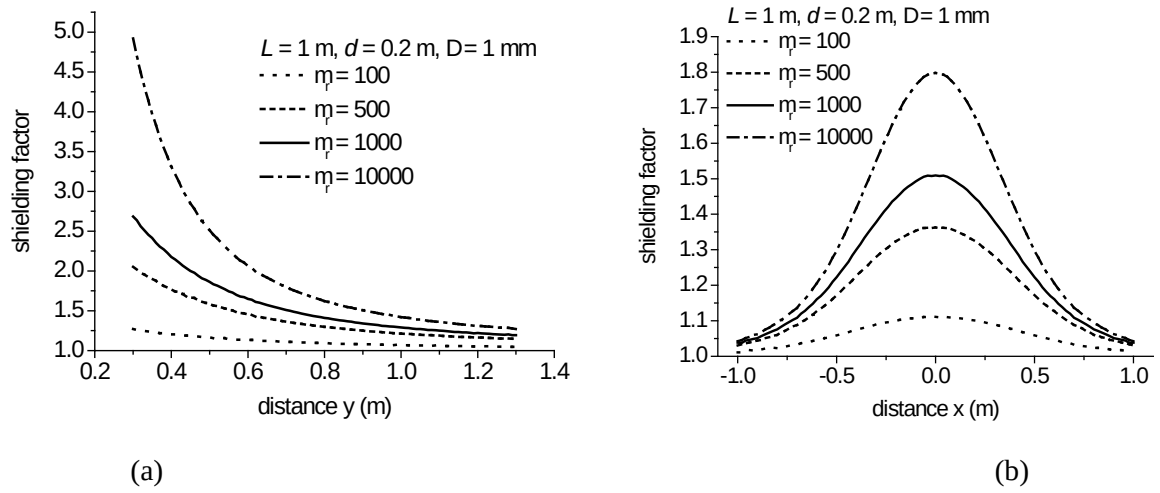

(a) (b)

Figure 2.3.9 *SF* of the flat shield of Figure 2.3.8(a) for different values of magnetic permeability: (a) plot along *y* axis at $x = 0$, (b) plot along *x* axis at $y = 0.7$ m.

The distance *d* between source and shield does not appreciably influence the shielding factor beyond the shield if the distance shield - measurement point is kept constant (Figure 2.3.10).

However, ***the shielding factor rapidly decreases when the distance shield - measurement point increases. At distances higher than the shield width, the shielding efficiency becomes virtually zero*** (see Figure 2.3.10).

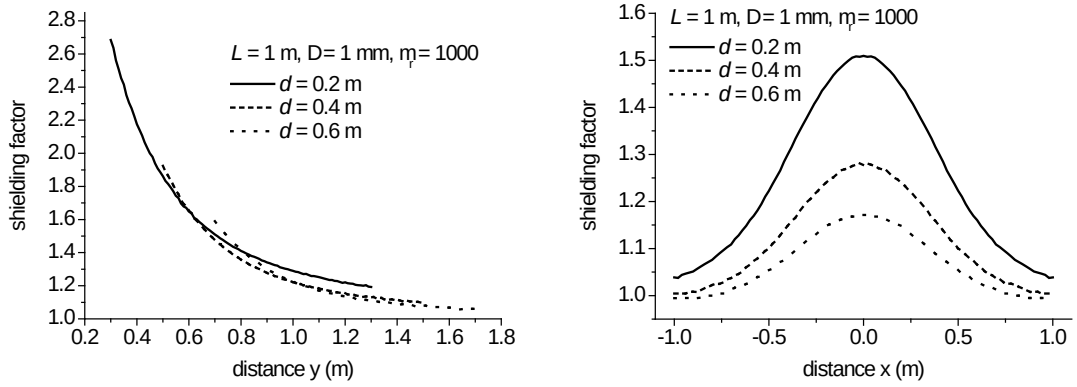

(a) (b)

Figure 2.3.10 *SF* of the flat shield of Figure 2.3.8(a) for different source - shield distances: (a) plot along *y* axis at $x = 0$, (b) plot along *x* axis at a distance of 0.5 m from the shield, (corresponds to $y = 0.7$ m, 0.9 m and 1.1 m respectively for $d = 0.2$ m, 0.4 m and 0.6 m).

The influence of shield width is significant. Increasing the value of *L* positively influences the shielding factor (Figure 2.3.11).

Error! Reference source not found.

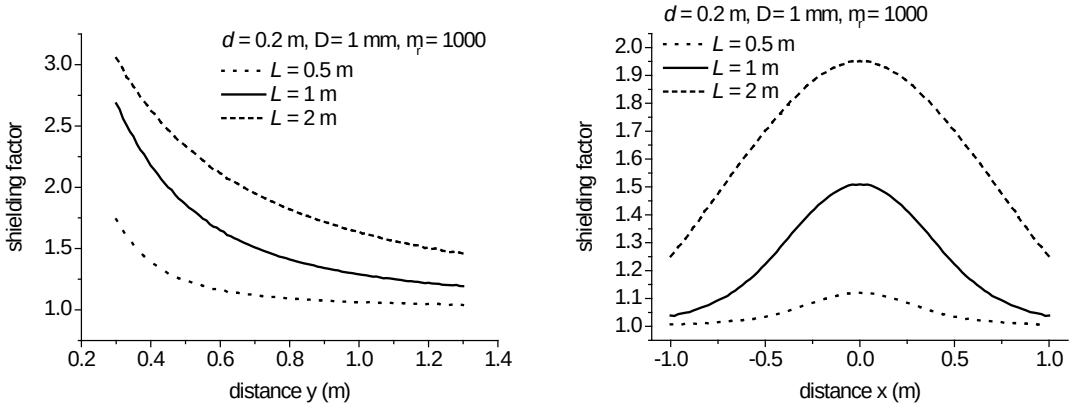

(a) (b)

Figure 2.3.11 *SF* of the flat shield of Figure 2.3.8(a) for different widths: (a) plot along *y* axis at $x = 0$, (b) plot along *x* axis at $y = 0.7$ m.

The shield thickness has a noticeable influence for the lower values (a few millimetres) but for higher values the increase of the shielding factor is lower, as shown in Figure 2.3.12.

The influence of the shield shape is important for ferromagnetic materials both when the shield is placed around the protected area and when it encloses the source. The U-shaped shield always increases the shielding factor with respect to a planar shield having the same with as the central part of the U-shaped shield (Figure 2.3.13).

When the shield arrangements make an angle (U-shaped, closed), the assumption of a perfect material-continuity is a condition unachievable in practice. Even when a good continuity is guaranteed by forming or welding the material, at the edges, it has a detrimental effect on the magnetic properties, due to the mechanical or thermal stresses. This effect is particularly significant when high-permeability materials are used (e.g. GO Fe-Si alloy or Mumetal). It can be overcome by a controlled thermal annealing that is only possible in the case of small size screening. The angle, achieved by layers of laminations, introduces unavoidable air gaps in the path of the magnetic flux flowing in the shield. The lack of continuity (e.g. a gap) gives rise to a significant reduction of the shielding effectiveness, which mainly affects the high-permeability materials (about a factor 2 for two gaps of 0.1 mm in the U-shaped shield of Figure 2.3.8(c) with a thickness of 1 mm).

All these calculations have been performed for single-phase sources, but similar results can be expected with three-phase systems.

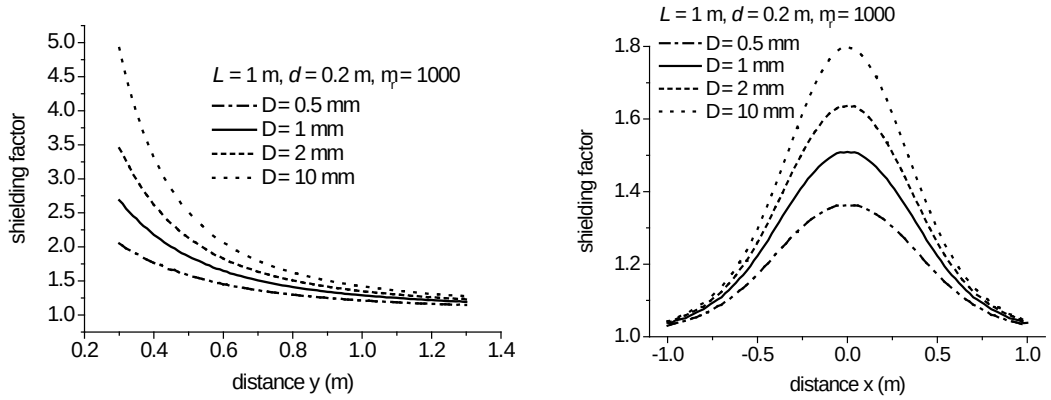

(a) (b)

Figure 2.3.12 *SF* for different thicknesses of the flat shield of Figure 2.3.8(a): (a) plot along *y* axis at $x = 0$, (b) plot along *x* axis at $y = 0.7$ m.

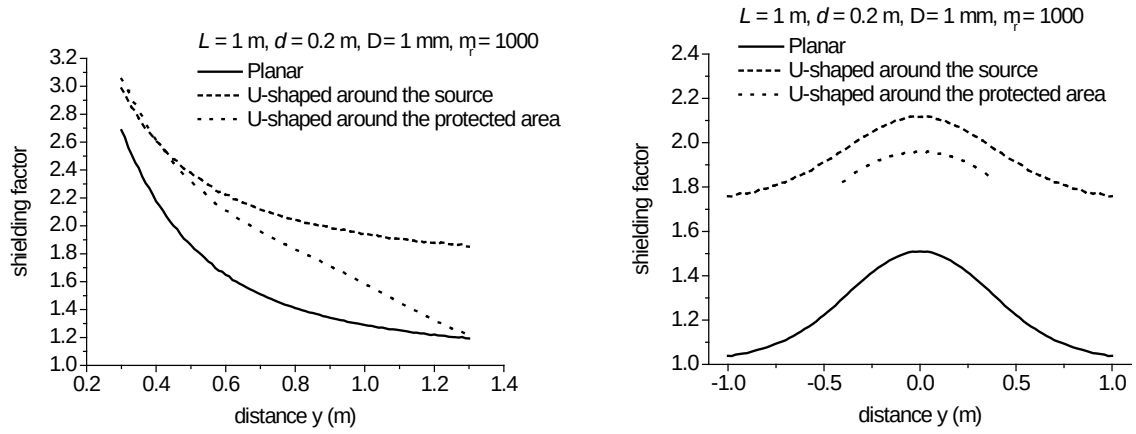

(a) (b)

Figure 2.3.13 *SF* for the three shielding shapes of Figure 2.3.8: (a) plot along y axis at x = 0, (b) plot along x axis at y=0.7 m.

2.3.2 (Pure) conductive shielding[7]

As it has been done for pure ferromagnetic materials, the way pure conductive materials repel the field lines is described followed by an analysis of the different shapes (open shields, closed shields).

2.3.2.1 The induced current shielding mechanism

When a region of space experiences a time-varying magnetic flux density $\boldsymbol{B}$, an electric field $\boldsymbol{E}$ is induced within this region, as described by Faraday's Law (see chapter 1). If a pure conductive material with electrical conductivity σ is placed in this region, the induced electric field drives an induced current density within it. This induced current constitutes an additional field source, superimposed to the main field source, that opposes the change in the imposed magnetic flux. The superposition of imposed and induced magnetic fields tends to "buck out" the imposed field, diverting the flux away from the shielded region in closed shields (Figure 2.3.14a [12]), while, in open shields, it produces a compression of the flux lines on the side of the source and a reduction of the magnetic flux density beyond the shields (Figure 2.3.14b).

[7] Also known as “shielding by eddy currents”

The induced current mechanism arises only when the imposed field is time-varying, so that the mechanism is not effective for DC fields and its efficiency increases with the frequency. In conductive materials the resulting shielding factor is a complex number at each point in space (its magnitude is the ratio of the field magnitudes with and without shielding and its phase is equal to the phase difference of these fields).

The shielding effect occurs in any electrically conducting material, which may or may not also have a permeability μ larger than μ_o. In an AC field with frequency f, the induced current density and total flux density decay exponentially into the material, away from the surface of the shield that faces the source, with a characteristic decay length $\delta = 1/\sqrt{\pi f \mu \sigma}$, which is referred to as the "***skin depth***" (see chapter 1).

In pure conductive materials, where $\mu = \mu_o$, the product $f \mu_0 \sigma$ can often be small enough that the skin depth δ is large in comparison with the shield thickness Δ. For example, at 60 Hz, the skin depths in copper and aluminium are 8.5 mm and 11.8 mm, respectively. Even with a 100-fold increase in frequency to 6 kHz, both materials have skin depths of the order of 1 mm. The skin depth is strongly reduced in ferromagnetic materials, which usually show a lower electrical conductivity, but greater magnetic permeability. When $\delta >> \Delta$, the induced currents flow uniformly over the shield thickness. By reducing skin depths with increasing frequency, the shielding factor can increase. However, beyond a certain point, the reduction of the skin depth value does not lead to an increase of eddy currents with frequency, limiting or reducing the shielding effects.

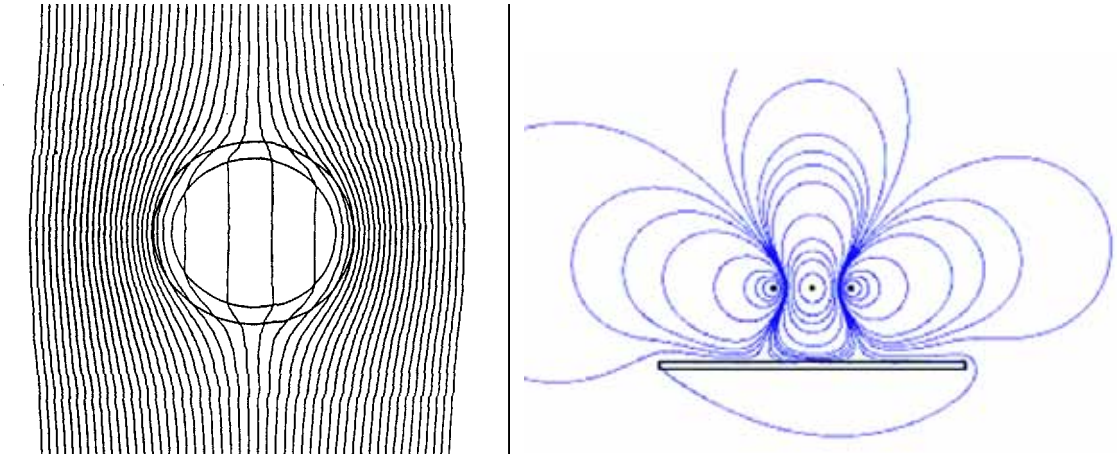

(a) (b)

Figure 2.3.14 "Repelling-like" displacement of the magnetic field lines by a pure conductive shield: a) closed shield with external source (homogeneous field), b) open shield (three-phase source)

The materials adopted for conductive shielding usually have electrical conductivity higher than 10 MS/m. Copper, aluminium and their alloys, formerd into thin sheets (thickness of some millimetres) are usually employed. Often the use of aluminium is preferred, due to its lower specific weight, which enables sensible reductions of the global weight of the shielding structure, without decreasing the shielding efficiency. Also pure iron (Fe) has interesting conductive properties, but at low frequency the prevalent shielding effects are due to its ferromagnetic behaviour.

The superconductive alloys represent a particular category of conductive materials. Their shielding properties are ideal, because, due to the Meissner effect, the magnetic field is totally rejected from the sheet. Therefore, within a closed superconductive shield the magnetic field everywhere is zero in the inner region. However, at the moment, the very low temperatures (few Kelvins) required by the superconductive phenomenon limit its application to laboratories.

2.3.2.2 Closed conductive shields (cylindrical or spherical)

In the same manner as for the flux shunting descriptions of section 2.3.1.2, for non-permeable, conducting shields that take the forms of long cylinders and spheres and that are thin both in comparison with the skin depth and the inner radius of the structure, the induced current analysis can be carried out for two separate source / shielded region configurations (uniform field imposed / shielded region inside and dipole source inside / shielded region outside). Uniform and dipole field solutions within the bulk of each region are spliced together by requiring continuity of normal magnetic flux density and a discontinuity in tangential magnetic field that is determined by a surface current density within the shield based upon the product of induced electric field, conductivity, and thickness [1], [2].

Again, for each of the four cases, the complex shielding factor is uniform throughout the shielded region, and again the uniform external field and the dipole source configurations satisfy reciprocity conditions for both the long cylindrical and spherical shield geometries - each shield provides the same complex shielding factor inside from an externally applied field as it does outside from an interior dipole source.

For ***a long cylindrical shield*** with permeability μ_o conductivity σ, inner radius a, and thickness Δ in a sinusoidally varying field at angular frequency ω, which is thin enough to satisfy the conditions $\Delta << \delta = 1/\sqrt{\pi f \mu_0 \sigma}$ and $\Delta << a$, the complex shielding factor (s) for either source configuration is expressed in terms of a magnetic diffusion time τ that is analogous to a circuit L/R time constant [1], [2]:

$$s = 1 + i\omega\frac{\tau}{2} \qquad \text{where } \tau \approx \mu_0 \sigma a \Delta \qquad (2.3.5)$$

For ***a spherical shield*** with permeability μ_o, conductivity σ, inner radius a, and thickness Δ in a sinusoidally varying field at angular frequency ω which is thin enough to satisfy the conditions $\Delta << \delta = 1/\sqrt{\pi f \mu_0 \sigma}$ and $\Delta << a$, the complex shielding factor for either source configuration is again expressed in terms of the magnetic diffusion time τ:

$$s = 1 + i\omega\frac{\tau}{3} \qquad \text{where } \tau \approx \mu_0 \sigma a \Delta \qquad (2.3.6)$$

Equation (5) for a long cylindrical shield and (6) for a spherical shield each make apparent the effects of increasing conductivity, radius, and thickness in improving induced current shielding by increasing the magnetic diffusion time τ and consequently the magnitude of the shielding factor.

The fact that the magnetic diffusion time is based upon the product of radius and thickness, rather than upon the square of the thickness of the shield, derives from the fact that the induced currents circulate around a large scale dimension of the shield. This leads to considerably better shielding in the regime where the skin depth is large in comparison with the shield thickness than would be estimated based upon a direct comparison of shield thickness with skin depth.

Of particular note is the dependence of shielding factor magnitude upon radius for a fixed shield thickness, which is opposite to the dependence for the flux-shunting mechanism. ***For the ferromagnetic shield, an increase in radius produces poorer shielding, because a larger total flux must be shunted through a fixed thickness. By contrast, for the pure conductive case, an increase in radius produces improved shielding, because the inductive coupling to the source is proportional to the area that intercepts the source flux, while the resistance that is presented to induced currents is proportional to the circumference of the shield***. The ratio of area to circumference produces the linear dependence upon radius in the magnetic diffusion time in (5) and (6).

Figure 2.3.15 shows the magnitude of the shielding factor, as given by (5) and (6), as a function of the frequency-magnetic diffusion time product $t \cdot \pi \cdot \mu \cdot \sigma \cdot a \cdot D$ for both long cylindrical and spherical shields. For a given value of $t \cdot \pi \cdot \mu \cdot \sigma \cdot a \cdot D$, the imaginary term in (5) is larger than the corresponding term in (6) by a factor of 3/2. In contrast with the results for the flux shunting mechanism, the long cylindrical shield provides somewhat better induced current shielding than the spherical shield.

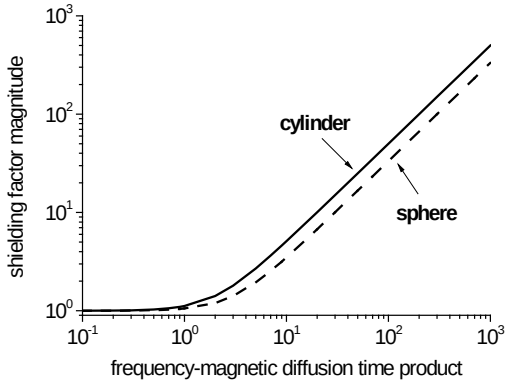

Figure 2.3.15 Shielding factor as a function of frequency-magnetic diffusion time product for a long cylinder shield and for a spherical shield.

2.3.2.3 Open pure conductive shields (flat shields)

Also in the case of pure conductive materials open shields are employed for large-scale screening or when an easy access to the region to be mitigated must be guaranteed. The shields usually take the form of thin sheets (of the order of millimetres or greater), possibly formed into a curved or partially closed shield. For these types of shield, the computation of the shielding effects requires the numerical solution of Maxwell equations.

The main parameters controlling the shielding efficiency are: the electrical conductivity of the material, the shield dimensions and thickness, the distance between source and shield, and the shield shape. A comprehensive analysis of their effect cannot be reported here.

Anyway some examples of their influence on the shielding performances of conductive shields are described in the following.

The analysis is developed by making reference to the same two-dimensional source, used for the ferromagnetic shields (lead-and-return conductor), but only with reference to the planar shield shown in Figure 2.3.8**Error! Reference source not found.**(a) (thickness D, electrical conductivity σ, width L)[8]. The shielding factor depends again on the position; the value is plotted along the y-axis (at $x = 0$) and along the x-axis (at $y = d + 0.5$, that is 0.5 m from the planar shield).

The electrical conductivity is an essential parameter for the effectiveness of the conductive shield.

As expected, the larger the conductivity, the larger the shielding factor will be. It is worth noting that, for the highest conductivity values, the best shielding factor is reached not in close proximity of the shield, but at a distance of some tens of centimetres (Figure 2.3.16). It must be noted also that, contrary to what happens with ferromagnetic materials, the *SF* does not drop at distances higher than the shield width.

In order to better understand the signification of these curves, the conductivities of the most common metals are listed in Table 2.3.2.

[8] Some information concerning U shaped shields can be found in section 5.3.4.2

Table 2.3.2 Conductivity of most common shielding materials (copper and aluminium are pure conductive materials).

Metal	Conductivity in MS/m
Copper	59
Aluminium	36
Iron	10
Steel	6
GO steel	2
Permalloy	1.8

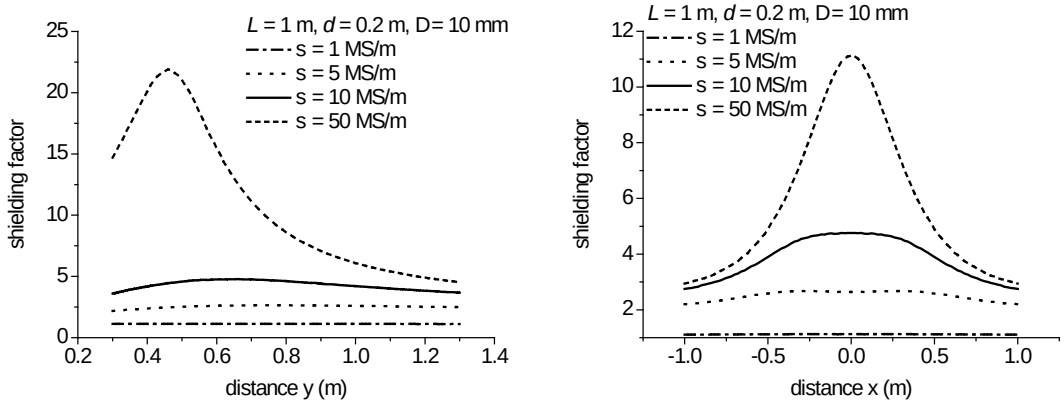

(a) (b)

Figure 2.3.16 *SF* for different electrical conductivities of the shield of Figure 2.3.8(a): (a) plot along *y* axis at $x = 0$, (b) plot along *x* axis at $y = 0.7$ m.

The influence of the shield width is very significant: increasing the value of L leads to an important increase of the shielding factor at distance. However the spatial distribution of the shielding factor is complicate and not always monotonic, as shown in Figure 2.3.17

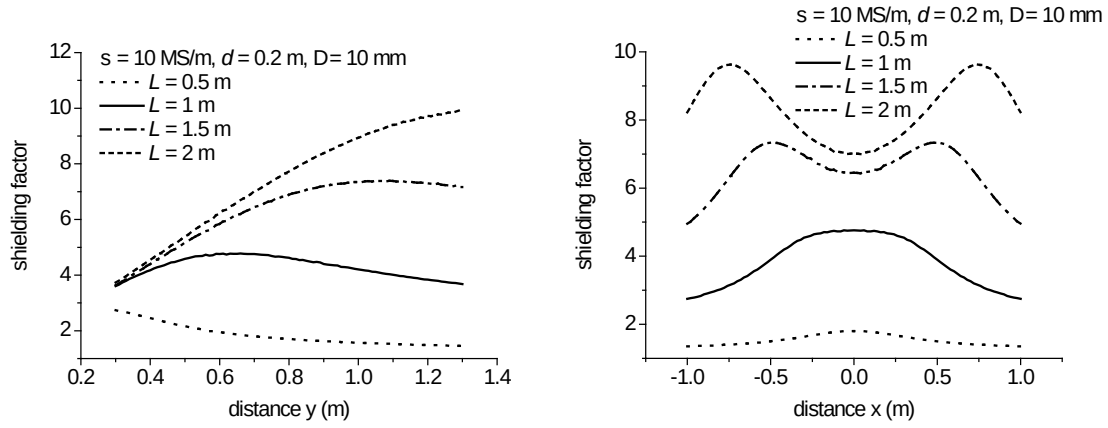

(a) (b)

Figure 2.3.17 *SF* for different widths of the shield of Figure 2.3.8(a); (a) plot along *y* axis at $x = 0$, (b) plot along *x* axis at $y = 0.7$ m.

The thickness of the shield is another important factor. The increase of thickness increases the intensity of eddy currents and consequently improves the shielding efficiency (Figure 2.3.18). However, at large distances from the shield, increasing the thickness above the skin depth fails to produce any significant improvement.

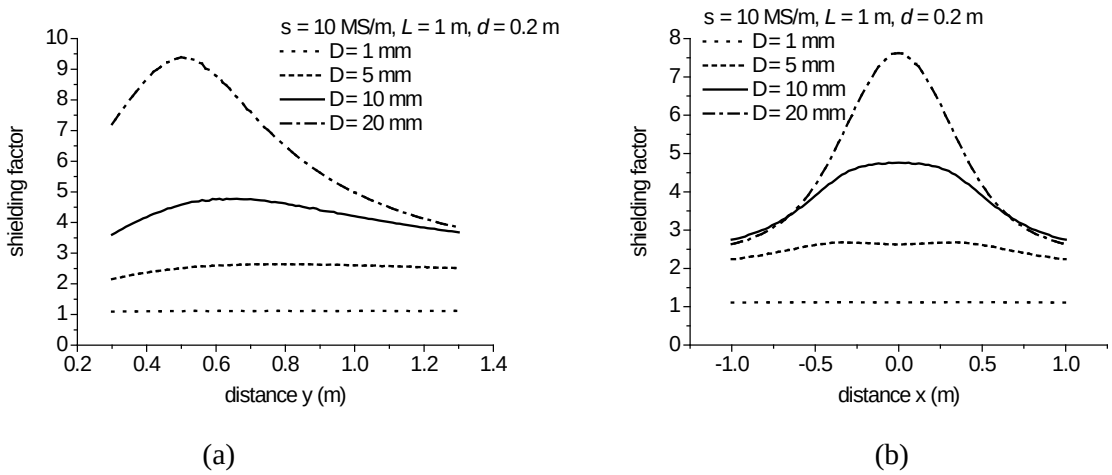

(a) (b)

Figure 2.3.18 *SF* for different thicknesses of the shield of Figure 2.3.8(a); (a) plot along *y* axis at $x = 0$, (b) plot along *x* axis at $y = 0.7$ m.

It is important to note that, contrary the effect with flat shields made of ferromagnetic materials, ***the shielding effectiveness of flat shields made of good conductive material does not reduce at distance from the shield greater than the shield width.***

A more straight evaluation of the influence of the shield features is given by using as parameter the product electrical conductivity by shield thickness, as both parameters have more or less the same influence on the shielding effectiveness (Figure 2.3.19).

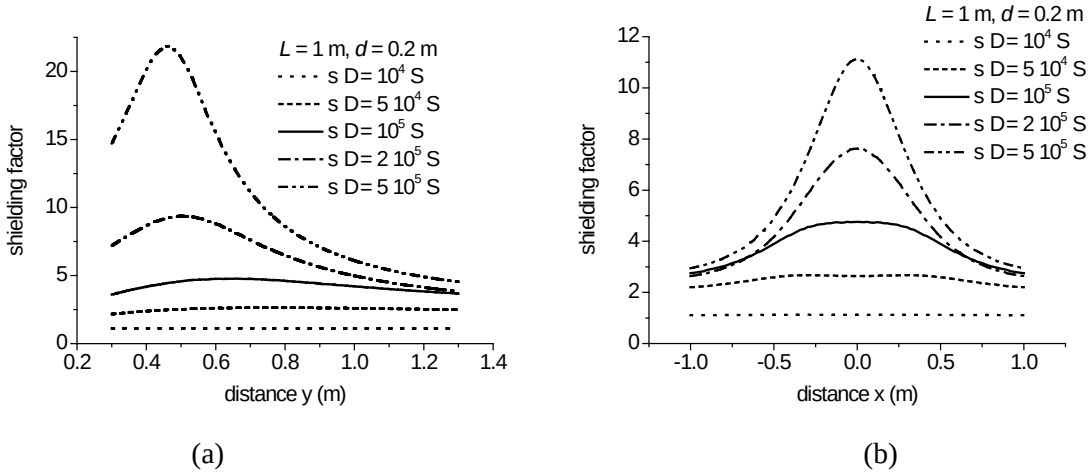

(a) (b)

Figure 2.3.19: *SF* for the shield of Figure 2.3.8(a) with different values of "conductivity x thickness"; (a) plot along y axis at $x = 0$, (b) plot along *x* axis at $y = 0.7$ m.

The distance *d* between source and shield does not noticeably influence the field beyond the shield in the area close to the conductive sheet; on the contrary, for locations far from the shield, the shielding effectiveness decreases with increasing distance *d* (Figure 2.3.20).

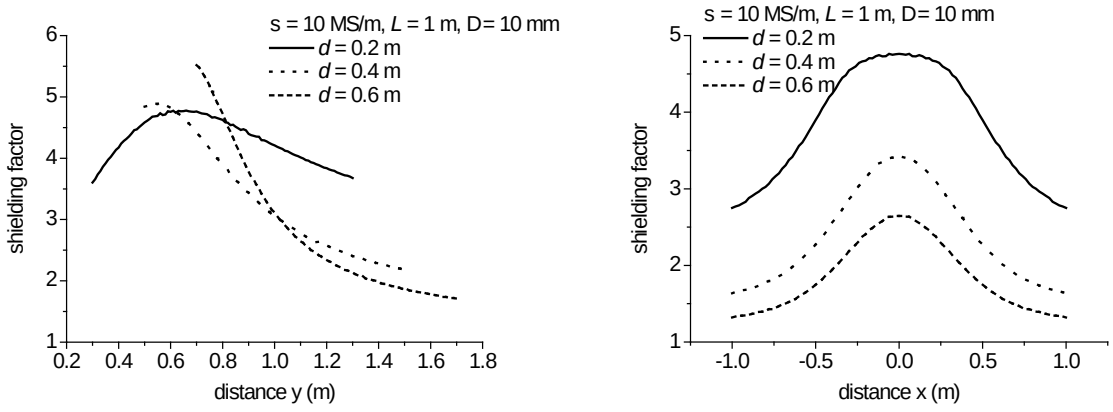

(a) (b)

Figure 2.3.20 SF for different source-shield distances of the shield of Figure 2.3.8(a); (a) plot along *y* axis at $x = 0$, (b) plot along *x* axis at a distance of 0.5 m from the shield (corresponding to $y = 0.7$ m, 0.9 m and 1.1 m respectively for $d = 0.2$ m, 0.4 m and 0.6 m).

2.3.3 Simultaneous effects of high permeability and conductivity

As shown in Section 2.3.1, a high permeability material can provide shielding through the flux shunting mechanism without any shielding effect by induced (eddy) currents. This is the situation in a dc field, or in an ac field if the material conductivity is too low for induced currents to significantly contribute to the shielding.

In the same way, as shown in Section 2.3.2, a conducting, non-ferromagnetic material can provide shielding through the induced current mechanism without any shielding by flux shunting.

This section describes shielding configurations that use materials that have both permeability μ larger than μ_o and electrical conductivity large enough for shielding by induced current to become significant. This is often the case for ferromagnetic material shielding an ac field.

Analytical descriptions of configurations that involve shielding materials that have both permeability $\mu > \mu_o$ and significant electrical conductivity σ are more complicated than those where only one shielding mechanism is involved. This is because the distribution of magnetic flux and induced currents are coupled to each other through a magnetic diffusion equation throughout the bulk of the shielding materials.

2.3.3.1 Closed metallic shields

Results from four such descriptions are provided here so as to generalize the results from the four descriptions in each of Sections 2.3.1.2 and 2.3.2.2. Again, analysis is carried out for both long cylindrical and spherical shields, and for both the uniform field imposed outside/shielded region inside and the dipole source inside/shielded region outside configurations.

As in Sections 2.3.1.2 and 2.3.2.2, the complex shielding factor in the models that are described here is uniform throughout the shielded region for each of the four cases; the uniform external field and the dipole source configurations are reciprocal, producing identical shielding factors for each geometry.

For a long cylindrical shield with permeability μ, conductivity σ , inner radius a and outer radius b in a sinusoidally varying field at angular frequency ω , the dependences upon radius of the fields within the shield involve first order modified Bessel functions depending on the skin depth d

Figure 2.3.21 shows, on log axes, the magnitude of the shielding factor that can be found in [5], as a function of shield conductivity σ for various values of shield relative permeability μ/μ_o, for a long cylindrical shield with inner radius a = 0.1 m, thickness D = 5 mm and source frequency $f = 50$ Hz. This figure makes apparent the relevance of the analyses of Sections 2.3.1.2 and 2.3.2.2, each of which involved only one shielding mechanism, to the description where both mechanisms are simultaneously present:

1) For values of conductivity s that are small enough that the effects of induced currents are negligible, only the flux shunting mechanism contributes to the shielding - the left end of each curve approaches the value of shielding factor that is given by (1) in Section 2.3.1.2 and is based only upon the shield dimensions and relative permeability.

2) The curve for $\mu / \mu_o = 1$, which describes a non-permeable conducting shield, has a dependence upon conductivity σ that agrees with the magnitude of the shielding factor given by (5) in Section 2.3.2.2 (shown as the upper dashed curve) for values of σ that are small enough that $d >> D$. However, when σ becomes large enough for the skin depth to be less than the shield thickness, the shielding factor magnitude increases more rapidly than is predicted by (5). In this regime (the right end of the $\mu / \mu_o = 1$ curve), induced currents and flux concentrate toward the surface of the shield that faces the source. The simpler analysis that leads to (5) assumes that, at any given angular position, the current density is uniformly distributed over the thickness of the shield, flowing in an axial direction on one side of the shield and returning in the opposite axial direction on the other side.

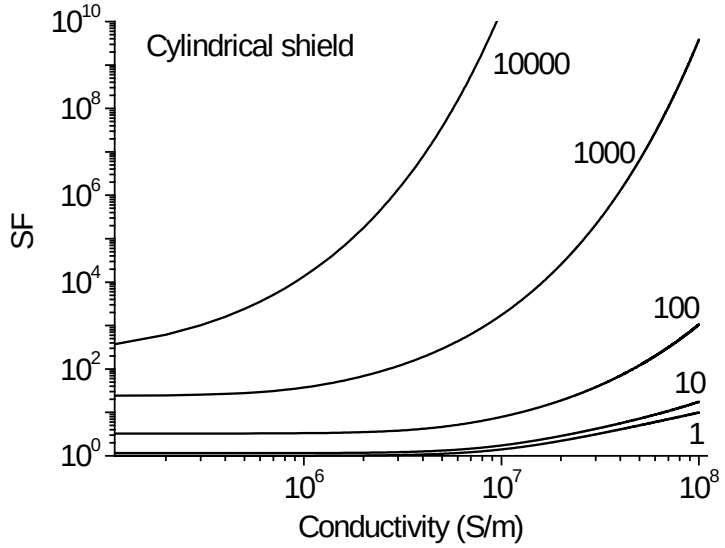

Figure 2.3.21 Shielding with simultaneous effects of permeability and conductivity for a long cylindrical shield. Shielding factor as a function of the electrical conductivity for different values of the relative magnetic permeability. Parameter values are: a = 0.1 m, D= 5 mm, f = 50 Hz[9].

For a spherical shield with permeability μ, conductivity σ, inner radius a and outer radius b in a sinusoidally varying field at angular frequency ω the dependences upon the radius of the fields within the shield involve complex hyperbolic functions depending again on the skin depth d.

Figure 2.3.22 shows, on log axes, the magnitude of the shielding factor, given in [5], as a function of shield conductivity σ, for various values of shield relative permeability μ / μ_o, for a spherical shield with inner radius a = 0.10 m, thickness Δ = 5.0 mm and source frequency f = 50 Hz. As for Figures 2.3.6**Error! Reference source not found.** and 2.3.15, the curves in Figure 2.3.21 and Figure 2.3.22, for long cylindrical and spherical shields, respectively, are quite similar but not identical. As was the case for Figure 2.3.21, the relevance of the analyses in Sections 2.3.1.2 and 2.3.2.2 is apparent in the regimes of Figure 2.3.22.

[9] These curves, initially computed at 60 Hz by J.F. Hoburg, have been redrawn at 50 Hz by A. Manzin.

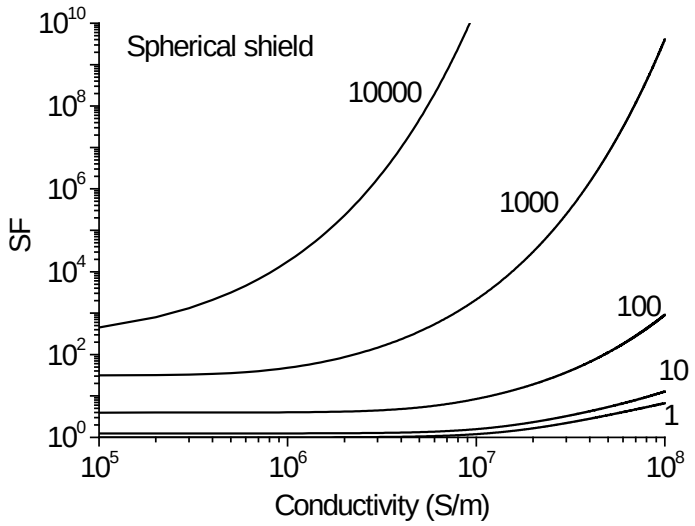

Figure 2.3.22 Shielding with simultaneous effects of permeability and conductivity for a sphere shield. Shielding factor as a function of the electrical conductivity for different values of the relative magnetic permeability. Parameter values are: a = 0.1 m, D= 5 mm, f = 50 Hz.

The examples in this section show that a material that has both permeability $\mu > \mu_o$ and conductivity σ can provide shielding in three separate regimes.

1) For values of conductivity that are too small for induced currents to be effective, the shielding is due only to flux shunting, and is the same as would occur with a dc source.
2) For values of conductivity that are large enough that induced currents circulating around the large scale dimensions of the shield contribute significantly to the shielding, but where the skin depth is large compared with the shield thickness, the shielding factor is increased (shielding is improved) from that due only to flux shunting, and can be analyzed on the basis of a description in which the circulating current is uniform over the shield thickness.
3) For values of conductivity that are large enough that the skin depth is less than the shield thickness, the shielding factor increases rapidly (shielding improves rapidly) with decreasing skin depth. Since the skin depth at a given frequency is determined by the product of conductivity and permeability, this regime occurs only for very high values of conductivity for a non-permeable material, but occurs at smaller values of conductivity with increasing permeability. This highly effective form of shielding can be analyzed only with a description in which the variation of circulating current density over the shield thickness is determined as part of the analysis.

2.3.3.2 Open metallic shields

The considerations that have been drawn for closed shields made of a material having both permeability $\mu > \mu_o$ and non zero conductivity σ cannot be entirely applied to the case of open shields. In particular, similar considerations can be made until the skin depth is large enough compared with the shield thickness: the presence of induced currents increases the shielding factor, so that the global shielding efficiency is improved. With the increase of the conductivity (or permeability) or with the increase of the frequency, when the flux penetration is not complete (skin depth lower than the shield thickness), the shielding efficiency is not monotonic. This effect can be explained when considering, in the case of open shield, that the additional shielding mechanism introduced by the presence of the electrical conductivity is mainly due to the appearance of an additional field source, which tends to contrast with that of the main one. The intensity of this additional source depends on the amplitude of the currents induced in the shield. If the flux penetration is reduced, also the induced currents tend to be limited, weakening the antagonist field. Also the

"magnetostatic" shielding effect is affected by the skin effect; in fact, an incomplete flux penetration reduces the cross sectional area of the shield, with a consequential increase of its reluctance.

As a consequence of the reduction of the skin depth, the shielding factor increases to a given limit and then reduces or remains almost constant. This behaviour can be observed from the results reported in Figures 2.3.22 and 2.3.24, making reference to a planar shield of side equal to 1 m, placed at a distance of 0.2 m from the source (see **Error! Reference source not found.**a). The electrical conductivity of the shield is fixed at 2 MS/m, while its relative permeability is varied from 1 to 50,000. Three values of the shield thickness are considered: 1 mm, 5 mm, 10 mm. The skin depths, at 50 Hz, are summarized in Table 2.3. The results plotted in the figures prove that when the skin depth becomes sensibly lower than the shield thickness, the SF reduces. In particular, the values of SF always increase with permeability when the shield thickness is small (1 mm), whilst non-monotonic behaviour is found with the increasing of the thickness. This is well evident from Figure 2.3.25, which reports the values of SF at point x = 0, y = 0.3 m.

Table 2.3.3 Skin depth for different values of relative permeability (with s = 2 MS/m and f = 50 Hz).

Relative permeability	Skin depth (mm)
1	50
100	5
1000	1.6
10000	0.5
50000	0.23

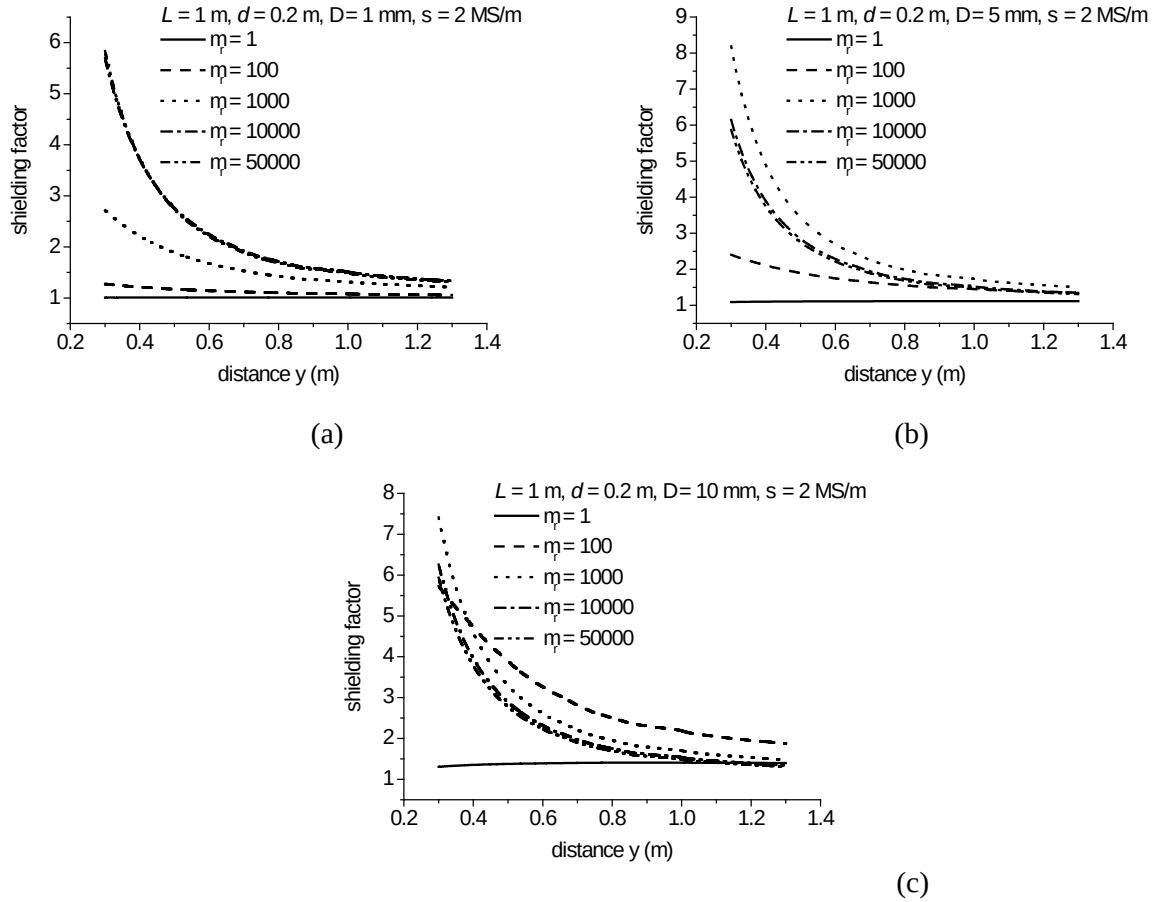

Figure 2.3.23 *SF* for planar metallic shields (Figure 2.3.8(a)) along the *y* axis at x = 0 for different values of the magnetic permeability: a) D= 1 mm, b) D= 5 mm, c) D= 10 mm.

These considerations are derived assuming a linear behaviour of the material (constant permeability). In the presence of non-linearities, the behaviour of the material can partially modify the results, particularly if local

saturations inside the shield appear. In these cases, taking into account the number of parameters affecting the global behaviour of the shield, it is not easy to deduce general considerations, and a specific analysis has to be performed for the considered case.

An example of the results obtained experimentally on commercial ferromagnetic materials are reported in Figure 2.3.26, which presents the shielding factors for flat and U-shaped shields composed of three different materials: 0.8 mm thick Low Carbon Steel sheet, 0.5 mm thick Non Oriented Fe-Si lamination, 0.3 mm Grain Oriented Fe-Si lamination in the rolling and transversal directions.

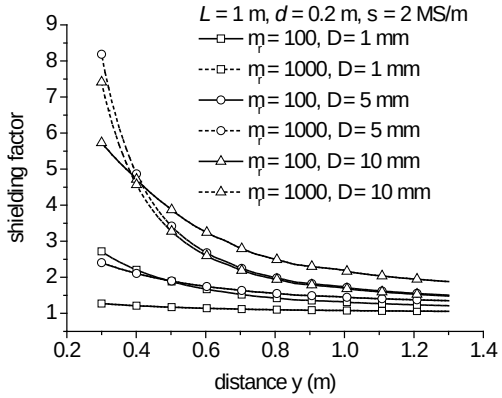

Figure 2.3.24 *SF* for planar metallic shields (Figure 2.3.8(a)) along the *y* axis at $x = 0$ for two values of the magnetic permeability (100 and 1000) and three values of the shield thickness D (1 mm, 5 mm, 10 mm).

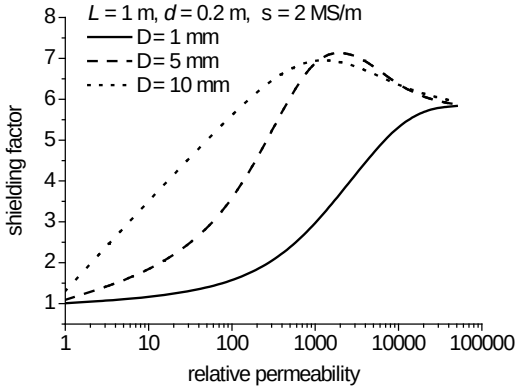

Figure 2.3.25 *SF* for planar metallic shields (Figure 2.3.8(a)) at $x = 0$, $y = 0.3$ m as a function of the relative permeability for three values of the shield thickness *D* (1 mm, 5 mm, 10 mm)

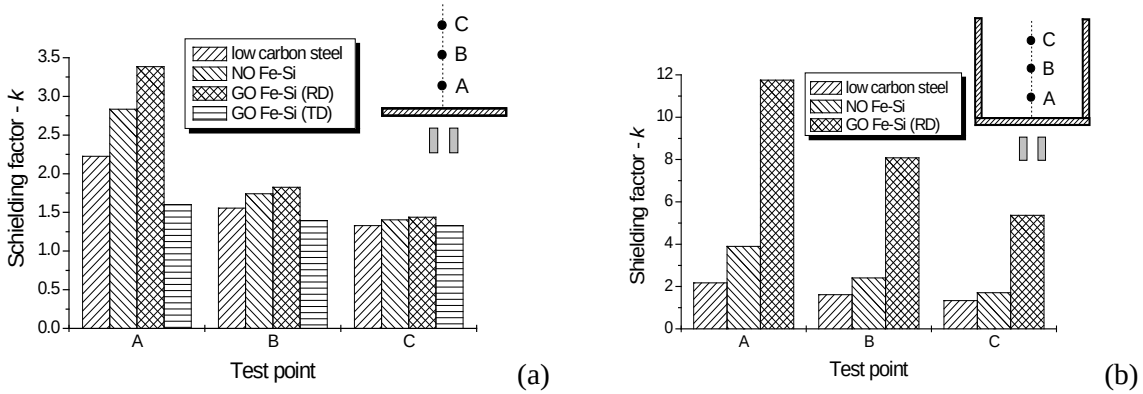

Figure 2.3.26 Shielding factor for some commercial magnetic laminations: plane (a) and U-shaped (b) configurations.

2.3.3.3 Multilayer shields

Since magnetic and conductive non-magnetic screens show complementary behaviours, a coupling between them can merge the advantages of both materials, improving the shielding efficiency. Thus multilayered shields, when composed of alternating high conductivity and high permeability materials, can provide enhanced shielding over shields composed of only a single layer [4, 10]. Multilayered shields are also required with Grain-Oriented ferromagnetic laminations, in order to provide an easy path for the differing magnetic fluxes directions.

In order to apply the principles that are described in this chapter, knowledge of material properties is essential. While electrical conductivities are relatively constant over a wide range of flux densities, permeabilities of ferromagnetic materials are generally nonlinear functions of the flux densities within the materials. Permeabilities at low flux densities (Rayleigh region) are typically one to two orders of magnitude smaller than those in the high permeability area that occurs at flux densities on the order of 0.01 - 0.1 T. At even higher flux densities (order of 1 T), ferromagnetic materials become saturated and permeabilities again become relatively small [6].

Setting aside the case of GO materials, the typical configuration of multilayered screens involves the coupling of a ferromagnetic lamination with a conductive sheet. Two layouts are possible: a) the ferromagnetic shield on the source-side with the conductive shield on the side of the protected area; b) the conductive sheet on the source-side with the ferromagnetic shield on the side of the protected area. A general comparative analysis between them becomes very complicate (or even impossible), because of the increased number of parameters controlling the multilayer shield behaviour; therefore a general rule cannot be stated. In addition to the geometrical and constitutive characteristics of each single shield, the distance between them seems to play in essential role in determining the shielding efficiency.

Examples for planar shields very close to each other:

- For single-phase systems parallel to the shield, configuration a) is found to be more efficient than b). It is important to note that in this case the addition of a third ferromagnetic layer (at the side of the area of interest) significantly reduces the shielding efficiency (“sandwich” configuration).
- For 3-phase systems parallel to the shield, the opposite conclusion is obtained.
- For a coil with the axis perpendicular to the shield the opposite conclusion is also obtained.

2.3.4 Corrosion

This chapter addresses the important question of the lifetime of metallic shields mainly when they are buried in the soil (shielding materials above ground can be easily controlled). However, this topic being very complex and not directly in the scope of the task force, it is not possible to go far into details and in particular to consider all the alloys that can be used.

2.3.4.1 Steel

Steel, with the exception of some specific alloys (stainless steel) that cannot be used for making magnetic shielding, is a material that will usually corrode quickly in the air and in the soil. Therefore it always requires a protective coating.

The most used coating is galvanization. It is also the most effective for long-term applications and mainly for structures buried in the soil because it offers also a protection against abrasion. Indeed, the three intermetallic layers that form during the galvanizing process are all harder than the substrate steel and have excellent abrasion resistance.

For buried structures, the needed thickness of the zinc protective coating highly depends on the soil characteristics. The properties of soil that have the most effect on the corrosion rate of zinc are aeration, moisture content (or time of wetness), pH, temperature, and resistivity:

- Aeration: favourable
- Moisture: unfavourable
- pH: basic is favourable, acid increases corrosion rate
- Resistivity: high soil resistivity is favourable

Figure 2.3.27 gives an idea of the effect of pH and resistivity (in W.cm) on the lifetime of buried steel.

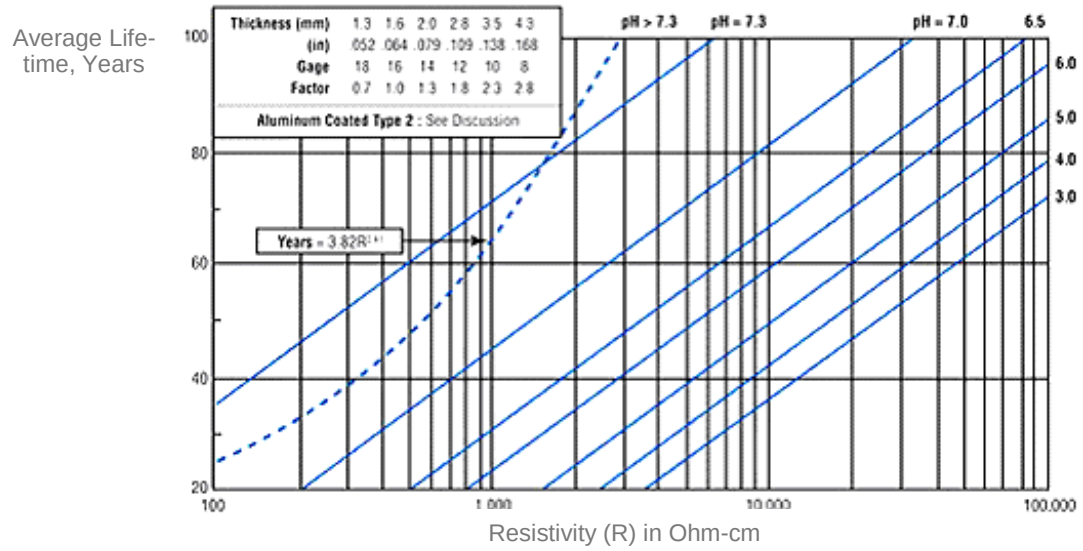

Figure 2.3.27 Average life-time against resistivity for galvanized steel buried in soil with the soil pH and the thickness of galvanization as parameters (National Corrugated Steel Pipe Association).

As the behaviour of galvanized steel in-ground is not as well understood as is the durability of these materials in above-ground applications, it is recommended to apply a zinc coating of at least 50 µm on any steel shielding intended to be buried in the ground.

2.3.4.2 Copper

Several factors can influence the corrosion of copper[10].

· **Corrosion by the soil**

Copper structures embedded in the soil (like water tubing) have an outstanding history of corrosion resistance in most underground environments. Copper does not naturally corrode in most clays, chalks, loams, sands, and gravels. Certain aggressive soil conditions, however, can cause it to corrode. The basic prerequisite for corrosion is the presence of appreciable amounts of moisture (bad drainage). Other factors that can facilitate the corrosion process include soils having: (1) elevated concentrations of sulfate, chloride, ammonia compounds, or sulfide; (2) poor aeration, which supports anaerobic bacteria activity; (3) large amounts of organic or inorganic acid; and (4) large oxygen or neutral-salt (especially chloride) differentials.

· **Galvanic corrosion**

Copper is normally cathodic to most commonly used underground metals and alloys such as steel, galvanized steels, and cast iron. Copper is however anodic to carbon, and corrosion could occur if cinders are used for backfill and contain appreciable amounts of carbon. It is also known that when copper is partially embedded in concrete and partially exposed to the soil, the embedded part will normally be cathodic to the other part, causing the deterioration of the latter in the immediate vicinity of the soil-concrete interface.

· **Corrosion due to DC stray currents**

Stray current corrosion or interference can occur on underground copper structures when uncontrolled direct currents exist in the area. This form of corrosion is related to the magnitude and direction of direct currents flowing in the earth through paths other than those intended. When stray currents flow onto the underground structure, no corrosion damage occurs because these areas are cathodically protected. These stray currents also cause no deterioration while they are flowing in and along the structure. However, the currents must eventually leave the structure, return to the earth, and flow to their source of generation. Areas where these currents leave the structure and enter the soil are anodic, and serious corrosion can occur at these locations.

[10] Edited version of an article which appeared in American Water Works Association Journal, August 1984 and is reprinted, with permission from American Water Works Association
www.copper.org/resources/properties/protection/underground.html

A common source of stray DC electricity is an impressed-current-type cathodic protection system such as those widely used by utilities and gas and oil transmission companies for the mitigation of corrosion on underground steel pipelines. Electric utility high-voltage direct-current (HVDC) transmission systems and DC-powered transit systems are also potential sources of stray direct current.

· **AC corrosion**

Copper can apparently be adversely affected by certain conditions in the AC system to which it might be grounded but the question remains very controversial. The widely use of copper for building earthing systems allows however to consider this risk as very low.

2.3.4.3 Aluminium

Like for copper, aluminium corrosion can be influenced by several factors[11].
Note that there are many different aluminium alloys; yet not all of them are suitable for shielding purposes, mainly when they are buried in the soil.

· **Corrosion by the soil**

Aluminium has a great affinity for oxygen but is also very quickly covered by a protective layer of oxide.
The main corrosion mechanism for aluminium occurs by puncture mainly in the presence of chloride (e.g. presence of salt). These punctures are usually superficial; yet, they can become locally severe (depending of the type of soil), tending to stabilise after 4 to 5 years. Their maximum depth seems to be about 1.8 mm after 7 years.

Generalised corrosion (important loss of weight) normally doesn't occur with aluminium alloys of high purity (> 99 %) that doesn't contain copper. The aluminium normally used for making shielding plates has a 99.5 % aluminium purity (1050A class).

This class of alloy is normally well resistant to corrosion if the ph of soil remain relatively neutral (3< ph < 9). One of the materials used for the controlled backfill (dolomite) is a double carbonate of calcium and magnesium. This material has normally a quite high pH and could affect the stability of the protective layer in presence of moisture. Practically, however, a natural coating of $Ca(AlO_2)_2$ appears, which is insoluble in water.

Taking this into consideration it can be concluded that buried aluminium plates will loose less than 100 µm thickness in 10 year and hence, that general corrosion will be avoided.

· **Galvanic corrosion**

Although aluminium in the soil will be partially protected by its hydroxide coating, it remains an electronegative metal that can be corroded in contact with more electropositive metals like steel and copper. Therefore it remains very important to avoid any contact with those materials.

· **Corrosion due to DC stray currents**

Aluminium corrosion by DC current is not well known and need apparently still to be evaluated (it seems that a cathodic protection would not be a solution for protecting aluminium from stray currents).

· **AC corrosion**

The risk of AC corrosion is very difficult to evaluate.
AC stray currents could involve, by local alcalinisation, dissolution of the natural protective coating. The current density threshold for starting an AC corrosion seems to be of about 70 µA / cm^2 .

Measurements performed on a short length of H shape shielding for a power cable, with no continuity between the plates, have shown current densities smaller than 1 µA/cm^2 . Computer simulations for a cable link with 1300 A in the conductors, in the absence of horizontal plates but with electrical continuity between vertical plates, have resulted in a equivalent current loss of about 60 µA/m or, taking into account the area of the plates, less than 7 nA/cm^2.

These results are quite reassuring but they are based on the hypothesis that the leakage currents are equally distributed on the surface of the plates. This statement, of course, is not always correct. This is one of the reasons why, in the H layout (see subchapter 5.3), it is advisable to hold a gap between vertical and horizontal plates and also why it is not advisable to protect the plates by a special coating which could have as result that the leakage currents concentrates on very small surfaces or on the edges of the plates.

[11] This section is based on a non-published study performed by CEBELCOR for the Belgian TSO, ELIA. Some of the references of this study are included in the references of this chapter.

2.3.5 Conclusions

Many geometrical and constitutive parameters concur together to determine the shielding efficiency of metallic shields, making arduous an exhaustive analysis of all the possible configurations. Thus, only general considerations on the influence of each single parameter can be deduced, as reported in the following conclusions, valid for all kinds of metallic shields.

Effect of shield shape

- Closed shields surrounding the area of interest are usually the most efficient, but they can mitigate the field only in a limited volume, which in addition becomes less accessible.
- Closed shields around the sources often provide lower mitigation, but their effect is extended to the whole surrounding space.
- Open shields using ferromagnetic materials are only effective in the vicinity of the shield.
- Open shields having a shape which partially encloses the area to be protected or the source, usually show higher shielding factor with respect to the planar ones but involve also more shielding material.

Effect of shield dimensions

- The increase of the shield thickness to reasonable limits improves the shielding efficiency, provided that its value does not greatly exceed the skin depth.
- In open shields also, the increase of the shield width increases the shielding factor.

Effect of magnetic permeability

- The larger the magnetic permeability, the larger the shielding factor will be. However, the permeability value depends not only on the material, but also on the operating conditions.
- Open shields usually work at low flux density, with corresponding reduced permeability values.
- Closed shields are usually operate with greater permeability values, but their performances can be significantly degraded by magnetic saturation and by the presence of air-gaps.
- At power frequency, the contribution to the shielding performances added by the electrical conductivity in popular ferromagnetic materials is generally not negligible.

Effect of electrical conductivity

- The greater the electrical conductivity, the greater the mitigation effect.
- Owing to the fact that the shielding mechanism is due to the induction of currents, the shielding effectiveness is highly dependent on the orientation of the field with respect to the source.
- In general the mitigation due to induced currents is lower near the shield, but it extends to the whole space whatever the shape of the shield is; on the contrary, open shields made of ferromagnetic materials exhibit high shielding factors in proximity of the shield, but their efficiency rapidly decreases with the increase of the distance.
- The use of multilayer shields composed of magnetic and conductive materials can provide very good solutions.

Effect of corrosion

- Copper is practically free of any corrosion problem except in case of dc stray currents.
- Aluminium is like copper but needs some more controlled conditions when buried in the soil.
- Steel needs always special protection measures against corrosion.

2.3.6 References

[1] H. A. Haus and J. R. Melcher - Electromagnetic Fields and Energy. - Englewood Cliffs, NI. Prentice Hall, 1989.

[2] M. Zahn - Electromagnetic Field Theory: A Problem Solving Approach - New York: Wiley, 1919.

[3] T. Rikitake. - Magnetic and Electromagnetic Shielding. - Tokyo: Terra, 1987.

[4] Handbook of Shielding Principles for Power System Magnetic Fields - EPRI, Electric Power Research Institute, Palo Alto, CA: Rep.- TR103630, vol. 2, sec. 2-3, 1994.

[5] J. R. Wait and D. A. Hill - Electromagnetic shielding of sources within a metal-cased bore hole - IEEE Trans. Geosci. Electron., vol. 15, pp. 108-112, Apr. 1977.

[6] R. M. Bozorth - Ferromagnetism Piscataway - NJ: IEEE Press, 1993.

[7] JF Hoburg - Principle of Quasistatic Magnetic Shielding with Cylindrical and Spherical Shields - IEEE Transaction on Electromagnetic Compatibility, Vol 37, No 4, pp. 574-579, November 1995.

[8] O. Bottauscio, M. Chiampi, A. Manzin - Numerical analysis of magnetic shielding efficiency of multilayered screens - IEEE Trans. Mag., Vol. 40, No. 2, pp. 726-729, 2004.

[9] O. Bottauscio, , M. Chiampi, D. Chiarabaglio, F. Fiorillo, L. Rocchino, M. Zucca - Role of magnetic materials in power frequency shielding: numerical analysis and experiments - IEE Proceedings Generat. Transm. and Distrib., Vol. 148, No. 2, 2001, pp. 104-110.

[10] O. Bottauscio, M. Chiampi, R. Conti, M. Repetto, M. Zucca - Some considerations about environmental ELF magnetic field reduction - EMC Europe, Tutorial Session No. 6, Brugge (Belgium), 11-15 Sept. 2000, pp. 112-121.

[11] O. Bottauscio, E. Carpaneto, M. Chiampi, D. Chiarabaglio, I. Panaitescu - Numerical and experimental evaluation of magnetic field generated by power busbar systems - IEE Proc.-Gener. Transm. Distrib., Vol. 143, n. 5, Sept. 1996, pp. 455-460.

[12] L. Hasselgren, J. Luomi - Geometrical Aspects of magnetic shielding at Extremely Low Frequencies - IEEE Transaction on Electromagnetic Compatibility, Vol 37, No 3, August 1995 pp. 409-420.

[13] D.O. Sprouts and M.E.J. Carlisle - Resistance of aluminium alliages to underground corrosion - Corrosion, vol 17, 125t, march 1961.

[14] W. French - Alternating current corrosion of aluminium - IEEE transactions on power apparatus and systems, vol 92, 1973, pp 2053-2062.

[15] Christian Vargel - Corrosion de l’aluminium - Dunod, ISBN: 2 10 004191 6, Paris 1999.

2.4 Impact of mitigation techniques on the operating conditions

When mitigation techniques are applied, modification to the operating conditions can result. This is due to the fact that the mitigation technique interacts with the magnetic field produced by the power installation and, hence, by reciprocity with the electrical parameters of the installation. The application of a particular mitigation technique, like a metallic shield, can also have some influence on the assembly and maintenance of the installation.

In this chapter, only the main parameters that could be addressed are shown; more details can be found in the respective subchapters of chapter 5 dealing with this particular topic.

2.4.1 Impact of conductor management

The techniques presented in subchapter 2.1 are normally applied to linear structures (overhead lines and underground cables), and their application may change the initial operating conditions of these installations. For example, compacting an overhead line reduces the inductances (series reactance) and increases the capacitances (shunt reactances) with, as result, that the line Surge Impedance Zc is reduced. If the surge impedance is reduced, the Surge Impedance Loading (SIL), which is equal to the line voltage squared divided by Zc, increases accordingly. The SIL is the value of power that may flow through the line with practically no interchange of reactive power with the system. According to [1] the typical increase in the SIL due to compaction increases by approximately 20 %; this means that line compaction not only reduces the EMF emission but also improves the theoretical power transfer capacity of the line.

On the other hand, as will be stated in section 5.1.5 and in [2], line compaction can have a negative impact on the audible noise and, to a lesser extend, on the radio interference level.

Concerning overhead lines maintenance, it is worth recalling that reducing the field at ground level, by reducing the phase-to-phase clearance, leads to an increase of the electric field in the vicinity of the conductors. This can have an influence on the work procedures for the labour force (e.g. painters, life-line workers) who have to climb on the towers. It is also well-known that compact lines, when they have a lower insulation level, exhibit a higher risk for outage.

In the same way that line compaction reduces the surge impedance, rearranging the phases of a two-circuit line in order to obtain the low reactance configuration leads also to circuits having a lower surge impedance and, hence to an improvement of the SIL of each circuit. Here again, the EMF mitigation method has a positive impact on the line operating conditions.

In relation to underground cables, reducing the phase-to-phase distance has a positive influence on the field level but a negative impact on the thermal behaviour and, hence, on the ampacity. Moreover the mechanical strengths in the case of a short circuit is higher where there is a short distance between phases. This is particularly the case with EHV cables (e.g. 400 kV) where placing the cables close together is not always possible.

2.4.2 Impact of compensation loops

In the case of overhead lines or underground cables, passive or active loops are not symmetrically coupled with each of the phase conductors. Hence they introduce an asymmetry in the field configuration and in the line parameters. This can create some unbalance in the line current, more important as the mitigation section increases. Moreover, in the case of passive loops, there is an increase in line losses, due to the current in the passive loop (see subchapter 5.1 for more details).

2.4.3 Impact of shielding by metallic materials

In subchapter 2.3 the technique of shielding by metallic materials (both high conductivity and ferromagnetic) was presented.

In relation to high conductivity materials, the temperature rise of conductive shields when installed very close to the source can affect the power rating of the electrical installation. For example, the installation of aluminium shielding close to power cables can reduce the heat dissipation and consequently the ampacity of the link. Although this fact is generally not important, it occasionally needs to be taken into account for calculating the energy transfer of the link or simply for assessing the cost of the losses. Other effects like the variation of the line impedance can generally be neglected.

Regarding the maintenance and the outage risks, shielding by metallic plates can be considered as an extra protection against mechanical aggressions (third party damages).

The same comments applicable to conductive shielding basically are also valid to ferromagnetic shields. It should be pointed out however, that the losses are usually lower in this latter method of shielding and hence, also, the possible impact on the ampacity. On the other hand, if the ferromagnetic shielding (pipe, raceway, etc) constitutes a greater protection against mechanical aggression than conductive shielding, they are themselves usually more difficult to repair in the case of a cable fault.

Finally, it should be pointed out that the interaction between source and shield, can sometimes lead to mechanical stresses (in case of short circuit) and vibration (under normal operating conditions).

2.4.4 References

[1] Increasing the transmission capacity of overhead lines – High Surge Impedance Loading Technique - O. Regis Jr on behalf of CIGRE WG B2.06 Electra 221 – August 2005

[2] The influence of line configuration on environment impacts of electrical origin - Cigré WG B2.06 Technical Brochure No 278 – August 2005.

3 METHODS TO ASSESS FIELD MITIGATION

In order to elaborate a mitigation design, it is important to have tools that can predict the magnetic field from a given source – or set of sources – before and after the planned mitigation operation. In this chapter, these resources are presented and are comprised by the following methods: analytical, numerical, optimization and experimental.

3.1 Analytical methods

Analytical methods are based on computation of the Biot-Savart formula or on the evaluation of a closed form solution of Maxwell equations, providing analytical expressions that explicitly include all the parameters that control the field distribution and intensity. These methods are often useful in cases in which the geometry of the problem has high symmetry or simplicity.

Their advantage is to provide immediate evaluations of the field quantities, given the geometrical and constitutive data of the domain under study and the features of the field sources. As a drawback, analytical methods are restricted to very simple geometrical configurations, with high degree of symmetry and in presence of material with linear behaviour. In practice, they can be applied mainly to two-dimensional problems when the shape of the domain under study can be easily represented by analytical formulae. In addition, they are not suitable to deal with nonlinearities, as the ones introduced by magnetic material behaviour.

To compute some of the long or cumbersome expressions involved in analytical methods, it can be helpful to use symbolic manipulation programs such as MATHEMATICA and MAPLE [1].

3.1.1 Biot-Savart formula

The magnetic field generated by the current flowing in conductors can be computed by the Biot-Savart formula, in absence of ferromagnetic materials in the surrounding region and assuming that electromagnetic effects (electromotive forces, eddy currents, displacement currents, etc.) can be neglected. In chapter 1 simple formulas were given for calculating the magnetic field produced by straight wires. These formulae can be generalised to wires having arbitrary shapes.

Biot-Savart formula (current based)

This formula allows computing the field due to a very thin wire of arbitrary shape. An infinitesimal wire segment is selected, with length *dl* and supplied by a current *I*,

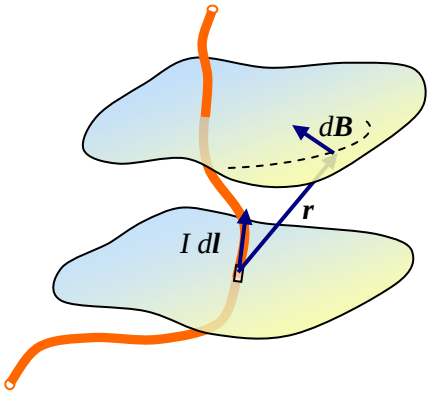

$$d\mathbf{B}(x,y,z) = \frac{\mu_o}{4\pi}\frac{I\, d\mathbf{l}' \times \mathbf{r}}{|\mathbf{r}|^3} \qquad (3.1.1)$$

$$d\mathbf{H}(x,y,z) = \frac{d\mathbf{B}}{\mu_o} \qquad (3.1.2)$$

Figure 3.1.1 The magnetic field from a segment of a current-carrying wire of arbitrary shape.

creates in the air a magnetic flux density *dB* and a magnetic field strength *dH*, where *r* is the distance between element *dl* and the point where *dB* is evaluated. By integrating along the whole conductor, vectors *B*(*x*, *y*, *z*) and *H*(*x*, *y*, *z*) are obtained.

It is also possible to compute the field from a distributed current inside conductors that have non-zero thickness. The procedure is to integrate infinitesimal contributions throughout the full conductor. Here the current density is used.

Biot-Savart formula (current-density based)

Considering a given volume *V*, where a known current density ***J*** is flowing, the magnetic field strength ***H*** in a generic point P is given by the following integral

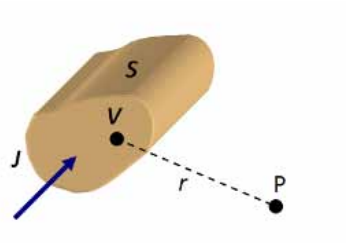

Figure 3.1.2 Evaluation of the field from a volumetric conductive element

$$\boldsymbol{H}(P) = \int_V \boldsymbol{J} \times \nabla\gamma \, dv \tag{3.1.3}$$

where γ is the Green's function given by

$$\gamma = 1/4\pi r \tag{3.1.4}$$

and *r* represents the distance between the source point and the point of evaluation.

The Biot-Savart formula cannot be employed for the evaluation of the magnetic field in presence of shielding materials. However, it is a useful tool for the quick evaluation of the magnetic field from various sources (e.g. three-phase cables, coils).

3.1.2 Solutions by Maxwell equations

The use of analytical methods in presence of shielding elements requires the direct solution of the Maxwell equations (see chapter 1). The analytical form of the solution depends on the geometry under analysis [2, 3], and can be derived using the method of separation of variables or the method of conformal mapping. In the following frames, the analytical solutions for a cylindrical shield, and an infinite and finite plane shields are presented

Cylindrical shield

An infinite cylinder (along *z* direction) is placed inside a uniform magnetic field strength $\boldsymbol{H}_e$ of pulsation ω. The internal and external radius are indicated respectively with *a* and *b*. The shield has thickness *t*, with relative permeability μ_r and electrical conductivity σ. The field $\boldsymbol{H}_i$ in the region inside the shield is given by:

$$\boldsymbol{H}_i = 2\frac{T_{11}T_{22} - T_{12}T_{21}}{T_{11} + T_{22} - (T_{12} + T_{21})}\boldsymbol{H}_e \tag{3.1.5}$$

where,

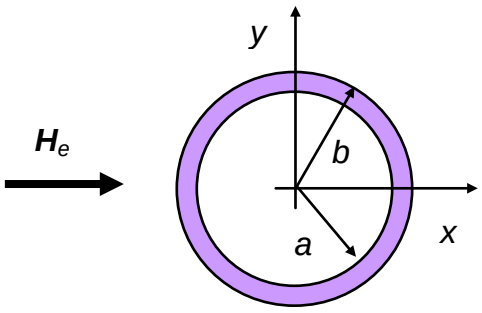

Figure 3.1.3 2-D shield with cylindrical shape.

$$T_{11} = (\gamma b)\left[K_1(\gamma b)I'_1(\gamma a) - K'_1(\gamma a)I_1(\gamma b)\right] \tag{3.1.6}$$

$$T_{12} = \frac{1}{\mu_r}(\gamma b)^2\left[K'_1(\gamma a)I'_1(\gamma b) - K'_1(\gamma b)I'_1(\gamma a)\right] \tag{3.1.7}$$

$$T_{21} = \frac{1}{\mu_r}\frac{\gamma b}{\gamma a}\left[K_1(\gamma b)I_1(\gamma a) - K_1(\gamma a)I_1(\gamma b)\right] \tag{3.1.8}$$

$$T_{21} = \frac{(\gamma b)^2}{\gamma a}\left[K_1(\gamma a)I'_1(\gamma b) - K'_1(\gamma b)I_1(\gamma a)\right] \tag{3.1.9}$$

and $\gamma = \sqrt{j\omega\mu_0\mu_r\sigma}$

In the previous expressions, *j* is the imaginary units, I_1 and I'_1 are the modified Bessel function of first order and first kind and its derivative, and K_1 and K'_1 are the modified Bessel function of first order and second kind and its derivative.

Due to the nature of Maxwell equations some other two-dimensional closed shields are also possible to solve. However any shape different from the circular, presented above, will encounter extreme difficulties. Another solvable case is an open shield that is infinite in two directions.

Infinite plane shield

The shield is supposed to be constituted by a sheet, infinite along *x* and *z* directions. The sheet has a thickness *t*, with relative permeability μ_r and electrical conductivity σ. The field sources, having pulsation ω, are constituted by *M* conductors; the generic conductor *m* (*m* = 1,..., *M*) is placed at the point (x_m, y_m) and a current I_m flows through it . The Cartesian components of the magnetic flux density in the region over the shield are expressed by:

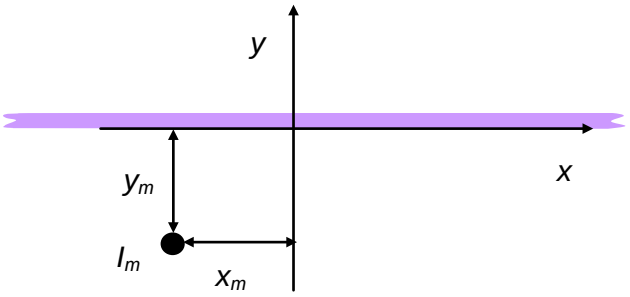

Figure 3.1.4 2-D shield infinite in the x and z axis.

$$B_x = -\frac{4W}{F}\int_0^{+\infty}\sum_{m=1}^{M}\frac{\mu_0 I_m}{2\pi}\times e^{-k(y-t-y_m)}\times\cos k(x-x_m)\,dk \qquad (3.1.10)$$

$$B_y = \frac{4W}{F}\int_0^{+\infty}\sum_{m=1}^{M}\frac{\mu_0 I_m}{2\pi}\times e^{-k(y-t-y_m)}\times\sin k(x-x_m)\,dk \qquad (3.1.11)$$

where $W = \dfrac{\mu_r k}{\sqrt{k^2 + j\omega\mu_0\mu_r\sigma}}$ (3.1.12), $F = (1+W)^2\times e^{kt} - (1-W)^2\times e^{-kt}$ (3.1.13) .and *j* is the imaginary unit.

Semi-infinite or finite open shields are also possible to solve analytically, yet, as shown below, this is achievable only if very ideal conditions are allowed.

Finite plane shield

The shield is supposed to be constituted by a sheet of width 2*L*, infinite along *z* direction. The sheet has a negligible thickness and ideal electromagnetic properties, so that two limit conditions are considered

- *PEC* (*perfect electric conductor*), having infinite electrical conductivity and permeability of the air
- *PMC* (*perfect magnetic conductor*), having infinite magnetic permeability and electrical conductivity equal to zero

The field source, having pulsation ω, comprises a conductor, placed at the point (x_0, y_0) with a current *I*. The Cartesian components of the magnetic field strength are given by

$$H_x = -\,\mathrm{Im}(\acute{A}) \qquad (3.1.14)$$

$$H_y = -\,\mathrm{Re}(\acute{A}) \qquad (3.1.15)$$

where

$$\acute{A} = -\frac{I}{2\pi}\left[\frac{1}{(t-t_0)} + \frac{1}{(t-t_0^*)} - \frac{1}{(t-j)} - \frac{1}{(t+j)}\right]\frac{(1+t^2)^2}{4lt}$$

for *PMC* (3.1.16)

$$\acute{A} = -\frac{I}{2\pi}\left[\frac{1}{(t-t_0)} - \frac{1}{(t-t_0^*)} - \frac{1}{(t-j)} + \frac{1}{(t+j)}\right]\frac{(1+t^2)^2}{4lt}$$

for *PEC* (3.1.17)

with *j* the imaginary unit,

$$t = \sqrt{\frac{L-(x+jy)}{L+(x+jy)}}$$

$$t_0 = \sqrt{\frac{L-(x_0+jy_0)}{L+(x_0+jy_0)}}$$

and t_0^* is the complex conjugate of t_0 .

By applying superposition, the proposed method is applicable to the presence of more sources.

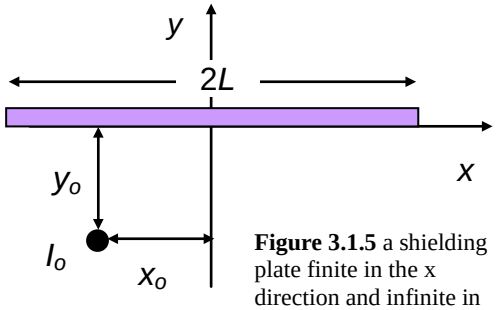

Figure 3.1.5 a shielding plate finite in the x direction and infinite in the z direction.

These examples have been used to produce the field distribution for pure conductive and pure ferromagnetic closed shields in chapter 2. The complexity of these analytical computations does not allow realistic assumptions to obtain practical shielding results.

3.2 Numerical methods

For the design of mitigation techniques, when analytical solutions are not available, numerical methods can be very helpful for the evaluation of the electromagnetic field quantities.

Computational methods are used as an alternative or combined approach, with respect to measurements, to evaluate the electromagnetic fields generated by the sources and the efficiency of mitigation techniques. The computational methods in electromagnetism are based on the solution of the Maxwell equations in their complete form or in a reduced form when simplifying assumptions can be introduced. This can be done by either analytical or numerical approaches.

The numerical solution of Maxwell equations is usually performed, in the area of physic and engineering, by different alternative methods. The most used techniques can be generically subdivided into volume methods (e.g. based on variational formulations), boundary methods (based on integral formulations) and hybrid methods. Volume methods are based on the discretisation of the entire domain under analysis and can be applied to strongly non-homogeneous domains. In boundary methods, the space is divided into linear, homogeneous and isotropic domains, the boundaries of which are discretized by surface elements. The hybrid methods are obtained by coupling the two approaches. Depending on the method, this can entail problems with infinite domains. The most common numerical techniques employed in electromagnetism can be so summarized:

- *Volume-element methods:*
  - Ø Finite Element method (FEM)
  - Ø Finite Difference method (FDM) and Finite Difference Time Domain method (FDTD)
- *Integral methods*:
  - Ø Integral equations (IE)
  - Ø Boundary Element Method (BEM)
  - Ø Method of Moment (MOM)
  - Ø Impedance method (IM)
- *Hybrid methods*:
  - Ø Finite Element – Boundary Element method (FEM-BEM)
  - Ø Finite Element – Boundary Element – Analytical (for thin-structures)

These numerical techniques are employed to solve the electromagnetic field equations in two-dimensional (2D) or three-dimensional (3D) domains, taking into account the actual geometrical structures and physical characteristics of the considered materials, as well as the features of the field sources (e.g. currents, charges, voltages). They are commonly used in research and technical activities for field calculations.

Basically, all the mentioned methods require a pre-processing phase, a solving phase and a post-processing phase. The pre-processing phase consists in:

- definition and discretisation of the problem geometry
- input of the physical characteristics of the materials
- input of the field source features

The solving phase consists in the definition and solution of the algebraic system of equations that can be derived following the considered technique. This phase is the most consuming with respect to the CPU time, depending on the complexity of the problem (e.g. 2D, 3D), giving rise to computational times ranging from some seconds up to several days on professional workstations. The post-processing phase allows the evaluation of the numerical results under different forms:

- local values of field quantities (electric field E, magnetic field strength H, magnetic flux density B, current density J)
- field lines of field quantities (E, H, B, J), showing the field orientation and distribution
- chromatic maps of the magnitude field quantities (E, H, B, J), showing possible critical points
- integral quantities (e.g. magnetic fluxes, currents, losses)

Even if numerical methods are powerful tools, they should be used with caution in order to avoid errors due to incorrect applications of the methodology. This calls for preliminary evaluations of the reliability of the numerical results, by comparison with other outcomes, obtained by experiments of by analytical methods in the case of simple problems.

The choice of the numerical method is determined by the characteristic of the problem to be studied and by a compromise between required accuracy, computational efficiency and memory requirements. The main features of the different numerical techniques for electromagnetic field solution, together with their merits and drawbacks are listed in the following.

3.2.1 Finite Element Method (FEM)

The finite element method is based on the solution of Maxwell equations in their differential form. This method is without doubt the most popular one in many fields of applications, from electromagnetism to mechanics and fluid dynamics.

The method is based on the approximation of the solution by means of the superposition of reconstructors (shape functions) having a simple analytical expression. By approximating the exact solution with a superposition of simple analytical functions, the differential operators can be computed explicitly, leading to the definition of algebraic matrix equations. In order to apply this approach, FEM requires the subdivision of the domain into a volume mesh, obtained by using different kind of elements (tetrahedra, hexahedra or cuboids for 3D problems or triangles or quadrangles for 2D problems). The reconstructors are usually associated with the nodes of the mesh. The use of such volume elements leads to an easy adaptability of the method to modelling complex shapes and to impose boundary conditions.

The matrix equations generated by FEM are largely sparse[12], allowing the use of optimized algorithms for their storage and solution. An important class of finite element methods is the so-called “edge element” of “facet element” method, which are based on the use of reconstructors that are assigned to the edges or to the face of the volume elements. These variants are particularly helpful for the solutions of 3D problems.

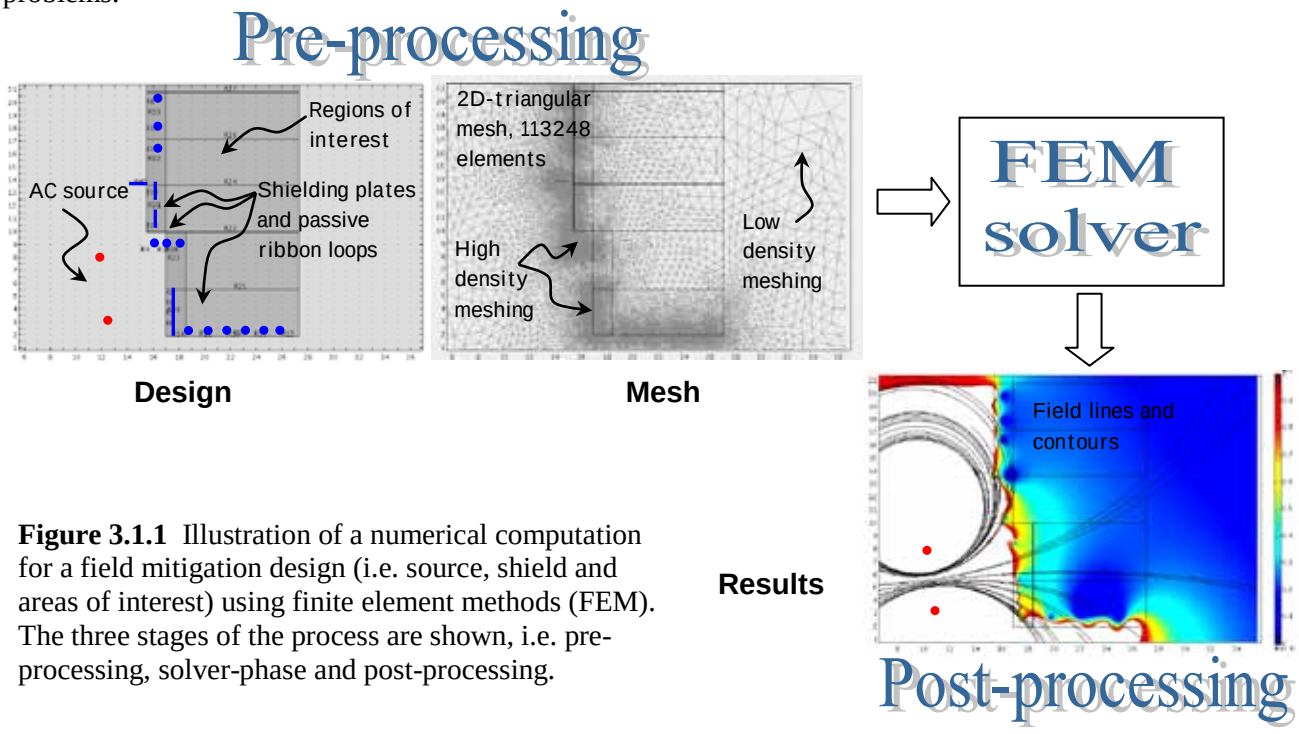

Figure 3.1.1 Illustration of a numerical computation for a field mitigation design (i.e. source, shield and areas of interest) using finite element methods (FEM). The three stages of the process are shown, i.e. pre-processing, solver-phase and post-processing.

FEM requires a finite domain, while the magnetic field is usually defined on an open space [4, 5]. In order to avoid inaccuracies introduced by the finite boundaries, the domain under study has to be significantly amplified, strongly increasing the computational burden. However, transformation techniques can be used to transform an infinite domain into a finite one.

[12] A sparse matrix is a matrix populated mainly by zeros. Sparse data is usually easily compressed and as a result memory usage can be significantly reduced.

3.2.2 Finite Difference Method (FDM)

The finite difference method is also based on the solution of Maxwell equations in their differential form. This approach starts from the approximation of the spatial derivatives with finite increments, leading to an algebraic system of equations where the unknown are usually the values of the electromagnetic quantity on the nodes of the mesh. It requires the subdivision of the volume into a regular mesh (usually parallelepipeds), which constitutes a severe restriction to the modelling of complex shapes and to the imposition of boundary conditions.

3.2.3 Finite Difference Time Domain (FDTD)

Although the finite difference approach can also be applied in the frequency domain, the Finite-Difference Time-Domain method is much more popular [6]. Maxwell's equations are directly discretized in space as well as in time on a staggered Yee-grid[13]. The solution is directly computed in the time domain in explicit time steps, whereby the field strengths in the computational space are set to zero at the beginning. This means that FDTD does not involve the solution of a matrix equation. Since the entire volume must be divided into cells, the number of unknowns is very large. However, unlike other formulations, the computational effort grows only linearly with the number of unknowns and the number of cells. It is used in some low-frequency applications (e.g. transients). Yet, FDTD most extensive use is at high frequencies (e.g. microwaves).

3.2.4 Integral Equations (IE) and Boundary Element Method (BEM)

The solution of integral equations is a powerful tool for the analysis of electromagnetic-field problems. A frequently used type of IE for scattering problems starts with Maxwell's equations and derive an integral expression for the electric field (EFIE) or the magnetic field (MFIE) via Green's functions.

There exist several direct and iterative algorithms for the solution of IEs. The most popular method is the method of moments (MoM) described by Harrington in the mid 60's. Similar approaches are known under the titles method of weighted residuals, method of projection, Galerkin method, and point matching method, Boundary Element Method (BEM) etc. Today, several computer codes based on MoM are commercially available.

In the case of Integral Methods, most of the computational time is required to compute the terms of the algebraic matrix that is usually fully populated. These matrix equations were originally solved by direct methods. Later iterative methods such as the conjugate gradient method or the most efficient GMRES method were also used to speed up the solution process of large systems.

IE methods are preferably applied for "open" problems, such as scattering problems including radiation in the free space. The application is restricted to models that can be described by homogeneous subregions with known Green's functions. The computational effort is roughly proportional to N^3, with N equal to the number of unknowns; consequently the problem size grows very fast.

3.2.5 Hybrid Finite Element-Boundary Element Method (FEM-BEM)

This method is based on a hybrid formulation, coupling the variational and integral approaches. The domain under study is divided into sub-domains that are treated by FEM or BEM formulations. The two sets of equations are coupled through the interfaces by imposing suitable continuity conditions. The advantage of this method is to put together the advantage of FEM in treating strongly non-homogeneous volumes with the advantage BEM to handle open boundary domains. As a drawback, this method is quite complex and some numerical instabilities can arise under particular conditions.

3.2.6 Hybrid Finite Element-Boundary Element (for thin-structures)

Due to the necessity of handling domains where the aspect ration between transversal dimensions is very high (a screen for shielding purposes can have transversal dimensions of some meters and thickness of few millimeters), specific mixed formulations have been developed and proposed in the scientific literature [7]. An important approach is constituted by the so-called "Thin-shield approximation", where the

[13] Kane Yee, in 1966, proposed staggering the vector components of E and H about cubic cells of a computational grid in such a way that each E-field is located midway between a H-field vector component and conversely. This scheme is very robust and solves several complications in FDTD formulations.

electromagnetic phenomena arising inside the shielding element are handled by an analytical approach, leading to a 2D finite element formulation on the shield plane. The shields and the sources are then coupled together by a 3D boundary element formulation.

3.2.7 Comments on numerical methods

A mitigation design problem can be characterized by sources, shielding structures and regions of interest. Once the sources are determined, the assessment of the field produced by them can be often determined by analytical methods, since no materials are usually involved at this stage. This analysis will suggest what type of mitigation technique can be used, as well as what structure and possibly which shielding materials could be used (see also chapter 4). Yet, to obtain the details of the mitigation design, it is often important to be able to predict the outcome of the interaction between the source field and the mitigation structure. The methods developed in this section are able to compute this interaction and, therefore, accomplish a mitigation design. Moreover, this design can be changed –in the computer– and new predictions can be obtained, therefore parametric tests and parametric designs are also possible.

It can be observed that there are advantages and disadvantages for each of these methods; therefore the designer has to make the most adequate choice according to the characteristics of the particular mitigation requirements. The way the problem is placed in the program is also important and is always most convenient to try to use approximations or search for symmetries of the shielding structure, such that 2D-simulations –instead of 3D– could be used.

FEM is the most used method for computations of mitigation designs at power frequencies. Several codes based on FEM and the other methods described in this section (e.g. FDM, MoM, FDTD, BEM) are commercially available. On the other hand, several research organizations have developed their own numerical codes for solving electromagnetic problems. Although they may neither be as versatile as commercial codes, nor completely user friendly, some of them can be obtained free of charge. There is also the possibility of solving a specific mitigation problem as cooperation between the code developer and the mitigation designer, especially if the problem has academic interest.

Recently, more elaborated numerical techniques have emerged, mostly related to optimization methods applied to field mitigation. Some of these include neural networks, shape-optimization and genetic algorithms [8], [9]. It is expected further development of these techniques to reach high precision in mitigation designs. Some of these techniques may include economical cost as a parameter of the optimization procedure [10].

3.2.8 References

[1] John H. Davis, *Differential Equations with Maple an Interactive Approach*, Birkhauser, 2000.

[2] Yaping Du, Cheng T C and Farag A S, *Principles of power-frequency magnetic field shielding with flat sheets in a source of long conductor.* IEEE Transactions on EMC, vol.38, No.3, August 1996.

[3] Olsen G and Moreno P, *Some observations about shielding of extremely LF magnetic fields by finite width shields,* IEEE Transactions on EMC, vol.38, No.3, August 1996.

[4] Anders Bondeson, Thomas Rylander and Per Ingelström, *Computational Electromagnetics*, Springer, 2005.

[5] Wassef K, Varadan V.V., Varadan V.K. Magnetic field shielding concepts for power transmission lines, IEEE Trans. on Magnetics, vol. 34, no. 3, pp. 649-654, may 1998.

[6] Allen Taflove and Susan C. Hagness, *Computational Electrodynamics: The Finite-Difference Time-Domain Method*, third edition, Artech House Publishers, 2005.

[7] Bottauscio O, Chiampi M, Conti R, Repetto M, Zucca M, *Some considerations about environmental Elf magnetic field reduction*, EMC Brugge 2000.

[8] Y.Q. Liu, P. Sousa Jr., E. Salinas, P. Cruz, J. Daalder, *"Continuum gradient based shape optimization of conducting shields for power frequency magnetic field mitigation"*, IEEE Transactions on Magnetics, vol. 42, no. 4, pp. 1215-1218, Apr. 2006.

[9] Celozzi S and Garzia F, *Active shielding for power-frequency magnetic field reduction using genetic algorithms optimization,* IEEE Proc-Sc. Meas. Technol, Vol.151, No1, January 2004.

[10] P. Cruz, C. Izquierdo and M. Burgos, *Optimal Design of active Shielding for Power Lines*, Proceedings 14th PSCC, Sevilla 2002, Session 24, Paper 2, p1-7.

3.3 Experimental

Experimentation within magnetic field mitigation techniques is related to the need of assessing a new idea or a concept. Often it can also be associated with testing a known technique where a solution to a mitigation problem is obtained from a set of parameters which need to be evaluated.

In the past, experimental testing required preliminary estimations and rigorous procedures had to be planned as sometimes unnecessary or redundant cases were not always possible to rule out before hand. However, as computer power moves up and numerical methods are becoming increasingly powerful, a new modality of experimentation, namely *experimental validation*, is emerging thanks to these advances and it is being adopted as modern approach. Computer simulations have the advantage that they are performed in a controlled and flexible environment and it is not uncommon that a diversity of cases - including "extreme" ones - are tested before any actual implementation or experiment is carried out, which is particularly advantageous when dealing with parametric tests. In this manner, for example, to create a certain mitigation design, a computer model is first elaborated and solved numerically; furthermore this model is contrasted against experimental data i.e. is *validated*. The result of an adequate choice of parameters upon this validated model, which fit certain desired physical conditions, will then represent the final mitigation design.

The cost of a field mitigation experiment is often the most critical factor in the determination of its feasibility. One way to reduce costs is to decide what characteristics of the design or the technique are to be tested and under what relevant conditions. According to the specific mitigation problem, three experimental options are possible: in-situ experiments, lab experiments and small-scale experiments.

3.3.1 In-situ experiments

These experiments are performed in actual scale and conditions (compare with 3.3.3) which includes the site (compare with 3.3.2) where the sources are located. The advantage in this case is that the experimental conditions are the closest to the actual ones. Consequently, in-situ experimentation can provide quite reliable measurements. However, the main hindrance is that the equipment or system to be mitigated may be already operative and it has to be disconnected from the feeding power to accommodate the experimental setup. Two different cases are considered

a) experiments at the installation stage (before the system starts operations)
b) experiments when the system is already operative

At the installation stage: In this case a large flexibility is often at disposal as experiments can be carried out without interfering with duty operations. For example, shielding of components can be tested in a substation for realistic values of currents; also, various mitigation structures (e.g. shielding in combination with conductor management) can be tested in underground cable systems. In this category fall, for example, new built substations, new underground cable systems [1] and new power line installations.

***When the system is already in operation*:** especial attention has to be placed in trying to cause minimum interruption to the services; in some cases backup systems can be connected to guarantee continuity of the services. However, the latter operation will add expenses to the total mitigation design. A good alternative is to coordinate mitigation experiments with other operations in the system that would require bringing temporarily the functioning of the system to a halt. Examples of these operations are renovation (long term), maintenance and inspections of the system (short term).

3.3.2 High-power lab experiments

To avoid disrupting a power system in operation it is sometimes convenient to perform mitigation experiments in a laboratory; more precisely in a high-voltage facility. Typical mitigation experiments that can be performed in the lab are: shielding of busbars, design of transformer connections, underground cable configuration and shielding. Moreover, experiments in the lab are very suitable for active compensation designs. Specifically developments of the additional circuitry and feeding to the compensating coils are typical lab operations. It is often more convenient, from the economical point of view, to perform these mitigation experiments only with the relevant part or section of the system which is assumed to be the source (or main source) of magnetic fields. For example, Figure 3.3.1 shows a MV/LV substation that was evaluated and the transformer connections were deduced to be the main source of magnetic fields affecting the floor above the substation. Experiments were carried out in the lab with a constructed model of this particular cable configuration. Then a specific mitigation design was developed and effectively implemented.

Figure 3.3.1 Identification of a part of the power system as the main source of magnetic fields; experiments with this section were performed in the lab which lead to an effective mitigation design.

Experimentation combined with computer simulations can represent various degrees of approach to a realistic mitigation situation. Yet, simplicity in the experimental procedures can be advantageous. For example, if a system of busbars inside a MV/LV substation is considered a source to be investigated experimentally, the designer may choose to test the magnetic field corresponding to that busbar system and its behaviour in relation to various mitigation designs or prototypes. An example is shown in Figure 3.3.2 where an experimental set-up is comprised by a 180 x 60 x 60 cm wooden frame, where 60 x 60 cm magnetic sheets can be disposed on the frame. Two external busbars are supplied by a 50 Hz single-phase system with currents of some hundred amperes. Numerical simulations were performed and the models were validated using the results of these experiments [2].

The influence of the cover of the switchboard can be estimated by simulation or -sometimes- even not taken it into account if the study deals with a relative comparison between two shielding designs. Naturally, considering the ferromagnetic cover as part of the test will add precision, but also complexity and extra costs to the experiment.

There are some ways to reduce complexity and cost of experiments, here some hints,

1) Making realistic and detailed computer simulations using 2D and, when necessary, 3D codes. Even for large computer times, the involved costs tend to be low when compared with the costs of some of the in-situ or lab experiments whose results can be predicted before hand by reliable simulations.
2) Starting with a low-current and relatively low-voltage source it is possible to generate high current sources by using multiple turns (Figure 3.3.3). This construction diminishes the need of a high-power facility.
3) Identifying carefully the most relevant sources of magnetic fields (involving not very relevant parts of the system can incur in unnecessary costs).
4) Using simplified models provided they give a reasonable trade with accuracy.
5) Even if the experimental stage is already taking place and data is being obtained, it is convenient to run some additional computer simulations based on this information to improve the experimental results.

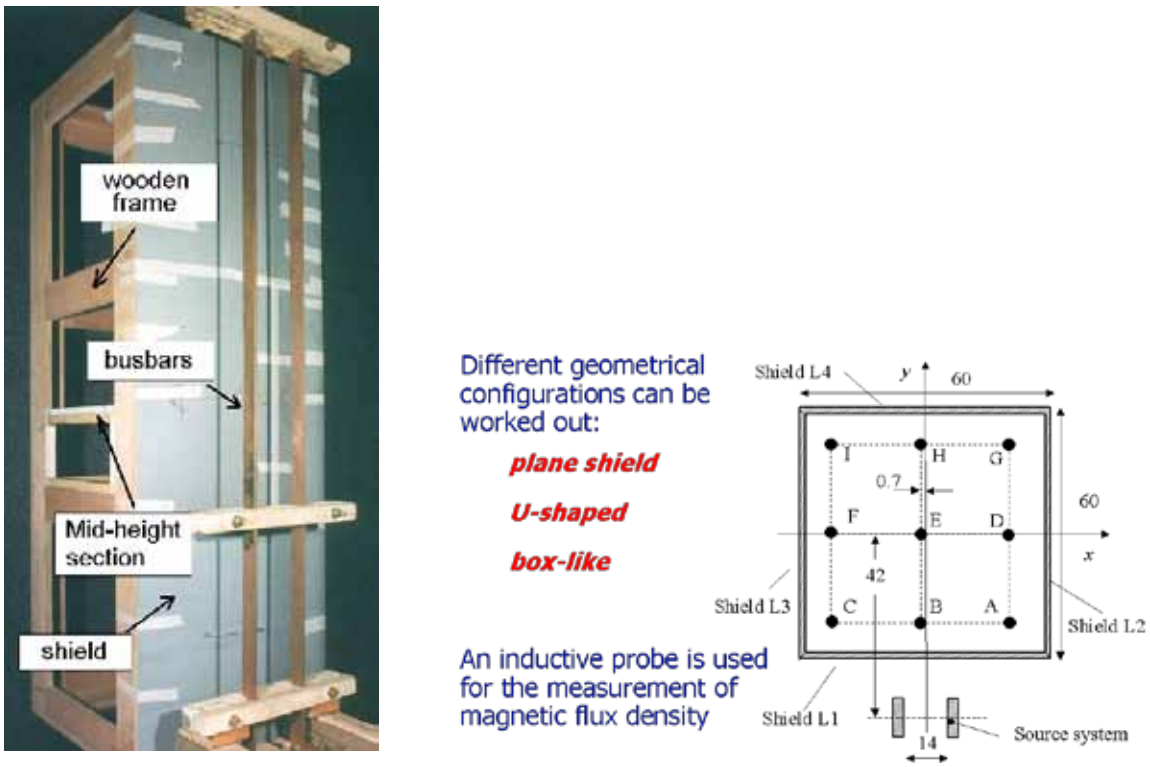

Figure 3.3.2 Experimental set-up for testing a busbar system and various shielding configurations; numerical simulations were performed and the numerical models were validated by these experiments [2].

Figure 3.3.3 By using multiple turns it is possible to generate high currents starting with a low-current source, this action diminishes the need of a high-power facility.

3.3.3 Low-power lab experiments

When designing techniques for mitigation of magnetic fields it is often necessary to perform experiments that can supply useful data. However, due to the size and weight of the elements involved (e.g. busbars, power cables and transformers) as well as the high voltages or currents implicated, performing these experiments may become a rather cumbersome endeavour, implying long and costly procedures. It would therefore be advantageous to have the possibility of reducing the total system and performing the test in a small space (for example a simple table in a low-power lab), having the option of using the results back on the mitigation design for the actual (large) system. In order to do this, we have to know the rules of how to transform the electrical parameters from one system to the other (Figure 3.3.4) and vice versa.

These rules can be obtained in a simplified way as follows. Assuming a system of sources and purely conductive (i.e. high σ and $\mu=\mu_0$) devices (such as coils, cables, busbars, aluminium or copper shield plates). It is also assumed that the sources operate within a quasi-static frequency range (e.g. power frequency and its harmonics). Naming x as the scaling factor, then length scales as $l' = x\,l$; surface as $A' = x^2$

A; and volume as $V' = x^3 V$. A current I is scaled assuming a scale-invariant current density J, i.e. J'(x', y', z') = J(x, y, z) or I'/A' = I/A, consequently $I' = x^2 I$. Thus, the current scales as the square of the scaling factor.

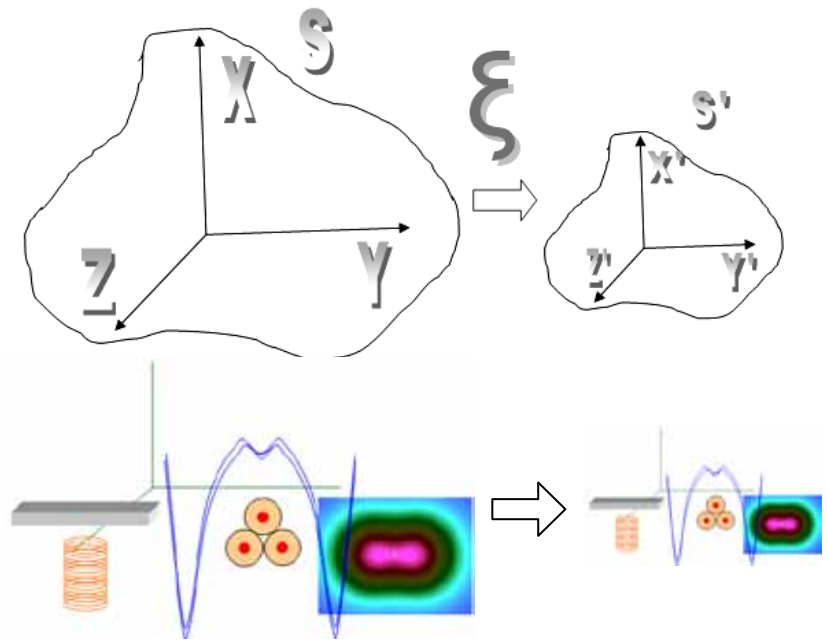

Figure 3.3.4 The system S can be scaled down to the smaller one S', providing an easy, flexible and cost effective experimental method of obtaining results for mitigation designs. This is possible, provided rules of transformation between the two systems are found.

Having units of length, the *skin depth* δ scales linearly: $\delta' = x\,\delta$. This expression allows the computation of a scaling rule for the frequency, as follows, $(2\pi\mu_0\sigma' f')^{-1/2} = x\,(2\pi\mu_0\sigma f)^{-1/2}$. Assuming scale invariance and homogeneity of the materials in both scales ($\sigma = \sigma'$), then the frequency scales as

$$f' = x^{-2} f \tag{3.3.1}$$

For example a *ten-times smaller* linear device needs a *hundred-times larger* operating frequency to behave in a invariant way in the new scale. Using Ampere's law in integral form ($\oint \mathbf{B}\cdot d\mathbf{l} = \mu_0 I$), it follows that the magnetic field **B** scales linearly with x,

$$\mathbf{B}' = x\,\mathbf{B} \tag{3.3.2}$$

Moreover, the shielding factors are

$$\begin{aligned}(SF)' &= (B_{BeforeShielding})'/(B_{AfterShielding})' \\ &= (xB_{BeforeShielding})/(xB_{AfterShielding}) = SF\end{aligned} \tag{3.3.3}$$

Equation (3.3.3) shows that the shielding factor SF remains unchanged under a scaling operation. This result makes things even easier:

Provided a shielding experiment (involving pure-conductive materials) is reproduced in small scale, the obtained shielding factors can also be applied to the original (large) design.

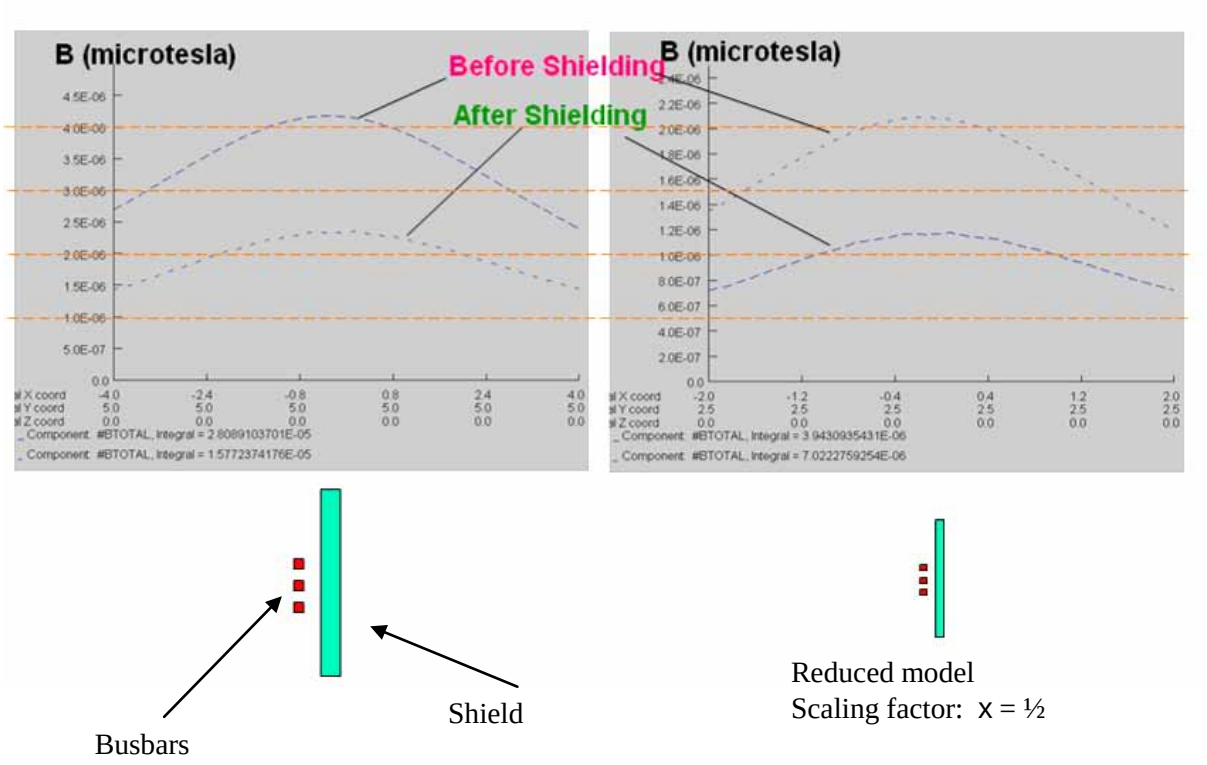

Figure 3.3.5 Scale invariance for a simple shielding configuration. In the large model (S) the field is computed at 4 m above the system while in the small one (S') at just 2 m. From the scaling principle, it is deduced that B' = 1/2 B, which is verified by computer simulation.

There are some problems that can emerge when trying to use a small-scale model. The main ones are:

- *Problem 1*: as the model goes smaller, the involved currents also go smaller but with the square of the scaling factor. Therefore the magnetic field produced by these currents will have a larger noise/signal ratio than the initial configuration. This may cause noticeable errors in the measurement of the field values.
- *Problem 2:* as the size of the system diminishes, the size of the B-field measuring device (e.g. a 3-coil based gaussmeter) does not. This causes error in the positioning especially when the scaling factor is $x \ll 1$.
- *Problem 3*: as the size of the system is reduced, the involved frequency increases inversely squared. For scaled models of 1/2, 1/3, 1/4, if the initial frequency is 50 Hz, then the new frequencies will be 200 Hz, 450 Hz and 800 Hz respectively. For a scaling of 1/10 the frequency goes up to 5 kHz, and for 1/100 it goes to 0.5 MHz, at these latter frequencies - and above - the sources start radiating and the scaling principle is not fulfilled for practical mitigation applications.
- *Problem 4*: the increase of frequency for reduced-scale systems requires the source feeding equipment to generate a signal of that frequency. Thus a signal generator is required. The trouble is that most signal generators have nearly no power output, therefore the generated fields from currents obtained in this way may be negligible.
- *Problem 5*: the systems of interest at actual scales are three-phase systems. However, it is not trivial to obtain a small, low-power three-phase equipment.

In fact, each of these issues has solutions,

- *Solution to 1*: We can use the fact that when a set of conductors (such as wires, coils, resistors) is given an input signal $i(\omega t)$, the magnetic field emitted by this arrangement at a point $\mathbf{r}(x,y,z)$ has the structure $B(x,y,z,t) = f(\mathbf{r},t) \times i(\omega t)$, which means that the magnetic field is linear with respect to the current. Therefore we can just increase the currents a certain proportion, decreasing in this way the noise/signal ratio, and we will know that in our system the field has also increased in that proportion.

- *Solution to 2*: positioning of the gaussmeter should be made carefully. A better solution is to design and use 3-perpendicular and concentric coils according to the scale of the experiment. In this way the measuring device is also scaled.
- *Solution to 3:* the scaling principle is easier to use when the scaling factors are not very large (nor too small with respect to unity). For practical purposes is better to use scaling factors that are within the range 1-1/10.
- *Solution to 4*: in order to insert power into the system, one can use an audio amplifier. This has been tested with rather good results.
- *Solution to 5*: it is possible to generate a 3-phase system of conductors by interconnecting two systems of single phase dipoles (as in Figure 3.3.3, but smaller). The phases of each dipole can be provided by a single source and phase-shifting capacitors.

Two examples of application of small scale experiments are shown in Figures 3.3.6 and 3.3.7, see also references [3] and [4].

Figure 3.3.6 Small scale arrangement (x =1/10) to model accurately a shielding structure of a large building affected by magnetic fields originated from a railway system with an AC current of frequency 16.67 Hz.

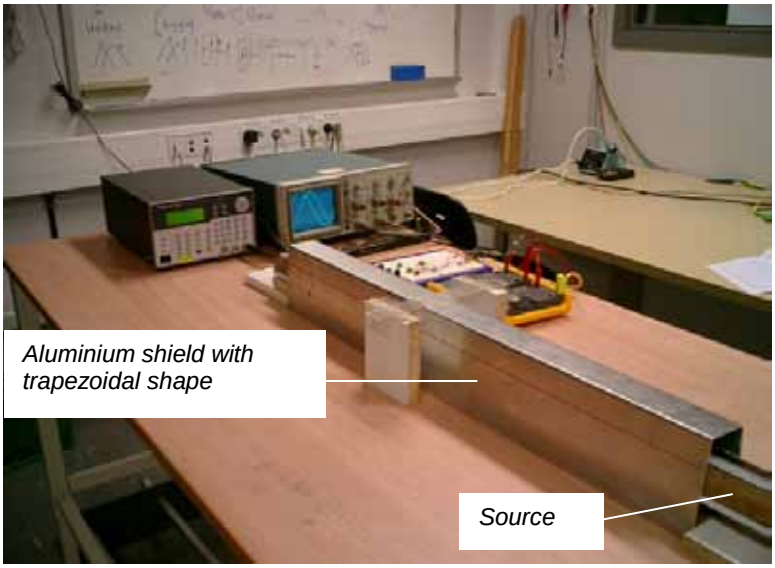

Figure 3.3.7 Small-scale experimental set up representing a trapezoidal-shaped shielding structure for a 3-phase underground cable system. The structure is scaled down six times (x = 1/6).

3.3.4 References

[1] G. Bucea and H. Kent, *"Shielding Techniques to Reduce Magnetic Fields Associated with Undergroud Power Cables: a Case Study from Sydney, Australia"*. CIGRE Session 1998, paper 21-201.

[2] O. Bottauscio, M. Chiampi, G. Crotti, A. Manzin, M. Zucca, *"Some considerations about passive shielding"*. Round Table on Magnetic Field Mitigation Methods, Proceedings of CIRED 2003.

[3] E. Salinas, Y. Q. Liu, P. Souza Jr. , J. Atalaya, P. Cruz , J. Daalder. *"Design and Validation of Power-Frequency Magnetic field Conductive Shielding for Underground Cables"* Proceedings of CIRED'2005, 18th International Conference and on Electricity Distribution, IEE Technical Report, Technical Theme 2, Power Quality and EMC, paper 97, pp 1-4, Turin, 2005.

[4] E. Salinas, J. Atalaya, Y. Hamnerius, C.J. Solano, D. Gonzales, C. Contreras, C. Leon, M. A. Sumari, S. Dimitriou and M. Rezinkina, *"A new Technique for reducing Extremely Low Frequency Magnetic Field Emissions affecting Large Building structures"*, The Environmentalist, Springer Netherlands, vol. 27, no. 4, pp 571-576, Oct. 2007.

4 MITIGATION STRATEGIES

After the detailed presentation of mitigation techniques in the former chapters, a relevant issue is to elaborate the strategy to follow, i.e. the choice of the most suitable mitigation technique.

The first thing a mitigation designer should do is to obtain a survey of the magnetic field distribution of the affected area. However, this is only possible when the source is in operation. If the mitigation design is to be performed before installation, this data will not be available. Yet, depending on the source, it is often possible to obtain the field distribution by computer simulation [1], [2], by experiments or by comparison from a similar source that is already in operation.

Another important consideration is the time variability of the magnetic field emission, which should be recorded and analysed. Measurements at certain time of the day could yield to wrong estimation of the field values. For a more complete understanding of the field behaviour, a registration of the magnetic field should be recorded for at least 24 hours (Figure 4.1). In some cases it is useful to have longer periods of variability, yet this depends on the specific type of source. By knowing the time-variability of the field it is possible to determine its maximum possible value.

Sometimes it is possible to obtain records of the currents that produce a magnetic field. Combining this information with the geometry of the conductors can lead to a simple assessment of the magnetic field and its sources. This procedure often allows the designer to decide upon the type of mitigation technique to implement.

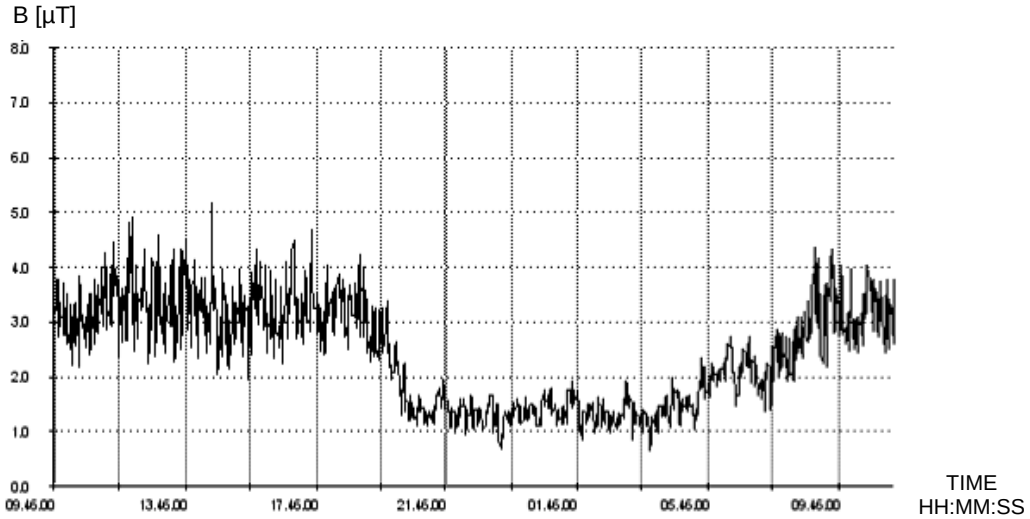

Figure 4.1 Typical 24-hours time variability of a magnetic field source.

Another important consideration is the direction of the vector field. Usually the recording of the field values is made with a three-axis gaussmeter providing RMS values of the field. However, knowing the direction of the field could sometimes be important when deciding what mitigation technique to use or how to design a chosen mitigation technique. For example if the field direction is known in the location where a shield or a compensating loop will be located, this knowledge will help to position the mitigation device perpendicularly to the field direction and therefore optimize its response. The direction of the field is not necessarily linear but it can be elliptically polarized as it happens in most cases with three-phase sources. Therefore, knowing this behaviour is valuable for the mitigation choice and design. An example is shown in Figure 4.2, where one of the conductors is very close to the affected region. The initial design in Figure 4.2-(a) is not effective since the field in the vicinity of the closest conductors behaves as if it was originated from a zero-sequence source. This knowledge and the simulations showing the directions of the eddy currents has helped to design a better shield represented in Figure 4.2-(b), which shows an extended shielding structure that redirects the induced currents creating effective current loops and resulting in a minimization of the field inside the enclosed region. This structure is made of a plate and ribbons. In some designs, both plates can be replaced by ribbons with further cost reduction.

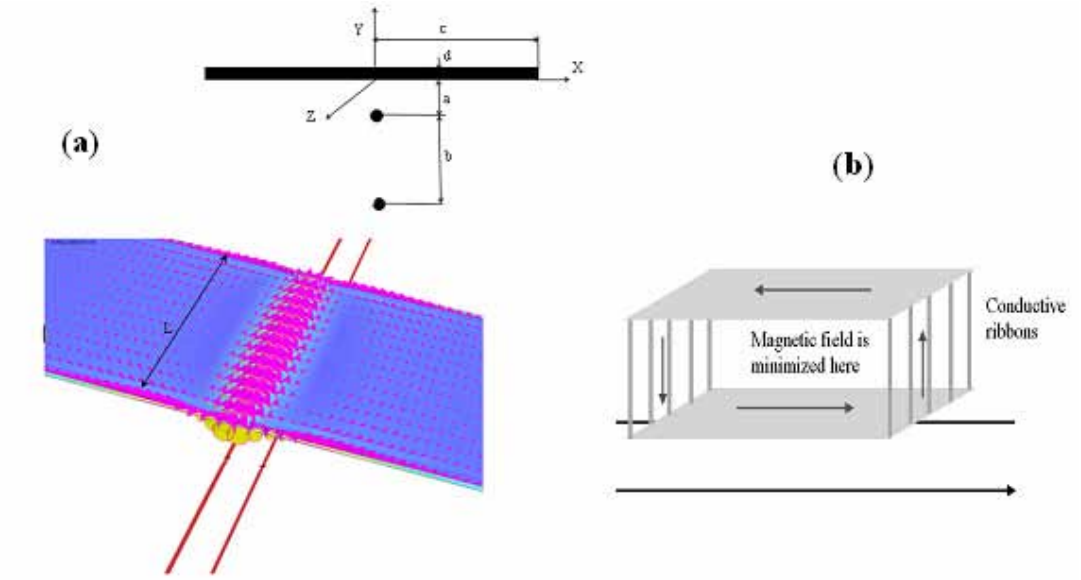

Figure 4.2 Example of the importance of vector field distribution on the design of a conductive shield: (a) eddy currents are accumulated in the edges (b) these currents are redirected implying a better mitigation.

4.1 Mitigation at the source or at the affected area

Another factor that determines the technique to use is the choice of the location where it needs to be applied, i.e. to the source or to the area of interest. This is not an easy question since the definition of the area of interest is not always unambiguous. However, it should be possible to characterize a general problem in which there are magnetic field sources and one or several areas of interest. There could also be a small region affected within this area. As a general rule, it can be suggested that it will be more cost-effective to mitigate at the source than at the area of interest. However, the choice can be different. For example in some cases where the source is rather large (e.g. long busbars); or if the purpose is to mitigate the field in a small region, e.g. a single house, then the option of mitigating the affected area is probably the most cost-effective choice (Figure 4.3).

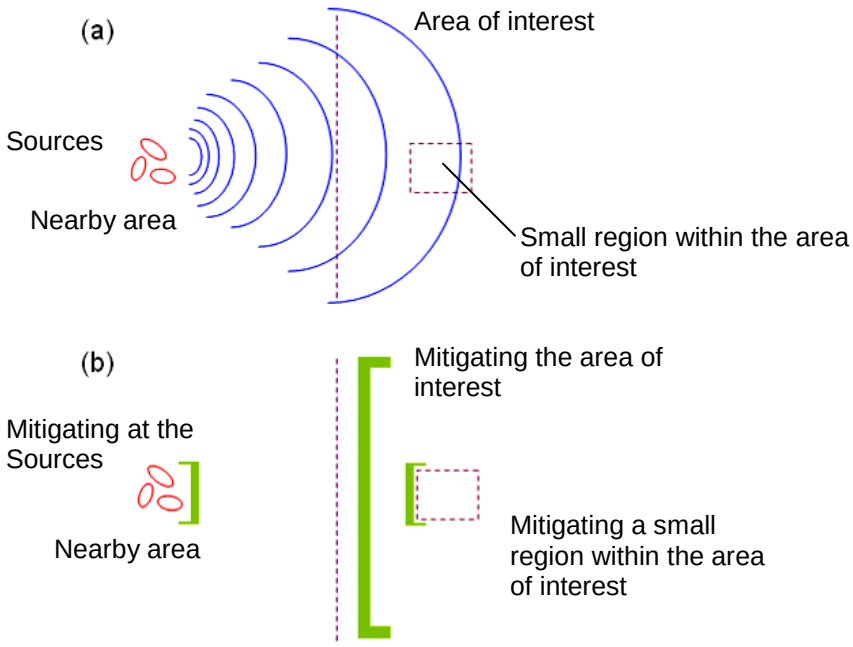

Figure 4.3 Three choices of mitigation, to be decided according to the specific problem. The green outlines are symbolic representations, not necessarily shields, and could represent a loop, an active device, or another mitigation action within that region.

4.2 Field mitigation research and innovation

The topic of magnetic field mitigation has in recent years become an activity having a fairly high demand and often, utilities, manufacturers and consulting companies dedicate serious efforts to provide solutions to requests from concerned customer. It is then surprising that techniques and methods commonly used in actual field mitigation operations (design and implementation) often do not engage much innovation. Also it is worth mentioning that results of research are seldom seen in the practical applications. Figure 4.4 shows the introduction of research in a magnetic field mitigation procedure. Research can often lead to innovations, which have the ability to improve the effectiveness of a mitigation operation.

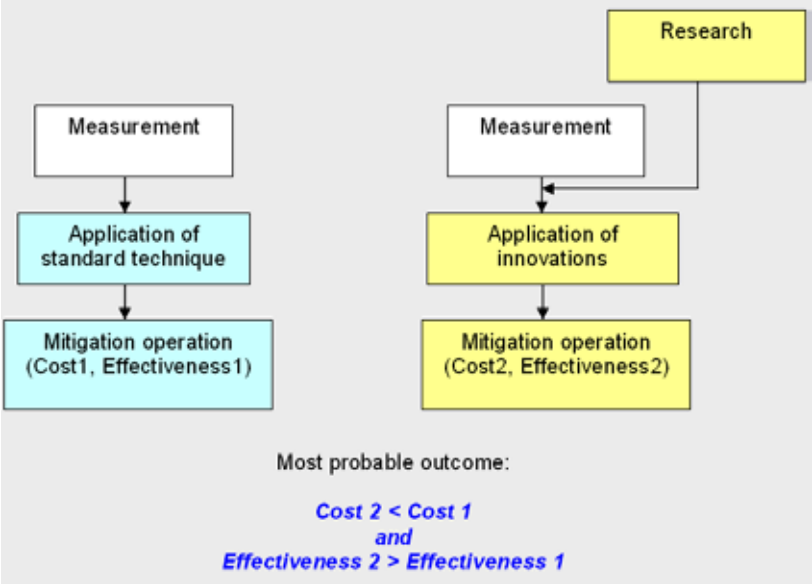

Figure 4.4 Introduction of research in a field mitigation procedure can lead to innovations, increase of effectiveness and cost reductions.

For example, the mitigation of the magnetic field in the vicinity of MV/LV substations, where the field is a complex superposition of many sources, is often solved by designing shields that cover the floor of the affected area, which usually results in costly and not very efficient mitigation. When a meticulous study is made of each component and of the way the field is originated in each source, the results of the investigation can lead to improvement in the techniques of field mitigation, representing more effectiveness and lower cost than standard techniques.

However, engagement in research will always involve extra costs (software development, experiments, and meetings, to mention a few). Thus, it may not be suitable for small operations, but could involve huge savings when the operation is large (e.g. mitigation of long underground cable structures or new power lines to extend a grid in a large city).

It is worth to observe that several of the examples in chapter 6 are the result of funded research activities, some of them as cooperation within industry and academia.

4.3 References

[1] A. Canova, F. Freschi, M. Repetto, M. Tartaglia – Identification of equivalent source system for electromagnetic field pollution evaluation – CIRED Conference, Turin, 6-9 June 2005.

[2] C. Song, G. Chen, C. Zhu, Z. Fu – A simplified method for magnetic field prediction of 110/10 kV indoor substations at design stage – CIRED Conference, Turin, 6-9 June 2005.

5 APPLICATIONS TO DIFFERENT PARTS OF THE ELECTRIC SYSTEM

In this chapter, the mitigation techniques proposed in chapter 2 are applied to different power installations, discussing the best alternatives that provide a high shielding effectiveness at a moderate cost. Both “ad hoc” simulations (based on methods presented in chapter 3) and results taken from other researchers are provided. In each case, a mitigation analysis for real installations is included, with the adopted solution. If the information is available, cost of the solution is also provided.

In all the cases, the strategy of mitigating the source has been adopted. In this way, a systematic analysis of the effect of the mitigation technique for each particular source can be performed. However, following chapter 4, a case-by-case study is required, and in some circumstances, the mitigation of the area of interest could be a more cost-effective solution.

The installations that have been considered in this chapter are:

- Overhead lines, from Extra High Voltage (EHV) to Low Voltage (LV)
- Underground high voltage cables, both in pipes and ducts
- Transmission and subtransmission substations
- Secondary distribution substations (MV/LV)

5.1 Overhead EHV and HV Power Lines

As for many other sources, and in accordance with the general principle described in Chapter 2, the magnetic field (MF) generated by transmission or distribution lines is substantially controlled by, besides the phase currents, the distance from the line, the distance between phase conductors and the line geometry [1].

To diminish human exposure to the MF produced by overhead (O/H) power lines it is generally impossible to reduce the line current without reducing the transmitted power (unless the line is upgraded to an higher voltage level that allows to keep the power unchanged while lowering current and losses). Similarly, it is often impossible, or at least inconvenient, to increase the distance from the line through modifications of the line route. Therefore, in many cases and mainly to face specific and local problems, other methods must be found that allow to obtain the desired result without compromising the reliability and safety of the electrical system and burdening as less as possible on the environment and on the territory.

The only really feasible technical solutions remain:

- increasing the height of the masts;
- acting on the conductors arrangement, including the splitting of the phase conductors [2,42];
- adding compensation circuits (passive and active loop compensation).

As shown in Figure 5.1.1, the first solution (increasing the height of the masts) is however useful only when a rather small reduction of the field is requested just within the line corridor, but no significant benefit can derive from such a solution if the area in which the field must be reduced is outside the line corridor, that is where the reduction is often more needed. For this reason, no further consideration will be given to this kind of solution in the sections that follow, with the exception of MV/LV overhead lines. The rest of the subchapter will instead be focused mainly on the latter two solutions. However, for the sake of completeness, mention will be also made of some other hypothetical methods that have been sometimes suggested.

5.1.1 Conductor arrangement and compaction

The analysis is considered for single-circuit, multi-circuit lines and split-phase lines.

5.1.1.1 Single-circuit lines

Rather simple numerical models [3] and relevant computer programs [4,5] are available to calculate the magnetic field generated by power lines. The basic formulation is the Biot-Savart Law applied to every line conductor, taking into account the sag between supports [4] or assuming straight conductors [5] at a height that will be the corresponding to the nearest conductor point to the desired calculation point [6].

Approximated formulae can also be used to calculate in a simple way the field in points far from the line conductors (that is at a distance of several times the phase-to-phase clearance), as shown in chapter 2. It was stated there that, compared with the flat configuration, the triangular configuration realises a magnetic field reduction by a factor of 1.4.

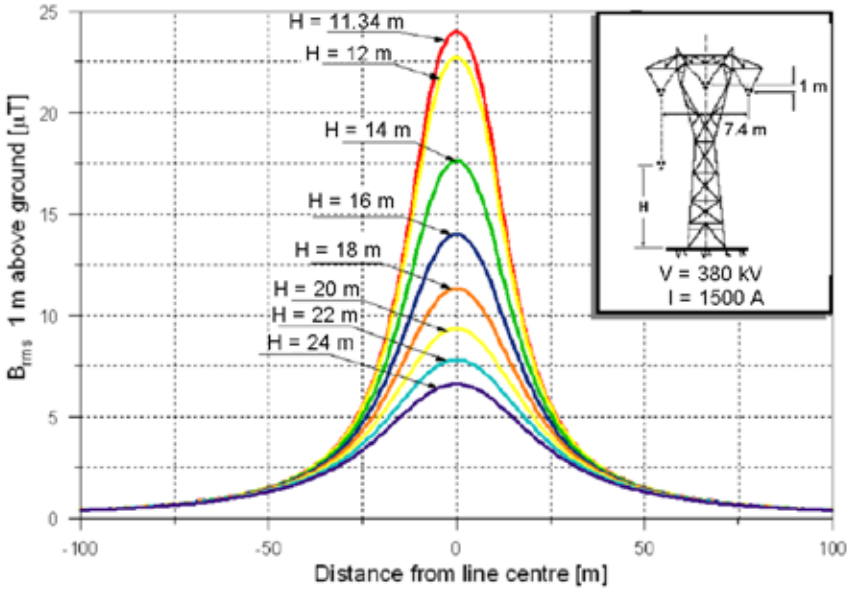

Figure 5.1.1 Field mitigation by increasing tower height.

For nearer distances to the line (i.e. inside the right of way), specially in transmission lines, the more accurate formulation should be used. If so, even within triangular configurations there are differences between arrangements. It can be shown that the "Ñ" (inverted delta) configuration is the best one (**Error! Reference source not found.**) followed closely by the alternate configuration ("▷"), not shown in the figure, and by the "D" (delta) configuration. In the four configurations of the figure, the clearance to ground from the lowest conductor is the same, as well as the phase-to-phase clearance.

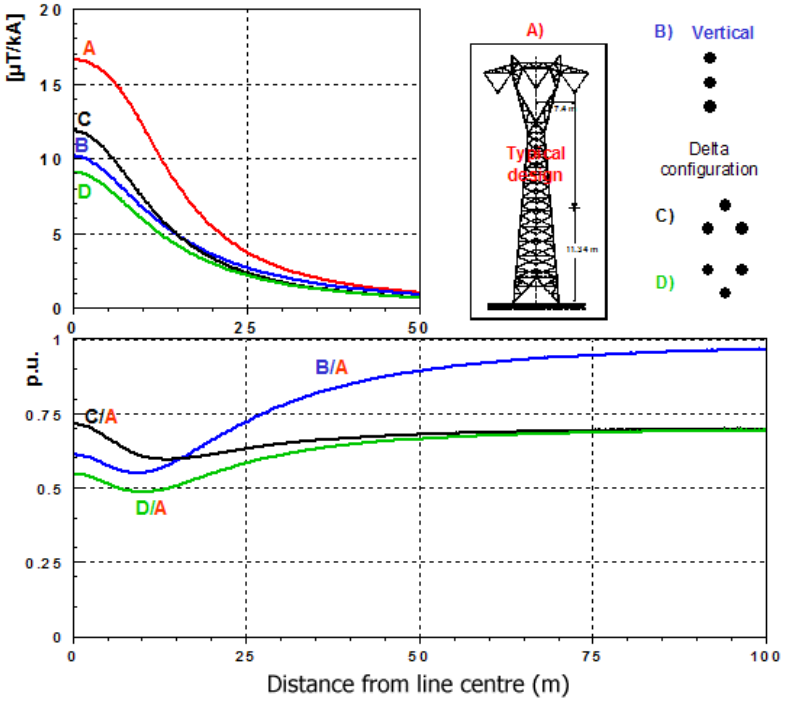

Figure 5.1.2 Comparison between the B-field lateral profiles, 1 m above ground, associated with four phase conductor arrangements (typical design corresponding to a 380 kV line).

As was seen in chapter 2, the field is proportional to phase-to-phase distance; therefore, "compaction" of the phase conductors makes it possible not only to reduce the space occupation but also to mitigate the magnetic field.

Note that the replacement of an O/H line with an equivalent underground cable may be seen as an extreme compaction of the phase conductors and therefore, apart from consideration of economical, technical and environmental problems, it represents a very effective solution. This method is briefly presented in 5.1.3. The limit to compaction is given by minimum live-line working air gap and insulating gap requirements, ruled by national or international standards and regulations [7,8]. The extremely compact lines are designed with clearances just lightly above these limits. The use of interphase insulating spacers to limit mechanical movement of phases relative to each other and the increase of total cross section of conductors (bundling) to avoid excessive levels of corona losses, audible noise and radio interferences rise the cost of these ultra compact lines [9].

Examples of O/H line compaction

A practical example of EHV compaction is the Swedish 420 kV T-tower inverted delta configuration (phase-to-phase distance about 7 m). The magnetic field can be reduced by a factor RF = 1.7 – 2.0 compared with conventional Swedish flat line (phase-to-phase distance = 9 m) (Figure 5.1.3). The cost of a 400 kV line with T-towers does not exceed that of similar portal towers [10]. Another inverted delta lattice-type design (phase-to-phase distance = 7.5 m) for 500 kV lines is presented in [11]. A reduction factor RF of 2.4 over conventional flat configuration (phase-to-phase distance = 12 m) is reported. If it is used a extremely compaction, the RF can be higher. For example, for the 420 kV T-Tower with a phase-to-phase distance of 4.2 m RF = 2.9 – 3.8, and for the 500 kV lattice-type design with an interphase distance of 5.3 m RF = 3.4.

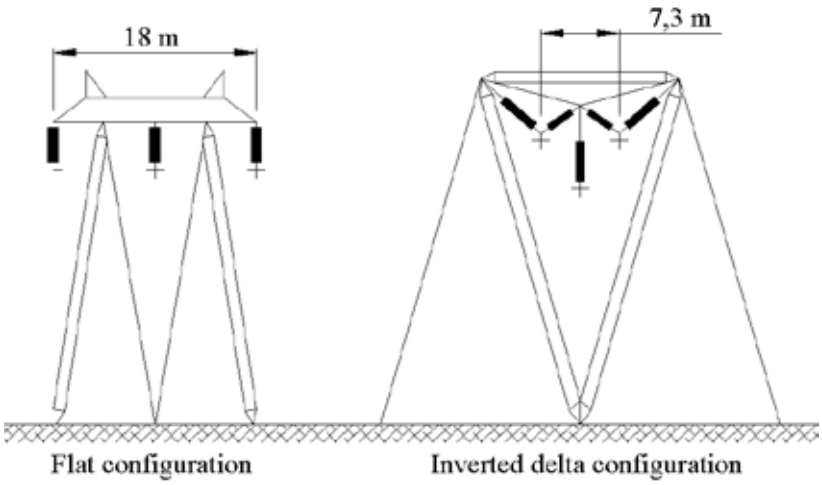

Figure 5.1.3 Flat and inverted delta Swedish tower types (420 kV).

For lower transmission voltages similar field reduction can be obtained by compaction. A further reduction is possible by the use of covered conductors, used today up to 110 kV. For example, a conventional three-height triangular lattice-type 132 kV line can be compacted to a pole-type with insulating arms with RF » 1.4 [12]. A practical experience is presented in [13], where an inverted delta tangent structure for a 115 kV line is designed and tested (Figure 5.1.4 b)). A reduction factor of 4 in relation with the standard H-frame tangent structure (Figure 5.1.4 a)) is reported. The final design was tuned to allow work practices.

(continuation)

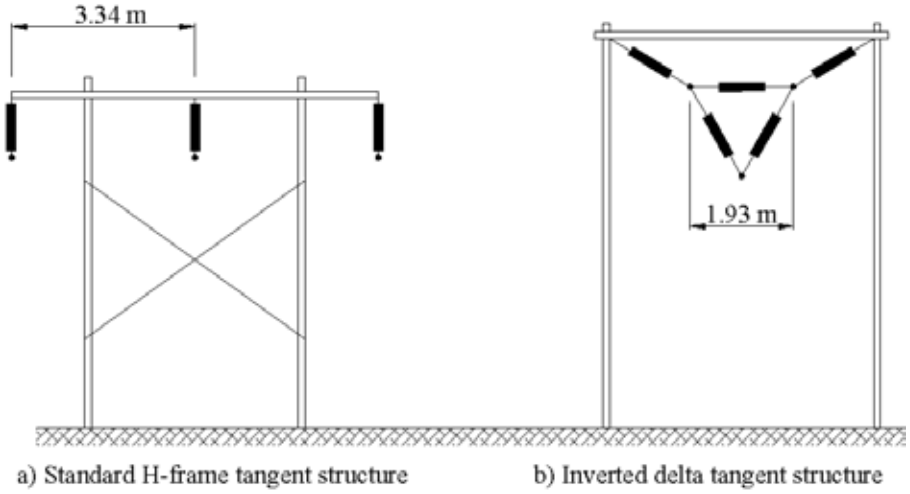

Figure 5.1.4 Conventional H-Frame and proposed inverted delta designs.

An experience related with the use of covered conductors carried out in Omaha (USA) is reported in [14]: this Aerial Spacer Cable System at 66 kV is basically composed of covered overhead cables separated by a spacer suspended by means of insulating brackets from conventional wood or metallic poles (Figure 5.1.5) by means of a messenger cable. The phase-to phase clearance is just 0.66 m. If this configuration is compared with the conventional three-height triangular, with phase-to-phase distance of 2.5 m a RF close to 4 is obtained. The increase of cost of this spacer cable system with respect to a conventional one is estimated to be of about 25 % [15].

Figure 5.1.5 View of an Aerial Spacer Cable System for a 66 kV line.

Another experience of covered conductors took place in Finland [16]. A test 110 kV line of covered LMF SAX conductor with vertical arrangement was built in 1996, being exploited successfully. Taking into account a phase-to-phase clearance of 1.8 m, this vertical configuration has a RF of about 2.5 at 30 m in relation to three-height triangular. The cost increase of this option is also estimated to be around 25 %. Other examples of compaction can be seen in [39,43,44,45].

5.1.1.2 Multi-circuit lines

In case of multi-circuit lines (such as double-circuit lines), also the geometrical arrangement of the single conductors of each phase plays an important role. In this case, however, it is necessary to know the direction (and relevant phase angle) of the currents in each circuit to determine the best solution. The background behind this phenomenon was explained in chapter 2.

In case of double circuit lines, with same current direction and amplitude in both circuits, phase reversal is the most effective way to reduce the field. Figure 5.1.6 shows the behaviour of the field with and without phase reversion for a 380 kV line. The field due to low reactance configuration is for every distance lower than super-bundle field, and the reduction factor increases considerably for several power lines at different voltages. However, in other cases, the field of low reactance configuration can be higher underneath the line (this fact depends largely on the layout), as can be seen in Figure 5.1.7.

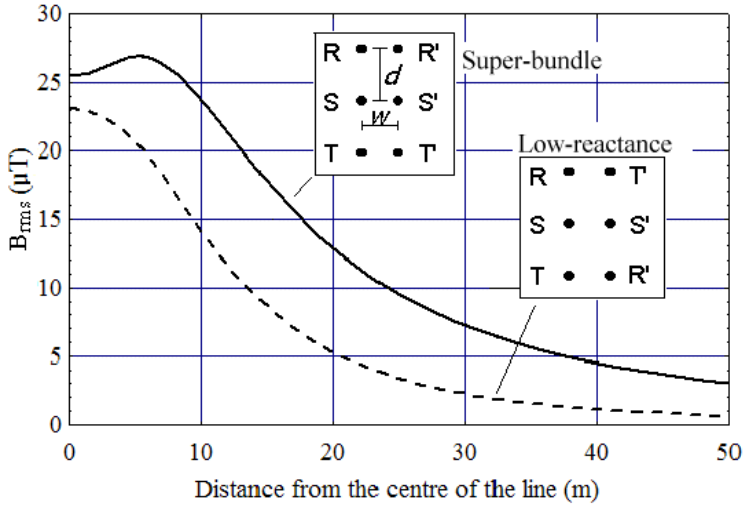

Figure 5.1.6 Lateral profiles of B-field at 1 m above ground produced by a 380 kV double-circuit line with and without phase reversion (I_1=I_2=1500A) (d = 8 m; w = 10 m).

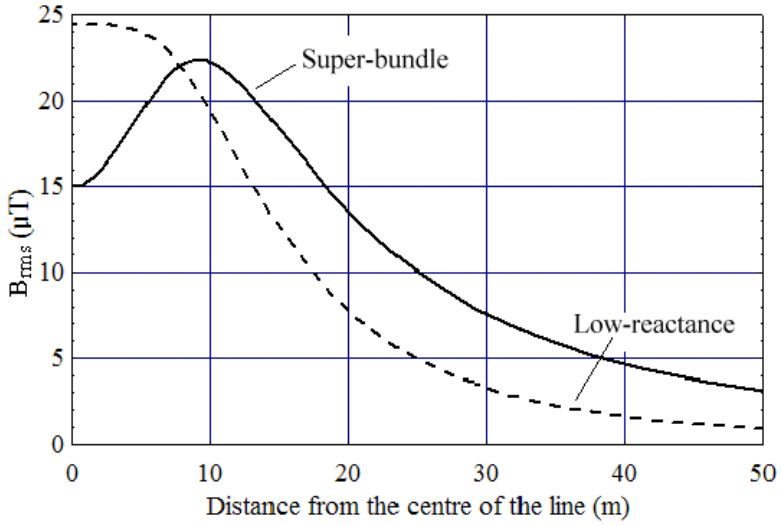

Figure 5.1.7 Case where the field underneath the line is higher with reversed phasing than without. (d = 8 m; w = 15 m).

5.1.1.3 Split-phase lines

The reversal phasing is the basis of the idea which is applied in the so-called “split-phase” line, whose theoretical analysis was presented in chapter 2. A “split-phase” line is a three-phase line, where one or more of the phases are split into two or more conductors, giving rise to considerably lower field levels. Examples of the advantages of a split-phase line are shown in Figure 5.1.8, where the fields generated by four different

splitting strategies are compared with that produced by a traditional "Ñ" configuration. If just one phase is split, the field decay rate is proportional to $1/r^2$, giving already a fair mitigation. For two phases split in 2 conductors (cases b and c), the field decays as $1/r^3$, and, for two phases split in 3 conductors ("star line", case d), as $1/r^4$.

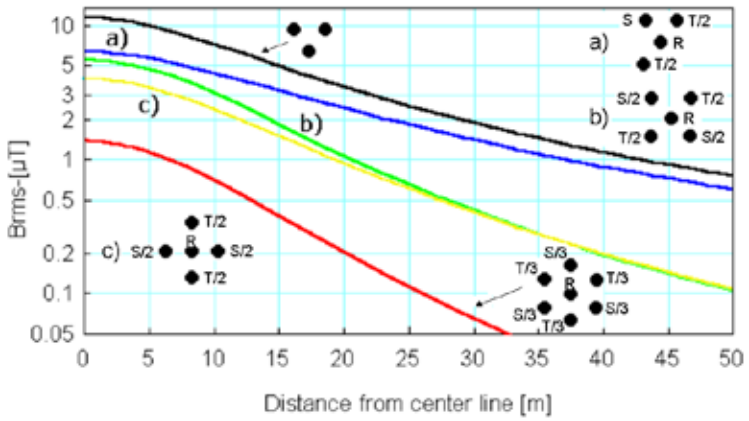

Figure 5.1.8 Comparison between the B-field lateral profiles, 1 m above ground, of a single circuit "Ñ" configuration line and three possible "split-phases" solutions (I: 1500 A; interphase distance: 5.5 m; minimum conductor to ground clearance: 11.34 m).

Examples of split-phase lines

There are few practical cases of split-phase lines. In [18] a 245 kV full scale test line is presented with a 5-wire arrangement similar to case b) in Figure 5.1.8 (distance between phases S/2 and T/2 = 4.61 m). The reduction factor under the line with respect to a horizontal configuration (phase-phase distance = 7 m) is RF = 8.3, with higher values alongside the transversal distance. Other example of possible configurations [9] is the compact vertical 5-wire ("brush type"), with reductions similar to the previous one (Figure 5.1.9, left). In the same figure there is an example of "star type" line.

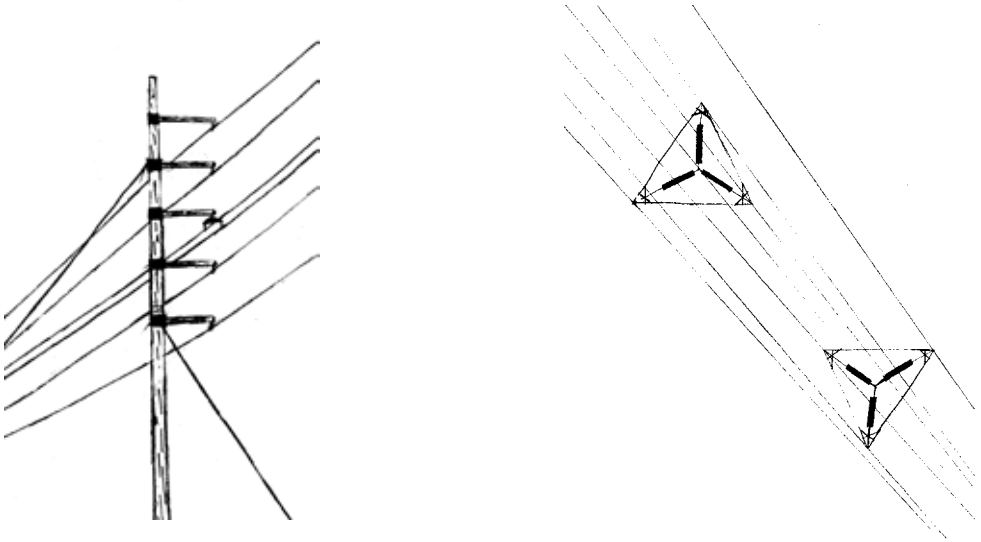

Figure 5.1.9 View of a 5-wire split-phase 115 kV line (left) and a 7-wire "star-type" (right) [19].

An additional potential benefit of split-phase lines is the significant reduction of the line surge impedance. By contrast, split-phase designs may produce significantly higher levels of audible and radio noise than traditional lines (cf. section 5.1.5). This problem, however, becomes important for voltages above 300 kV. For example EPRI has evaluated that each split-phase of a 500-kV line may require two bundles of two or three conductors each, of the same diameter as that of a traditional three-phase 500 kV line. Thus, the required total cross-sectional area is practically twice that of a traditional line. Therefore, the cost of this option will be substantially higher than that of a traditional line. In any case, it is important to note that the split-phase option can be applied as a local solution involving a limited number of spans.

It is however to be noted that the transformation of a single circuit line into a double-circuit line with the suitable phase arrangement realises, de facto, a split-phase solution, but offering the enormous advantage to allow the utilisation of towers whose design is already available. Figure 5.1.10 shows, by way of an example, what could be obtained in the case of a 132 kV line.

It has to be mentioned, however, that making from a single circuit line a double circuit line with the same total power spread on both circuits is only possible for a few spans of an existing line which has not been designed for being upgraded into a two circuits line. Otherwise it would mean that the line could never be exploited with its full foreseen capacity.

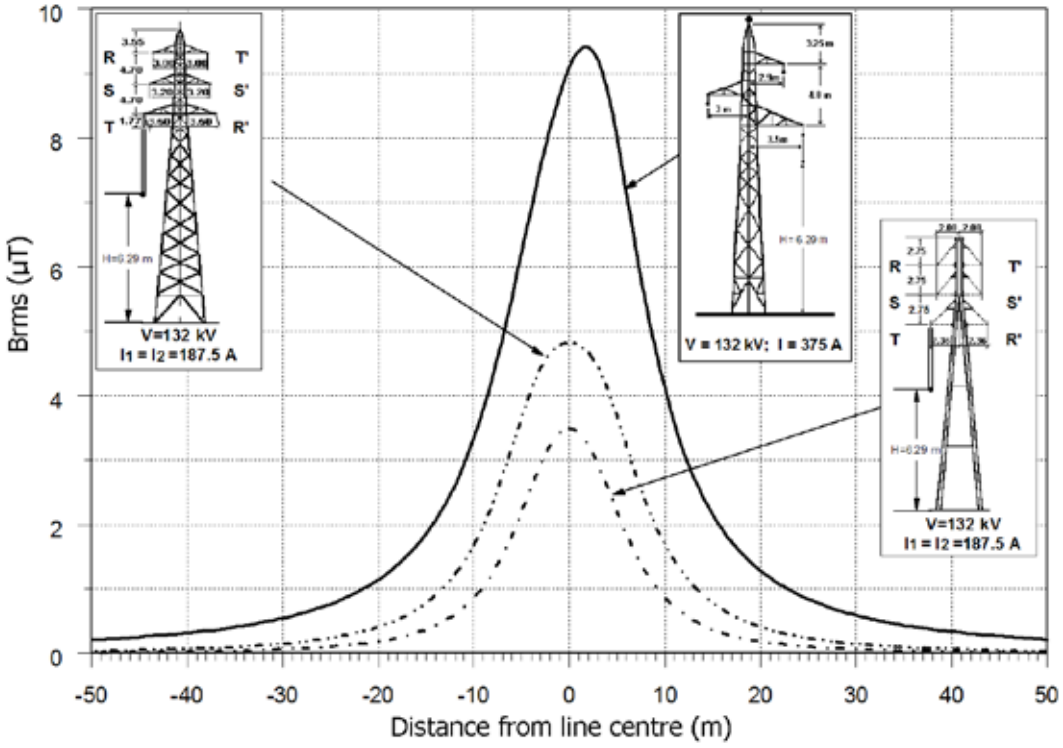

Figure 5.1.10 Comparison between the B-field lateral profiles, 1 m above ground, of a single circuit 132 kV line in use in Italy and two possible "split-phases" solutions obtained by using a standard double circuit line and a compacted one.

Examples of transitions from single circuit to double circuit configuration

In Figure 5.1.11 an example of transition from single circuit to double circuit configuration is shown. The 130 kV line is equipped with twin conductors per phase, which enables phase splitting very easily. Three concrete poles were installed and replaced the original wooden poles through an area with single family and apartment houses in Tornhaga, Kungälv in western Sweden. The reduction was 80 % as anticipated. The total cost was 144 000 € (1996 euros).

(*continuation)*

Figure 5.1.11 Example of transition from single circuit to double circuit configuration (Sweden).

Another example is depicted in Figure 5.1.12. The single circuit 132 kV line Scorzè – Camposampiero (Mirano, Italy) was converted in one span (close to a primary school) to an antisymmetrical double circuit configuration, limiting the field to 0.2 mT [45].

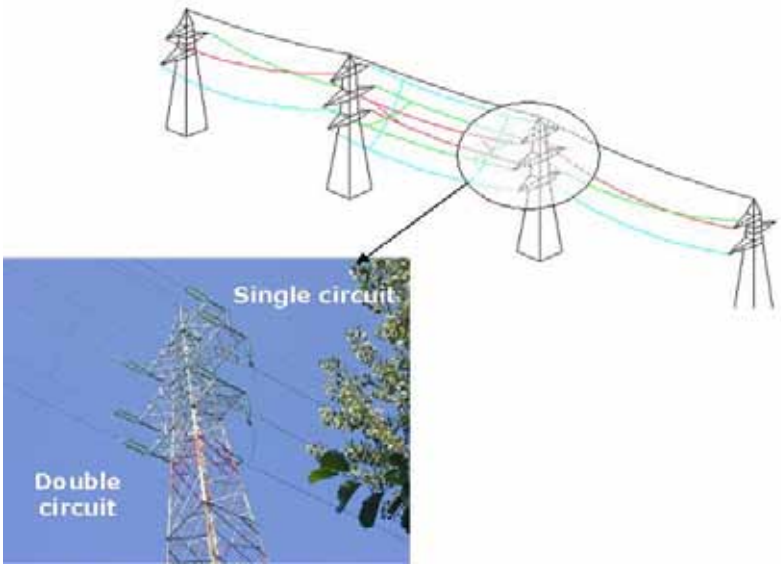

Figure 5.1.12 Example of transition from single circuit to double circuit configuration (Italy).

5.1.2 Compensation by induced or injected currents in secondary circuits

As was seen in chapter 1, two different techniques are possible: passive and active compensation.

5.1.2.1 Passive compensation

As described in Chapter 2, a shielding effect may be the result of a field created by the currents induced in an additional passive circuit under the influence of the original field to be reduced.

In the case of power lines, additional conductors at or close to ground potential (and properly arranged and connected to create a loop) can be installed, parallel to the line, to reduce the magnetic field. Theoretical analysis of passive shielding applied to overhead lines can be found in [2,19,20,21,22]. The impedance of shield wires is mainly determined by the wire inductance. Thus, to reduce the impedance of the shield wires, which control the intensity of the induced current, series capacitor compensation is inserted.

The optimum design of a compensating loop requires the definition, by means of suitable computer programs, of the placement of shield wires (which depends on the type of line configuration and the affected area location, symmetrical or asymmetrical), the loop conductor resistance and of the series capacitance. Compensating loop can be designed to reduce the magnetic field levels in an entire cross section of a line or in part of it or in a defined volume nearby the line corridor.

Figure 5.1.13 shows the results of calculations performed to define a possible solution for a case involving a single circuit horizontal 380 kV overhead line. A reduction factor of 1.7 under the line is obtained, growing slightly alongside transversal distance. This type of line is the most feasible to be shielded by this method. The reduction is important with an affordable cost, due to the fact that it is not needed to refurbish the towers or leave the line out of service. Other loop designs for horizontal lines are shown in [23,24].

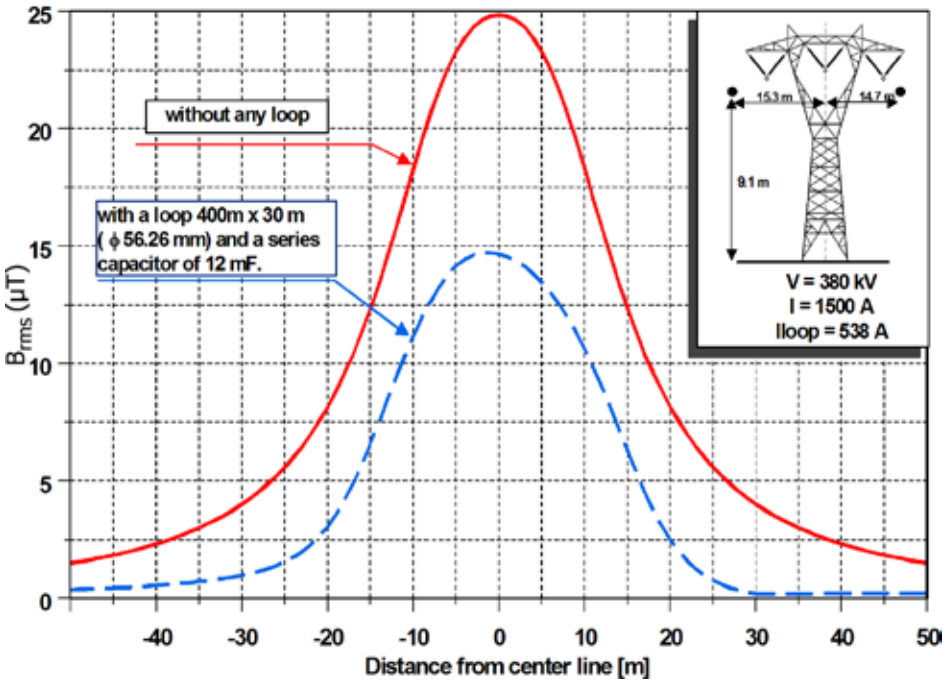

Figure 5.1.13 Comparison between the B-field [mT] lateral profiles, 1 m above ground, before and after the application of a compensating loop to a single circuit 380 kV line (computed values).

Even higher field reductions can be obtained. In 1996 the Electric Power Research Institute (EPRI) and the New York Power Authority (NYPA) designed and installed a passive loop system for the New York Cross-State Corridor, which contains two 345 kV flat lines. A 10 fold reduction of the average field over an area, outside the right of way, extending up to 30 m from its edge was experimentally observed [19,25,26] (width of the right of way = 91 m).

This method has also been proposed for other line configurations. A 3-wire shield for a Swedish inverted delta line is analysed in [27]; it involves two low-resistance conductors replacing ground wires and an underground cable (Figure 5.1.14). Although right underneath the line the field is higher with the shield than without (RF » 0.5), at about 7 m from the line the RF starts to increase up to about 1.6 at 30 m.

Although the cost of purchasing and installing passive loops should be quantified on a scheme by scheme basis, some estimations that have been proposed are illustrative. Paper [23] shows that the cost of compensating a 345 kV flat line is about 50,000 $/km (1992 dollars). Assuming a line cost of about 200,000 $/km, leads to a relative cost of 1.25. Similar results are obtained in [28]. In [24] a passive loop for Swedish

400 kV flat lines was designed and tested. The total cost of a 100 m loop was estimated about 74.000 $ (1995 dollars). In [26] the cost of passive loops installed in New York Cross-State Corridor was estimated in 930,000 $/km (1997 dollars). The cost differences between these estimations are mainly due to loop mitigation effectiveness and the inclusion or not of different items: losses capitalisation, design and engineering costs, etc.

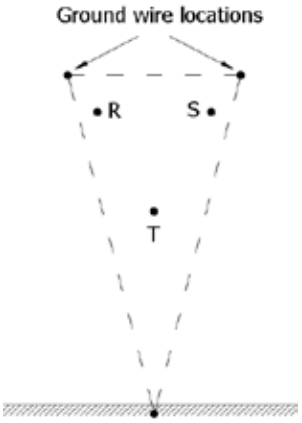

Figure 5.1.14 3-wire shield for the inverted delta configuration [29].

As stated before, this method is feasible for existing lines, with the more attractive feature that there is no need to refurbish the line. However, difficulties of installation on existing facilities and visual impacts make this solution difficult to implement [17]. Nowadays it is considered feasible to solve specific problems.

Another possibility for applying this technique is to incorporate the loop on the proper line support structures and to install this type of structures in new lines. In [28] the cost increase for installing 400 kV flat line supports with two conductors added is estimated 15300 €/span. This leads to a relative cost of 1.15. In [9] the relative cost of a similar configuration for a 500 kV line is estimated to be about 1.06. Finally, in [29] an integrated design for 66-145 kV lines is presented. It is composed of a single-circuit vertical configuration with an upper ground wire that also serves as one of the loop conductors, and a lower conductor wire that closes the loop. With this arrangement it would be technically feasible to build complete lines. In this case, line losses can increase up to about 8 % (cf. section 5.1.5).

5.1.2.2 Active compensation

In this approach, which is mentioned here only as a theoretical basis, the field created by the line conductors is cancelled by creating an equal but opposite field. Imposing shield wire currents using external power sources represents a feasible engineering option, especially when passive loops, even with an optimum arrangement and series capacitor compensation scheme, are not sufficient for achieving the desired shield wire currents. The calculation of optimum injected current to the active shielding is easy to obtain for the simplest shield configurations, like two-wire, three-wire and four-wire shields [19,22,40]. More complex shields have been proposed, although for mitigation of the interest area [41]. A feedback circuit sensitive to the magnetic field measured at the locations to be shielded would controls the power source. The practicality of this option needs however to be demonstrated, due to the requirement for more sophisticated equipment than in the passive shielding. On the other hand, less stringent shield characteristics (conductor resistance, location) are required. If, in the future, reliable standardised control and power injection systems would be marketed, this option could become competitive, as shown in [27,30].

In principle, the above-mentioned approach could be used also for shielding small apparatus such as video display units.

5.1.3 Other hypothetical mitigation methods

A mitigation method, hybrid between split-phase and passive/active loop, is the four-phase case, developed and patented in Sweden [31], but not put into practice yet. It consists on a flat configuration made up of one split-phase whose conductors are outside the other two phases, and forming a loop (Figure 5.1.15).This arrangement is planned to be used on existing Swedish 220 kV old lines with portal towers that do not need to be changed (old lines have fairly long distances between the legs and short spans, which enable to hang in two phases (in V-chains) between the legs instead of one and still have enough distance to each leg), which

makes this method cost-effective [17]. The field is decreased by a factor about 9 with passive capacitive compensation, and up to 24 with active compensation.

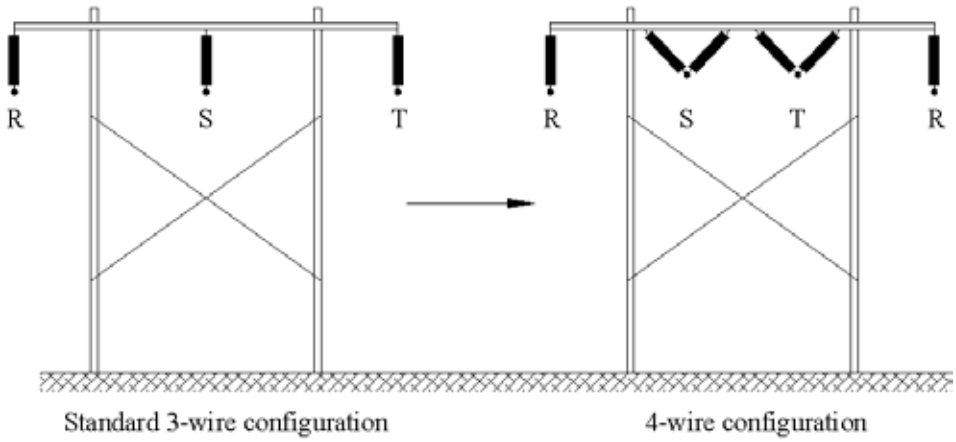

Figure 5.1.15 Conversion of a standard H-frame tangent structure to 4-wire one.

Other possibilities to reduce the field of overhead lines are, besides the use of underground cables [12], uprating to a higher voltage [17] and replacing three-phase line by six-phase [32]. Neither of these methods are considered in a first approach when facing a practical case.

Indeed, even if cables (especially if they are laid down separate and in a flat arrangement) may generate higher MF right above the cable than under the equivalent O/H line, their MF lateral profile decreases with distance from the center of the cable system much more than that of an O/H line (Figure 5.1.16). In addition, MF from power cables may be reduced with suitable techniques (cf. subchapter 5.3).

The major drawbacks of underground cables are the need to compensate the high admittance to ground by means of inductive shunts (only for higher EHV and long links), and the higher cost of the cable. About 10 years ago the underground cable/overhead line capital cost ranged from 5-10 for 110-219 kV lines to 15-25 for 363-764 kV [33]. Today, thanks to the dry insulation, the ratio for EHV lines has dropped until around 8. Even in relation with environmental issues there are factors other than visual impact (disturbance of flora and fauna, constraints on farming) that make this aspect controversial [34].

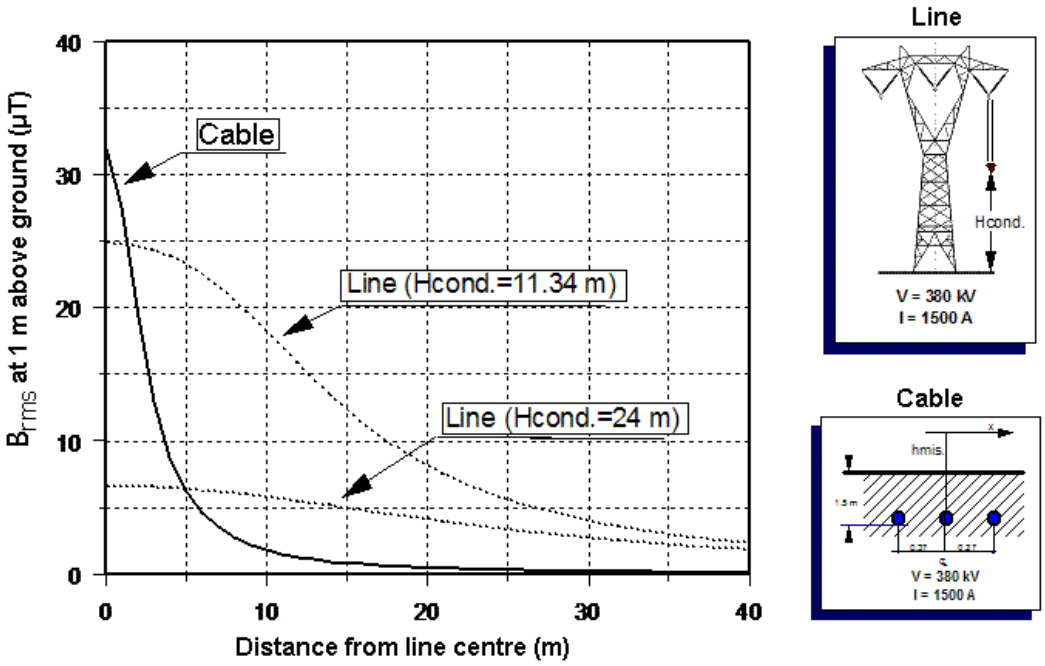

Figure 5.1.16 Lateral profiles of B-field at 1 m above ground produced by a 380 kV single-circuit overhead line (at two different conductor to ground clearances) and a 380 kV single-circuit cable, both carrying the same power.

The benefit of six-phase lines is that the phase-phase distance can be reduced (higher compaction). However, the field decay is with $1/r^2$, so this configuration is not so advantageous, taking into account the cost for implementing six-phase lines.

5.1.4 Parameters affecting the mitigation efficiency

The previous analysis has been developed taking into account some simplifying assumptions: balanced current (neither inverse nor zero sequence) in the line and effect of ground wire currents neglected. Although in most of the real cases of transmission lines these assumptions are reasonable, it would be advisable to know how the presence of these parameters can affect (positively or negatively) on the final RF of the mitigation method chosen. Without trying to be exhaustive, in this section some general rules are provided, and some numerical results of influence of these aspects on reduction factor are shown.

5.1.4.1 Ground wires current

When a transmission line has one or two ground wires, due to the geometrical asymmetry of these wires in relation to phase conductors, an electromotive force is induced in them, generating a current between them and to ground (this analysis assumes that the ground wire is not insulated from the towers). The net ground wires current acts like a homopolar phase current, generating a field that decays inversely with distance (cf. chapter 2). This field adds to the theoretical balanced three-phase field, changing slightly the mitigation effectiveness. This variation can be an increase or decrease, depending upon the value of the net ground current. If the mitigation method provides an increase in net ground wire current in relation with the original configuration, a small reduction in RF is obtained. On the contrary, if the mitigation method provides a reduction in net ground wires current a small increase in RF is observed. As an example, without attempting to be exhaustive, Table 5.1.1 shows the quantitative results obtained for 400 kV super-bundle double-circuit configuration (phase-phase distance = 8 m; ckt1-ckt2 distance = 15 m) when presence and absence of ground wires are considered. The compaction generates more net ground wires current and the effectiveness is lower than theoretical modelling without ground wires. The phase reversing generates less net ground wires current, and the effectiveness is slightly higher.

Table 5.1.1 Reduction factors at three distances from the line for a super-bundle double-circuit configuration when compacting and converting to low-reactance in presence and absence of ground wire.

Type of modelling	Compaction(1)	Low-reactance
	0/30/50 m	0/30/50 m
No ground wire	0.70/1.31/1.33	0.63/2.31/3.46
Two ground wires	0.71/1.27/1.25	0.69/2.42/3.64

(1) Phase-phase distance = 6 m; ckt1-ckt2 distance = 10 m

5.1.4.2 Non-balanced current

In relation with unbalance, it arises from untransposed lines and from multiple lines sharing one physical right-of-way. The presence of inverse sequence current does not change significantly the mitigation effectiveness. The presence of homopolar current reduces usually the effectiveness. The reduction of RF is higher as the mitigation method is more effective. A typical example of this behaviour is the low-reactance configuration, highly effective on balanced lines, but not so in presence of homopolar current at certain distance from the line centre [35]. Table 5.1.2 shows the results obtained for the same line than in Table 5.1.1, with no ground wires and balanced and non-balanced currents.

5.1.5 Effects of mitigation techniques on other performance aspects of overhead lines

Although the main aim of the designs proposed previously is the reduction of magnetic field generated by the line, it is inevitable that other performance aspects of the line change simultaneously. This behaviour raises the convenience of studying, in a case-by-case base, the influence of the proposed MF mitigating design on these additional aspects, like electric parameters (electric field, corona effect, unbalance, losses), reliability, maintenance, etc.

Table 5.1.2 Reduction factors at three distances from the line for a super-bundle double-circuit configuration when compacting and converting to low-reactance in presence and absence of balanced current.

	Compaction	Low-reactance
	0/30/50 m	0/30/50 m
Balanced current	0.70/1.31/1.33	0.63/2.31/3.46
Presence of inverse seq. (2 %)	0.70/1.31/1.33	0.63/2.30/3.46
Presence of homopolar seq. (2 %)	0.69/1.31/1.32	0.57/1.76/2.25

In relation to electrical parameters, the most influenced in a negative sense is the corona effect. Unfortunately, it is verified that the most effective methods to reduce MF, like compaction or split-phase, provoke an increase in corona effect. Therefore, the final low-field design must be balanced with allowed corona levels. Without attempting to be exhaustive, Table 5.1.3 shows, in a qualitative sense, the variation of electrical parameters, in relation to the horizontal configuration, for some of the mitigation designs considered [36]. It can be seen that two of the more effective methods to reduce MF (conversion from super-bundle to low-reactance configuration and phase-split) generate an increase in corona effect, both audible and radio interference. Moreover, if the line is compacted, the corona effect is even more intensified. In cases of ultra compaction it is needed to reduce this effect to certain limits, resulting in thicker conductors and/or, more effective, more subconductors per phase. It is interesting to note that, in the cases of passive/active loop the MF reduction has a neglected effect on corona performance. Regarding 132 kV, corona effect can be neglected, even in cases of extreme compaction.

Table 5.1.3 Effect of magnetic field reduction on other electrical performance aspects of HV/EHV lines.

Method	Magnetic Field	Electric Field	Audible Noise	Radio Interference	Unbalance
Height increase	$	$	$	$[1]	=
Layout	$	$	=	#	$
Compaction	K	K	J	#	$
Vertical super-bundle " low-reactance	$K	K	#	#[2]	$K
Phase splitting	$K	K	#	#	$
Passive/active loop	$K	$	=	=	=

[1] Starting from certain distance (about 50 m) the effect is the opposite

[2] It rises lightly from about 30 m off

In relation to passive compensation another aspect that should be tackled is the increase of line losses. A simple calculation can provide us a rough estimation. If a line completely compensated is assumed, a typical single loop current of 1/3 of line current, and loop conductor equal than line conductor, the losses increase is 7.4 %. Taking into account that normally only a small portion of the line is compensated (several hundreds of meters), the losses increase is negligible.

Issues regarding reliability are mostly related to compaction of the line. A key parameter is the minimum distance phase conductor-structure, because it states the insulation level and, therefore, the probability of outages due to overvoltages. It has been checked [2] that a small relative reduction of this distance in relation to values used nowadays has as a consequence a higher relative increase of outage frequency. Therefore, in the design of low-MF lines is preferable to avoid the existence of grounded parts of the tower in the way between phase conductors (e.g. inverted delta).

The modification of the phase configuration, or the phase-to-phase clearance, implies also a change in the procedure to carry out line maintenance routine tasks, especially live-line working. The final design has to allow the development of these tasks, compatible with the minimum allowed clearances. An experience related with this is reported in [13], where the design process of a new compact 115 kV lines is described. During the field tests the increase of pole separation and the spacing between the crossarm and conductors was needed.

5.1.6 Concluding remarks

The main methods for reducing the magnetic field produced by overhead power lines have been presented. However, some of the methods considered here are still at a research stage and their final design should be adapted to specific conditions. It is not always easy to carry out a precise estimate of their pros and cons from the technical, economical and environmental points of views. Nevertheless, an attempt to point out the main advantages and drawbacks of each of the considered solutions in comparison with traditional overhead lines has been presented and is summarised in Table 5.1.4. It has to take into account that the estimated relative cost has to be considered as an approximation (the table has been constructed from numerous sources), and that more precise results would require a case-by-case analysis. Moreover, it is important to note that the cost of every design has been calculated for new lines. If the aim is making an intervention on an existing line, higher or lower cost could be obtained. Finally, in the case of passive and active loops, the estimated cost is only the compensating structure cost, not the line cost.

5.1.7 References

[1] B.J. Maddock: "Overhead line design in relation to electric and magnetic field limits". *Power Engineering Journal*, September 1992.

[2] H. Olsson, P. Pettersson, A. Eriksson: "Reduction of transmission line magnetic fields -possibility and contraints". *CIGRE* 1990 Session, paper 36-101.

[3] "Electric and magnetic fields produced by transmission systems. Description of phenomena - Practical guide for calculation". *CIGRE* Technical Brochure No. 21, 1980.

[4] EMFWorkstation 2.51, Electric Power Research Institute, 3412 Hillview Avenue, Palo Alto, California, 1996.

[5] The Fields 2.0 Program, Southern California Edison Company, 6090 North Irwindale Avenue, Irwindale, California, 1992.

[6] A.V. Mamishev, R.D. Nevels, B.D. Russell: "Effects of conductor sag on spatial distribution of power line magnetic field". *IEEE* Trans. on Power Delivery, Vol. 11, No. 3, pp. 1577-1586, July 1996.

[7] "National Electric Safety Code", 2002 Edition, IEEE, New York, 2002.

[8] IEC Standard 60071-2: "Insulation coordination. Part II. Application guide"

[9] V.S. Rashkes, R. Lordan, "Magnetic field reduction methods: efficiency and cost". *IEEE* Trans. on Power Delivery. Vol. 13, No. 2, pp. 552-559, April 1998.

[10] A. Eriksson, L. Söderberg, R. Ruritz : "Economical and technical conditions for the introduction of compact 420 kV AC and DC lines into Swedish urban areas. *CIGRE* Symposium, Leningrad, 3-5 June 1991.

[11] P. Villa, A. Bertazzi, M. Leva : "Compact transmission line with inverted delta configuration" . *CIGRE* 2002 Session, paper 22-103.

[12] R. Conti: "Riduzione del campo magnetico". AEI dic. 2001.

[13] T.J.F. Ordon, K.E. Lindsey, "Considerations in the design of three-phase compact transmission lines". *ESMO-95* Proceedings, pp. 108-114.

[14] M. Kuhlenengel, C. Landinger, S.Bello, G. Grenier, K. Psilopoulos, "Development and installation of a 69 kV Aerial Cable System". *IEEE* Transmission and Distribution Conference, vol. 2, pp. 836-41, Apr. 1999.

[15] T.J. Orban: "Spacer Cable Revisited", Transmission and Distribution World, Dec. 2002.

[16] Y. Ojala, T. Leskinen, M. Latineen, A. Hinkkuri: "110 kV overhead transmission Line with covered conductors", *CIGRE* 1998 Session, paper 22/33/36-10.

[17] "High Voltage overhead lines. Environmental concerns, procedures, impacts and mitigations". *CIGRE* Technical Brochure No. 147, 1999.

[18] G. Hennigs, A. Eriksson, U. Jonsson: "Compacted overhead lines with low magnetic fields". *CIGRE* 1996 Session, paper 22-204.

[19] "Electric and Magnetic Field Management Reference Book". Electric Power Research Institute, 3412 Hillview Avenue, Palo Alto, California, 1999.

[20] Yamazaki, T. Kawamoto, H. Fujinami: "Requirements for power line magnetic field mitigation using a passive loop conductor". *IEEE* Transactions on Power Delivery, Vol. 15, No. 2, Apr. 2000.

[21] A.R. Memari, W. Janischewskyj: "Mitigation of magnetic field near power lines". *IEEE* Transactions on Power Delivery, Vol. 11, No. 3, Jul. 1996. **

[22] P. Cruz: "Analysis, calculation and mitigation techniques of magnetic fields created by transmission lines" M.S. thesis (in spanish), Universidad de Sevilla, 2000.

[23] R.A. Walling, J.J. Paserba, C.W. Burns: "Series-Capacitor compensated shield scheme for enhanced mitigation of transmission line magnetic fields", *IEEE* Transactions on Power Delivery, vol. 8, No. 1, pp. 1577-86, Jan. 1993.

[24] A. Larsson, U. Jonsson, J. Sjödin: "Design, test and cost of a magnetic field cancellation loop near swedish 400 kV line", *Power Tech* Proceedings, Stockholm, Sep. 1995.

[25] B. Shperling, L. Menemenlis-Hopkins, B. Fardanesh, B. Clairmont, D. Childs: "Reduction of magnetic fields from transmission lines using passive loops". *CIGRE* 1996 Session, paper 36-103.

[26] EPRI Report, "Passive Shielding System for the NYPA 345 kV Cross-State Corridor", Report TR-111718, Dec. 1998.

[27] U. Jonsson, A. Larsson, J.O. Sjödin, “Optimized reduction of the magnetic field near Swedish 400 kV lines by advanced control of shield wire currents. Test results and economic evaluation”. *IEEE* Transactions on Power Delivery, Vol. 9, No. 2, pp. 961-969, Apr. 1994.
[28] P. Cruz, C. Izquierdo, M. Burgos: “Magnetic field mitigation in power lines with passive and active loops”. *CIGRE* 2002 Session, paper 36-106.
[29] H. Böhme, R. Paschen, A. Bertazzi, G.G. Di Marco, E. Elli, A. Catenacci: “Overhead transmission lines: design aimed to reduce the permitting time”. *CIGRE* 1998 Session, paper 22/33/36-07.
[30] P. Cruz, C. Izquierdo, M. Burgos: “Optimal design of active shielding for power lines”. 14th *Power System Computation Conference* Proc., Session 24, Paper 2, page 1, Sevilla 2002.
[31] P. Pettersson: “Principles in transmission line magnetic field reduction”. *IEEE* Transactions on Power Delivery, Vol. 11, No. 3, pp. 1587-93, July 1996.
[32] J.R. Stewart, S.J. Dale, K.W. Klein: “Magnetic field reduction using high phase order lines”. *IEEE* Transactions on Power Delivery, Vol. 8, No. 2, pp. 628-636, Apr. 1993.
[33] “Comparison of high voltages overhead lines and underground cables. Report and guidelines”. *CIGRE* Technical Brochure No. 110, Dec. 1996.
[34] “Overhead or underground? The National Grid Approach”. National Grid, UK, 2002.
[35] R.G. Olsen, D.C. James, V.L. Chartier: “The performance of reduced magnetic field power lines: theory and measurements on an operating line”. *IEEE* Transactions on Power Delivery. Vol. 7, No. 4, pp. 2046-53, Oct. 1992.
[36] J. Rogier, convenor, "The Influence of Line Configuration on Environment Impacts of Electrical Origin". *CIGRE* Technical Brochure 278, 2005.
[37] R. Conti, A. Giorgi, R. Rendina, L. Sartore, E. A. Sena: "Technical Solutions To Reduce 50 Hz Magnetic Fields from Power Lines". *Power Tech.* Proc., Vol. 2, Bologna 2003.
[38] R. Brown, T. Landers, J. Stewart, L. Oppel: “Six-phase succesfully applied to utility transmission system”. *CIGRE* 1998, paper 22/33/36-01.
[39] D. Tsanakas, G. Filippopoulus, J. Voyatzakis, G. Kouvarakis, “Compact and optimum phase conductor arrangement for the reduction of electric and magnetic fields of overhead lines”. *CIGRE* 2000, paper 36-103.
[40] Linear Research Associates, “Large-volume ELF Magnetic Field Compensation”. Interim Summary Report, Oct. 1995.
[41] M. Reta-Hernández, G. Karady, “Attenuation of low frequency magnetic fields using active shielding”. Electric Power System Research, vol. 45, pp. 57-63, 1998.
[42] A. Bazzani, M. Samanna, M. Bosco, “Analysis of a mathematical model to study reduction methods in the emission of magnetic field produced by high-voltage overhead power lines”. EMC Europe, Sep. 2002, Sorrento.
[43] M. Awad, M. Swidan, H. Moustafa, R. Radwan, “The egyptian experience for electric & magnetic fields and radio noise with compact and traditional towers”. *CIGRE* 1998, paper 22/33/36-09.
[44] R. Behncke, A. Clark, H. White, P. Opaschaitat, “500 kV compact line design for the greater Bankok area”. *CIGRE* 1998, paper 22/33/36-12.
[45] L. Yafang, Y. Yichao, W. Huiren, G. Xuehai, Z. Kaixian, D. Chun, G. Dongsheng, “Study of 500 kV compact transmission technology”. *CIGRE* 1998, paper 22/33/36-11.

Table 5.1.4 Main features of techniques proposed to reduce magnetic fields generated by HV and EHV overhead lines (in comparison with traditional design).

Technique	Advantages	Drawbacks	Voltage (kV)	Relative Cost[(1)](pu)	RF[(2)] 0/30/50 m	Relative cost/RF 30 m
Underground cables	- Small visual impact - No noise	- Bigger problems in network operation - Bigger complexity in fault repair and maintenance works with consequent increase in outage rates - Impact of trenches on flora and fauna - Bigger limitations in land use within ROW	132[(3)]	5 – 8	1.9/16.5/16.6	0.3 – 0.61
			400[(4)]	8 – 10	1.1/26.2.0/26.4	0.57 - 0.95
Moderately compact lines	- Lower visual impact due to the compacted design of the tower - Reduction of line surge impedance	- Reduced mechanical performances limiting their use - Heavy limitations in the possibility to carry out live line maintenance by using the available techniques and procedures	132[(5)]	0.95 - 1	1.2/1.4/1.4	0.71
			400[(6)]	0.95 - 1	2.2/2.4/2.1	0.42
Ultra compact lines			132[(7)]	1.4[(8)]	2.1/3.1/3.1	0.47
			400[(9)]	1.8[(8)]	2.9/3.8/3.5	0.47
Covered conductors			132[(10)]	1.25[(11)]	2.2/3.3/3.2	0.38
Split-phase lines	- Important reduction of line surge impedance	- Greater visual impact due to the bigger number of conductors and of mast complexity - Bigger structural complexity of masts and limitation in the possibility to carry out live line maintenance by using the available techniques and procedures	132[(12)]	1.4[(8)]	2.6/9.2/13.4	0.15
			400[(13)]	1.6[(8)]	3.6/6.0/7.7	0.27
Four-phase line	- Easy to adapt on existing portal lines		400[(14)]	-	1.4/3.6/8.8	-
Compensated passive loop suspended on external poles	- Feasible for already built lines - No need to stop service	- Greater visual impact due to the bigger number of conductors and the aditional loop supporting structures - Point-dependent effectiveness - Feasible only for local applications	132[(15)]	0.5[(16)]	1.2/11.0/9.1[(17)]	0.04
			400[(18)]	0.3[(19)]	1.6/14/8.5[(17)]	0.02
Active loop suspended on external poles	- Feasible for already built lines - No need to stop service	- Greater visual impact due to the bigger number of conductors and the aditional loop supporting structures - Complexity of the equipment - Low reliability nowadays - Point-dependent effectiveness - Feasible only for local applications	132[(20)]	0.35[(21)]	1.2/24.8/10.1[(17)]	0.015
			400[(22)]	0.25[(23)]	1.6/20.3/6.8[(17)]	0.012

[(1)]Relative Cost = capital cost of chosen design/capital cost of conventional three-height triangular line (132 kV simplex, Figure 5.1.) or horizontal line (400 kV, duplex, p-p distance = 9.7 m).
[(2)]RF: Magnetic field reduction coefficient or reduction factor = field of conventional line / field of chosen design.
[(3)] Underground configuration: flat; interphase spacing = 0.25 m; depth = 1.6 m.
[(4)] Underground configuration: flat; interphase spacing = 0.37 m; depth = 1.6 m.
[(5)] triangular "▷" configuration [12].
[(6)] Inverted delta configuration [27] (Swedish T-Tower).
[(7)] Inverted delta configuration [13].
[(8)] See [9].
[(9)] Inverted delta configuration, quadruplex, interphase distance = 4.2 m.
[(10)] Inverted delta configuration, p-p distance = 1.3; phase-to-pole distance = 1 m.
[(11)] See [16].
[(12)] See Figure 5.1.10.
[(13)] Pole-type support: p-p distance = 7.3 m; circuit-to-circuit distance = 9.3 m.
[(14)] p-p distance = 9.7 m.
[(15)] Horizontal line configuration (triangular not suitable), with p-p distance = 4.2 m; p-g distance = 6.3 m and loop of 400*25 m at 6 m of height, conductor resistance = 0.015 Ω/km, capacitor = 14 mF.
[(16)] It has been assumed that the line cost is 90,000 €/km.
[(17)] The field profile is not symmetric. Lower values are obtained for mitigation at the other side of the line.
[(18)] See Figure 5.1.14.
[(19)] See [23,28].
[(20)] Similar line than [(15)], with active loop of 400*25 m at 6 m of height.
[(21)] See [23,28]. It has been assumed that cost of power converter + control = 12,000 €.
[(22)] Active loop in the same location than passive one (Figure 5.14).
[(23)] See [23,28]. It has been assumed that cost of power converter + control = 9,000 €.

5.2 Overhead MV and LV distribution lines

The foundations underlying the mitigation of MF generated by MV and LV distribution lines is identical to HV and EHV lines. Therefore, the methods are sensibly the same, and this subchapter could be suppressed. However, some specific characteristics of these types of lines can make the mitigation strategy quite different, and therefore the solution adopted. It is not the aim of this subchapter to make a thorough revision of all the aspects around this topic, because it is out of the scope of the report, but to present some key ideas around the MF mitigation in these kind of lines, pointing out the major differences with the previously reported HV and EHV lines. More detailed analysis can be found in [1-6].

5.2.1 Comparison between distribution and transmission lines

The main differences between distribution and transmission lines could be summarized in the following:

- On a distribution line the magnitude of the current vary from the substation side to the end of the feeder, due to the presence of distributed loads [3].
- At distribution level there are different existent systems (3-wire 3-phase, 4-wire 3-phase, 2-wire 1-phase, 5-wire) where the neutral wire management broads from the absence in the line (case of primary distribution level in most European countries) to the presence together with the phase conductors and also multi-grounded (case of USA). This non-uniformity of the distribution lines systems makes more necessary to analyse in a case-by-case base technical and economical assessment of every mitigation method.
- Regardless of the distribution method, the current unbalance at distribution level is higher than at transmission level, and vary up and down the line [3]. This fact can make a mitigation method inefficient.
- The distribution systems that have a multi-grounded neutral wire, an unknown percentage of the neutral current flows into the ground or other conductive objects, making difficult to know the current path, and increasing the ground-level MF (chapter 2).
- The lower voltages between phases can make more feasible the use of covered and insulated conductors.
- In case of balanced current, due to the shorter phase-phase clearance the field mitigation is only of interest in an affected area near the line, typically 10 m. Due to the lower height of conductors, this makes more effective simply to raise the poles.

5.2.2 Mitigation methods for distribution lines

A summary of the methods is shown in Table 5.2.1 [4], where the typical MF reduction levels at 10 m from the line are shown. The highest mitigating methods are the ABC (Aerial Bundle Cable), the underground line and the spacer cable [7]. Their effectiveness is however conditioned by the absence of unbalance. Another main drawback of these methods is the cost. Their use is more feasible when other issues must be satisfied (reduction of visual impact, reduction of outages). A method less costly could be the split of the line, but it is also strongly conditioned by the unbalanced current. Other set of techniques (use of tree wires, armless construction and increase of ground clearance) are less mitigating-effective, but a significant reduction can be obtained, with the advantage of a lower cost and an allowed higher unbalance level, specially the increase to ground clearance. Eventually a compaction of the line can be tried, with no changes in the conductor, like reducing the span length or replacing string by post insulators. The reduction obtained is low, about 25-45 %, and the cost depends mainly of the original span lengths of the line section to be mitigated. A last technique, passive loop, has also been considered. The main drawback is that to obtain a reasonable reduction of about 35 % it is needed to use for the loop a conductor of much lower resistance (about 0.12 W/km) than conventional for MV lines, with the additional cost that it implies.

In addition to these general methods, for net current lines (e.g. multi-grounded 4-wire 3-phase) it is needed simultaneously to take control of the ground return current levels. Therefore, specific actions must be taken in this sense:

- Balance of phase currents by changing phase arrangement of loads connected to a 3-phase line [8] or converting laterals single-phase to 3-phase lines
- Increase of neutral conductor size
- Implementation of 5-wire system instead of 4-wire one [9].

Table 5.2.1 Main characteristics of different mitigation techniques.

Mitigation technique	Reduction level (%)	Installation cost	Global performance over conventional	Effect of unbalanced current
Small compaction	25-45	Low	Lower	Low
Crossarms ® armless	~ 60	Low/medium	Lower	Medium
Tree wires	~ 60	Medium	Higher	Medium
Spacer cable	~ 80	High	Higher	High
ABC	100	Very high	Higher	High
Underground line	~ 90	Very high	Higher	High
Phase split	70-80	Medium	Lower	High
Increase clearance to ground	25-60	Low/medium	Lower	Low
Compensation loop	35	Medium	Lower	Medium

Aerial Bundle Cable

The Aerial Bundle Cable consists on twisting the phase-conductors of the cable. An example is shown in Figure 5.2.1, where the magnetic field is reduced at ~60% with respect to the case of straight conductors. Anyway, it must be evidenced that the twisting produces a component of the magnetic field parallel to the conductor system which can alter the efficiency of possible conductors shields [10].

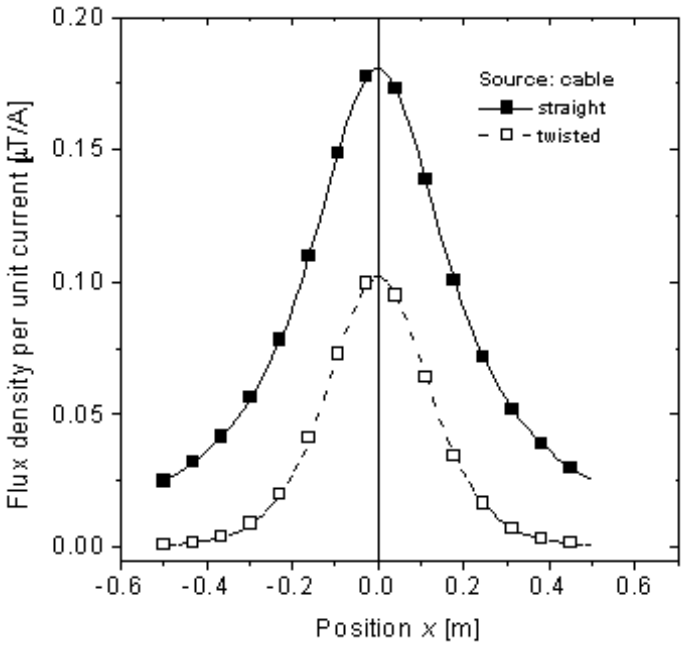

Figure 5.2.1 Effect of cable twisting. Diagram of *B* (unitary values) along a transversal direction at a distance from the cable of 0.2 m.

5.2.3 References

[3] E. A. Leeper: “Silencing the Fields. A Practical Guide to Reducing AC Magnetic Fields”. Symmetry Books, Boulder, Colorado, 2001.

[4] “Electric Distribution System Magnetic Fields”, Wisconsin Utilities Assoc., Madison, WI, 1993.

[5] S. Rodick, P. Musser: “Evaluation of measures and costs to mitigate magnetic fields from transmission and distribution lines”, 37th Rural Electric Power Conference, 25-27 April, 1993.

[6] P. Cruz: “Reduction of magnetic fields from overhead medium voltage lines”, 17th International Conference and Exhibition on Electricity Distribution (*CIRED*), Barcelona, 12-15 May 2003.

[7] B. Cestnik: “Consequences of Slovenian environmental legislation regarding non-ionizing radiation on new medum-voltages lines”, 16th International Conference and Exhibition on Electricity Distribution (*CIRED*), Amsterdan, 18-21 June 2001.

[8] A.S. Farag, J. Bakhashwain, T.C. Cheng, Y. Du, L. Hu, G. Zheng, D. Penn, J. Thompson: “Distribution Lines Electromagnetic Fields: Management and Design Guidelines”. Proceedings *CIGRÉ* Session, 2000, Paper 36-105.

[9] T.J. Orban: “Spacer Cable Revisited”, Transmission and Distribution World, Dec. 2002.

[10] T. Chen, J. Cherng: “Optimal Phase Arrangement of Distribution Transformers Connected to a Primary Feeder for System Unbalance Improvement and Loss Reduction Using Genetic Algorithm”. *IEEE* Transactions on Power Systems, Vol.15, No. 3, pp. 994 -1000, Aug. 2000.

[11] D. J. Ward, J. F. Buch, T.M. Kulas, W.J. Ros: “An Analysis of the Five-Wire Distribution System”. *IEEE* Transactions on Power Delivery, Vol.18, No. 1, , pp. 295 -299, Jan. 2003.

[12] L. Lindberg: “Reduction of magnetic fields from electric power and installation lines”. *IEE* Proc. Sci., Meas. Technol., vol. 145, no. 5, Sep. 1998.

5.3 Power cables

This sub-chapter addresses the different ways magnetic fields produced by power cables can be mitigated. The principles used are described in chapter 2 and more particularly in section 2.3. However, only methods that have been applied in the field or for which measuring results are available are presented here.

5.3.1 Relevant factors influencing the magnetic field levels

Before presenting the different mitigation methods it is worth recalling what are the main cable characteristics that will play a part in the generation of the magnetic field.

5.3.1.1 Cable formations

The reduction of ELF magnetic fields produced by power cables can become an important concern due to the fact that they are sometimes laid very close to inhabited areas.

As for overhead lines, the magnetic field due to power cables with balanced currents is proportional to the distance between conductors and normally inversely proportional to the square of the distance[14] between the observation point and the centre of the cable layout (cf. section 2.2). Therefore, even if the distance between conductors is much smaller than for an overhead line, in a narrow area above a power cable the magnetic field can be of the same order of magnitude or even higher than under an overhead line.

The main difference between an overhead line and an underground cable is the rapidity of decay of the field with the distance of the circuit.

Usually the cables are installed in a ***trefoil*** formation. This allows a good symmetry of the phases and, hence, no influence on the balance of the currents. Fortunately, it also gives rise to the lowest possible magnetic field pattern. However, when a very high current carrying capacity (ampacity) is required, it is not always possible to install the cables in trefoil. For thermal dissipation reasons some distance is needed between the conductors. In that case, the cables are usually installed in a ***flat (horizontal)*** formation with distances of several tens of cm between the axes of the conductors (typically 25 cm).

It is also important to note that the cables are practically always laid in flat formation (with a typical distance between cable axes of 40 or 50 cm) in the vicinity of the junction boxes. With such a layout, the magnetic field strength, in a limited area above the conductors, can become at ground level higher than that produced by an equivalent overhead line (cf. **Figure 5.3.3**).

As an example, **Figure 5.3.1** and **Figure 5.3.2** show, for both formations (assuming balanced currents) and for three different measurement positions above ground, the decrease of the field with the distance to the axis of the cable layout. In both cases, the cables are buried at a depth of 120 cm, have a diameter of 10 cm and are carrying a current of 1 kA. In the horizontal arrangement the distance between phases is 25 cm. In can be seen from these figures that the field ratio between both formations is about 3 (a factor 1.4 relative to the ratio between triangular and flat formation and a factor 2 relative to the mean distance between the axes of the cables).

Figure 5.3.3 shows the typical field pattern produced by both cable formations compared to that produced by a typical 150 kV overhead line[15]. It is important to note here that, contrary to the effect of the overhead line, the measuring distance above ground (or the cables buried depth) is very important for underground cables, at least in the direct vicinity of the link.

Besides the trefoil and the flat formation, other formations like the vertical formation are also sometimes applied. Details about their influence on the field levels can be found in [17] and in many other publications.

More examples of field patterns for different formations including the vertical one and the double circuits are described in [23].

[14] In some cases, however, the proportionality is linear or cubic

[15] Vertical formation with 10 m clearance to ground and 5 m between phases

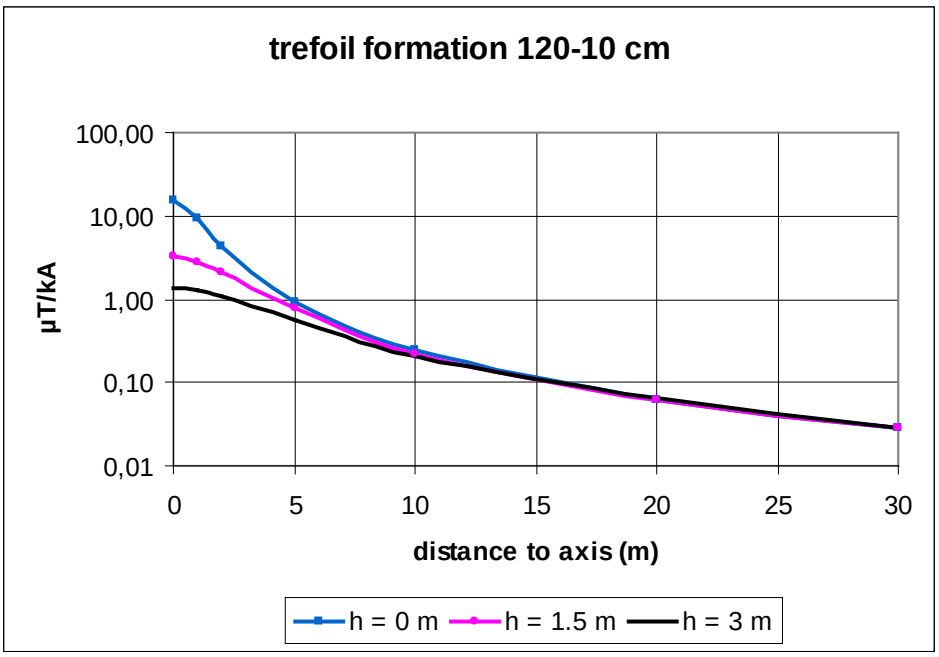

Figure 5.3.1 Trefoil formation - Field pattern at three different levels above ground (buried depth 120 cm, distance between axis of conductors: 10 cm).

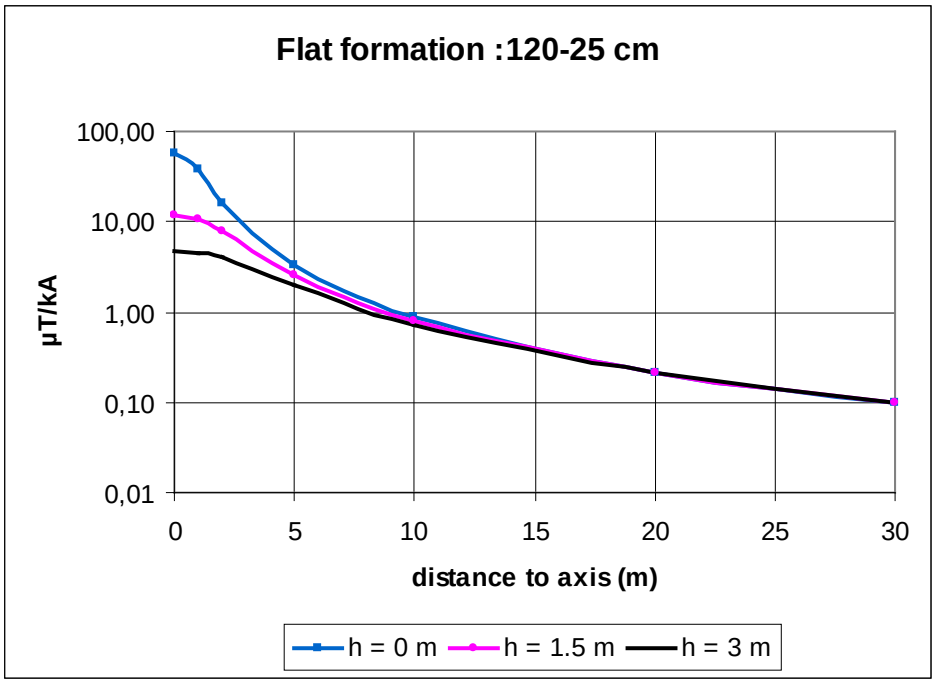

Figure 5.3.2 Flat formation - Field pattern at three different levels above ground (buried depth 120 cm, distance between axis of conductors: 25 cm).

The $1/r^2$ field decrease is only valid for single-core cables laid in flat or trefoil formations; for multiconductor cables like the classical MV lead-sheathed cables, the three conductors are normally twisted and form a helix with a pitch ranging from 1.5 to 2 m (about 1 m for overhead LV bundles).

This conductor arrangement greatly reduces the field at distances larger or of the same order of magnitude as the pitch[16]. Simplified expressions for calculating the field produced by twisted conductors can be found in [17], [19].

[16] The field decay becomes practically exponential

Table 5.3.1 gives the order of magnitude of the field produced by a LV bundle (or 3 conductors cable) and by a 3 conductor MV cable, both having a pitch of 1 m, in comparison with the same cables supposed to be untwisted (as in single core cables but with a smaller distance between the conductors). The currents are assumed to be balanced and equal to 100 A.

As seen from the table, at a distance to the cable equal to half the pitch, the field is already reduced by nearly a factor of 3, whereas at a distance equal to the pitch this factor raises up to 20.

Table 5.3.1 Typical magnetic field strength produced by a current of 100 A in MV and LV cables

Field level in µT for I = 100 A	Distance between conductors	Distance to the axis of the cable (m)				
		0.2	0.5	1	2	5
LV twisted bundle	15 mm	13	0.9	0.03	< 0.01	< 0.01
LV – not twisted	15 mm	16	2.5	0.6	0.16	0.03
MV – 3 conductors	30 mm	26	1.8	0.06	< 0.01	< 0.01
MV single core	30 mm	32	5	1.2	3.1	0.12

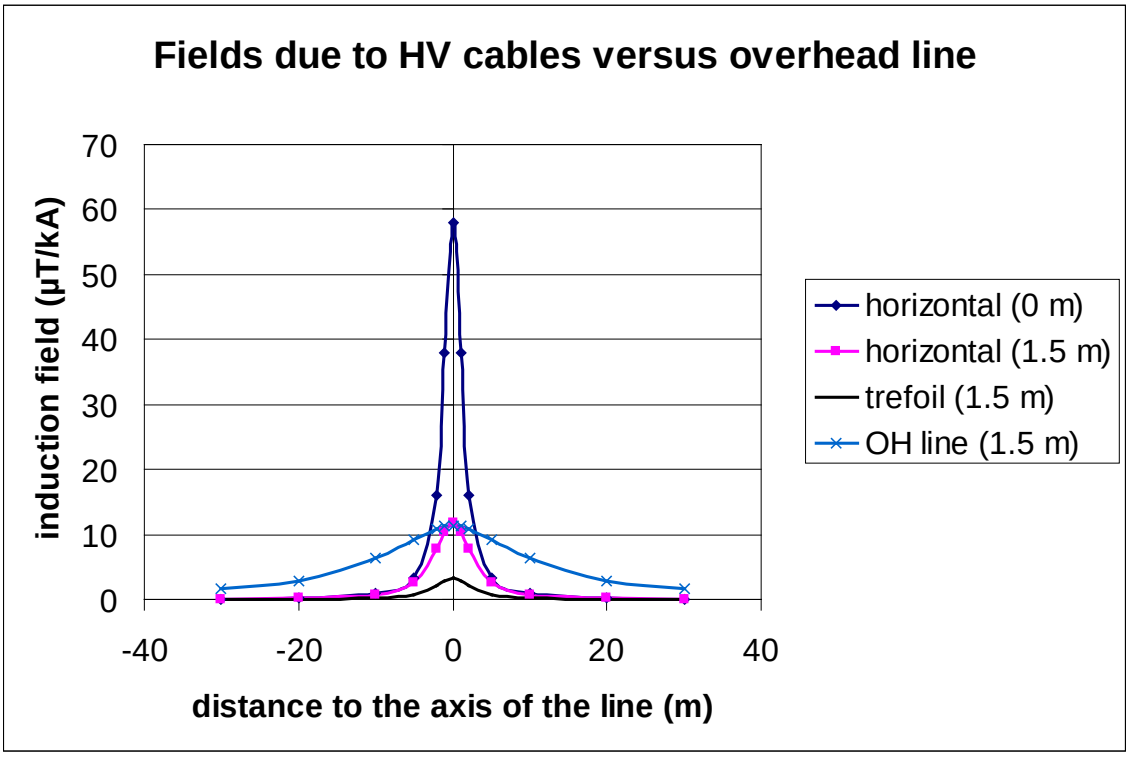

Figure 5.3.3 Comparison between underground cable and overhead line for two cable formations and measuring heights of 0 or 1.5 m above ground.

5.3.1.2 Cables led in ducts, pipes or tunnels

In most cases power cables are directly buried in the ground with or without the use of a specific backfilling (sand, dolomite…) in order to protect the cables against sharp rocks and/or to better control the heat dissipation.

However, in some cases ducts or pipes are first placed in the trench usually with one cable in each, or soil ducts are drilled and the cables are pulled into them afterwards,. Such methods, described in [23] and [24] are mainly used when the access to the cable is difficult or time limited during the installation (crossing of routes, vicinity of factories, urban area…) Ducts, generally embedded in concrete, are also used when it is impossible to bury the cables at a sufficient depth.

The main feature of these laying techniques, as far as magnetic fields are concerned, is that the distances between conductors and between conductors and ground level will generally differ from those of

classical buried cables. More particularly, the phase-to-phase distance of the classical trefoil formation is higher when the cables are led in ducts, leading to higher field levels. Also for the flat formation the phase to phase distance needs sometimes to be higher when the cables are led in ducts because the heat dissipation is not controlled as well as with the cables led directly in the soil.

Another laying technique is the use of tunnels that can be built for different purposes. The positioning of the cables in the tunnel (on steel trays, in concrete…) will depend on what the tunnel was built for (metro…). Vertical arrangements or arrangement with more than 2 circuits can easily occur. In all these cases, if mitigation methods need to be applied, it will probably not be just above the link, as for underground cables, but it can improve the reduction of the field below or beside the link.

5.3.1.3 Sheath currents - unbalanced currents

All the field levels mentioned in 5.3.1.1 have been calculated assuming balanced currents and no currents in the sheaths. This is only true for trefoil arrangements and/or for single point grounding of the shield/sheath.

In most practical situations with multi-point grounding (***solid bonding***), zero sequence currents and currents induced by the geometrical asymmetry of the layout will flow in the cable sheaths (and in the extra earth conductors if any) reducing the magnetic fields by the same mechanism as the passive loop technique (cf. 5.3.3) but also with the risk of reducing the ampacity [3], [15], [16], [26]. In order to avoid this ampacity reduction, the cable sheaths need to be specially designed (higher conductivity or cross section) leading to a higher diameter and a higher mechanical rigidity. Therefore, although useful for reducing the magnetic field, current flows in the sheaths are usually – at least in HV systems - avoided by periodic cross bonding of the conductors and/or the sheaths.

Unbalanced currents can always be considered as being the sum of three components: 2 symmetrical (balanced) components (direct and reverse) and a zero-sequence component. The total field results, of course, from the vectorial addition of the fields produced by each component separately. Knowing that the direct and reverse component of the total field differ only by their magnitude and by their phase angle rotation, their behaviour with the distance to the source and with respect to a possible mitigation technique (shielding) will normally be the same[17]. This is not the case for the zero-sequence components: Knowing that part of the zero-sequence currents returns to the source by the earth (instead of the cable sheath), they will produce magnetic fields decreasing linearly with the distance (instead of the distance squared). Moreover this part of the zero sequence field is not attenuated by the shielding methods described in the next sections[18].

5.3.2 Field mitigation by phase splitting

The phase cancellation technique described in chapter 2.1.3 can theoretically be applied for HV cables, e.g. by splitting two of the three phases in four cables and putting them symmetrically around the third phase leading to a layout of five cables (in flat formation or in a concentric formation). However, this solution, although very efficient for mitigating the field [26], is rarely applied, mainly due to its cost and to the difficulty to follow curves.

It has to be noted that the additional slitting of the third phase can be seen as the transformation of a single circuit cable to a double circuit with the suitable phase arrangement. However, in the most general case of a double circuit, the identification of the optimal laying configuration is more complex since it depends not only on the laying geometry of each circuit but also on the distance between the circuits.

In all cases, for the same number of individual cables and the same overall cross section, a compromise has to be found between the field reduction and the ampacity reduction.

5.3.3 Shielding by loop compensation (field cancellation methods)

As for overhead lines (see subchapters 2.2 and 5.1) it is possible, to some extend, to apply passive compensation for mitigating the field.

With a single cable circuit in flat formation the mitigation achieved remains however limited (about a factor of 2) as can be seen in **Figure 5.3.4** for a 132 kV cable in flat formation with a current of 250 A.

The effectiveness can be improved (by about a factor of 3) by adding a tuning capacitor but it remains an expensive solution due to the high capacitance value required for compensating the loop inductance. Smaller capacitances, however, could be obtained with a multiturn loop.

[17] Notwithstanding the fact that shielding techniques can introduce space asymmetries in the resulting field

[18] because the shield doesn't encompass entirely the circuit formed by the cable and its return path.

Higher effectiveness has been achieved without capacitive compensation for a double circuit link, as it is shown in chapter 6.2.

Although not highly efficient, loop compensation is an inexpensive technique that can sometimes be used in existing installations where the cables are led in tubes by pulling the loop across the existing tube (see example in chapter 6.2).

Several co-axial loops of the same diameter installed near each other to form a kind of coil can help in achieving an improvement of the shielding factor. This technique has been used for mitigating the field produced by junction boxes.

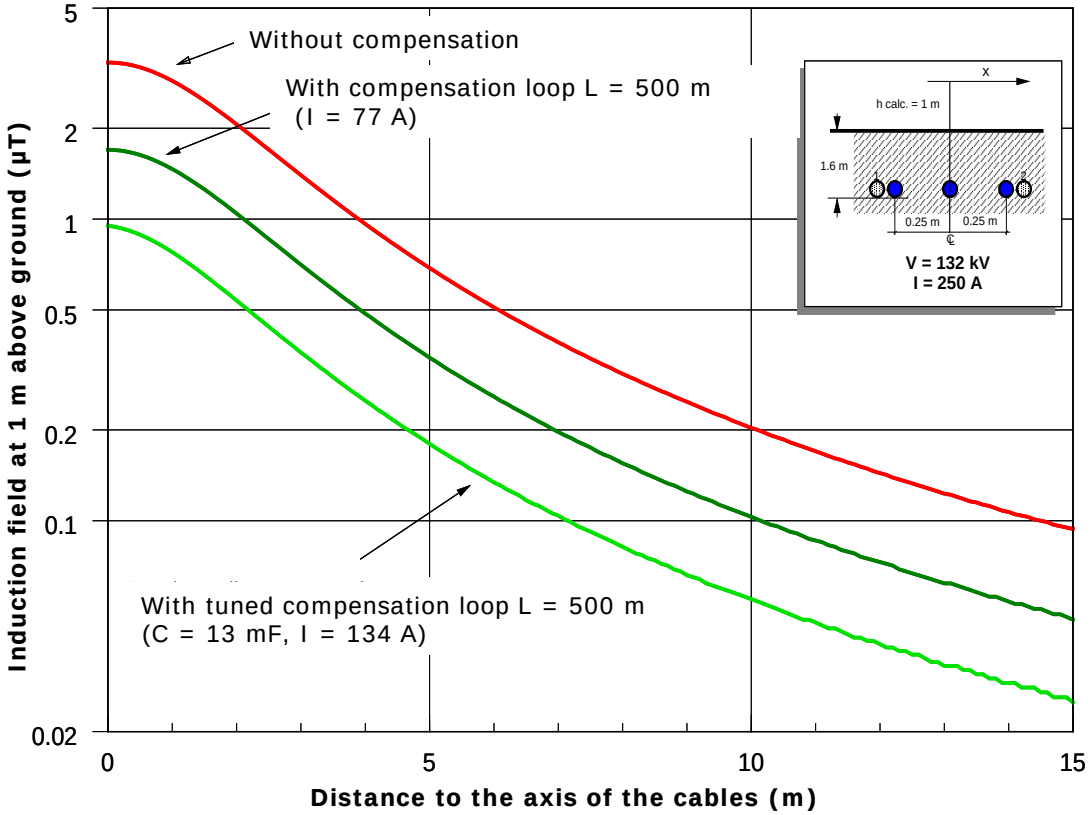

Figure 5.3.4 Field compensation by a single passive loop (with or without capacitive tuning).

5.3.4 Shielding with high conductivity materials

As explained in subchapter 2.3, the shielding mechanism involved with the use of high conductivity materials is basically the same as that occurring in the loop compensation technique or with multigrounded cables (without cross bonding), i.e. the induced currents (here eddy currents) produce a field that partly cancels the original field.

As far as conductive materials are concerned, two materials are usually considered: copper and aluminium. Both materials have their own advantages and disadvantages: Copper has a higher conductivity but also a higher cost[19] (and weight) than aluminium. Copper is also well known to withstand corrosion whereas the corrosion of buried aluminium is less known (cf. 2.3.5). Although copper is easier to assemble by soldering than aluminium, modern welding techniques under passive atmosphere (TIG…) also allow for the local assembly aluminium plates.

In the following sections mainly aluminium plates will be considered but the conclusions can easily be extrapolated to copper plates taking into account that 3 mm copper plates are more or less equivalent, as far as the shielding effectiveness is concerned, to 5 mm aluminium plates.

Three main layouts have been taken into consideration: flat (horizontal) screen or plane screen, U-shaped screen, and H-shaped screen and the open square screen.

5.3.4.1 Flat screen

A relatively simple way to mitigate the field produced by a 2 or 3 phases cable system ***in flat formation*** is to install horizontal plates as close as possible above or under the cable.

Screen thickness

Plates with 2 mm thickness already give fair results. However, the effectiveness clearly increases with the thickness as far as the latter remains smaller than the skin depth at power frequency (about 12 mm for aluminium, 9 mm for copper).

Screen width

As stated in chapter 2, the main problem with this kind of layout is that the shielding effectiveness usually strongly decreases with the distance to the centre of the plate, with, as a result, that the shielded field presents two peaks in the vicinity of the edges of the plate. To avoid this it is necessary to use a plate with sufficient width. Therefore it is suggested, as proposed in [11], to introduce the parameter $R = L/2h$ defined as the ratio of the screen half-width to the distance between conductors' barycentre and screen surface (assuming also the distance d between the conductors is small with respect to L).

It can be shown, for a two conductor circuit and a plate thickness of 5 mm, that R needs to be larger than 6 in order to obtain a field that remains always decreasing with increasing distance to the source (the so called "bell's behaviour"). Values of R larger than 2 need to be reached in order to reduce significantly the edge effects. With shielding of a smaller thickness the effectiveness, of course, is reduced together with the edge effects. Hence R can be reduced accordingly.

Screen continuity

For manufacturing reasons, the screen is normally divided into smaller elements placed near each other with or without air gaps.

It has been shown [12] that the shielding continuity between the different elements is not absolutely necessary. The presence of gaps reduces the eddy currents and the global shielding effectiveness but this effect decreases with the observation distance[20]. On the contrary, near the boundaries of the gaps, due to the fact that the eddy currents are flowing in opposite directions, there is a strong enhancement of the field which behaves a little like a compressed fluid leaking through the gaps. This enhancement remains even if the plates have a small overlap (but poor contact with each other). In fact, it decreases continually with the importance of the overlap, but it becomes difficult to estimate how far this decrease is due to the absence of a gap or to the increase in thickness. A good way to avoid this enhancement and to approach the theoretical

[19] And, therefore, is sometimes robbed when used as shield to protect the cables or to mitigate the fields !

[20] Even if this effect decreases with distance, the global shielding effectiveness remains lower in the absence of electrical continuity than in its presence. Hence, it is always advisable, for a single layer shield, to weld the plates together.

result achieved with a continuous screen is to use a double layer of aluminium plates, each layer being shifted by half the length of one plate with respect to the other layer, (as bricks in a wall). In this case the resulting effectiveness is close to that of a single continuous screen with the same global thickness.

It is important to note here, that the quality of the electrical contact between layers doesn't play any part in the shielding effectiveness.

Practical results with aluminium plates

Due to the relative little influence of the longitudinal subdivision of the screen, 2D numerical models based, among others, on the finite-element method (FEM) coupled with the boundary-element method (BEM) give fair results[21] and allow for any sensitivity analysis of the best solution for solving actual problems.

Figure 5.3.5 shows the comparison between calculation (2D FEM-BEM model) and measurements for a screen installed at 27 cm[22] above the axis of a three phases system in flat formation (distance between phases: 25 cm). The agreement is quite good although the calculation refers to a 6 mm continue screen (99.5 % aluminium), whereas the measurements are made on a 3 mm double layer discontinue screen.

It has to be noted, as already mentioned in chapter 2, that the shielding effectiveness decreases with the distance to the screen. In many cases this fact is not a major drawback because the non-mitigated field also decreases with the distance to power cables.

Figure 5.3.6 shows measurement results in a plane orthogonal to the cables for the same layout as in **Figure 5.3.2**.

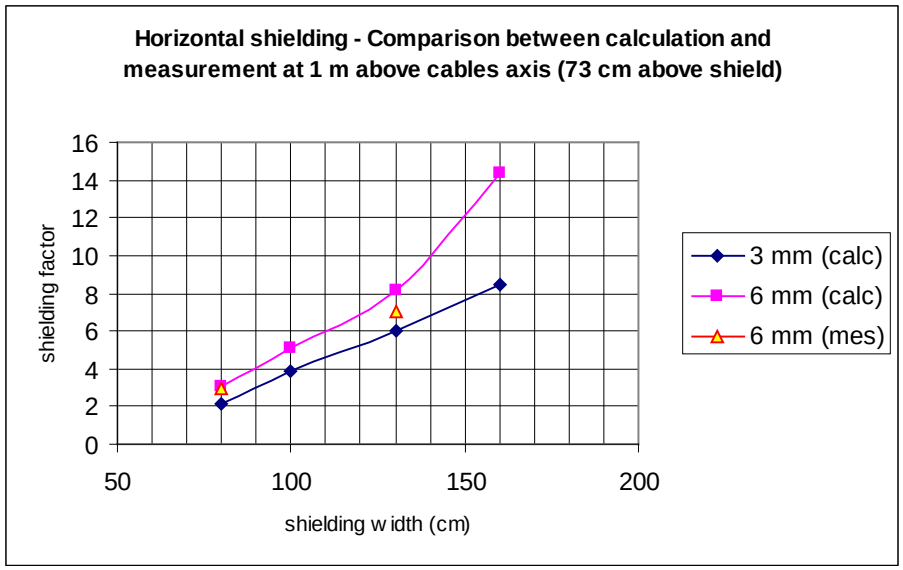

Figure 5.3.5 Shielding effectiveness of horizontal aluminium plates.

The screen is made of plates of respectively (length x width) 200 X 130 cm and 150 X 100 cm installed in double layer with total overlaps. The total length of the experimental full-scale model is about 8 m.

As in **Figure 5.3.5**, the graph shows clearly the influence of the factor *R* on the effectiveness: even a small increase of the screen width brings an important improvement on the global results. The figure also shows that the effectiveness decreases with the measurement height above the shielding and with the lateral distance. However, these observations are not necessarily confirmed by other experiences. In particular, concerning the effect of the decrease with the lateral distance, there is certainly an influence of the finite length of the model that reduces the shielding effectiveness at distance. The results shown are thus conservative.

Practical results with copper plates [21]

Using copper plates of 3 mm thickness and 1 m width installed at 10 cm above the axes of a flat formation of cables a SF of about 5 can be achieved at 2.5 m above the cable and of about 4 at some distance from the

[21] See section 3.2

[22] This corresponds to the typical thickness of a controlled backfilling (e.g. dolomite) above 2000 mm^2 alu power cables

link. Curiously about the same SF is achieved at distance when the screen is laid at the same distance from the cables but under the cables. Vertically above the cables the SF is however reduced to about 3.

With this layout the total Joule losses in the screen are about 20 to 30 % of the losses in the cable.

More interesting is the result achieved with copper plates installed at the same distance above and under the cables. In this case the SF is quasi constant and close to 20 !

Care must be taken when such high SF are achieved with conductive materials that the losses remain acceptable.

It has also been shown that the shielding effectiveness of a flat screen installed above and/or under a cable in trefoil formation was very poor (SF » 1.5).

Flat conductive shielding is thus not suitable in this case unless its width is very large [26]. This conclusion results also from the work presented in 5.3.6.2

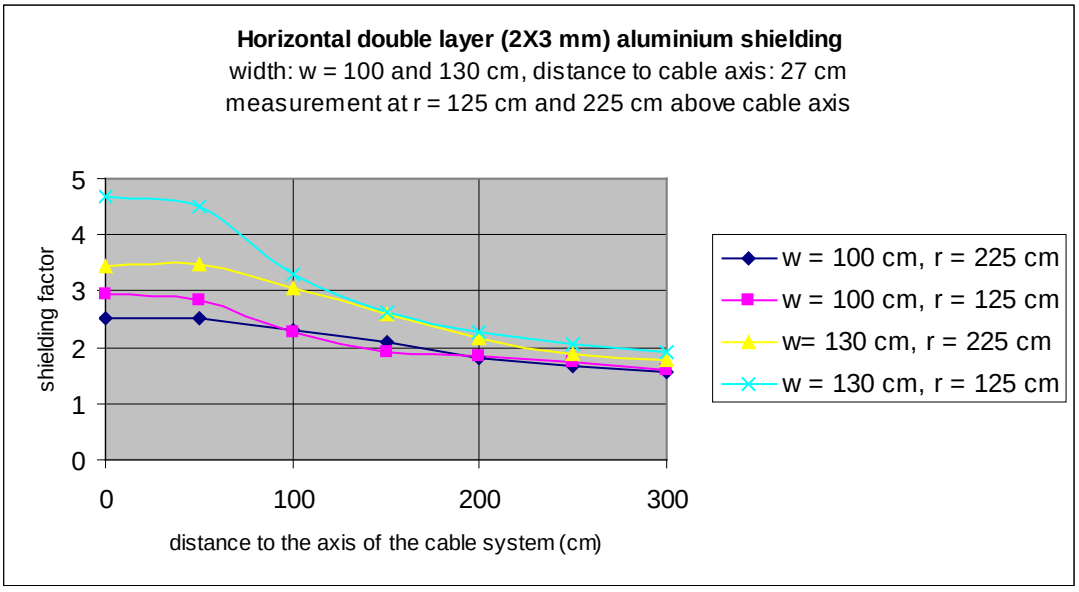

Figure 5.3.6 Decrease of the shielding effectiveness with the measuring distances.

5.3.4.2 U-shaped screen

It has been shown by many studies that the U-shape screen usually exhibits the best performances.

In fact, as shown in [12], for the same shielding area and contrary to what happens with ferromagnetic shields, a U screen has no greater effectiveness than a horizontal screen but it requires a narrower trench than that for a horizontal screen of the same total width before bending.

One problem, however, with U-shaped screens is that, contrary to what happens with plane screens, there is an absolute need to get a good contact between the vertical parts of each shielding element (assuming, of course, a non continuous screen).

This is schematically highlighted in **Figure 5.3.9** where the eddy currents flows freely in the horizontal part of the screen without the need to have a contact between plates, whereas, the induced currents cannot flow in the lateral part of the screen if there is poor electrical contact between successive elements.

This point is further discussed in the next section dealing with H-shaped screens.

Nevertheless, with the layout shown on figure 7, made of 2 mm plates of 100 cm (length) x 200 cm (width) formed to achieve vertical parts of 40 cm and bonded together (by bolds) in the longitudinal direction, a shielding factor of 4 has been achieved up to 1.5 m above the screen. This shielding effectiveness is also less dependent on the height of the measurement than with plane screens.

A shielding factor higher than 10 can be obtained with 5 mm plates welded together in order to achieve an excellent electrical contact. This is shown in Figure 5.3.8 taken from [22], where the comparison is made between the effectiveness of a flat screen and that of an inverted U-shaped screen of the same width (1 m) but not of the same area taking into account the “legs” of the U-shaped screen. In this figure the cable

carrying 375 A is led in horizontal formation at a depth of 160 cm with a phase-to-phase distance of 25 cm. The horizontal part of the screens is at a distance of 10 cm above the cables.

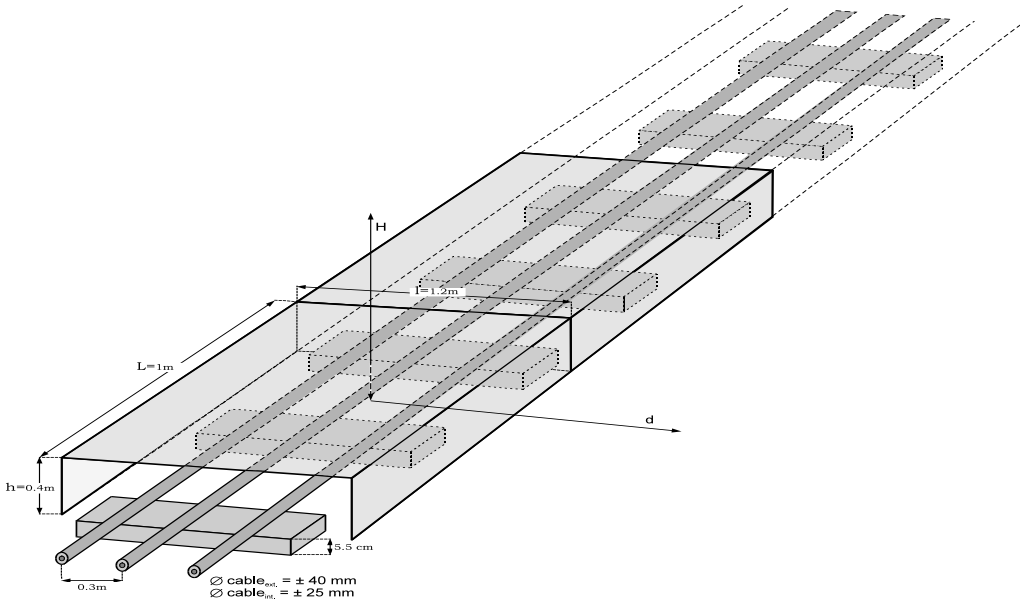

Figure 5.3.7 Typical U-shaped formation.

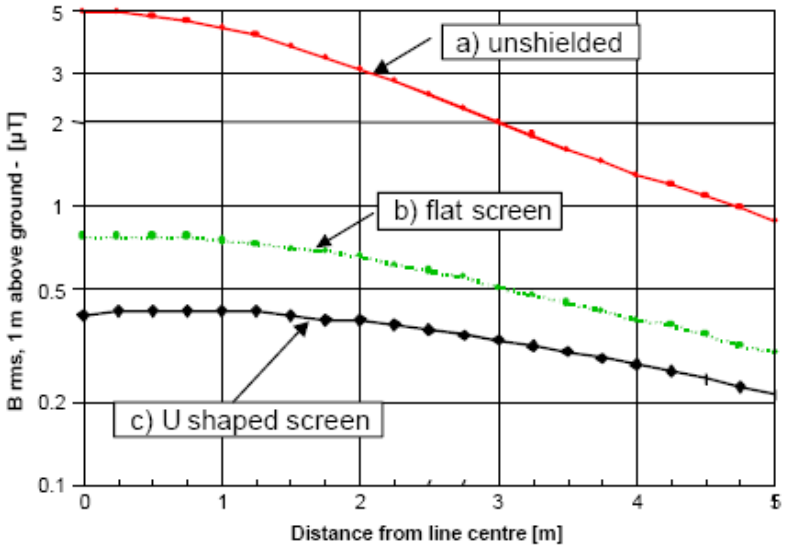

Figure 5.3.8 Effectiveness comparison between flat and U-shaped screens.

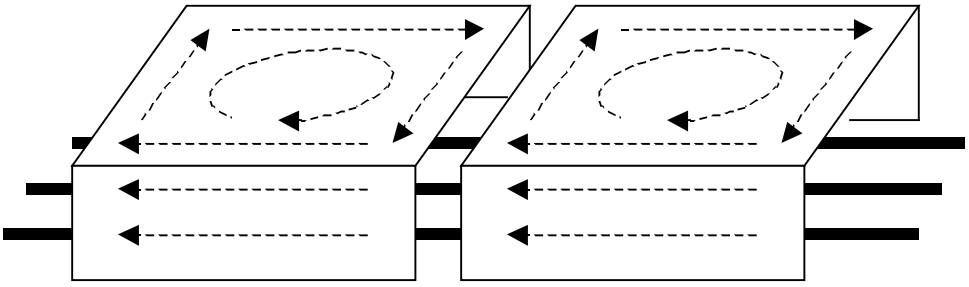

Figure 5.3.9 Induced currents in a U-shaped screen.

Another problem with U-shaped screens is their difficulty of installation. For cooling reasons, power cables need sometimes to be buried in a controlled backfilling (e.g. dolomite) that needs to be compacted. The presence of a U-screen layout makes the operation very difficult. For that reason, instead of using formed plates, it is easier to use an equivalent layout made of three plates: two vertical and one horizontal. This layout is known as the H-layout.

5.3.4.3 H-layout

In the H layout (**Figure 5.3.10**) and [18], two vertical plates are installed in the trench before filling with the first layer of backfilling. After the cable installation and a second layer of backfilling, the horizontal plates can be installed forming, with the vertical plate an H section.

Screen continuity

When 2D calculations are performed without explicit constraints for the currents, considering that the screen is infinite in the third direction, it is assumed that the sum of the induced currents in each part of the H (i.e. I1 for the horizontal plate, I2 for the vertical left plate and I3 for the vertical right plate) are equal to zero (I1 + I2 + I3 = 0), i.e. that the three parts are connected at infinity. The contact between vertical and horizontal plates is therefore only considered at infinity. Taking this assumption into account, it can be shown that the contact, and even the gap, between vertical and horizontal plates is not important at finite distance.

Actually, the screen is not infinite and it becomes necessary to assume that the induced current in each individual part of the shielding is zero at infinity (I1 = I2 = I3 = 0). With that hypothesis, however, the calculation shows that the screen is totally inefficient, even with a good longitudinal contact between plates !

However, if the assumption is that I1 = 0 and I2 + I3 = 0 at infinity or, in other words, that the circuit formed by the vertical plates is closed, the calculations show again a good shielding effectiveness.

Practically this results in two important factors:

1. Contrary to what happens with the plane screen, and likewise the U-shaped screen[23], a good continuity needs to be ensured between consecutive vertical plates.
2. The electrical circuit formed by the vertical plates needs to be closed at each extremity of the shielded area.

The value of the contact resistance between plates, although very important, needs not to be as low as the serial resistance of each individual plate because the inductance of the global circuit plays an important part in the limitation of the induced currents.

On the other hand, it has been shown experimentally that, for the flat cable formation, the longitudinal continuity of the horizontal plates is not important at all.

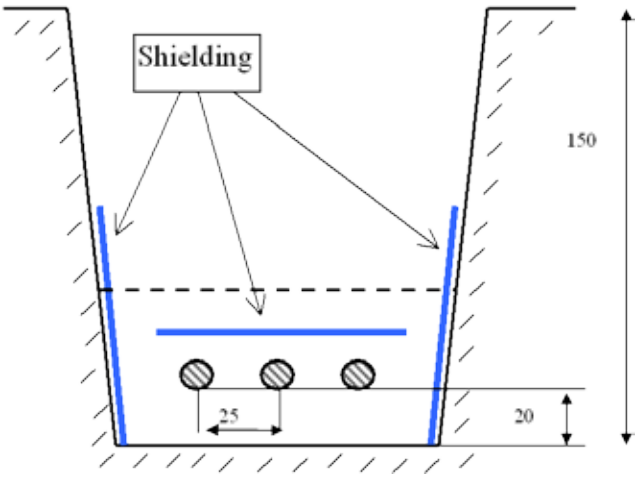

Figure 5.3.10 H-layout with typical distances for a flat formation (measures in cm).

[23] This longitudinal continuity seems however to be less important for U-shaped shields because, in each individual element, thanks to the continuity with the horizontal plate, the circuit is closed.

Screen thickness

Taking into account the limitation in shielding effectiveness due to contact between consecutive vertical elements, and on the basis of calculations, it can be shown that increasing the screen thickness above 3 mm does not bring a real improvement in the shielding effectiveness. On the other hand, for mechanical and corrosion withstand reasons, it is not safe to use screens that are too thin. Hence, the value of 3 mm seems to be a good choice for this type of aluminium shielding.

Shielding effectiveness

Depending on the dimensions of the screen and of the quality of contacts between the successive vertical elements, shielding factors ranging from 5 to 20 can be achieved with the flat formation (see **Figure 5.3.11**).

In any case the contact between plates has to be made by welding techniques.

For the trefoil formation, however, the shielding factor is smaller and it can be justified to add a forth plate under the formation (cf. 5.3.4.4).

It is also important to mention that the shielding, although symmetrical, introduces an asymmetry in the field pattern, which depends on the phases order rotation in the cables. In **Figure 5.3.11**, this order is TSR from left to right.

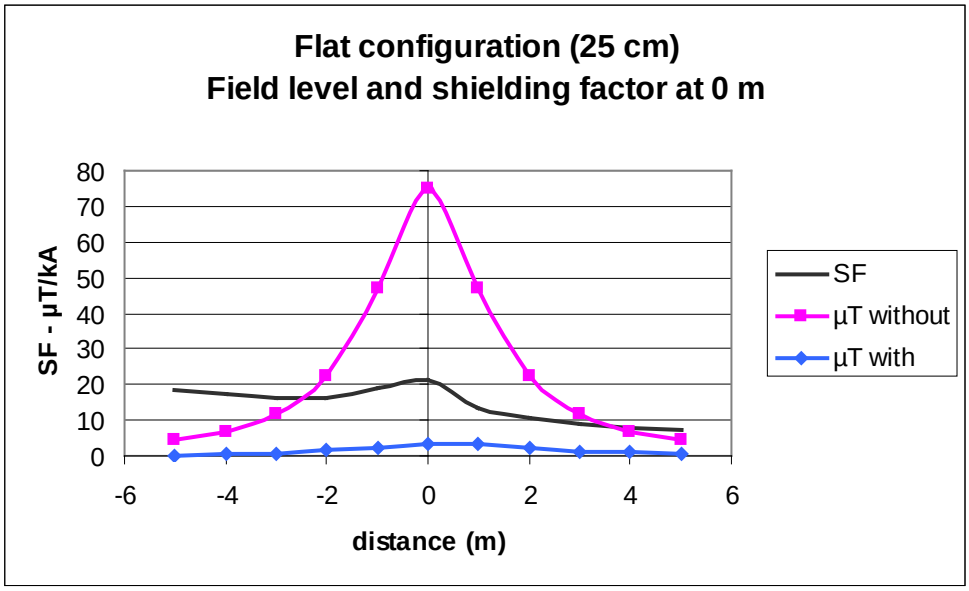

Figure 5.3.11 Flat formation - Calculated shielding factor (SF) and relative field (µT/kA) at ground level with and without shielding assuming a good continuity between vertical elements.

Losses

For the flat formation, although the current in the vertical plates can approach 1/3 of the current in the cables, the main (calculated) Joule losses are concentrates in the horizontal plates where they can approach half of the PU losses of the cable for a distance of 15 cm to the axis of the cables (typically 20 W/m, kA). These additional losses, however, have practically no influence on the thermal behaviour of the cables.

A practical example of this kind of H shielding technique is given in chapter 6.2.

5.3.4.4 Open square layout

For the trefoil formation, as also shown in 5.3.6.2, the effectiveness of the H layout is lower than for the flat formation. Therefore it is advisable to also add shielding plates under the cables in order to form, together with the other vertical and horizontal plates a kind of square or rectangle.

Contrary to what happens with the flat formation, there is a need, with the trefoil formation, to also ensure longitudinal continuity of the horizontal plates.

However, similarly to the H layout, no contact is needed between horizontal and vertical plates, except at the ends of the shielding section to allow closing the current loop (as with the H layout). In this way, a shielding effectiveness close to 10 can be achieved.

Figure 5.3.12 shows a practical example achieved on an existing 150 kV link. At both extremities of this 3 mm thick shielding (20 m length), small bridges (bended plates of 60 cm width) have been welded between the horizontal and the vertical plates in order to achieve the electrical continuity.

With this layout, a theoretical effectiveness of 9 has been computed. This could not be verified accurately by measurement because the mitigated field was of the same order of magnitude as the field produced by an overhead line located in the vicinity. However, the measurement indicated an effectiveness certainly higher than 6.

Losses

The (calculated) losses with the trefoil formation are significantly lower than with the flat formation in the H layout (about 1 to 5 W/m, kA).

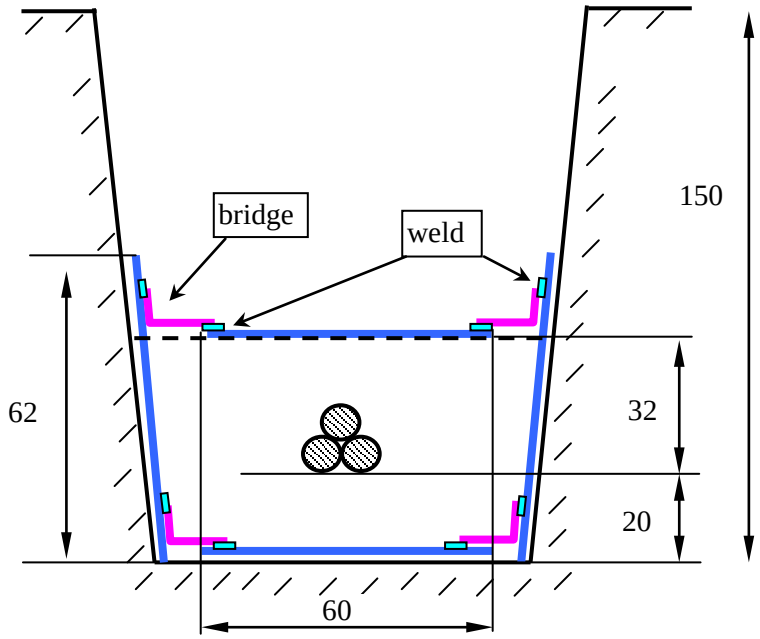

Figure 5.3.12 Open square-layout with typical distances for a trefoil formation (measures in cm)

5.3.5 Shielding with ferromagnetic materials

The second class of shielding materials concerns ferromagnetic materials and more particularly steel alloys like low carbon steels or grain oriented silicon alloys. These materials, as well as the physics of the involved mitigation mechanisms are described in section 2.3. As is highlighted in this section, both shielding mechanisms – the ***flux shunting mechanism*** and the ***eddy current mechanism*** – are also present.

5.3.5.1 Flat screen

It has been shown in chapter 2 that the effectiveness of open screens made of ferromagnetic material is usually weaker than that of equivalent high conductivity materials, mainly at some distance from the cables.

In particular for planar screens and for a flat formation of the cable conductors, ferromagnetic materials have always had a lesser effectiveness than conductive materials [17]. The contrary happens for a vertical formation, but vertical formations are not often encountered in practice.

At short distances from the cables however, (typically less than 3 m) and more particularly above the cables, a fair effectiveness can be achieved.

As an example, according to [14], a flat 5 mm steel plate with a permeability of 1000 and a width of 2 m installed at a height of 80 cm above the axes of a flat formation of cables leads to a SF of up to 5 at 2 m above the centre of the layout, up to 4 at a lateral distance of 1 m and about 2 at 2 m lateral distance.

A parametric sensitivity analysis shows that the optimum width is between 1 and 2 m; larger widths lead to an increase of the field at the edges of the plates. Also the distance between plates and cable reaches an optimum at about 80 cm.

5.3.5.2 U-shaped screen

As with conductive screens, the effectiveness of ferromagnetic screens increases when the screen is formed into an inverted U-shaped shield partly surrounding the conductors. According to [3] and [5], with 6 mm steel plates, shielding factors of up to 20 or 25 can be achieved just above the shielded area but, although not analysed in these experiences, the effectiveness decreases strongly with the distance to the conductors.

Therefore, as for the flat screen, unless for locally reducing the field, U-shaped ferromagnetic shielding doesn't seem to be an appropriate solution for mitigating the fields at distance.

5.3.5.3 Closed shielding

When the screen completely surrounds the three-phase cable system offering to the field lines a closed magnetic circuit, the shielding effectiveness can become very high. In this case, indeed, shielding factors up to 50 (or even higher depending of the steel magnetic properties and thickness) can be achieved as shown in **Figure 5.3.12** taken from [13]. In fact the shielding effectiveness becomes very sensitive to the permeability when the shielding is closed or exhibits a very small gap.

Other calculations based on the finite element method [14] lead to shielding factors of up to 25 using a rectangular duct of 5 mm thickness and a permeability of 1000. The authors of this paper, however, found an important sensibility related to the position of the cables within the tube. For good results the cable shouldn't lie directly against the shielding.

Parametric sensitivity analyses shows that a thickness between 3 and 5 mm is a good compromise between effectiveness and weight. Above 5 mm the improvement becomes negligible.

The effectiveness of a ***ferromagnetic tubular screen***, contrary to that of a conductive one, decreases when the diameter increases, but remains, for practical values (< 2 m), better than that of a conductive pipe of the same diameter [17].

However, in spite of its high effectiveness, the pipe system can lead to difficulties in the laying operations and in the successive pull-in of the cables, mainly for very tortuous paths.

Another way to achieve a ferromagnetic tubular shielding is to wrap several layers of magnetic-core laminates (used to manufacture magnetic cores for transformers) around cable circuit [9]. This method although quite efficient, remains difficult to apply in the field and requires special protection against corrosion.

The difficulties in achieving a tubular shielding can be overcome by using a more industrial approach – sometimes called the "***ferromagnetic raceway***" system - and highlighted in **Figure 5.3.13** taken from [20]; it allows for the cables to be laid in the shielding instead of drawing them in.. This technique is based on a closed conduit made of two parts, a base and a cover, and solidly fastened together by clips or by welding.

The effectiveness depends, of course, on the permeability of the material, but also – at least for very high permeability's – on the quality of the contacts between base and cover. However, contrary to the effect of high conductivity materials, it is the absence of gaps that is more important than the quality of the contacts.

With Ultra Low Carbon steel of maximum permeability 4900, shielding factors between 12 and 22 (depending of the contact pressure between base and cover) have been achieved at 1 m above soil with the cables buried at 1.6 m underground.

The system described in [20] and in [26] is modular with single pieces, 3 meters long that can be easily installed . Each section of the raceway has a slightly conical shape that allows for overlapping with the next section.

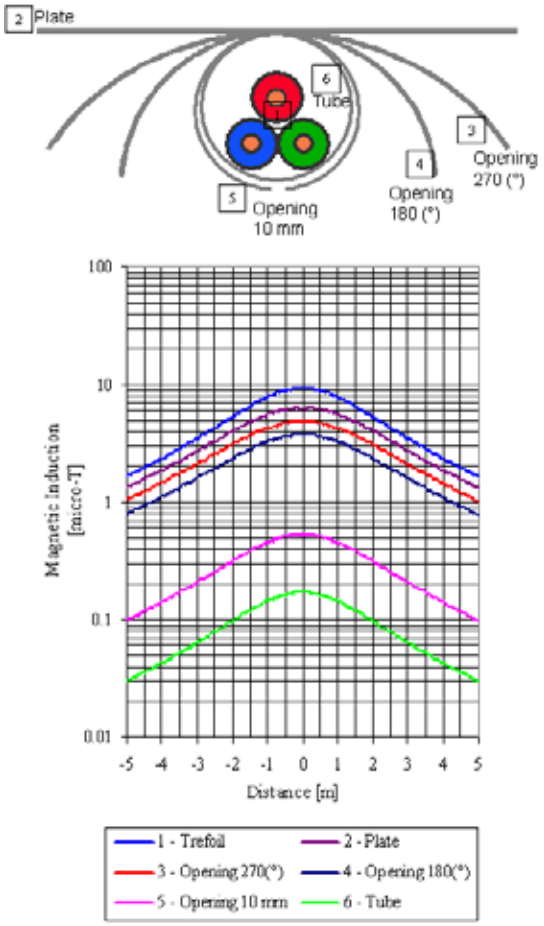

Figure 5.3.12 Increase of the shielding effectiveness with the screen progressively formed to produce a closed magnetic circuit around the source (field at 1 m above soil with 1500 A in the conductors).

5.3.5.4 Losses

The losses induced into ferromagnetic pipes can be computed according to IEC60287-1-1 (2.4.3 Losses in steel pipes) [25], where an empirical formula is given for the trefoil and cradle[24] formation. These two formations give substantially different values, so that the trefoil arrangement should always be preferred in order not to introduce a significant derating. Slightly different values are expected according to variations in the permeability and conductivity of the steel.

The losses induced into the raceway are similar to that computed for trefoil cables in ferromagnetic pipes, with the same mean raceway diameter and cable diameter. The result is the sum of the two effects due the use of better quality steel (loss reduction) and poor geometric factors (loss increase).

According to some calculations performed with ultra low carbon steel, losses should remain low (a few W/m, kA) , mainly due to the eddy currents (not to the hysteresis).

[24] Open formation laid on the bottom of the pipe

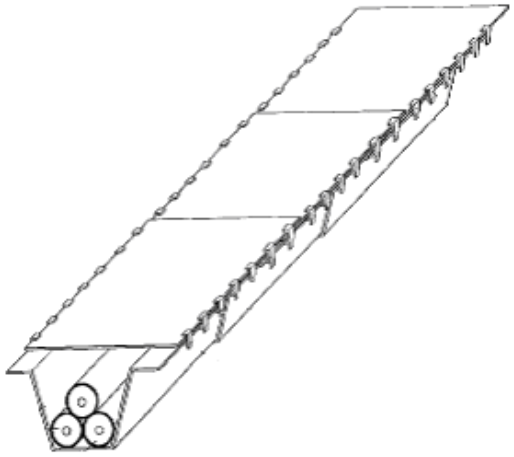

Figure 5.3.13 Closed ferromagnetic conduit comprising a base and a cover.

5.3.6 Comparison of methods' effectiveness

This section attempts to synthesise the main results presented in the previous sections, and taking also into account section 2.3.

5.3.6.1 Classification of the methods in the function of their effectiveness

In order to compare the different methods described above the authors of [26] have tried to give some quantitative information by calculating for a 1000 mm2 Al 150 kV single circuit cable system (single-core, 100 mm diameter, laying depth of the cable axis: 1.15 m, current: 1 kA) the maximum magnetic flux density (B_{max}) at ground level and the horizontal distance from the axis of the cable system (R_o) at which B at ground level becomes less than 3 μT. The results of these calculations are shown in Table 5.3.2 where they have been completed for the case of the H shaped aluminium shielding.

Table 5.3.2: Comparison of the main cable mitigating techniques.

	Mitigation solution applied to the reference conductor arrangement	**B_{max} (μT/kA)**	**R_o (m)**
0	Reference conductor arrangement: flat formation; phase to phase distance: 250 mm.	63.0	5.3
1	Changed conductor arrangement: plane configuration; phase to phase distance: 100 mm.	26.0	3.2
2	Changed conductor arrangement: trefoil; phase to phase distance: 100 mm.	19.5	2.7
3	Split-phase configuration: two of the three phases are split in four cables and put symmetrically around and in contact with the third phase cable.	2.4	0.0
4	Solid bonding (3 mm thick aluminium sheath).	15.0	2.4
6	Installation of a passive loop (close to the external phases)	26.5	3.2
7	Installation over the cables of a plane aluminium shield (width: 1 m; thickness: 5 mm – shield-to-cable distance: 50 mm)	10.9	2.4
8	Installation over the cables of a U shaped aluminium shield (width: 0.7 m; height of vertical lateral parts 0.15 m; thickness: 5 mm – shield-to-cable distance: 50 mm)	7.6	1.4
9	Installation over the cables of a H shaped aluminium shield (width: 0.9 m; height of vertical lateral parts 0.8 m; thickness: 3 mm – horizontal shield-to-cable distance: 150 mm)	3.1	0.5
10	Pipe or raceway type, high permeability ferromagnetic shield (cables in trefoil configuration)	<< 3.0	0.0

5.3.6.2 Shielding effectiveness versus configurations and material used

A direct comparison of different configurations with cables in either flat formation or trefoil formation has been performed at the Unit of Applied Electricity of the University of Liège. In each case, the two main shielding materials currently used, aluminium and steel, are compared in order to highlight the two shielding mechanisms.

Particular attention is drawn to the importance of the contacts between the different parts of the shield. The main results of this study are presented here.

It has to be noted that the purpose of these calculations in no way to define a master choice but just to show the complexity of the shielding mechanisms and the influence of each parameter on the shielding effectiveness. In particular the choice of other material properties (copper instead of aluminium, high permeability steel) can lead to different results.

Configurations

The source of the magnetic field is given by three-phase cables in both flat and trefoil formations. The screens are made of a maximum of four plates in perfect electrical contact or not. The material is either aluminum ($\sigma=3.8\ 10^7\ \Omega^{-1}m^{-1}$) or steel ($\mu_r=500$, $\sigma=10^7\ \Omega^{-1}m^{-1}$). It is important to note that the absence of electrical contact between plates of ferromagnetic material does not mean the presence of any gap and, hence, any change in reluctance.

For the flat configuration, the distance between the cables axis is 25 cm and the screen dimension is 80 cm x 30 cm.

For the trefoil configuration, the distance between the cables axis is 11 cm and the screen dimension is 40 cm x 40 cm. The shield thickness is 3 mm. The reference RMS current in the cables is 1000A.

All the considered configurations aim either to confirm some previous results presented in this chapter and chapter 2.3 or to give complementary results.

The shielding factor is computed for all the cases and is shown via numeric values on a grid in the vicinity of the shield (the grid step in both horizontal and vertical directions is 0.20 m)[25]. As an advantage of such a representation, a quick look at the shielding factor at several positions or along various directions all around the shield can be obtained without limiting the solution to particular horizontal or vertical distributions. A direct comparison between shielding factors for different configurations is also made possible.

In addition, for each configuration, the kind of shielding effect is illustrated in the corresponding map via the drawing of the flux lines (the zero phase of the left cable is chosen as a reference), showing either a flux compression or a flux shunting. Contour lines of the RMS magnetic flux density are also shown around the shields; the first inner line indicates the 20 mT level, decreasing by successive steps of 2 mT from one line to the other. The smaller the region inside the inner line, the higher the shielding effect.

For a parallel presentation of the results with flat and trefoil formations, the corresponding figures have the same numbering.

Results and comments for the cables in flat formation

The shielding factors obtained with a closed shield made of aluminium and steel plates with perfect electrical contacts between all or some plates, or no contact at all, are shown in **Figure 5.3.14**.

It can be seen that the electrical contacts, more particularly between the vertical plates, are always in favor of a good shielding effectiveness. With the steel plates, in the absence of a good contact, a maximum shielding factor is obtained in the direct vicinity of the shield while it rapidly decreases at distance up to a constant value. An increase of the magnetic permeability of the plate can, to a certain extent, lead to an increase of the shielding factor.

A reverse U-shape shield is considered as well in **Figure 5.3.15**, showing again the importance of good electrical contacts, mainly between the two vertical plates. These plates are indeed to be connected at their ends to offer a large loop, from one side to the other, to the eddy currents.

A shield made of two horizontal plates on both sides of the cables is shown to give the same shielding factor irrespective of the electrical contact between the plates (**Figure 5.3.16**). In this

[25] It is important to note that the computed figures cannot always be extrapolated at large distance from the shield, mainly when it is made of steel (ferromagnetic material)

configuration, the aluminium plates give a better shielding factor than the steel plates, which is also the case for the single horizontal plate above the cables (**Figure 5.3.17**).

A shield made of two vertical plates to the left and right sides of the cables is shown to be only efficient if a good electrical contact between the plates exists (**Figure 5.3.18**). The aluminium plates here also give a better shielding factor than the steel plates.

Results and comments for the cables in trefoil formation

The shielding factors obtained with a closed shield made of aluminium or steel plates with perfect electrical contacts between all or some of them, or no contact at all, are shown in **Figure 5.3.20** and **Figure 5.3.19**. It is important to note that the influence of the contact between plates is similar for both materials. This feature highlights the fact that the eddy currents also play an important part in the use of ferromagnetic materials.

Contrary to the effect of the flat configuration, a good contact only between the vertical plates (including the closed loop at the shield ends) is not sufficient to ensure a high effectiveness; a good contact needs to be made also between horizontal plates. The same conclusion applies for the reverse U shaped shield (Figure **5.3.20**) and, logically, shields made with only vertical or horizontal plates are less efficient.

Generally speaking, the shielding effectiveness appears always to be smaller in comparison with the flat layout, at least for the aluminium shielding. This statement, however, needs to be addressed carefully. Indeed the size of the shield has been significantly reduced when moving from the flat formation to the trefoil formation, whereas it is well known that the effectiveness of conductive materials increase with the size of the screen.

This feature is highlighted in Figure **5.3.23**, where for the same configuration as in **Figure 5.3.20** (top), i.e. for a perfectly closed shield, the size of the plates is increased from 40 cm up to 80 cm. In particular with a shield of 55 x 55 cm, the amount of material is exactly the same as for the flat formation. In this case the loss of effectiveness of the aluminium with respect to the flat formation is only about 20 %.

Cables in flat formation

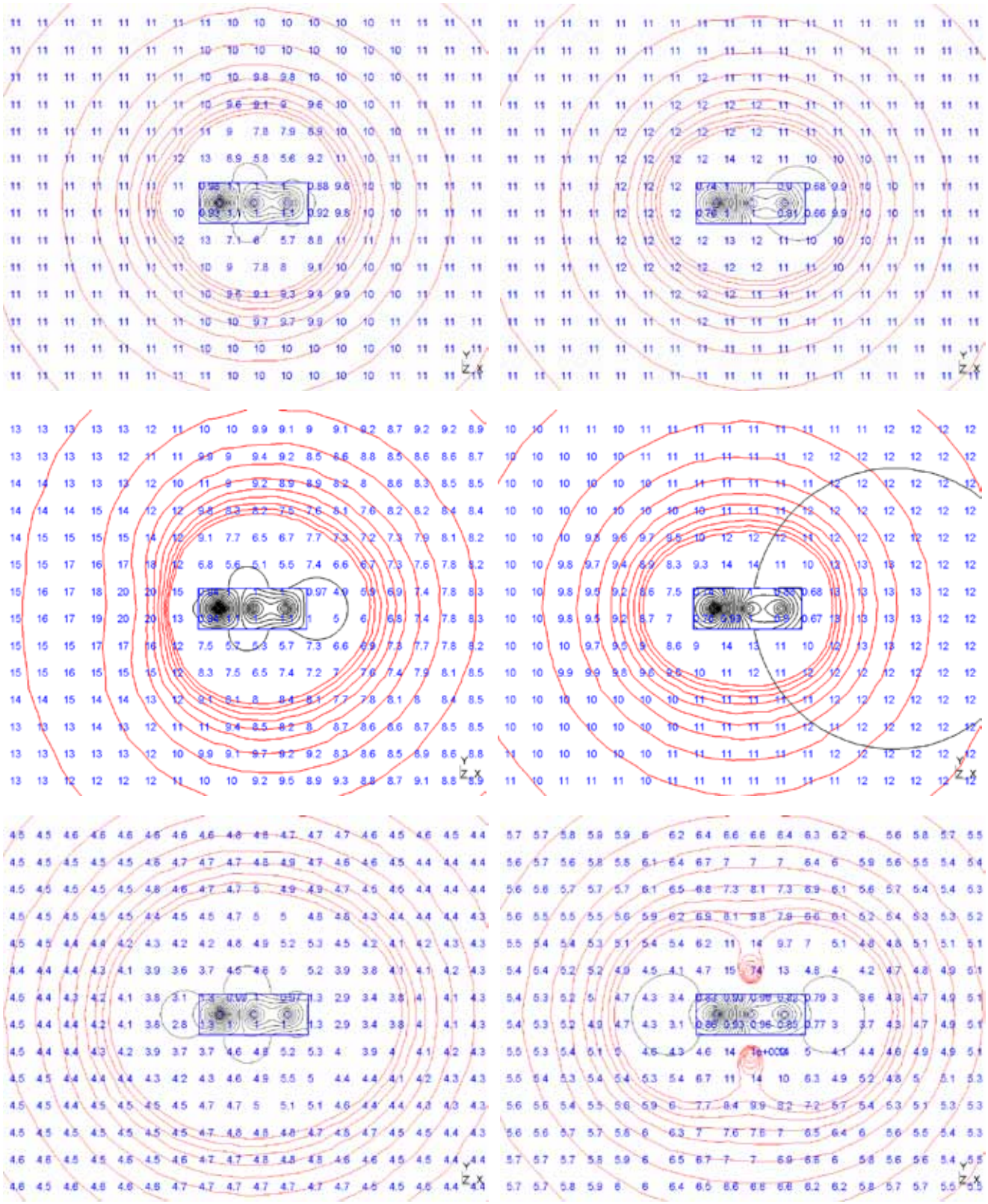

Figure 5.3.14 Shielding factor maps for a closed shield (*left:* Aluminium, *right:* Steel);
- Perfect electrical contacts between all plates (*top*),
- Perfect electrical contacts between the vertical plates only or between respectively the vertical plates and the horizontal plates (*middle*)
- No contact (*bottom*).

The grid step in both horizontal and vertical directions is 0.20m.

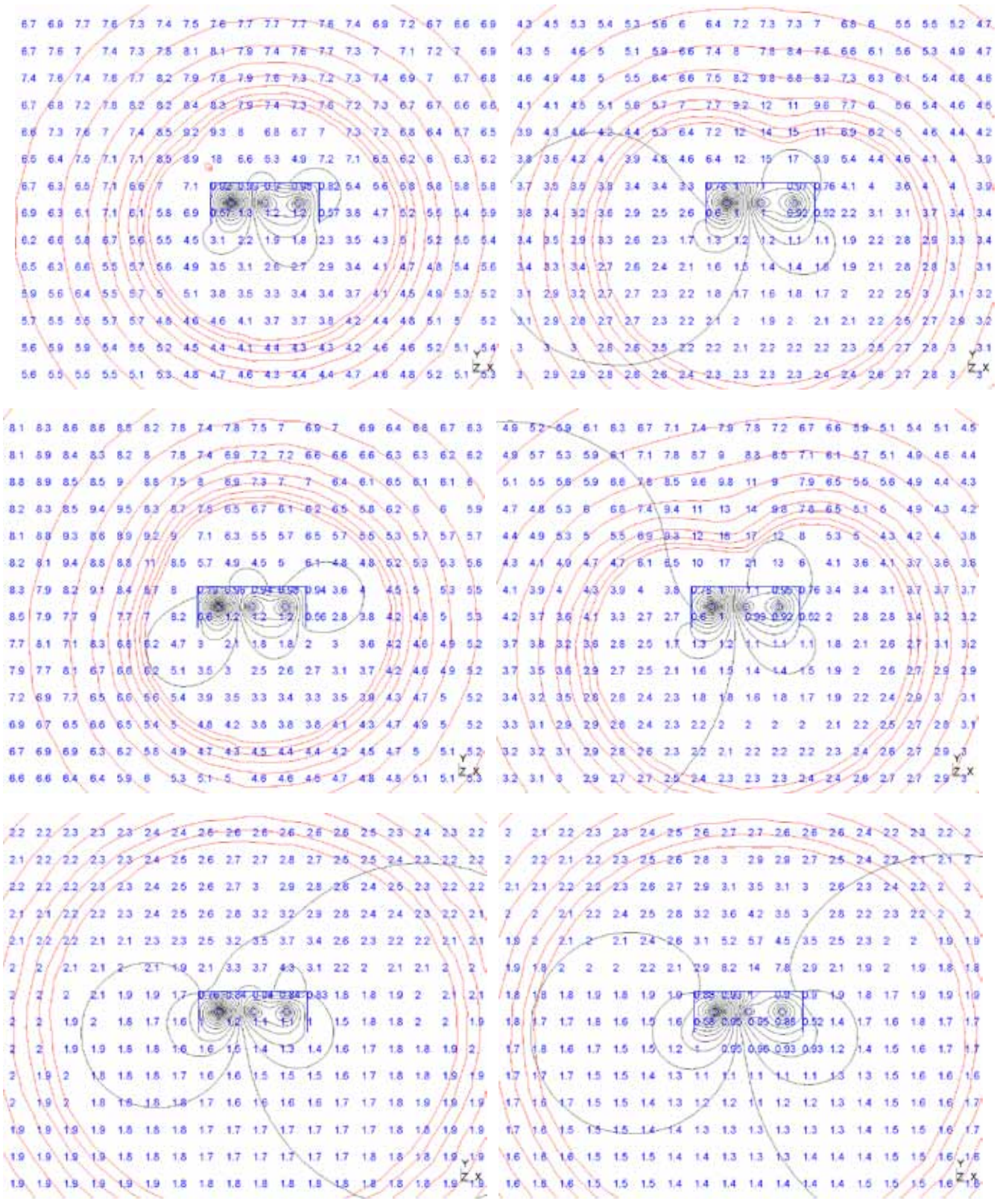

Figure 5.3.15 Shielding factor maps for a reverse-U shield (*left:* Aluminium, *right:* Steel)
- Perfect electrical contacts between all plates (*top*)
- Perfect electrical contacts (at plate ends for loop connection) between the vertical plates (*middle*)
- No contact (*bottom*).

The grid step in both horizontal and vertical directions is 0.20m.

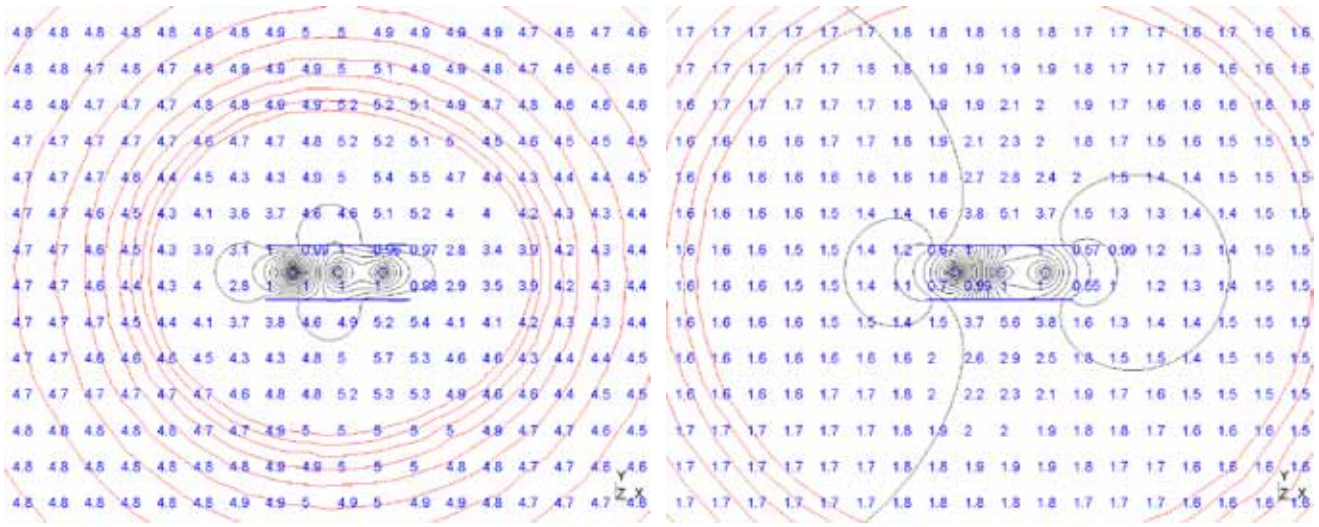

Figure 5.3.16 Shielding factor maps for two horizontal plates above and bellow the cables with or without perfect electrical contacts at plates ends for loop connection (*left:* Aluminium, *right:* Steel)

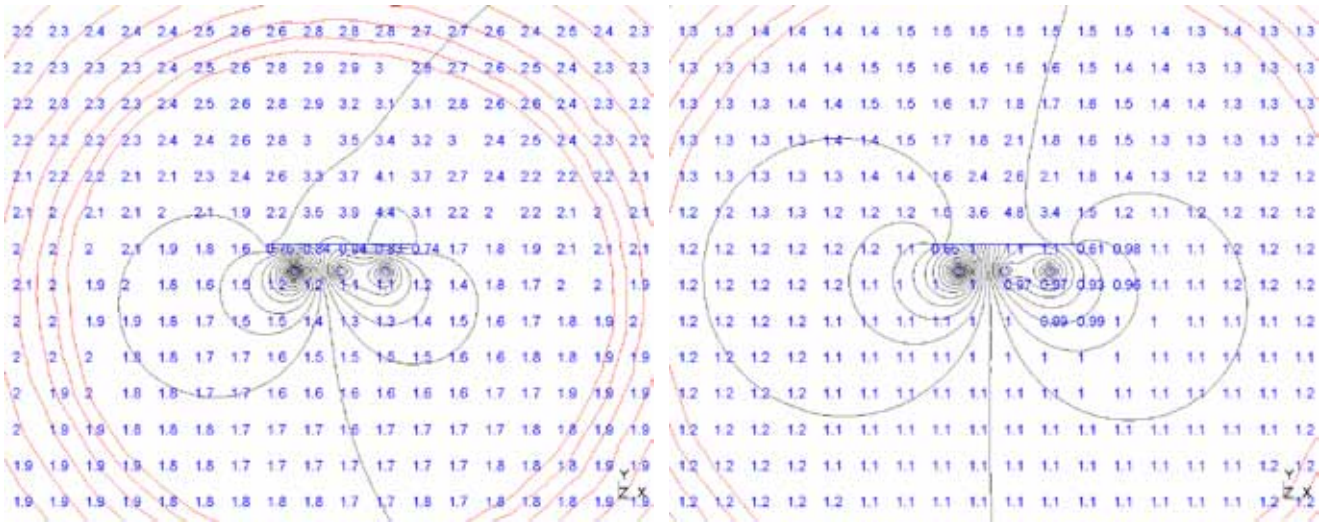

Figure 5.3.17 Shielding factor maps for a single horizontal plate above the cables (*left:* Aluminium, *right:* Steel).

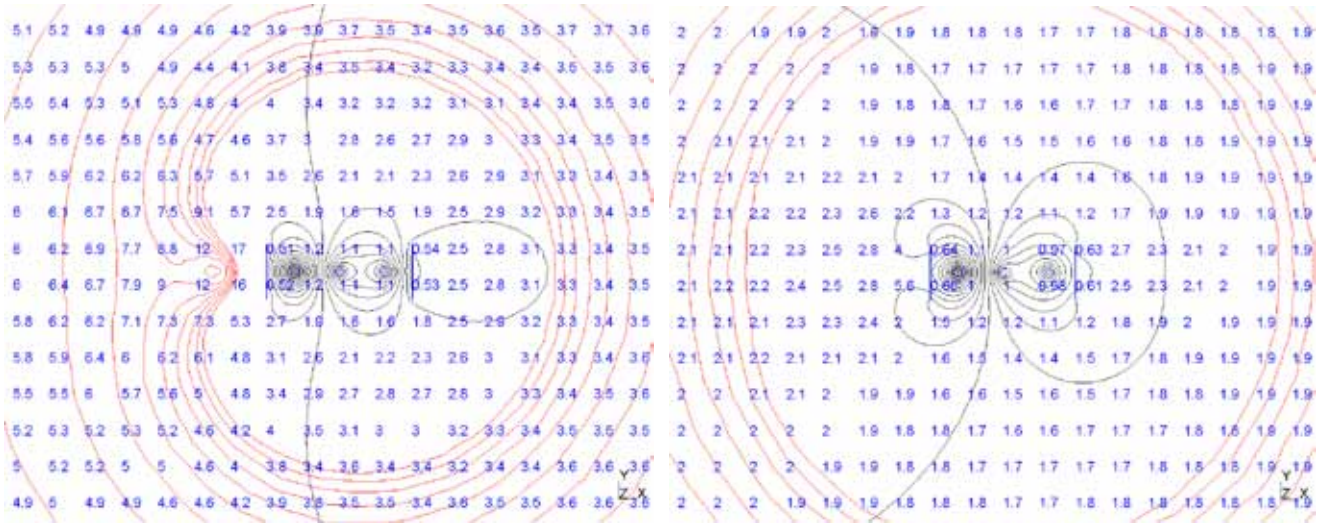

Figure 5.3.18 Shielding factor maps for two vertical plates on left and right sides of the cables with perfect electrical contacts between the plates at plate ends for loop connection.
(*left:* Aluminium, *right:* Steel)
The grid step in both horizontal and vertical directions is 0.20m.

Cables in trefoil formation

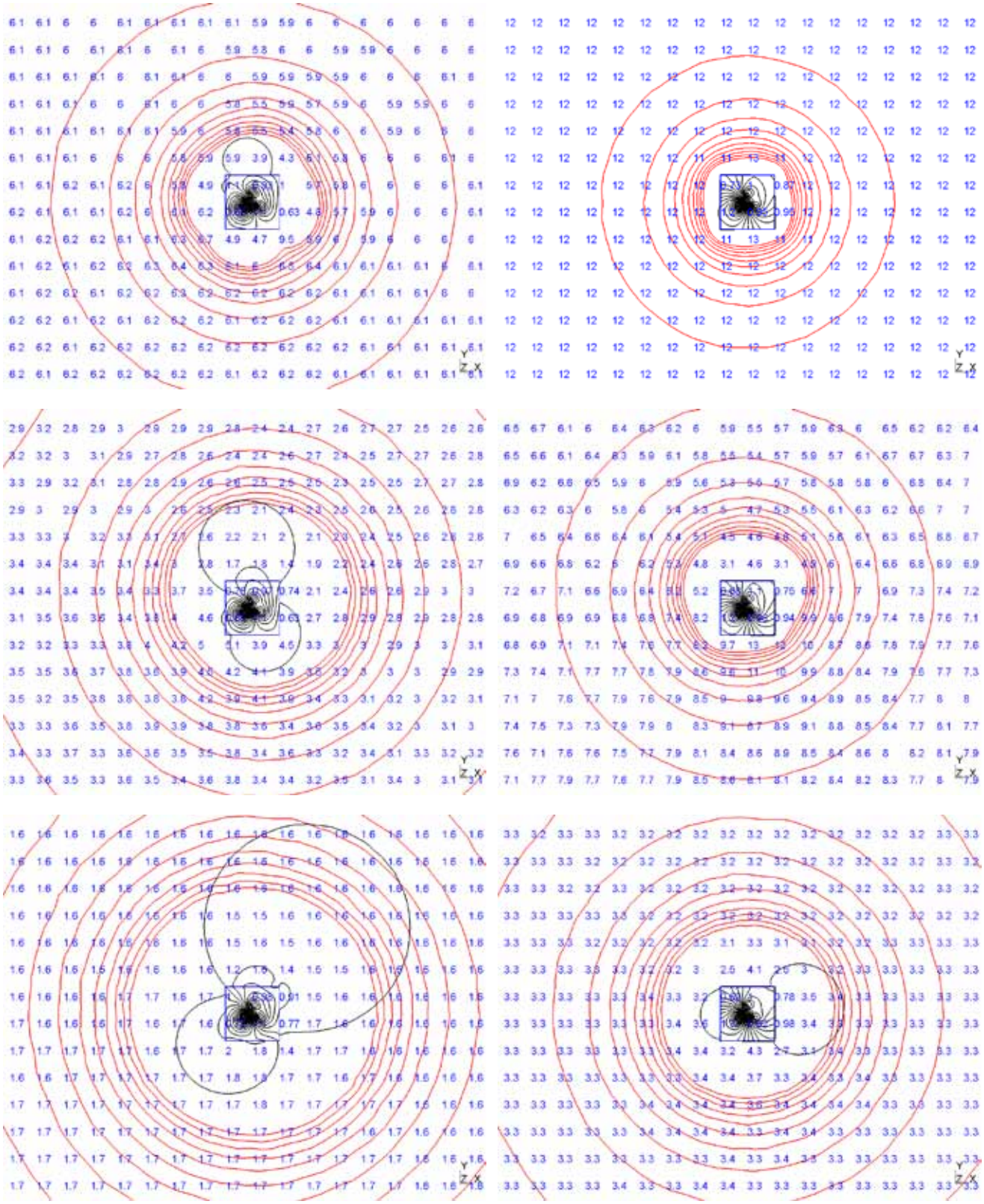

Figure 5.3.20 Shielding factor maps for a closed shield (*left:* Aluminium, *right:* Steel)
- Perfect electrical contacts between all plates (*top*)
- Contacts only between the vertical plates and the bottom plate (*middle*)
- No contact (*bottom*).

The grid step in both horizontal and vertical directions is 0.20m.

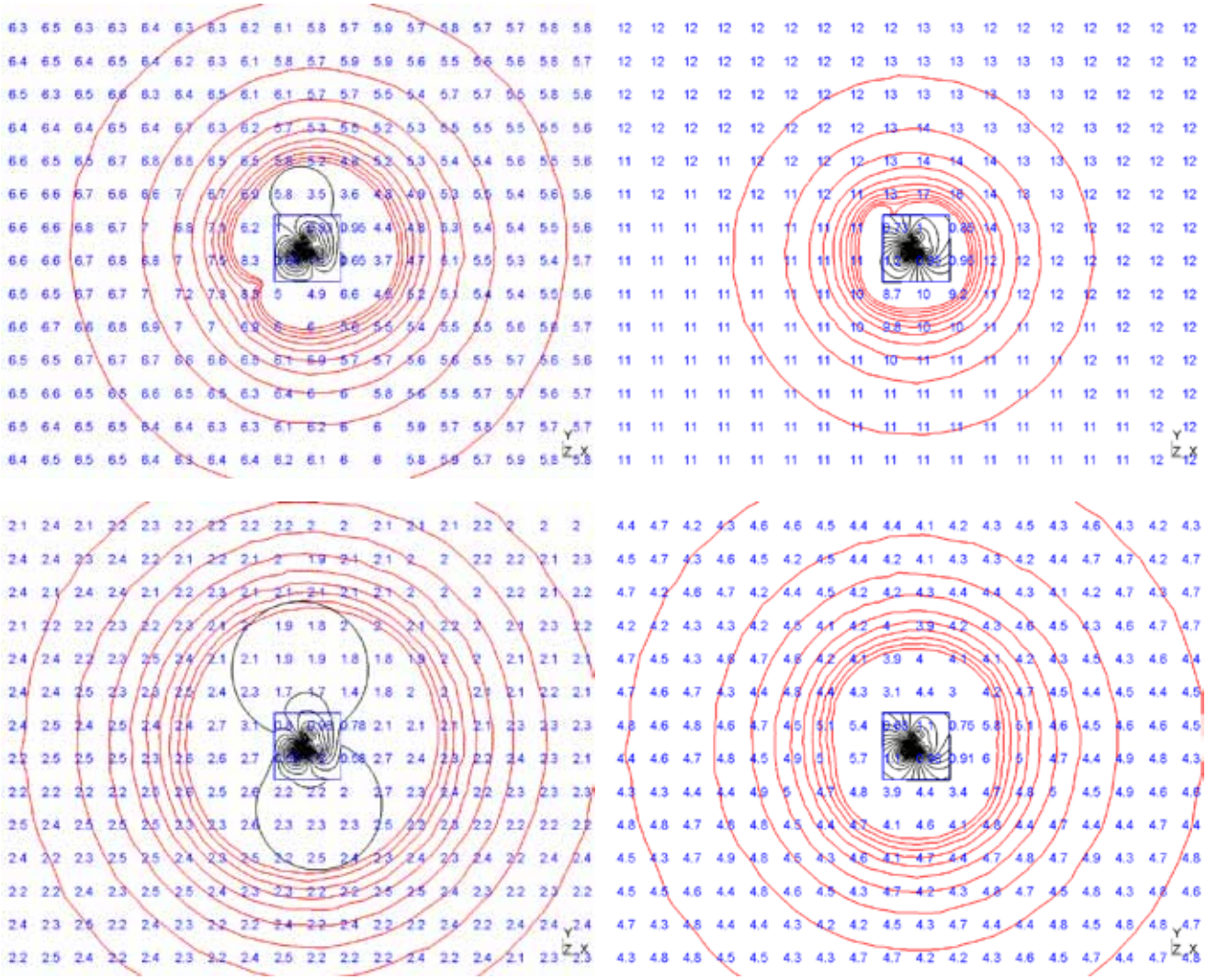

Figure 5.3.19 Shielding factor maps for the closed shield (*left:* Aluminium, *right:* Steel)
- Perfect electrical contacts at plate ends between the vertical plates and between the horizontal plates (*top*)
- Perfect electrical contacts between the vertical plates only (*bottom*).
The grid step in both horizontal and vertical directions is 0.20m.

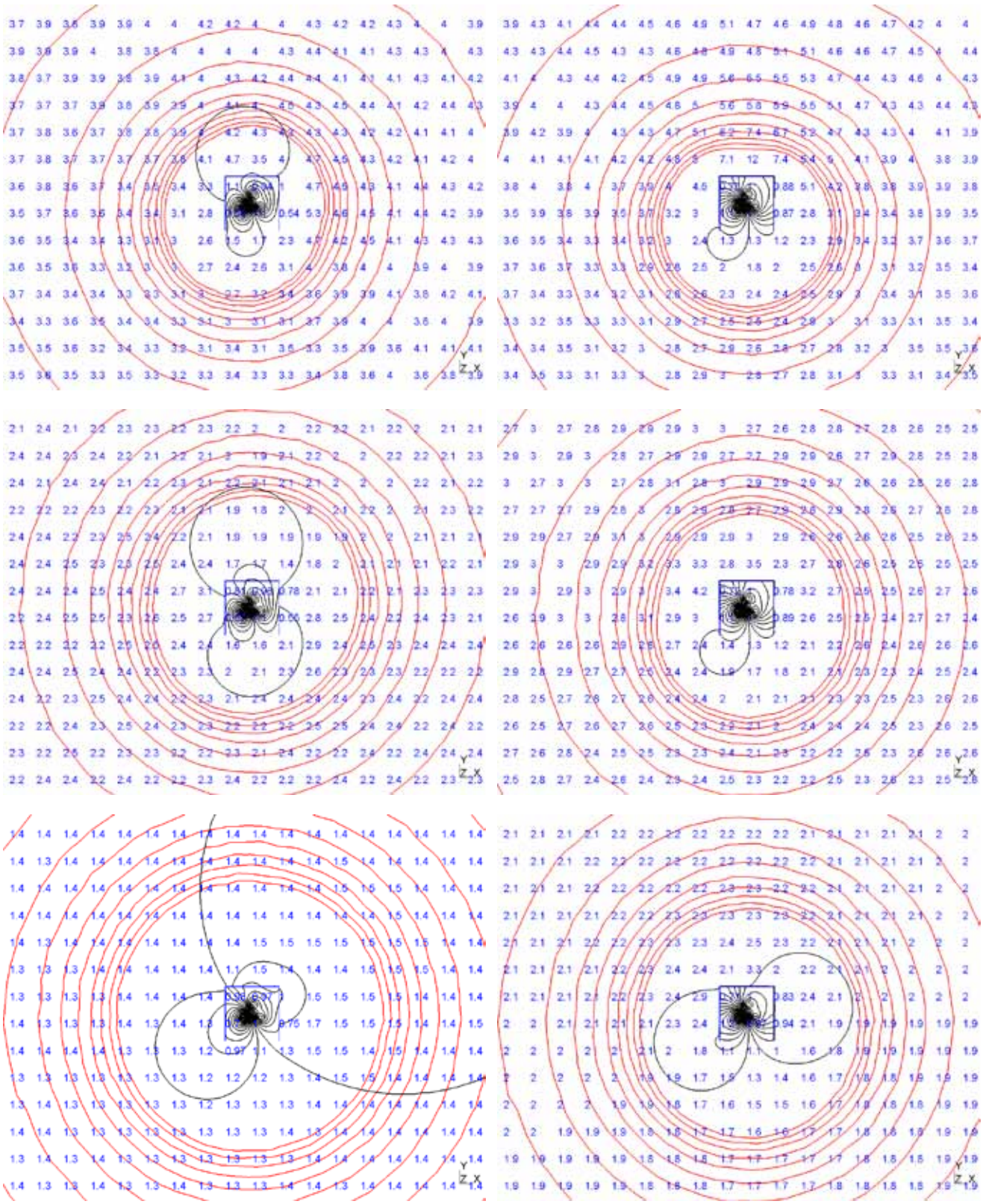

Figure 5.3.20 Shielding factor maps for the reverse-U shield (*left:* Aluminium, *right:* Steel)
- Perfect electrical contacts between all plates (*top*)
- Perfect electrical contacts (also at plate ends for loop connection) between the vertical plates (*middle*)
- No contact (*bottom*).

The grid step in both horizontal and vertical directions is 0.20m.

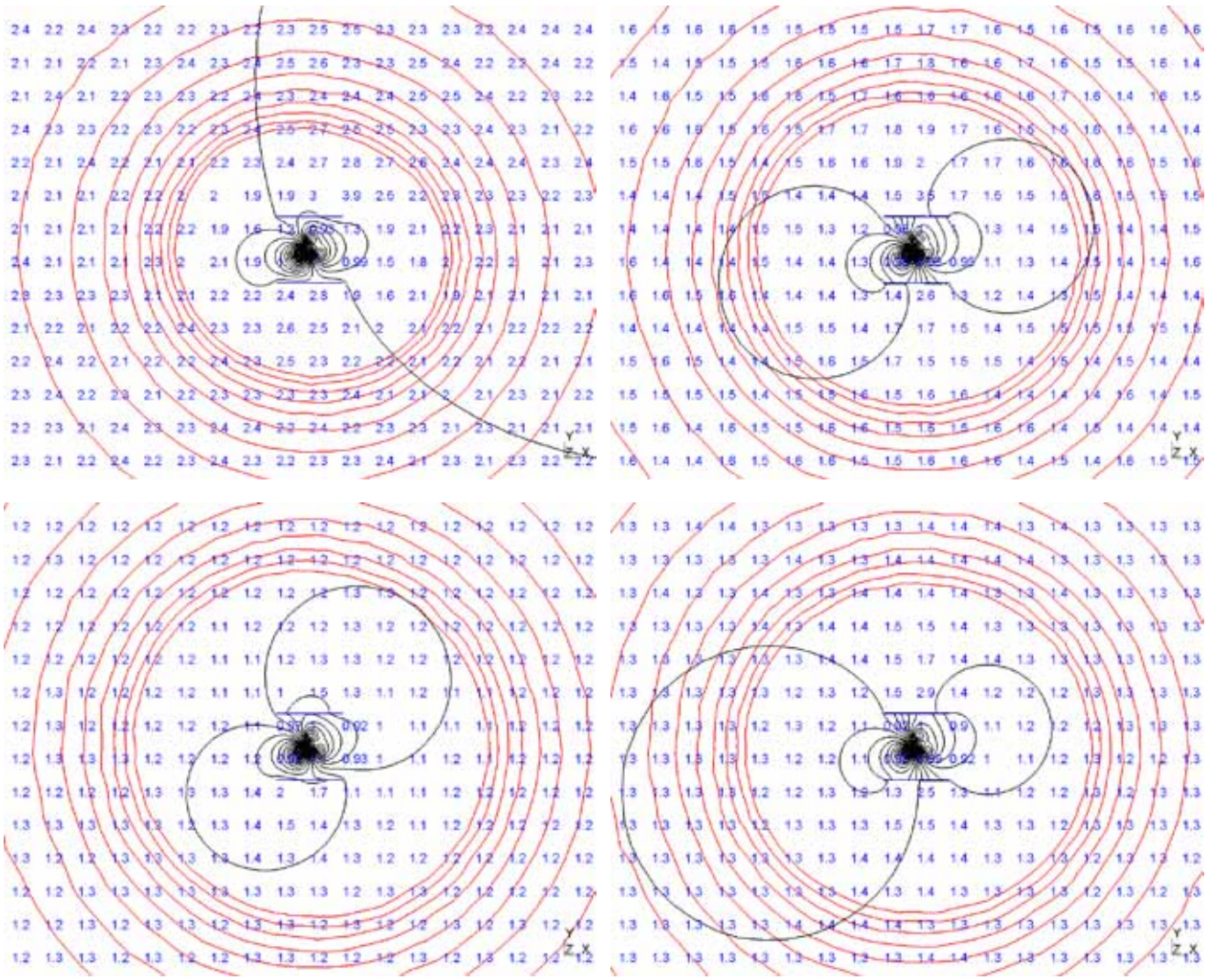

Figure 5.3.21 Shielding factor maps for two horizontal plates above and bellow the cables (*left:* Aluminium, *right:* Steel)
- Perfect electrical contacts (at plate ends for loop connection) between the plates (*top*)
- No contact (*bottom*).
The grid step in both horizontal and vertical directions is 0.20m.

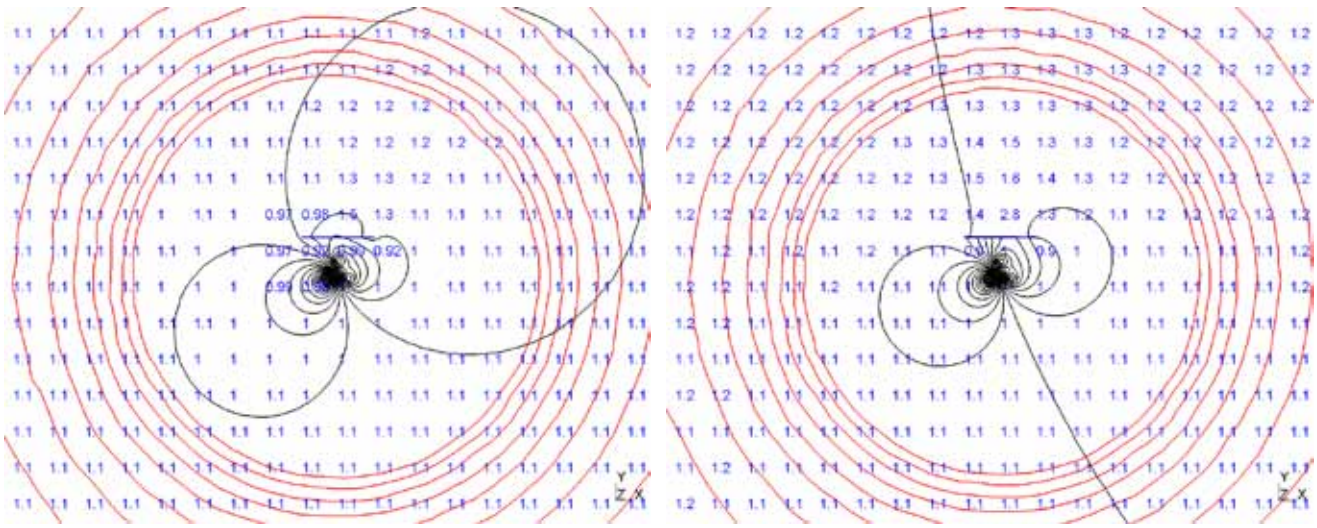

Figure 5.3.22 Shielding factor maps for a single horizontal plate above the cables (*left:* Aluminium, *right:* Steel).
The grid step in both horizontal and vertical directions is 0.20m.

Shields with increasing sizes (cables in trefoil formation)

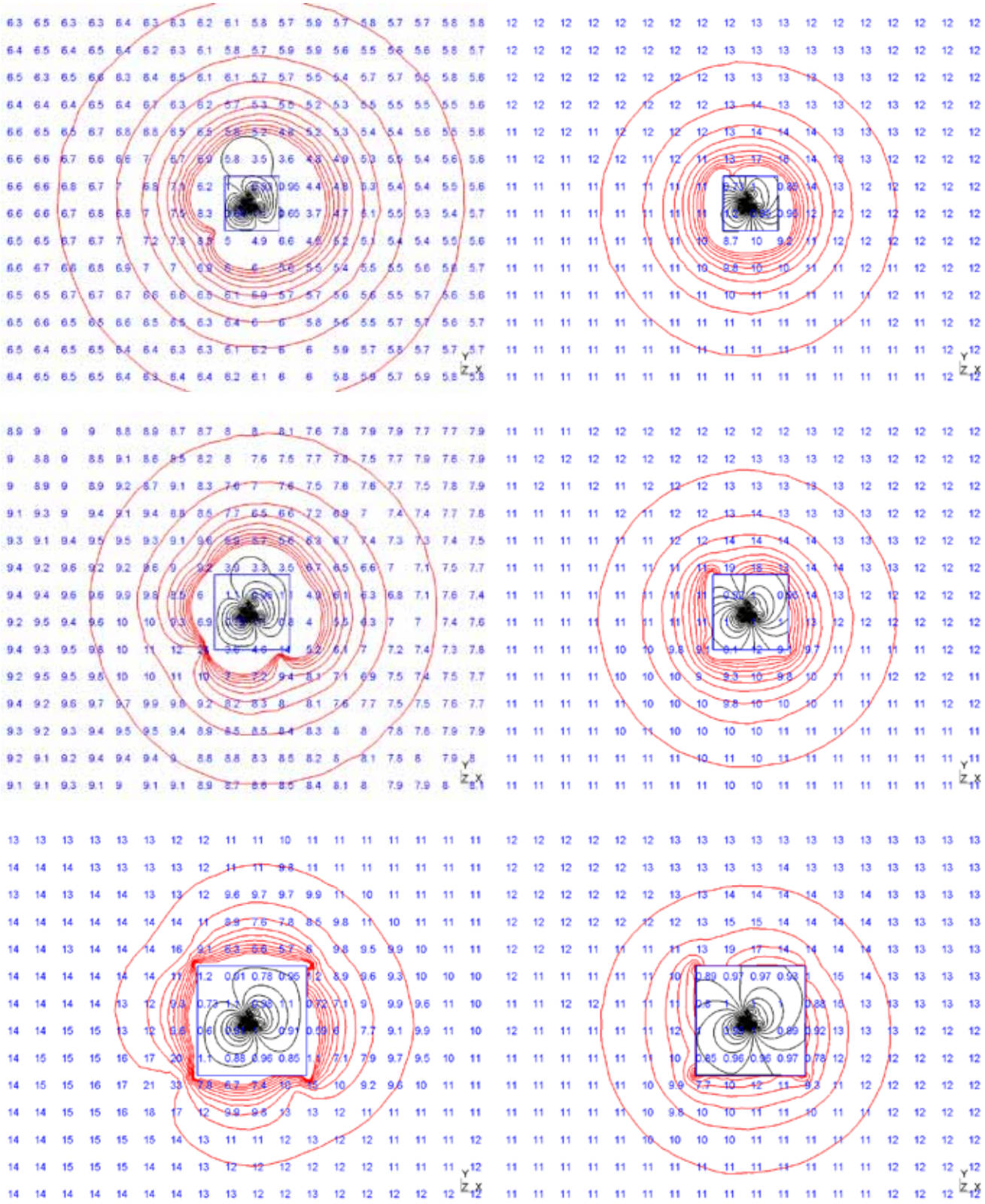

Figure 5.3.23 Shielding factor maps for closed shield with perfect electrical contacts between the vertical plates and the horizontal plates (*left:* Aluminium, *right:* Steel)
Screen size 40 cm x 40 cm (*top*), 55 cm x 55 cm (*middle*) and 80 cm x 80 cm (*bottom*).
The grid step in both horizontal and vertical directions is 0.20m**.**

5.3.7 Advantages and disadvantages of the different shielding materials

It is not easy to conclude on whether it is better to use conductive or ferromagnetic material for shielding power cables. However, in order to facilitate the choice, the main features of both shielding techniques using metallic materials have been summarised in the following table.

Feature	Conductive materials	Ferromagnetic materials
General	The effectiveness, although sometimes weaker than that of closed ferromagnetic screens, is more homogeneous in the space. Even if the shield doesn't encompass completely the current-carrying conductors, it remains effective at distance.	Closed ferromagnetic shields (tubular shape, raceway type) exhibit the highest effectiveness. However, ferromagnetic screens that don't encompass completely the current-carrying conductors, are only effective adjacent to the screen
Dimensions	For a given thickness, the larger the shield dimensions, the highest the effectiveness.	For a given thickness, the dimension of the shield has few influence on the effectiveness
Continuity	A good electrical continuity is generally needed between the shielding elements. This can only be achieved by soldering or welding techniques and can sometimes become rather expensive	Gaps have to be avoided between the shielding elements and good electrical contact is important but welding is generally not needed.
Corrosion	Copper exhibits the best resistance to corrosion. Aluminium has also a good resistance if the pH of the soil remains under control	All the ferromagnetic materials are subject to corrosion and need to be protected (e.g. by galvanization).
Losses	Joule losses can become quite high if the required effectiveness is high	For the same effectiveness, the losses are generally lower than for conductive materials
Impact on ampacity	Shield heating can become a problem if the shield is very close to the cables. However, generally, the shield is in direct contact with the soil which also has a heat dissipation effect (radiator)	The impact on the cable ampacity is usually low.
Material costs	Aluminium alloys are reasonably cheap and less expensive than copper or most coated high permeability steel for the same effectiveness. Copper plates installed above the cables can sometimes be stolen.	Good ferromagnetic materials like permalloy ("Mumetal") or transformer laminates (GO steel) are often expensive. However some special alloys like Ultra Low Carbon steel with high permeability are much cheaper and quite efficient.
Installation costs	Most shields can be built on site with simple easily available metallic plates. Shields made of aluminium or copper plates are rather easy to install and can follow the trench irregularities or the changes in the cable layout (e.g. junctions). As the shield may be open, cable installation is generally not affected Copper and mainly aluminium are lighter than ferromagnetic materials.	Most shields need special factory made elements (tubes, profiles, clamps…) Closed shields require special parts to follow the trench irregularities and the curves of the cable route. For tubular shields, the cables need to be pulled. This can be an advantage or disadvantage (fast recovering of the trench) Ferromagnetic material are generally not suitable for shielding existing links
Maintenance	Shielding elements can normally easily been removed for cable repair	Tubular shields can become a problem as they cannot be easily open (two elements conduit) or if filled with concrete

5.3.8 References

[3] Transmission Cable Magnetic Field Management - Power Technologies Inc - EPRI TR-102003 – Project 7898-37 – Final Report June 1993.

[4] Magnetic field in HV cable systems 1) systems without ferromagnetic components - CIGRE guide 104 - JTF 36-01/21 - June 1996.

[5] Magnetic field calculation in underground cable systems with ferromagnetic components - CIGRE - JTF 36-01/21 (SC 21 Doc 96/13) - 1996 (unpublished).

[6] R.G. Olsen - On low frequency shielding of electromagnetic fields - 10th International Symposium on High Voltage Engineering – Montréal – 1997.

[7] L. Hasselgren, J. Luomi - Geometrical Aspects of Magnetic Shielding at Extremely Low Frequencies - IEEE Trans on EMC vol 37, No 3, August 1995.

[8] A.S. Farag et alii - Implementation of shielding principles for magnetic field management of power cables - Electric Power System Research 48 (1999) pp 193-209 – Elsevier.

[9] G. Bucea, H. Kent - Shielding Techniques to Reduce Magnetic Fields Associated with Underground Power Cables - CIGRE Session 1998, paper 21-201.

[10] O. Bottauscio, M. Chiampi, D. Chiarabaglio, F. Fioillo, L. Rocchino, M. Zucca - Role of magnetic materials in power frequency shielding: numerical analysis and experiments - IEE Proc. Gener. Transm. Distr., Vol 148, No 2, March 2001.

[11] A. Canova, A. Manzin, M. Tartaglia - Evaluation of different Analytical and Semi-Analytical Methods for the Design of ELF Magnetic Field Shields - IEEE Trans. On Industry Applications, vol 38, no 3 May/June 2002.

[12] O. Bottauscio, D. Chiarabaglio, M. Chiampi, M. Repetto - A numerical Approach to the Design of Conducting Shields for ELF Magnetic Field Reduction - ETEP vol 12 No 2, March/April 2002.

[13] A. Bolza, F. Donazzi, P. Maioli - Campi ellettrici e magnetici: possibilità offerte dagli elettrodotti in cavo – Pirelli Caci e Sistemi 2000 - CIGRE 2002 Paris: Group 21, PS1, Q 4.

[14] P. Argaut, J.Y. Daurelle, F. Protat, K. Savina, C.A. Wallaert - Shielding technique to reduce magnetic fields from buried cables- Jicable 1999 – A 10.5.

[15] A.S. Farag, T.C. Cheng and al - Magnetic field modelling and management for transmission underground cables- Jicable 1995 – D 2.7.

[16] G.G. Karady & al.-The Feasibility of Magnetic Field Reduction by Phase Relationship Optimization in Cable Systems - IEEE trans. on Power Delivery, Vol 13, No 2 - April 1998.

[17] M. D'Amore, E. Menghi, M.S. Sarto - Shielding techniques of the low-frequency magnetic field from power lines- IEEE 2003.

[18] A method for applying a magnetic shielding along an AC power line - European patent application EP 1598911 A1.

[19] Y. Du, J. Burnett – ELF magnetic fields from nonaroured multi-core power cables – IEE Proc. Sci. Meas. Tecnol. Vol. 146, 2-8 – 1999.

[20] Method of screening the magnetic field generated by an electrical power transmission line and electrical power transmission line so screened - Patent application WO 2004/034539.

[21] Cipollone A, Fabbri A, Zendri E.- Techniques for shielding underground power lines to minimize exposure to ELF magnetic field in residential areas - EMC Europe 2002, Sorrento.

[22] R. Conti, A. Giorgi, R. Rendina, L. Sartore, E.A. Sena - Technical solutions to reduce 50 Hz magnetic fields from power lines - Proceedings of Power Tech 2003, Bologna 23 - 26 June 2003.

[23] General guidelines for the integration of a new underground cable in the network Cigré Technical Brochure 250 by WG B1.19 –2004.

[24] Construction, laying and installation techniques for extruded and self-contained fluid filled cable systems. - Cigré Technical Brochure 194 by WG 21.17 –2001.

[25] IEC 60287-1-1– Electric cables – Calculation of the current rating - Part 1-1: Current rating equations (100 % load factor) and calculation of losses.

[26] R. Conti, F. Donazzi, P. Maioli, R. Rendina, E.A. Sena - Some Italian experiences in the utilization of HV underground cable systems to solve local problems due to magnetic field and other environmental issues - CIGRE Session 2006, paper C4-303.

5.4 Substations

Substations are some of the most common sources of magnetic fields. They have been studied in the MF mitigation literature [1]-[5] comparatively as much as power lines and underground cables. Yet, there are remarkable differences between the field produced by these sources and the latter two, which also imply differences in the techniques applied for their field mitigation. In this section, these differences will be highlighted and schemes for mitigation of the emitted field from these sources will be presented. The focus will be on secondary (MV/LV) in-house (residential) substations. There are more substation types that can sometimes be considered relevant sources, for example outdoors, rural and industrial substations, which will be briefly described in this section. Attention is also paid to HV/MV substations including the gas insulated type. Still, field characterization and mitigation techniques for the latter types can often be deduced from the techniques developed for secondary substations.

5.4.1 Residential secondary (MV/LV) substations

Secondary substations represent the last stages of the electric network before reaching the customers loads. Inside substations, as the MV voltage is transformed down, the current increases at the LV side. Depending on the geometry of conductors/connections at this side, a composed –and relatively high– magnetic field is generated. A simplified illustration of an in-house substation is shown in Figure 5.4.1. An assumed area of interest is located above the substation[26] and some typical field values are displayed.

The main characteristics of these sources, and the ones that differentiate them from power lines and underground cables, are:

1) complexity
2) local concentration
3) proximity

Complexity: the field from residential secondary substations is often the result of an intricate superposition of fields originating from various sources, which involves vector and phase compositions. Usually, the measured field in the area of interest is not easy to predict analytically or even with 2D approximations. Instead, 3D-numerical computations are often necessary. In comparison, the magnetic field originating from power lines or underground cables is rather predictable, mainly due to several regularities in magnitude, direction and polarity, in addition to conductor configuration symmetries, which are common for these sources [6].

Local concentration: viewed externally, the field from most residential substations decays in all directions (contrary to power lines and underground cables, where there is often a privileged direction of field constancy). Moreover, substations contain sources of which the field decreases quite rapidly with distance; some of their components can even be considered as punctual sources having typically a $1/r^3$ field decrease. The local concentration characteristic is useful in the design of mitigation techniques for these sources.

Proximity: another characteristic of these sources is that they are commonly located in close vicinity to areas where people live or stay for extended periods of time. Then, although the field of these sources decreases rapidly (property 2), it can still affect nearby areas (e.g. Figure 5.4.1).

In order to mitigate the magnetic field from secondary substations, the designer needs to study the contribution of various substation parts. The result of this analysis can determine the parts with relevant contribution to the total field and distinguish them from the ones with lesser or negligible contributions. In this way, mitigation devices (e.g. shields, compensating loops) can be located strategically to achieve effective field reduction in the area of interest. It is therefore useful to look at the general characteristics of various components of secondary substations, each viewed as individual sources of power-frequency magnetic fields. The list of possible sources is:

- busbars
- transformers
- low-voltage cables
- low-voltage connections
- high-voltage cables
- neutral/stray currents

[26] Areas of interest are not necessarily located above secondary substations. They can also be adjacent to the sources or even beneath.

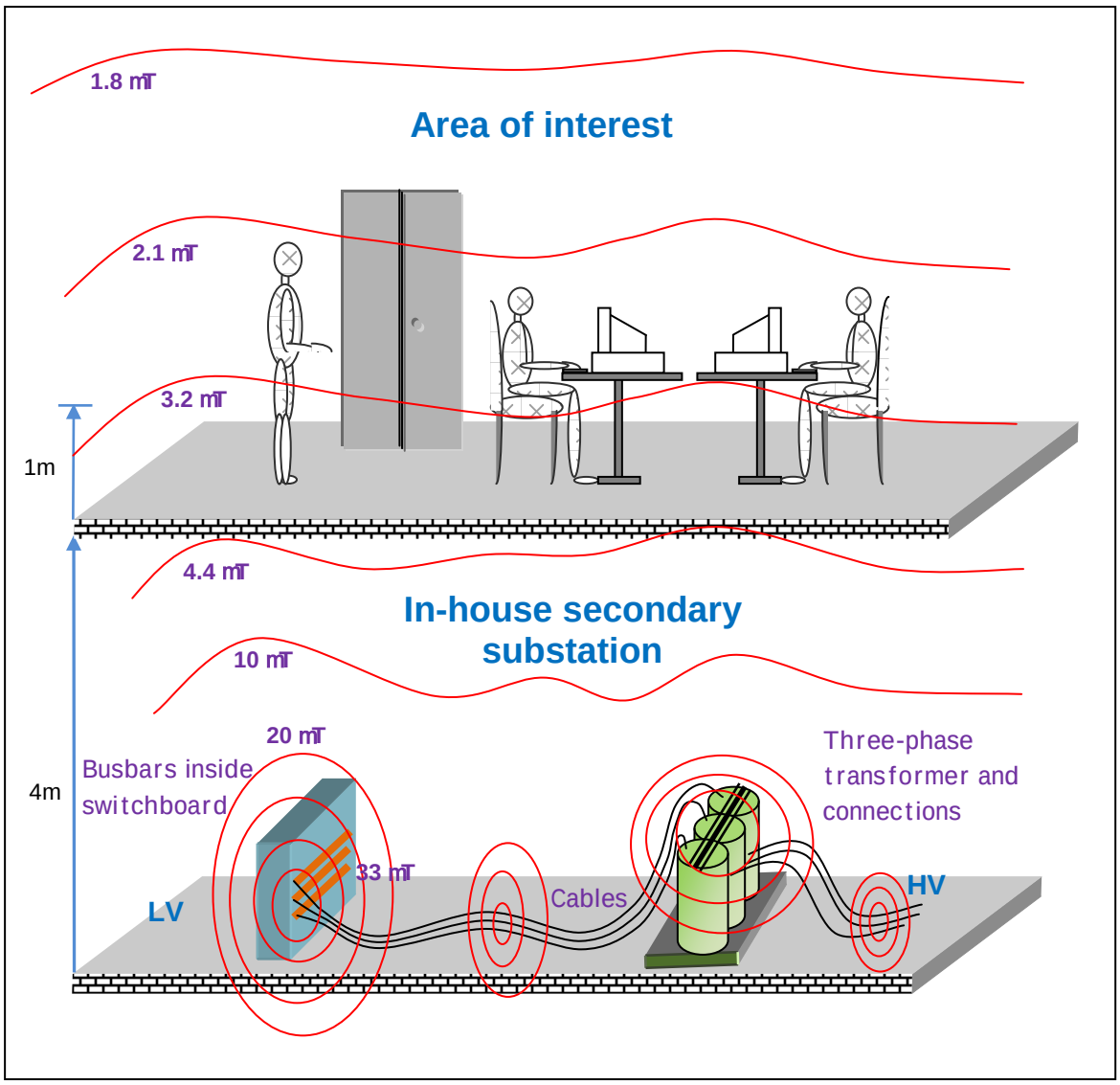

Figure 5.4.1 Illustration of some typical magnetic field values (in microtesla) originating from an in-house secondary substation situated in the cellar of a building. A usual configuration of major sources and distances is also shown.

Mitigation techniques can be developed for each individual source and, therefore, the designer has to solve more than one mitigation problem and needs to spend some time composing, pondering and interpreting the possible individual solutions. Yet, this seemingly tedious procedure appears to be more practical than attempting to solve at once the global problem arising from the superposition of all the sources [1], [7], especially when the most relevant sources have been identified.

5.4.1.1 Busbars

Non insulated busbars are major sources of magnetic fields (due to the distance between each individual bar); they are made of aluminium, copper or aluminium covered by copper and they are the most efficient devices to transport electricity within a substation. LV busbars are the only ones discussed in this section because they often carry large currents (in the range of hundred of amperes sometimes even over thousand amperes). Busbars can have any shape configuration. Yet, these shapes are made of straight segments (Figure 5.4.2), which allow the use of simple analytical methods for determining the individual contributions to the emitted field.

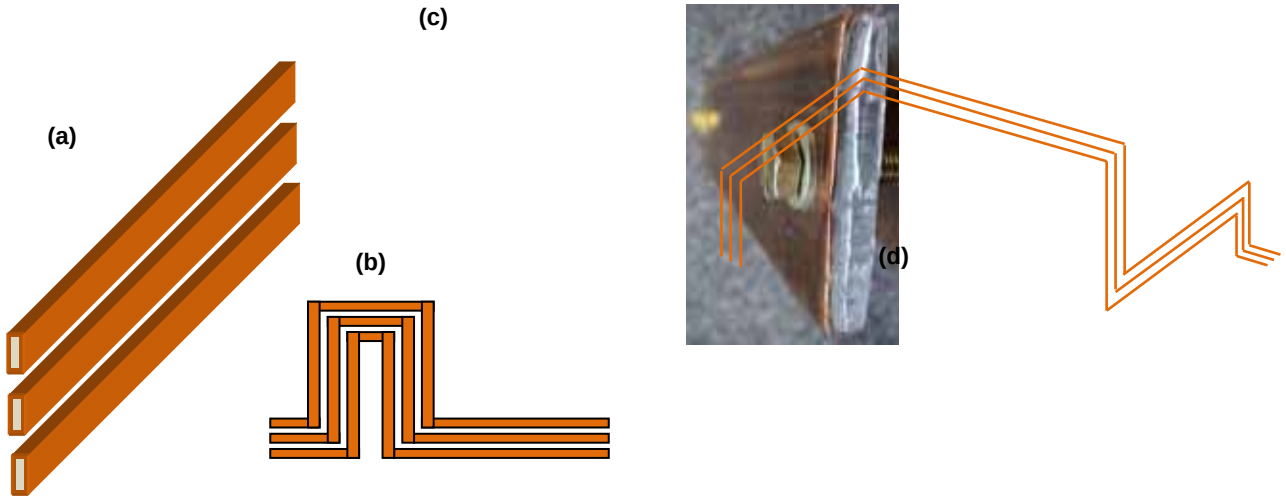

Figure 5.4.2 Busbars are major sources of magnetic fields, usually composed of straight sections (a), (b) made of copper or (covered) aluminium (c) and having sometimes intricate shapes (b), (d).

It should be noted that, like with power cables, it is usually possible to perform a field assessment assuming that the busbars are infinitely thin wires because the area of interest is usually at a sufficiently large distance from the busbars with respect to the geometric radius of each component (Figure 5.4.3)

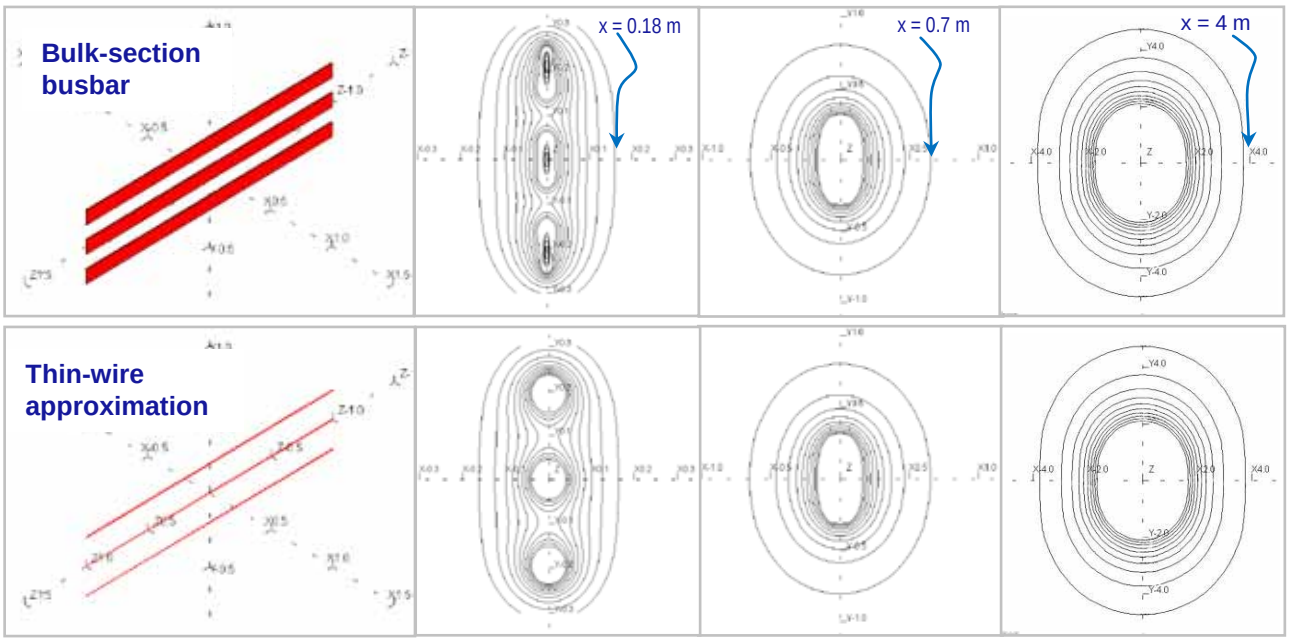

Figure 5.4.3 Approximation of solid busbars by infinitely-thin conductors; for large distances (i.e. in the area of interest) there is practically no distinction between the magnetic field values emitted by both systems.

The field from simple busbar arrangements is easy to compute analytically (for example, using the formulations of chapter 1.1). Even for complex busbar configurations, the field is evaluated using simple programming. Yet, computing interactions of these fields with shields or passive loops - for mitigation purposes - requires more elaborated software [3], [7], [8].

2D approach is valid for long (i.e. several metres) and straight busbars systems. For short busbars (e.g. 2 m long) the border effects can be significant, therefore 3D computations are often necessary. Another case in which 3D approach is necessary is when the geometry involves complex structures. Figure 5.4.4 shows a system that is long, yet due to the switchboard requirements (i.e. measurements, controls and connections) it contains corners and bends. Thus, 3D approach is needed to resolve this system accurately. The system is embedded in a FEM grid, so the effect of a shield structure can be evaluated.

Figure 5.4.4 also gives the field before and after a shielding plate (Aluminium, 17 m × 2m × 3mm) is placed in front of the busbars. The system is fed by two transformers and carries two different currents, 600A and

900A. The highest field values at the level of interest (y = 4m) are due to the two kinks. These kinks, although short in length, affect noticeably the field in the area of interest [9].

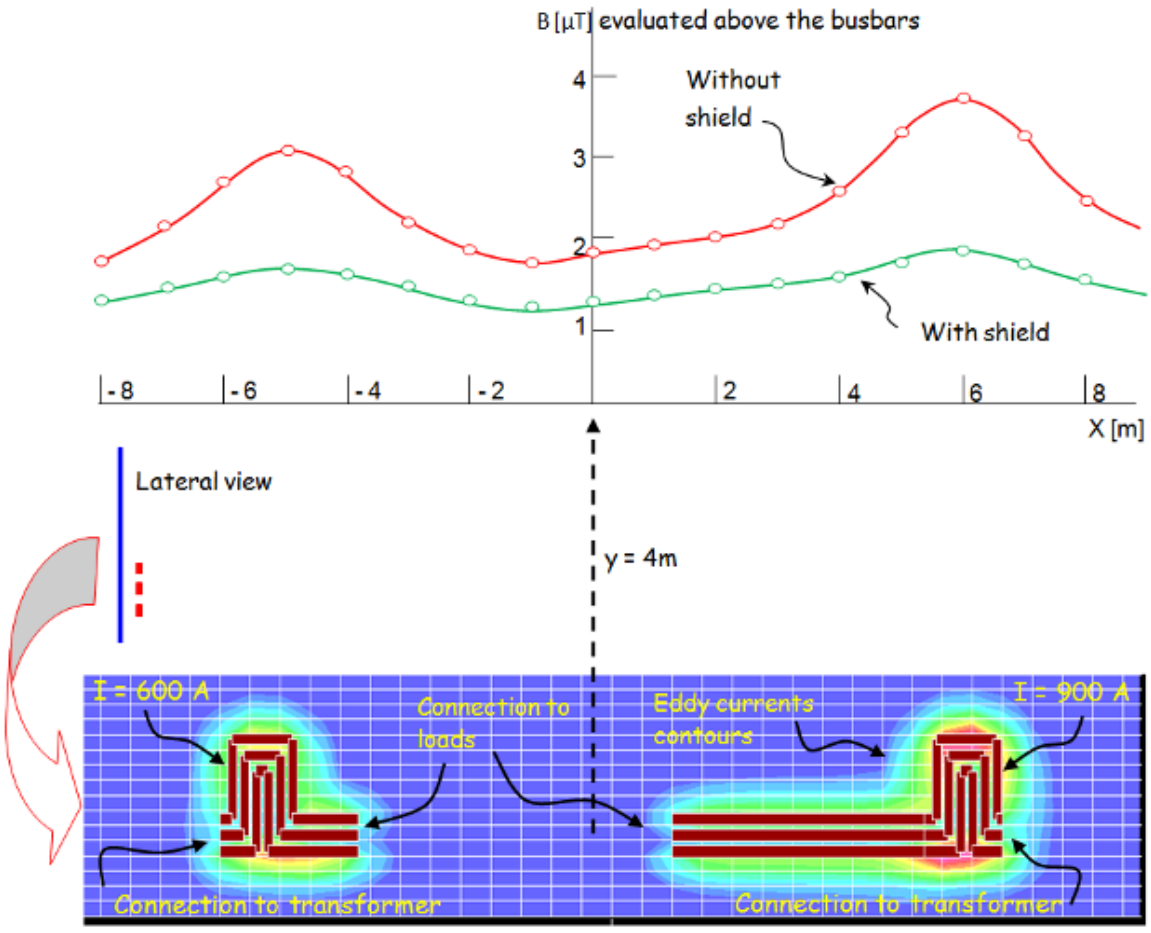

Figure 5.4.4 Evaluation of the field at 4 m above a 13 m long busbar system with a shield (Al, 3mm) placed at 0.2 m from the system; the computational FEM grid uses parallelepiped elements.

In order to understand better the way that fields generated by busbars can be mitigated, a particular - yet representative - system is analysed. It consists of a 3-phase busbar system carrying 500 amperes and a shield in front of it. Results from 2D-simulations with the method of *absorption of boundary conditions* [10] are used to benchmark various shielding arrangements (Figure 5.4.5), all cases use the same amount of material, i.e. constant volume[27], which enables useful comparisons as cost effectiveness can also be evaluated.

In **case (0)** the field is due to the source alone without any shield, the corresponding analytical and numerical computations have a good matching. **Cases (1)-(5)** represent aluminium flat shields ($\sigma = 3.77 \times 10^7$ S/m) with the same volume and mass, located at the same distance to the source (0.2 m). The field is taken in the area of interest at 4 m above the system; where the field does not vary much locally. **Case (6)** is also a flat shield with the same volume than the previous cases but the material is iron (Fe, with $\sigma = 10^7$ S/m and $\mu_r = 200$). **Case (7)** represents the effect of bending the plate of case (4). **Case (8)** is motivated by eddy-current distribution and is intended to save material from the previous case (7); it is based on aluminium ribbons joined together at the far edges.

[27] Except in case (8).

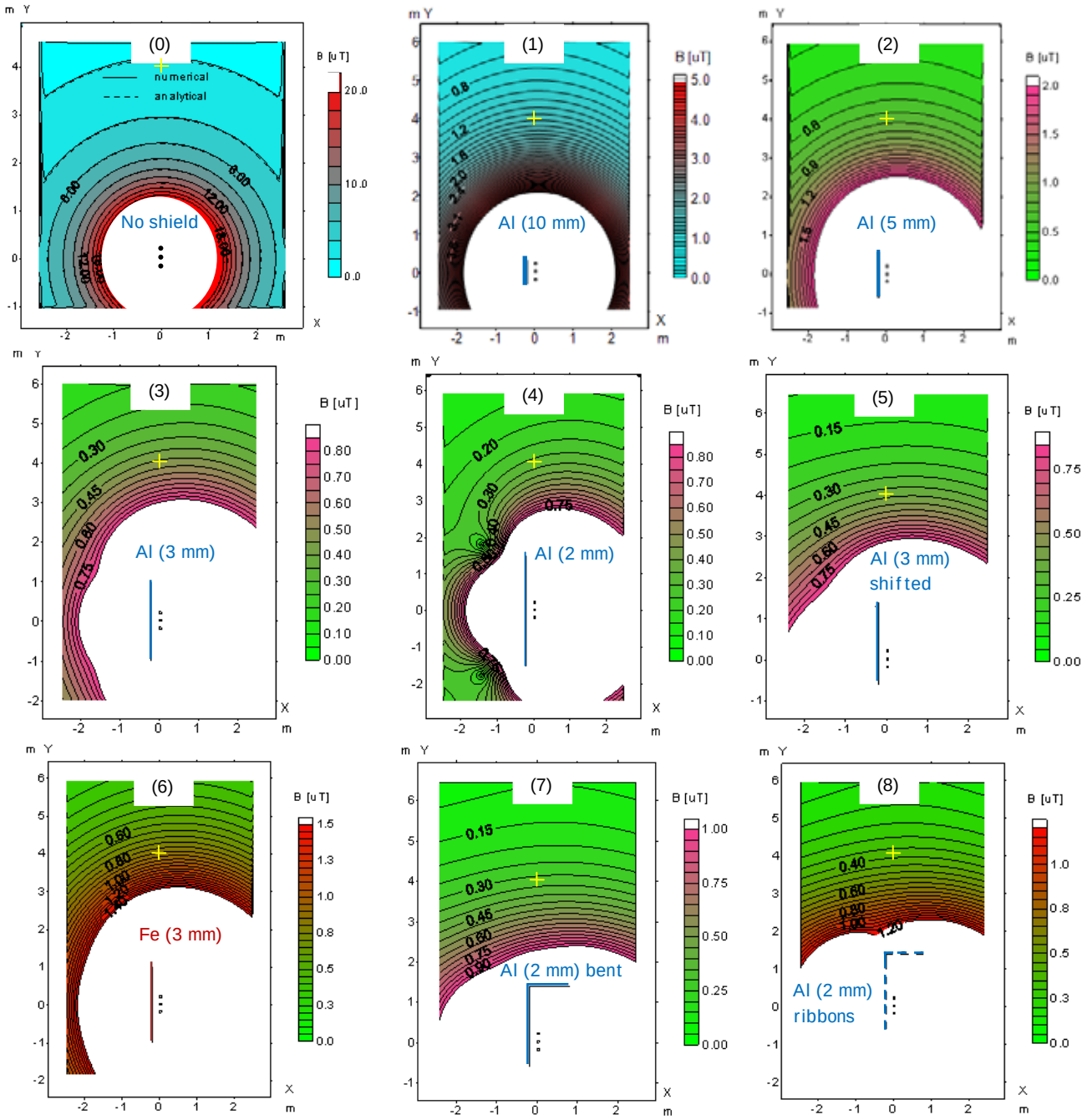

Figure 5.4.5 Benchmarking of various shielding arrangements for busbars. Constant volume is kept in most cases to be able to evaluate cost effectiveness.

The results are summarised in Table 5.4.1 and can be interpreted as follows:

The larger the surface of the shield (screen height in 2D), the better the shielding factor in the area of interest. This can be explained by the higher influence in that region of the eddy currents running on the upper edges of the plates. Thicker plates and shorter in height have good shielding factors in the near region (e.g. at the other side of the plate) but fail to "control" the field in the area of interest (far region). For the same properties attributed to upper edge currents, a small shift upwards of the shield will increase a bit the mitigation in the area of interest. Iron (**case (6)**), is also compared to aluminium (**case (3)**); as this is an open shield (see also 2.3.1.3), the ferromagnetic plate provides good results only in the vicinity of the plate but not in the area of interest [11]. Case (7), which is similar to case (4) but with the aluminium plate bent, also provides a slight improvement. The structure of case (8), based on aluminium ribbons, surprisingly leads to a relatively good shielding factor and it saves 40% material. The only disadvantage of case (8) is that busbar systems that contain vertical segments will not bring much reduction in areas above these segments because they will be perpendicular to the ribbons and, therefore, related eddy currents will not be effective.

Table 5.4.1 Shielding factors for various busbars shielding arrangements.

Case		Screen thickness d [m]	Screen height H [m]	Screen's material	Details of the geometry	SF = B_0/B at (x=0, y=4m)
	0	-	-	-	no shield	1 (B_0 = 2.17 μT)
Same Volume	1	0.01	0.6	Al	centred	1.6
	2	0.005	1.2	Al	centred	2.9
	3	0.003	2	Al	centred	4.67
	4	0.002	3	Al	centred	6.7
	5	0.003	2	Al	shifted upwards	5.6
	6	0.003	2	Fe	centred	2.5
	7	0.002	2+1	Al	bent	6.73
	8	0.002	1.8 (ribbons)	Al	ribbons and bent, it saves 40% of material	5.59

The effect of the switchboard enclosures can also be computed. Yet, depending on the manufacturer, there is a diversity of designs and inner components. Besides the mainframe (usually made of low-conductivity steel) there can be metallic doors, glass windows, openings on the front side and in the bottom of the structure. In Figure 5.4.6 (a)-(b) two different types are shown.

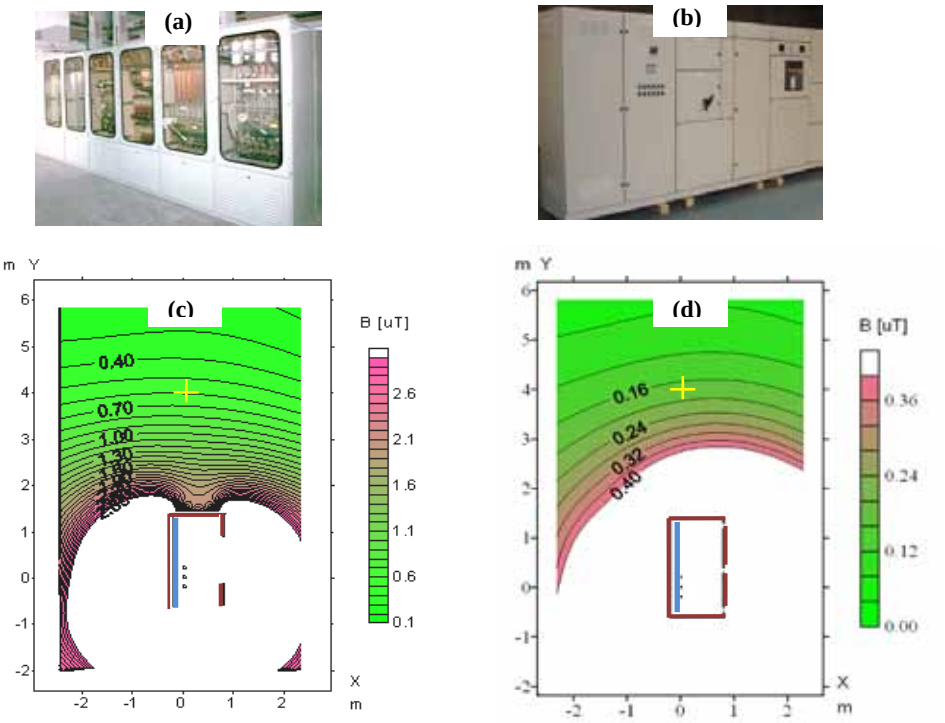

Figure 5.4.6 Two examples of switchboard enclosures (a), (b) and simulations for two cases of busbars and shield inside switchboard covers (c), (d).

Numerical simulations for two distinctive cases of the arrangement, {busbars + shield + cover} are also presented in Figure 5.4.6 (c)-(d). Each case has an overall outer dimension of 2m x 1m containing a shield 2m high and 5mm thick attached to the back of the switchboard; the material of the cover is steel having relative permeability $\mu_r = 150$ and conductivity $\sigma = 0.5 \times 10^7$ S/m. The first case, Figure 5.4.6 (c), has a front glass window and open bottom for under-floor connections. The second case, Figure 5.4.6 (d) has a nearly closed cover, but it has 5 mm gaps around its front doors. Combined mitigation effects of shield and steel cover give shielding factors of 8.2 and 12.5 for (c) and (d) respectively. Besides bars and cover, actual switchboards contain diverse materials structure and circuitry compacted in the enclosure. The influence of these items is assumed to be small, yet in some cases not negligible. Thus, the technique presented here is only a relatively good approximation. Another observation is that this technique can be generalized to other busbars or conductors systems involving more complex arrangements.

In reference [6], a more elaborated technique is presented involving 2 passive shields (Shield1: 1010-steel and Shield2: aluminium) and active cancellation loops located adjacent to the switchboard (Figure 5.4.7). The

structure of the switchboard is modelled as a combination of dipoles and quadrupoles and, from these results, the compensating loops are designed. The active loops (4 turns) are fed by a sensor coil and a control circuit. Measurements are performed in front of the second shield - at 1m above the floor and in an area of 5mx5m. Strong edge effects are observed and resulting averaged (in the area of interest) shielding factors, <SF>, are:

- <SF> = 2 when cancellation loops are used alone
- <SF> = 4 when the 1010-steel is used alone
- <SF> = 6 when the Al shield is used alone
- <SF> = 9 when aluminium and 1010-steel are used
- <SF> larger than 20 when aluminium, 1010-steel and loops are used

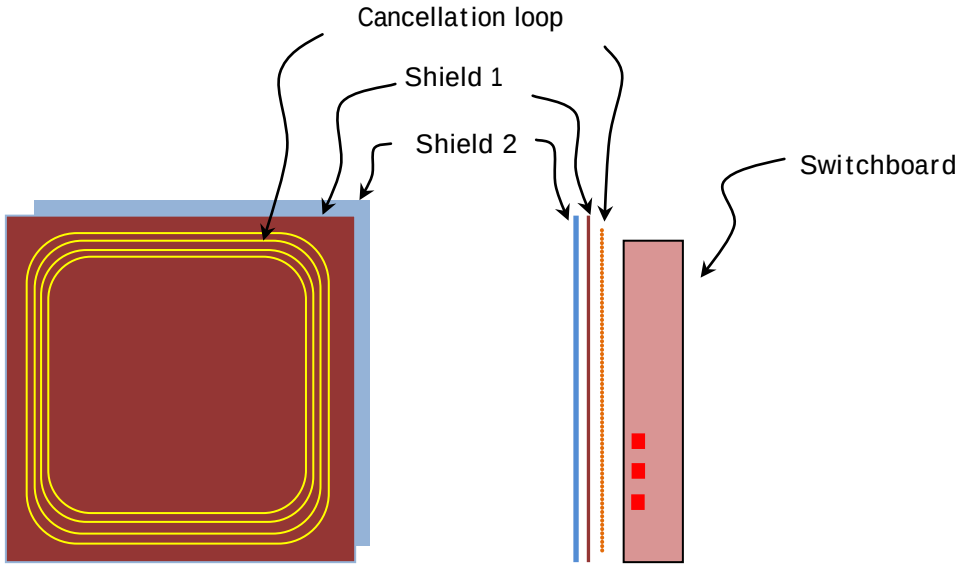

Figure 5.4.7 Active and passive shielding techniques applied to field mitigation of a busbars.

Active loops ensure dipole cancellation while passive shields take care of the higher order multipole shielding [6], a simpler version was highlighted in section 2.1 of this guide. Since it can be obtained by a single shield, the cost of the technique for achieving shielding factors up to 6 is much lower than that of the combined active and passive shielding procedures (although they achieve larger factors).

5.4.1.2 Transformers

Substation MV/LV transformers, dry or oil immersed, are typically in the range 100 kVA to 2000 kVA. Nevertheless, some of the mitigation tools presented here can also be applied or generalized to larger transformer sizes. The measurement of the magnetic field around transformers, at a few metres distance, often yields values above 1 microtesla, especially when they are not encapsulated (e.g. dry transformers). Moreover, these values often do not decrease with the distance as one would expect. Since the leakage field of a transformer is generated by coils, they should decrease as $\sim r^{-3}$ at distances larger than the source size. Moreover, if the transformer is in a ferromagnetic enclosure (e.g. oil-immersed) the field outside the enclosure should be negligible. To illustrate this point, Figure 5.4.8 shows the influence of the core and a possible external cover on the field produced by the coils of a transformer at full load. Taking these considerations into account, it becomes clear that the main field generated outside the transformer has another explanation.

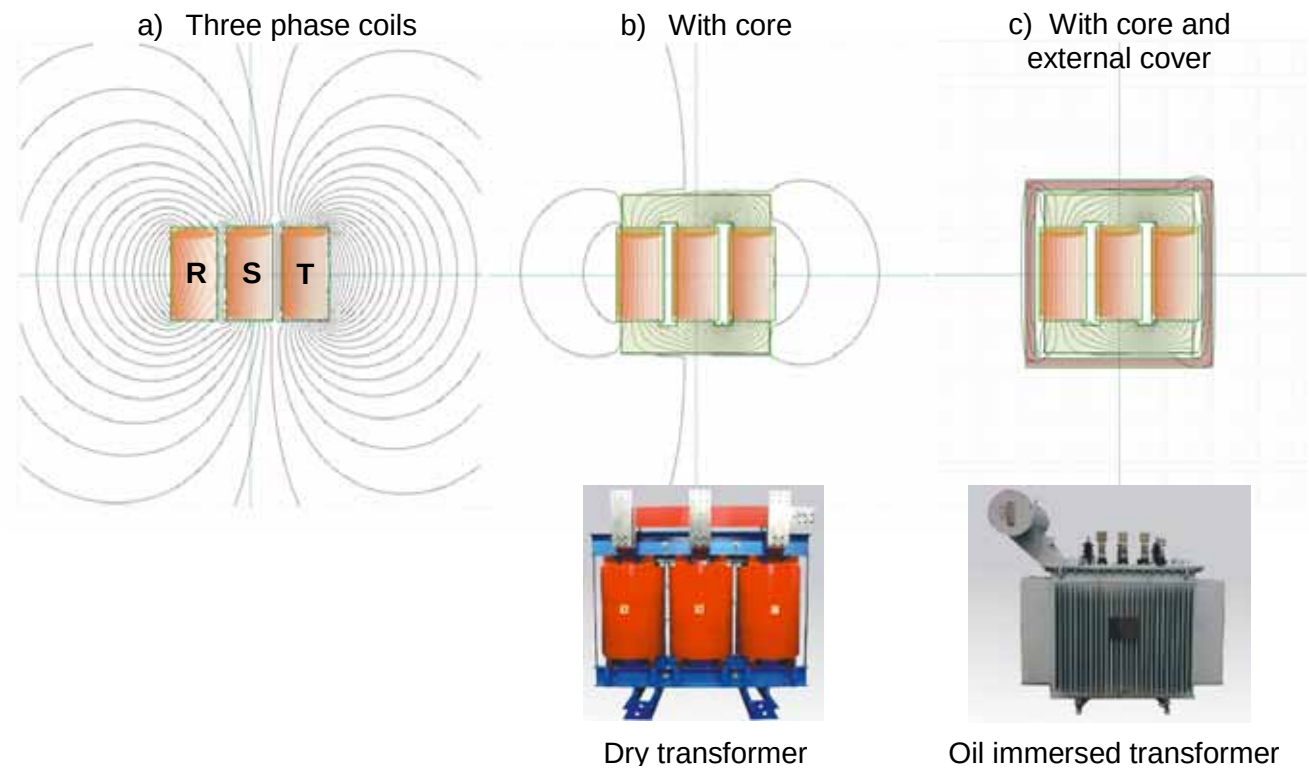

Figure 5.4.8 Illustration of the magnetic field originated specifically from a three-phase substation transformer.

Indeed, the main field sources are the external LV connections of the transformer. In fact it is the separation between the phase terminations which is the origin of the problem and becomes often the most contributing source to the substation total field (Figure 5.4.9), see also [2], [7] and [9].

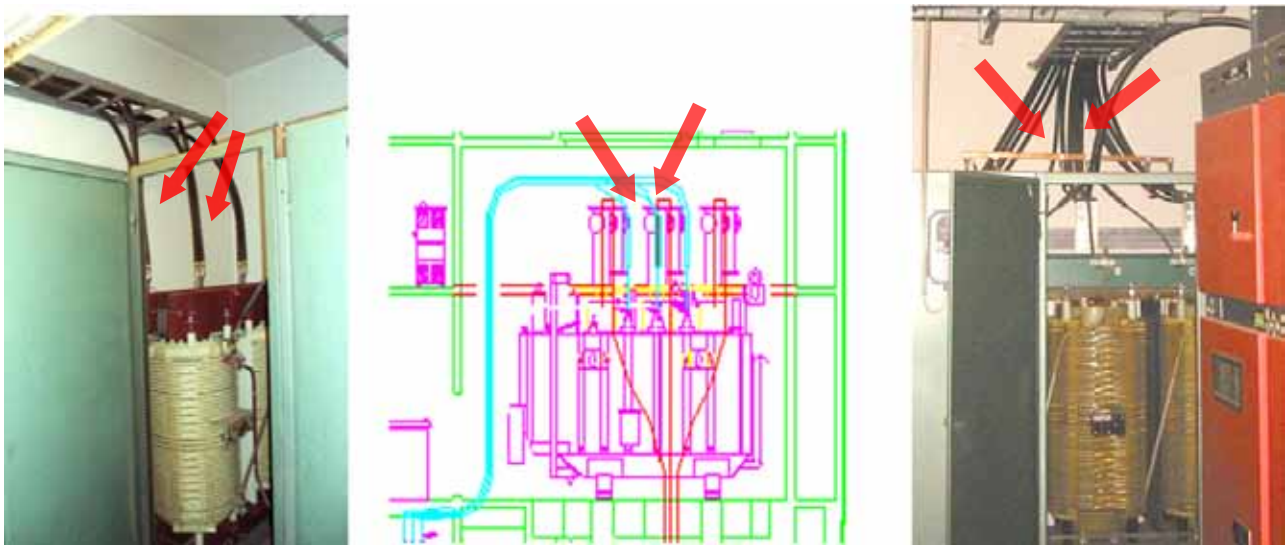

Figure 5.4.9 Various examples of the actual sources of magnetic fields attributed to transformers; they consist of the loops formed by the separation of the LV connections.

The best –and also most cost-effective– mitigation method for the field around transformers consists in phase management, by keeping the phases mixed as soon as they leave the transformer (Figure 5.4.10). It can provide high shielding factors. This operation can, of course, be improved if the connections are led to follow a path located as far as possible from the area of interest.

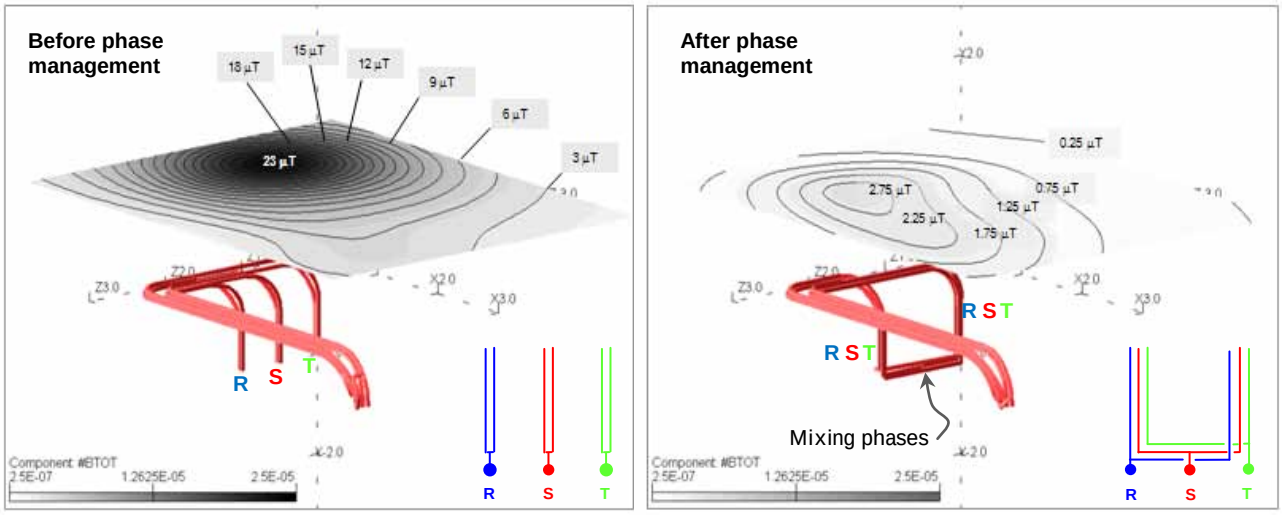

Figure 5.4.10 Mixing phases on the LV connections as a cost-effective mitigation technique that provides in this example shielding factors of around 10.

Other techniques are mentioned in the literature [4], [9], [12] for complementing (enhancing the overall mitigation) the phase management technique (or use instead of), in case of difficulties. As an example, Figure 5.4.11 represents the field mitigation achieved with a shielding installed above a transformer. The case on the left figure represents the field from a single aluminium shield, while, on the right, a double layer is used made of aluminium and a high permeability material. The ferromagnetic layer is quite effective but the cost of the material is important.

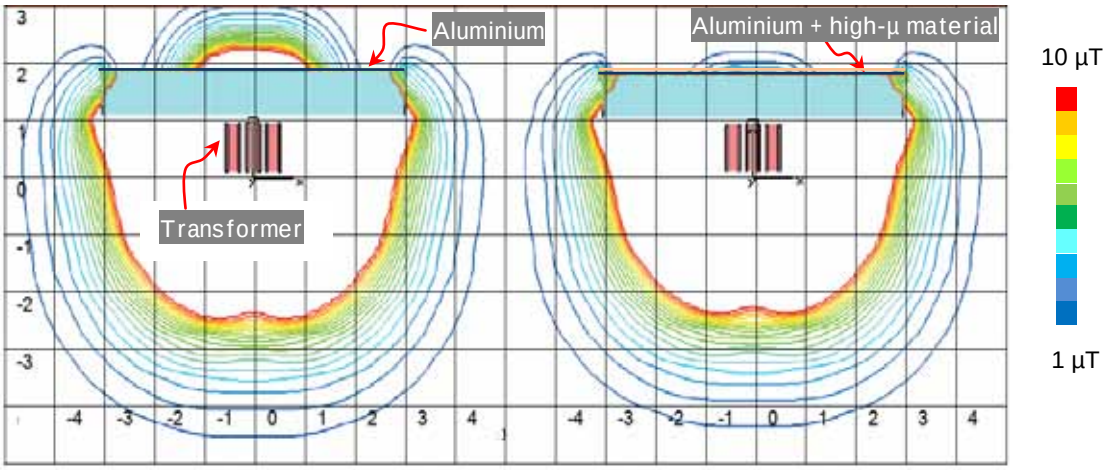

Figure 5.4.11 Applying shielding above a 1000kVA transformer as suggested in [12].

Another mitigating method is to encapsulate the transformer together with its connections in a closed metallic box. Figure 5.4.12 shows an example of a conductive box made of 5mm-thick aluminium applied to a 800 kVA dry transformer. The comparison between shielded and unshielded cases shows a shielding factor of about 7 in the region of interest located above the transformer.

Unshielded transformer **Aluminium-shielded transformer**

Figure 5.4.12 A metallic cover box (right) can be applied to a dry-type unshielded transformer (left).

5.4.1.3 Other sources of magnetic fields in substations

The main sources responsible for the field level encountered in the vicinity of a distribution substation have been discussed above. Yet, cables and HV connections can provide non-negligible contributions to the total field. In order to design a more general mitigation strategy, the contribution of all the conductors (except the ones due to the transformer coils) can be simulated numerically [3] (Figure 5.4.13). Methods based on the techniques developed in the previous chapters of this guide can generally be applied for mitigating these fields. Phase cancellation should be the first technique to attempt before trying shielding (using the classical methods used for underground power cables). Stray currents, due to unbalance in the loads, can be a serious problem, as shielding techniques cannot work on homopolar components. However shielding techniques can be applied to 4 conductor systems when there is no current in the earth. On the other hand, magnetic absorbers, i.e. cylindrical cores made of ferromagnetic multilayer structure and applied to a conductor set can change the impedance of the circuit and, hence, reduce the stray currents and their related field, which decreases with the distance r according to 1/r.

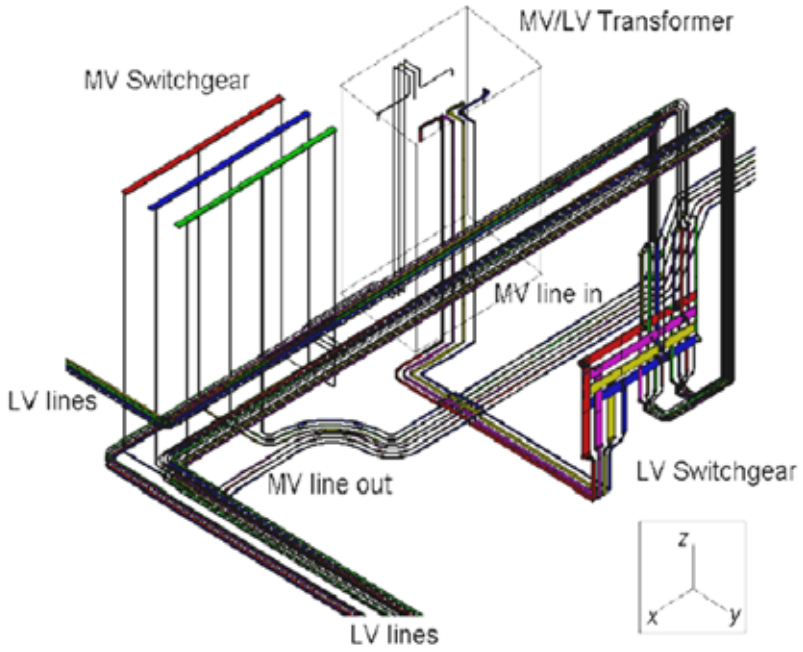

Figure 5.4.13 Considering all the contributions from the conductors in a MV/LV substation.

5.4.2 Rural substations

In a rural environment it is common to have an open-type substation, consisting of a single transformer with its corresponding MV and LV switch gears (e.g. in [13], an 11/0.4 kV substation of this type is analysed). A fence limits access to the substation. Areas of interest for mitigation - where people spend extended periods of time - are seldom in close proximity to this type of substation. In case this closeness takes place, some of the available mitigation techniques are similar to the ones for indoor MV/LV substations; for example phase and cable re-arrangements at the LV sides. On the other hand, some techniques are not applicable. The absence of walls, for example, makes shielding not feasible. Still, a good mitigation technique for this case is probably distance management, i.e. extending the limits of the fence in the initial configuration.

Figure 5.4.14 Substation in a rural area.

5.4.3 Industrial substations

Typically, when dealing with substations for residential distribution in a crowded urban environment, field mitigation focuses in a region neighbouring the substation, i.e. near the upper or possibly lateral boundaries. In the case of industrial substations (Fig 5.4.15), as in the previous case of rural substations, it seldom happens that public houses are in close proximity to the field sources. Yet, it could happen that offices and other spots inside these industrial compounds become areas of interest for mitigation purposes.

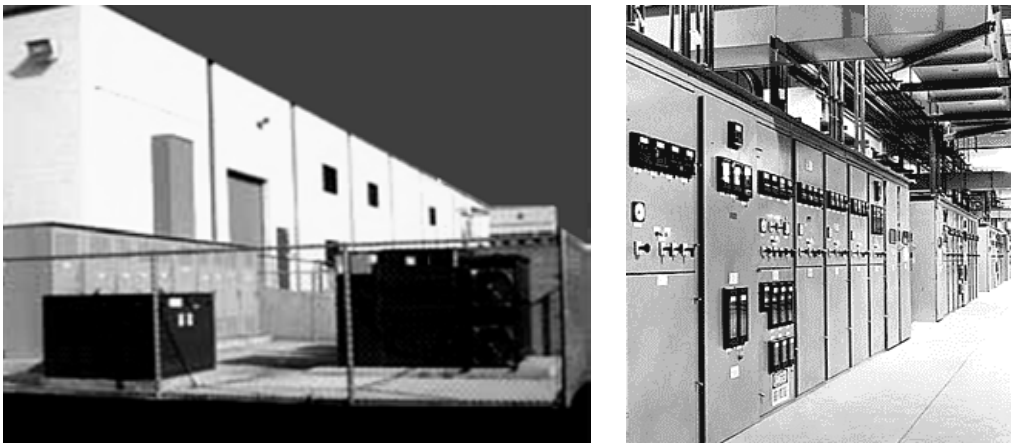

Figure 5.4.15 Two types of substations in an industrial environment.

As a result of the large loads involved, a substation in an industrial environment is usually driven by higher power than their residential or rural equivalents; currents are also larger and so are their magnetic fields. Not surprisingly, the substation components are also physically larger. An example of the latter is the system of busbars, which, in industrial backgrounds, tends to be particularly long when there is a need to feed power to a large number of loads. This characteristic induces the associated field to have an extensive spreading.

Analysing the typical case of offices above an industrial substation, the solution of modifying the arrangement of the electrical components inside the substation (such as increasing the source distance from the affected area) could provide interesting results, but it is generally not applicable to existing plants, taking into account the cost of the

modification and the technical constraints. Disregarding this solution, the mitigation of the magnetic fields has to be obtained by the use of passive shields. An interesting case of this type involving partial shielding (region of interest just above the substation) is presented in Figure 5.4.16. The shielding was performed by using layered plates made of combined materials, namely aluminium (2mm thick) and ferromagnetic (0.3 mm thick GO Fe-Si laminations). The field levels measured before and after the shielding in the area over the substations are reported in Figure 5.4.16. A maximum shielding factor of about 10 is obtained by this solution. The methods dealing with this type of field are described in [13].

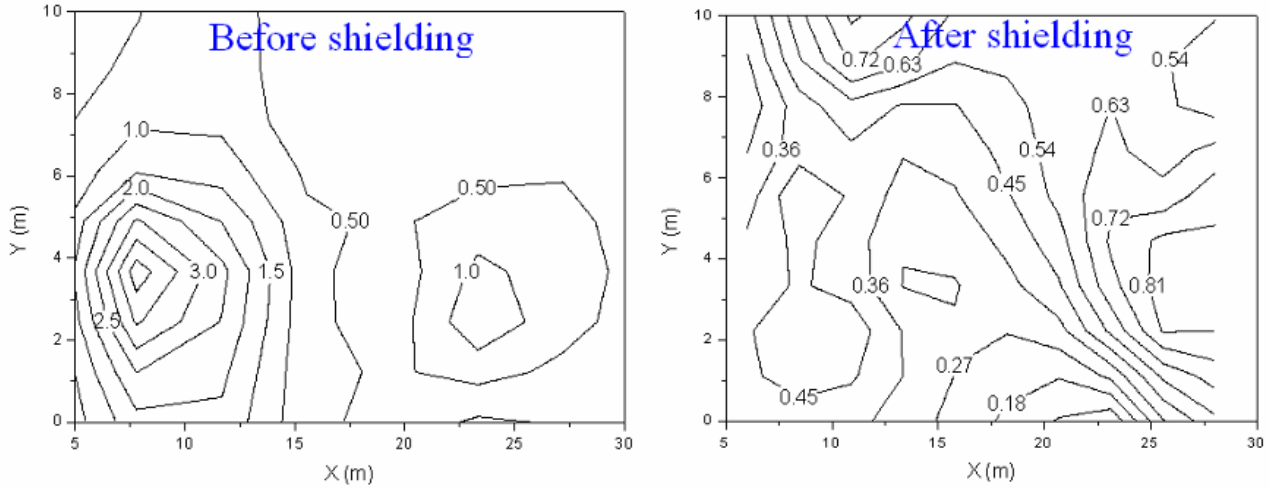

Figure 5.4.16 Mitigation of the field over the ceiling of an industrial substation; magnetic field levels (in microtesla) before the shielding (left) and magnetic field levels after the shielding (right).

5.4.4 HV/MV substations

In the case of HV/MV or simply HV substations, the power and size of the components are even larger than in the previously studied cases. The voltages involved are typically in the range of several hundreds of kV reduced to tens of kV (e.g. 110/20 kV, 275/33 kV, 400/110 kV). Currents involved are also large; therefore higher magnetic fields are expected. A relevant issue related to field mitigation is to identify the areas of interest. The fields inside this type of substation are rather complex and often mixed with fields associated with switching operations (transients) which are beyond the scope of this guide. Since the interest is mainly in areas of public exposure, these regions are often located far from this type of substation. However, in some cases dwellings can be located in relative close proximity to the substation (e.g. at tens of metres distance) and still falling within the range of influence of the substation magnetic fields. Noteworthy cases are HV gas insulated substations, which can be located in close vicinity to residential dwellings and are also studied here.

In standard HV substations, the strongest magnetic field around the outside of the substation are originated from the power lines or underground cables arriving or leaving the substation. The field from transformers, busbars and other devices can be very high in the vicinity of the source; yet, it mostly remains within the substation.

In order to analyze the field of a HV substation, both experimental and computational methods are used. Depending on the desired degree of approximation to achieve, a simple structure or a rather detailed one can be assumed for the source components. The levels of complexity can be characterized in the following way [14],

- Level 1: modelling only bus conductors and their associated phase currents. Minor geometrical variations in the conductors are ignored.
- Level 2: expanded model including neutral reactors, concentric neutrals for underground distribution feeders, neutral conductors for overhead distribution feeders and transmission line overhead ground wires.
- Level 3: substation grounding system, connections to this system and neutral connections to ground rods at the distribution poles are added to the model
- Level 4: to take account of localized distortions of the magnetic fields, effects caused by induced eddy currents in ground conductor loops and non-energized structures are modelled to properly generate the contribution to the field from these circulating currents.

Then the distribution of the magnetic flux density is computed by dedicated software based largely on the Biot-Savart law.

In Figure 5.4.17, the conductor structure of a typical HV substation 500/275 kV is shown; it has been adapted from [15]. Some of its power components include transformers (1B-3B), disconnectors, circuit breakers, and truss frames for supporting conductors. This substation is connected to 500 kV (TL-1, TL-2) and 275 kV (TL-3-6) double circuit (1L, 2L) power transmission lines. The magnetic field values were measured at 1m above the ground surface, using a portable magnetic field sensor. The mayor magnetic field contribution to a region surrounding the substation is on the shadowed area, i.e. the outgoing secondary overhead lines.

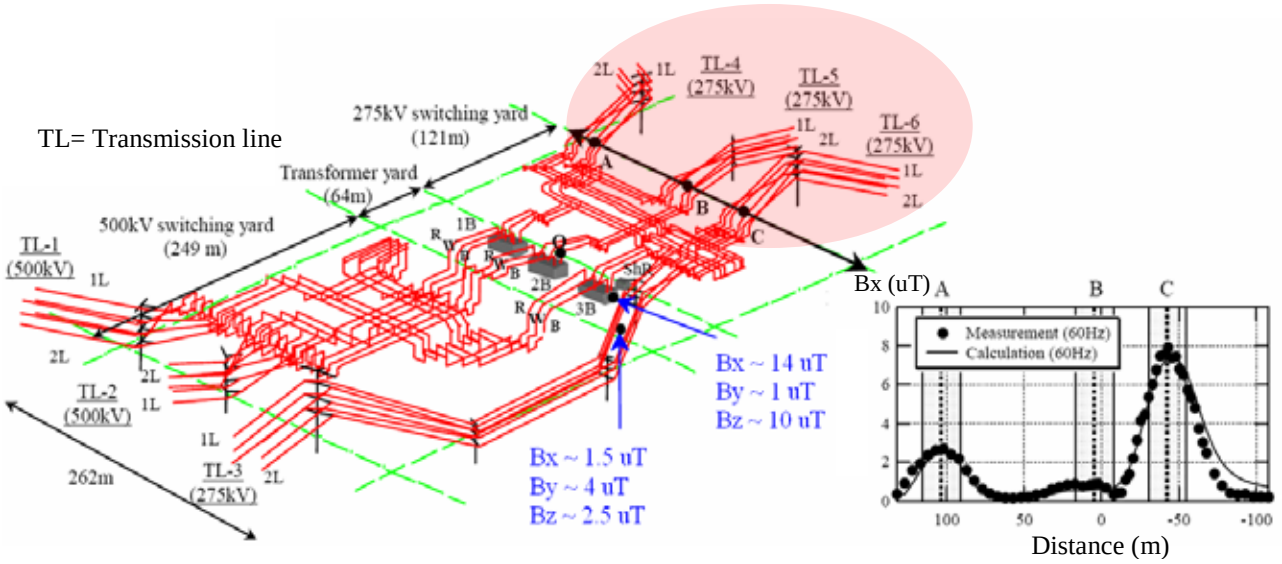

Figure 5.4.17 Magnetic field sources of a typical HV substation (500/275 kV). The major contribution of the magnetic field, to a region surrounding the substation, is in the coloured area; adapted from [15].

The three-phase power line currents were also measured using current transformers; they are displayed in Table 5.4.2. Relatively large current fluctuations in time are expected and can be realized from the intervals shown in this table. Moreover, the currents of sources TL-6 and the secondary bus (275 kV) are significantly larger than the others and can be identified as the actual causes of the field that reaches the area of interest, which is located outside the substation fence and is within or close to the coloured area.

Table 5.4.2 Current amplitude ranges of the various substation sources.

Power line	**TL-1**	**TL-2**	**TL-3**	**TL-4**	**TL-5**	**TL-6**
Current range [A] rms	300~600	100~200	500~650	500~1300	400~1000	2700~3500

Power line	**1B 2nd**	**2B 2nd**	**3B 2nd**	**500 kV Bus**	**275 kV Bus**
Current range [A] rms	400~900	400~850	380~900	100~400	2000~3000

The complex arrangements of conductors were simulated and the values of magnetic flux density were computed at 1m above the ground over the area of the substation (262m x 424m). The field contour lines were plotted every 2 μT and are displayed in Figure 5.4.18.

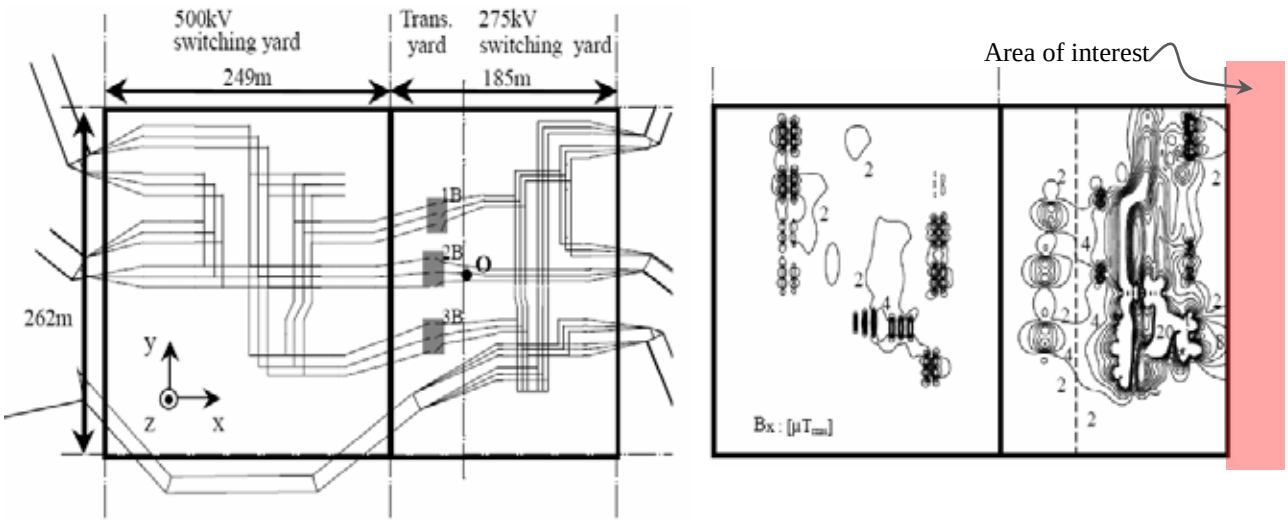

Figure 5.4.18 Top view of the conductors of the 500/275 kV substation (left) and the results of simulations showing the contour plot distribution of B_x and the area of interest (right); adapted from [15].

The results of the simulations confirm that the fields that lie on the secondary (MV) side of the substation are the ones that contribute most to the peak values and the field extending outside the limits (i.e. fence) of the substation define the area of interest. In general, the way the magnetic field behaves in this area depends on the particular characteristics of each substation case.

Reference [16] explores a similar situation on a 400/110 kV substation. The magnetic field values are evaluated on a set of 21 points around the low-voltage side of the HV substation. The field variation along distance - on the road leaving away from the fence - is shown in Figure 5.4.19. The highest value is 1.74 μT and it diminishes to negligible values along the road. Higher values were found along a second (line 2) on the high-voltage side within the HV substation fence. However, these latter values seldom relate to areas of interest.

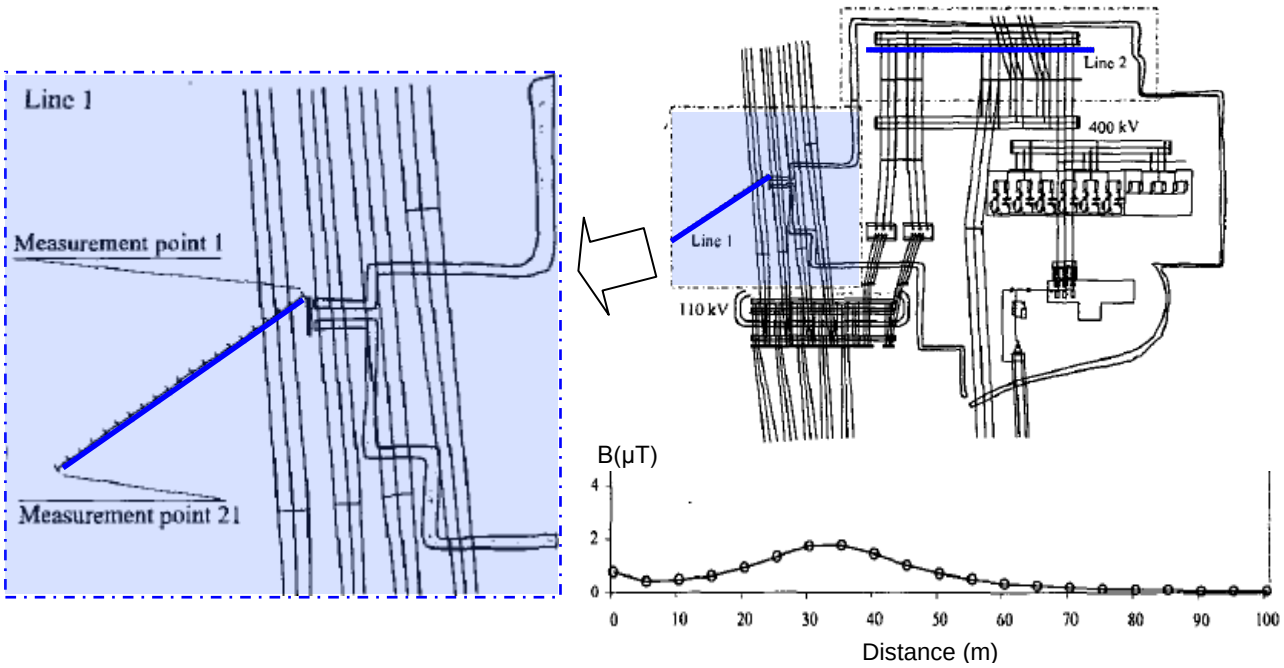

Figure 5.4.19 Magnetic field values along the road away from the fence of a 400/110kV substation; adapted from [16]

Once the field from a HV substation is known as well as its properties, field mitigation techniques can be proposed, designed and implemented. Here some considerations, [17-20]

- A good mitigation technique is distance management from the HV installations. Moving the affected area or extending the fence some reasonable number of metres can take care of the field that is inherent to a low voltage substation as this should decrease by itself with the distance.
- Unwanted values of magnetic fields may still persist at certain distances along some direction located at the LV side. This is evidently due to of the transmission lines carrying along the high currents from the LV side. If an affected area is close to this path, the mitigation techniques to apply are the ones developed for transmission lines or cables (sections 2.1, 2.2, 5.1, 5.2, 5.3 of this guide).
- Seldom, yet possibly, some field mitigation operation can be performed within the limits of the fence of the substation (e.g. related to EMC). In this case, due to the complexity of the field's direction and magnitude, the suggested technique is the use of conductive or ferromagnetic shields on the specific affected area.
- Circulating currents in some structures supporting equipment can cause noticeable distortions in the magnetic field, usually resulting in field reduction [14]. This consideration can be advantageous when developing a mitigation strategy for a HV substation.
- Unbalance in the 3-phase currents, harmonics content and neutral currents can affect the magnetic field distribution. This can play an important role in the design of a mitigation technique.

5.4.5 HV Gas insulated substations (GIS)

In recent years, Gas Insulated Substations (GIS), where the conductors and contacts are insulated by pressurized sulfur hexafluoride gas (SF6) have gained growing interest due to its exceptional property of volume savings in space-constrained sites. Compact GIS can therefore be found in urban residential environments. These characteristics make the surroundings of a GIS become areas of interest in the context of this guide.

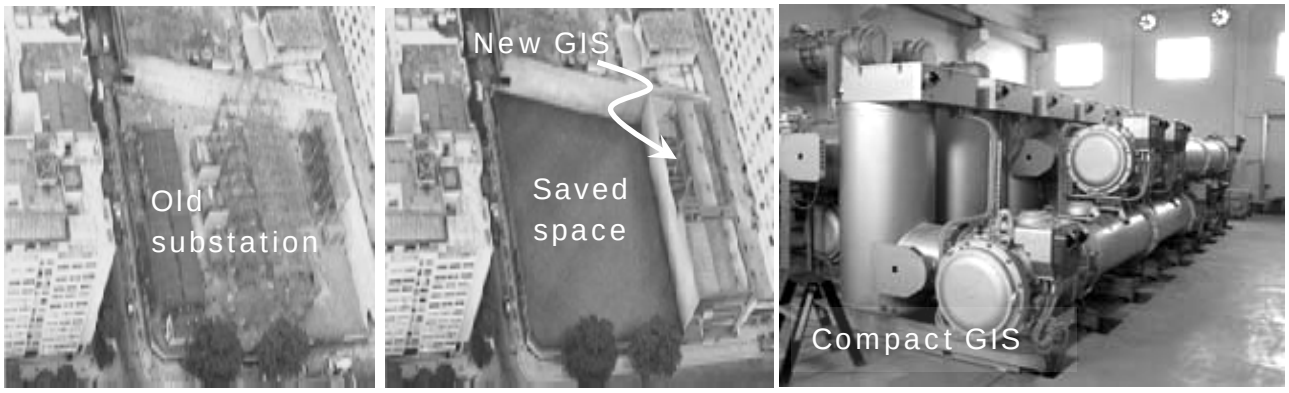

Figure 5.4.20 Space-saving characteristic of gas insulating substations (GIS) makes these substations ideal for operation in urban residential environments.

Due to the compact nature of the GIS (the phase conductors are closer) and the shielding effect of the sheath current, emitted magnetic fields around the equipment are thought to be lower than in conventional substations. Yet, their closeness to public areas makes a closer investigation of these sources worthwhile [21-23].

In Figure 5.4.21, magnetic flux density distributions under balanced and unbalanced current conditions are shown for two 500/275 kV substations, open-air and GIS types. Field distribution in an open-air substation is more influenced by the unbalanced current conditions than that in gas insulated case. This is mainly due to the sheath effect. The steep reduction of the magnetic flux density in a gas insulated substation is also remarkable compared to that in an open-air substation.

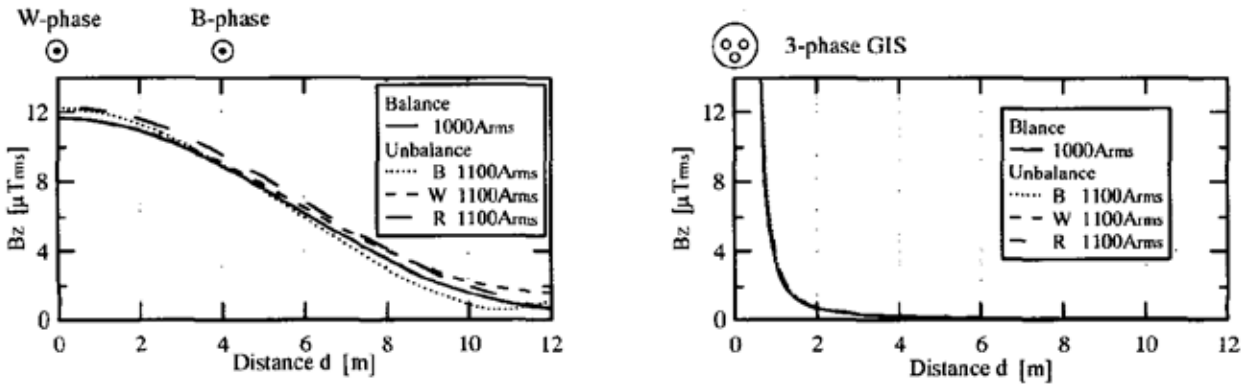

Figure 5.4.21 Comparison of magnetic flux density between open-air substation and gas insulated substation by different current condition [22].

In Figure 5.4.22, the effect of raising the bus structure for double bus 34.5/4.8 kV GIS substation is shown. The purpose of this comparison is to determine the best configuration to minimize the field inside and specially outside the substation. In Figure 5.4.23 the effect is shown of using compaction techniques by minimizing the space between conductors within minimum allowable clearance of the circuit. In both cases magnetic field reduction has been demonstrated [21].

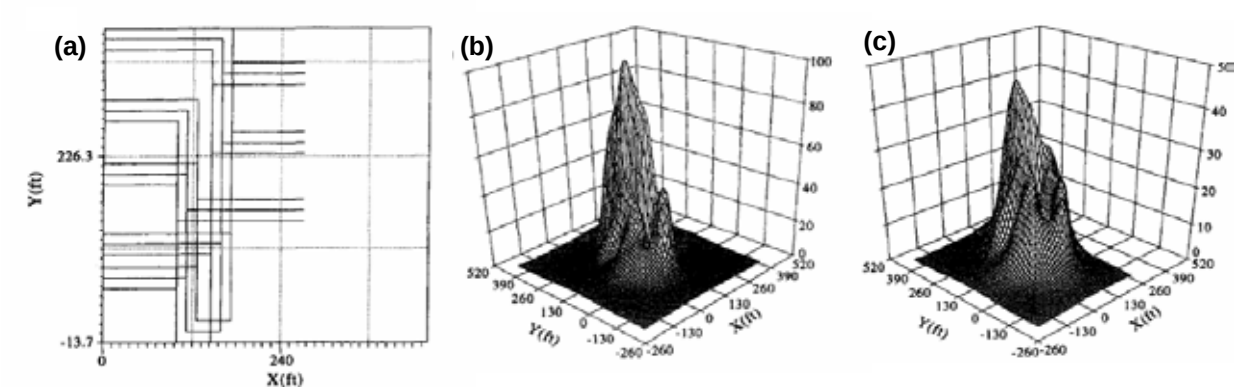

Figure 5.4.22 Simulation of the magnetic field (mG) of the double bus design of a 34.5/4.8 kV GIS substation (a) and the effect of raising the normal bus structure 10 feet (3 m) higher: (b) field values for normal configuration (c) field values for 3 m-high configuration; adapted from [21].

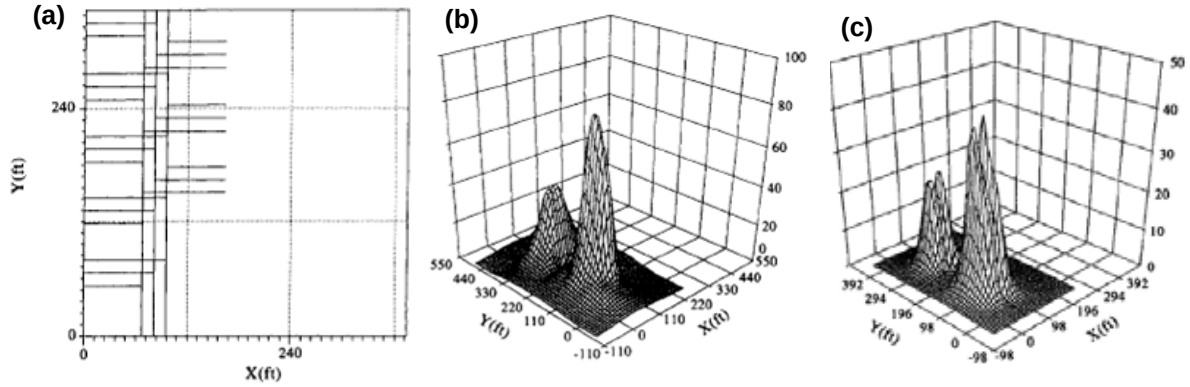

Figure 5.4.23 Simulation of the magnetic field (mG) of a single bus design of a 34.5/4.8 kV GIS substation (a) and the effect of bus structure compaction, (b) field values for normal configuration, (c) field values for 0.2 m compact bus; adapted from [21].

The study of magnetic fields originated from high voltage substations shows a diversity of voltage transformation characteristics (Table 5.4.3); in most of the cases the field was measured and simulated. Roughly speaking, fields inside the substations give peak field values within the range of 10 to 20 μT, while at the borders (e.g. fence, wall or other areas of interest) the magnetic field doesn't exceed a few microtesla, diminishing rapidly along the distance perpendicular to cables or overhead lines exiting the MV side of the substation.

Table 5.4.3 Magnetic field studies of HV substations showing the diversity of voltage characteristics.

Type	**Open air**							**GIS**		
Voltage (kV)	115/13.8	500/275 and 77/6.6	400/110	230/110	115/21	132/11	500/220 and 500/66	34.5/4.8	500/275	110/20
Reference	[14]	[15]	[16]	[17]	[18]	[19]	[20]	[21]	[22]	[23]

5.4.6 Synthesis and additional remarks

The components of a secondary substation yield a rather complex emission pattern, yet the possibility of studying the field emitted by individual sources, and superposing the effects afterwards, helps to work out effective mitigation designs.

Busbars are major sources of magnetic field in secondary substations. Their behaviour in a far region can be predicted rather accurately by analytical computations. However, taking into account the cover of a switchboard and the implementation of a metal shield, it becomes necessary to make use of a dedicated code to model the problem numerically.

Magnetic field emissions of transformers are, in priority order, due to: i) LV connections, ii) coils, and iii) ferromagnetic nucleus; at relatively large distances (> 3m) the contribution of the last two sources is negligible.

Residential and industrial substations differ in power levels. Due to their heavy loads, industrial substations components carry more current and, hence, produce higher magnetic fields

Table 5.4.4 Field mitigation techniques used for MV/LV (secondary) substations.

Source	Strategy	Technique	Method
Short Busbars (residential)	Mitigation at the source	Conductive shielding (e.g. aluminium) Passive compensation	3D-FEM or Integral methods Lab experiments
Long Busbars (industrial)	Mitigation at the source could be too cumbersome. Thus mitigation at the affected area may be needed	Conductive or ferromagnetic shielding Active compensation	2D-Numerical methods Analytical
Transformers	Mitigation at the source, concentrating on the connections at the secondary side	Phase cancellation Distance management	3D-Numerical Experiments with the relevant parts (connections on the secondary side)
Cables	Mitigation at the source	see section 5.3	Analytical 2D-FEM

A HV substation can be of one of two types, an open-air (standard) substation or a gas insulated one. In the first case, the region where the magnetic field is the highest is where the LV feeders are located and the transmission lines (or underground cables) leave the substation. An efficient mitigation technique is distance management. In reference [16] it has been shown that the field diminishes relatively fast along the direction leaving the LV side.

Recently, HV gas insulated substations (GIS) have been receiving increasing attention due to their compactness. This property also allows locating them near urban and residential locations. Various characteristics

of these substations can be optimized (for example conductor distance or bus heights) to achieve mitigation in surrounding areas. As they are often indoors, mitigation using metal shields is also possible.

5.4.7 References

[1] Hasselgren, L. Luomi J., "Geometrical Aspects of Magnetic Shielding at Extremely Low Frequencies", IEEE Transactions on Electromagnetic Compatibility, **Vol. 37**, No. 3, Aug.1995, pp 409-420.

[2] Quinchon L, and Popiel L, Cired Conference 99, Nice, May 1999.

[3] Bottauscio O, Chiampi M, Crotti G, Manzin A, Ribaldone P, and Zucca M, "Design of magnetic shields in MV/LV substations by three dimensional modeling and experimental analysis", EMC Europe 2002 Sept 9-13, 2002 Sorrento.

[4] Garzia F, Geri A, Active "Shielding Design in a Full 3D Space of Indoor MV/LV Substations Using Generic Algorithm Optimization", IEEE 2003.

[5] Haselgren, L., Möller and Hamnerius, Y.,"Calculation of magnetic shielding of a substation at power frequency using FEM", IEEE Trans. Power Delivery, **Vol. 9**, No. 3, July 1994. pp. 1398-1405.

[6] Hiles L., Olsen G., Holte C., Jensen R., and Griffing L., "Power frequency magnetic field management using a combination of active and passive shielding technology", IEEE Transactions on Power Delivery, **Vol.13**, No.1, January 1998.

[7] D. Fulchiron, J. Delaballe "Reduction of the low frequency EMF emission of MV/LV substations" Cired Conference, Barcelona, 12-15 May 2003.

[8] T. Keikko, J. Koinititty and L. Korpinen, "Calculations of Magnetic Fields from Indoor Distribution Substation Busbars", pp. 2309-2314, IEEE, 2000.

[9] Salinas, E., "Mitigation of Power-Frequency Magnetic Fields with Applications to Substations and Other Parts of the Electric Network" Technical Report **No.410**, Chalmers University of Technology, Gothenburg, Sweden, 2001.

[10] A. Taflove and S. C. Hagness, "Computational Electrodynamics: The Finite-Difference Time-Domain Method", 3rd ed. Norwood, MA: Artech House, 2005.

[11] Salinas, E., "Conductive and Ferromagnetic Screening of 50 Hz Magnetic Fields from a Three-Phase System of Busbars". Journal of Magnetism and Magnetic Materials, **Vol. 226-230**, 2001, pp. 1239-1241.

[12] A. J. Casura, T.P. Heuscher, J. Bader and L. Kueng, "Simulation of shieldings and mitigation methods for the electromagnetic field of a transformer", CIGRÉ 2006: C4-305.

[13] A. Canova, F. Freshi, M. Repetto and M. Tartaglia, "Identification of Power Frequency Industrial Magnetic Field Sources for Shielding purposes", Industry Applications Conference, 2004 and 39th IAS Annual Meeting. Conference Record, **Vol. 2**, pp 768 – 773. 2004.

[14] W. K. Daily and F. Dawalibi, "Measurements and Computations of Electromagnetic Fields in Electric Power Substations", IEEE Transactions on Power Delivery, **Vol. 9**, No1, 1994.

[15] M. Shimizu, A.Yoshida, K. Kato and H. Okubo, "Quantitative Evaluation of ELF Electromagnetic Environment at Substations" CIGRE Session 2002, paper 36-105.

[16] T. Keikko, S. Kuusiluoma, T. Sauramäki, and L Korpinen, "Comparison of Electric and Magnetic Fields near 400kV Electric Substation with Exposure Recommendations of the European Union," IEEE, pp. 1230-1234, 2002.

[17] I.O. Habiballah, M.M. Dawoud, K. Al-Balawi and A. S. Farag, "Magnetic Field Measurement & Simulation of a 230 kV Substation", Proceedings of the International Conference on Non-Ionizing Radiation at UNITEN, ICNIR 2003.

[18] William F. Horton and Saul Goldberg, "Power-Frequency Magnetic Fields and public health" CRC Press, Ch. 6, pp 93-108, 1995.

[19] I. Said, A.S. Farag, H. Hussain, N.A. Rahman, "Measurement of Magnetic Field from Distribution Substations in Malaysia" Australian Universities Power Engineering Conference (AUPEC), 2004.

[20] A.T. Wilson, P.J. Wallace, D.C. Smith, "Magnetic Field Effects in the Victoria Transmission System-Design and measurement" Cigre, 1990 Session, Paper 36-103.

[21] A.S. Farag, T C Cheng, L Hu, D. Penn and J. Thompson, "Study for optimal design of gas insulated substations (GIS) to reduce magnetic fields", Electrical Power & Energy Systems, **Vol 19**, No 3, pp 185-194, 1997.

[22] K.Sakai, K.Kato, H Okubo and A. Matsumoto, "ELF Magnetic Field Measurement and Calculation in 500kV Gas Insulated Substation", IEEE, pp.1220-1225, 2002.

[23] T. Sauramäki, T. Keikko, S. Kuusiluoma, L. Korpinen, "Exposure to Electric and Magneticd Fields at 110 kV Gas Insulated Substation (GIS) IEEE, pp. 1226-1229, 2002.

6 EXAMPLES OF MAGNETIC FIELD MITIGATION

This chapter presents some actual cases where magnetic field mitigation techniques have been applied. The design methods as well as the implementation procedures to achieve mitigation are mentioned. Shielding factors or pre- and post-mitigation magnetic field illustrations are also presented.

6.1 VDU interferences in residential electrical facilities[28]

The six cases briefly summarised here are all related to mitigation measures applied in order to reduce interferences on cathode ray tubes (CRT) video displays units (VDU). Although this kind of interference can presently be solved by using LCD or TFT screens, the mitigation methodology remains very useful.

6.1.1 Case study 1: Substation (various shielding techniques)

Installation:

A distribution substation in an office building with Low Voltage (LV) cables suspended from the ceiling of the substation as shown in
Figure **6.1.24**. The computer VDU affected area is directly above the substation cables.

Modification:

- Relocation of the cable from ceiling to floor using new cables and replacing the LV switches with compact circuit breakers. Where relocation of cables is not practical, existing phase cables are packed in trefoil configurations with additional shielding installed around cable trays using several layers of transformer-core steel.
- Two-layer shielding using transformer core steel sheets (Nippon ZDKH27) were installed on the substation's ceiling for additional shielding of LV cables extending from transformer bushings.

Results:

Measured magnetic flux density (MFD) at desk level in the office area directly above the substation before modification ranged from 1 to 20 mT. After substation modification, the computer interference in the affected area was adequately mitigated and the MFD levels were reduced to 0.2 to 1.5 mT as shown in the lower part of
Figure **6.1.24**. Field reduction ranges from 10 to 20 fold were achieved at the office area with previous highest MFD.

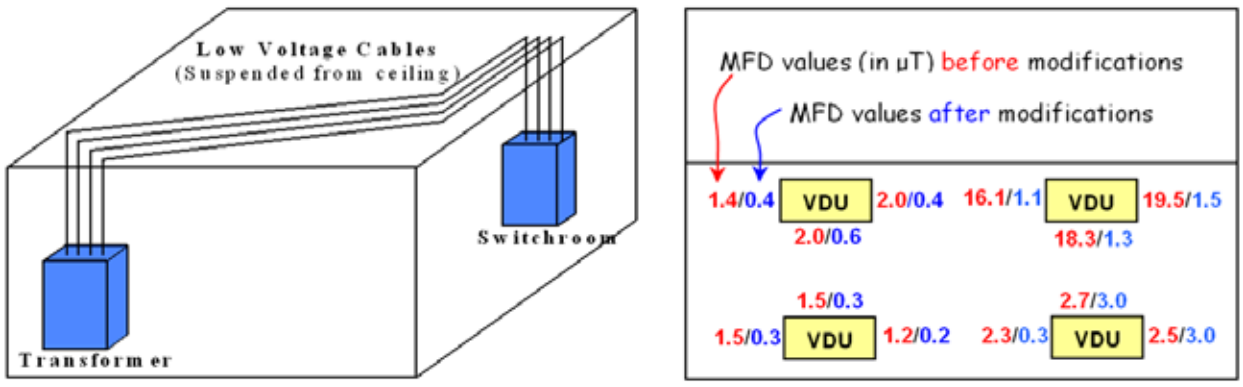

Figure 6.1.24 Case study 1: substation cables suspended from the ceiling (left). On the floor above the substation field was measured around desks with VDUs before and after mitigation (right).

28 Source: T. Dovan, R. Owen, K Nuttall, B. Howard (Australia) – Electra No 181, December 1998

6.1.2 Case study 2: Substation (distance management)

Installation:

A 22 kV/750kVA distribution substation in an office building with LV cables and switch suspended on the substation's ceiling as shown in Figure 6.1.2-a
-a. Computer VDU affected area is directly above the substation cables.

Modification:

Relocation of the existing LV cables from ceiling to floor as shown in Figure 6.1.2-b.

Results:

The measured MFD at desk level in the office area directly above the substation before modification ranged from about 1 to 5 mT. After substation modification, the computer interference in the affected area was sufficiently mitigated and the MFD levels were reduced to 0.2-1.8 mT as shown in Figure 6.1.2-c. At VDU locations, a field reduction of about 10 fold was achieved.

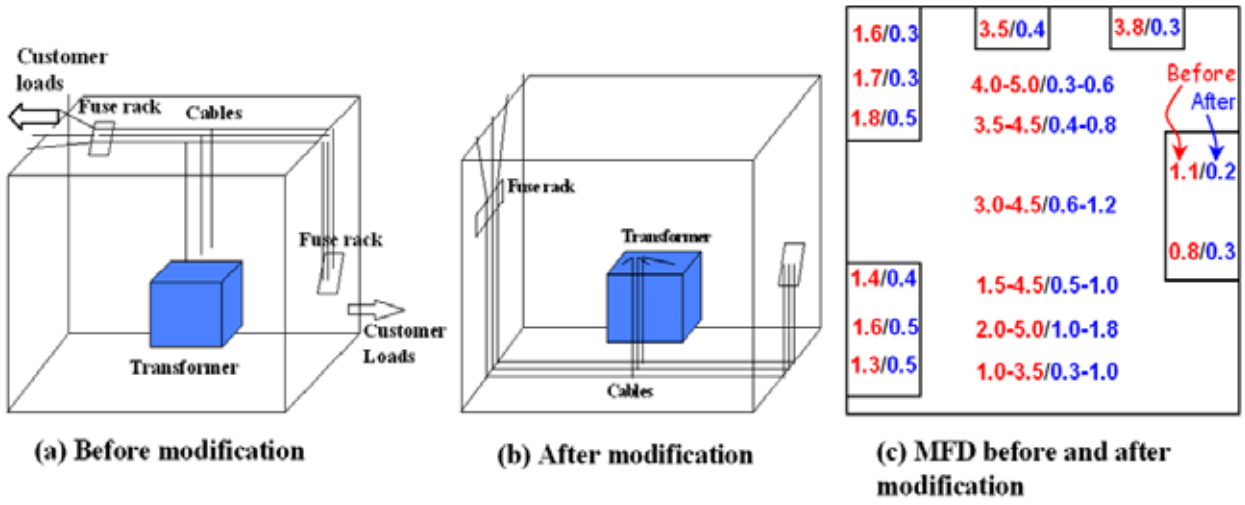

Figure 6.1.25 Case study 2: in-house substation with low voltage cables on the ceiling. The modification consisted of relocation of the LV cables.

6.1.3 Case study 3: Transmission lines

Installation:

Office buildings located at 20 to 30 m from the centre-line of a double circuit 220 kV transmission line. The measured MFD in office areas next to easement/right-of-way (ROW) ranged from 1 to 4 mT.

Modification:

Reverse phases of the double circuit line from abc/abc arrangement to abc/cba arrangement as shown in Figure 6.1.3.

Results:

The VDU interference was reduced to an acceptable level under normal operating condition with both circuits in services. If one circuit of the two circuits is taken out of service for maintenance, interference will occur for a short duration this can be avoided by carrying out maintenance work during non-office working hours. A comparison of ground-level MFD for the two operating conditions is given in Figure 6.1.4.

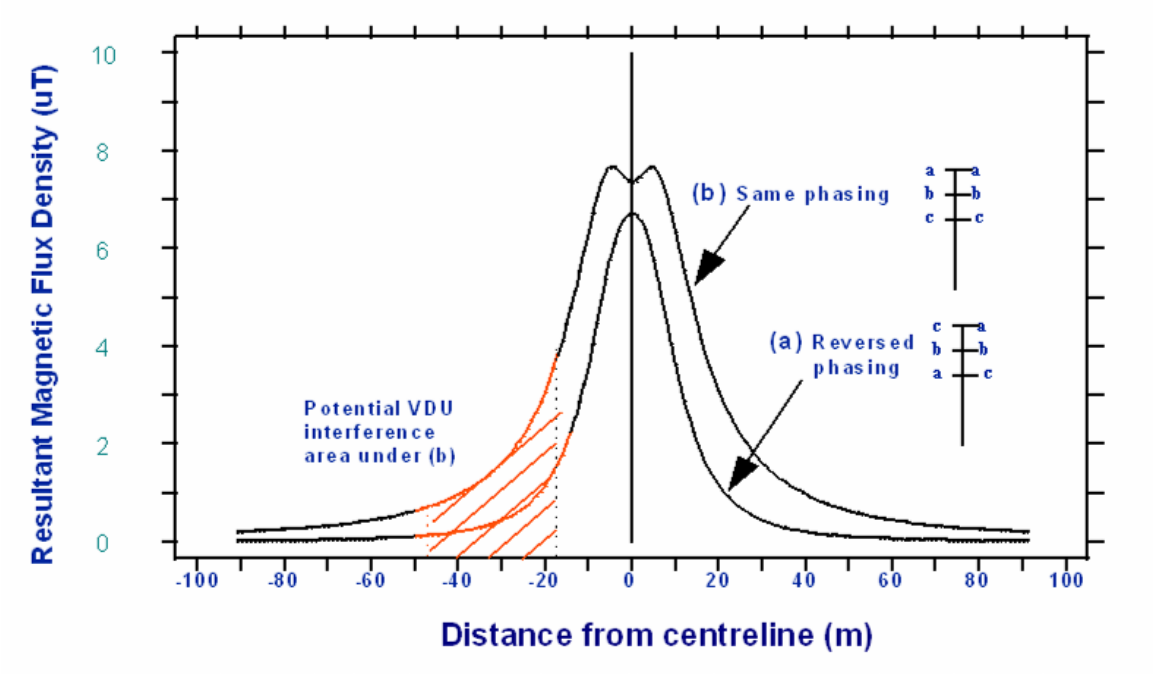

Figure 6.1.3 **Case study 3: calculated MFD under the line (Phase current in each circuit = 500A).**

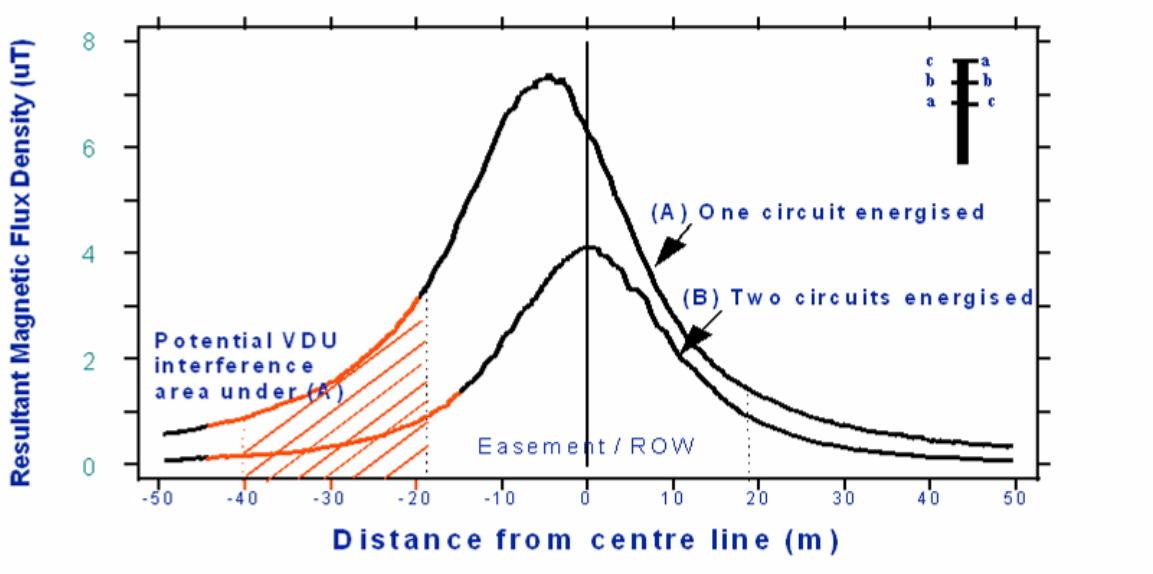

Figure 6.1.4 **Case study 3: measured MFD for two operating conditions (Same total current ~ 760A).**

6.1.4 Case study 4: Distribution lines

Installation:

This case study involved 415/240V "open-wire" distribution lines running along two sides of an office building, with line to building separation of about 1 to 2 m. Several VDUs on second-floor offices of the building were affected.

Modification:

The LV conductors outside were replaced by aerial bundled cables (ABC) for the spans along to the building walls.

Results:

MFD reductions ranging from 4 to 5 fold were achieved in the office areas and the interference was adequately mitigated. Summaries of the MFD measurements before and after conductor replacement are presented in Figure 6.1.5 (respectively left and right).

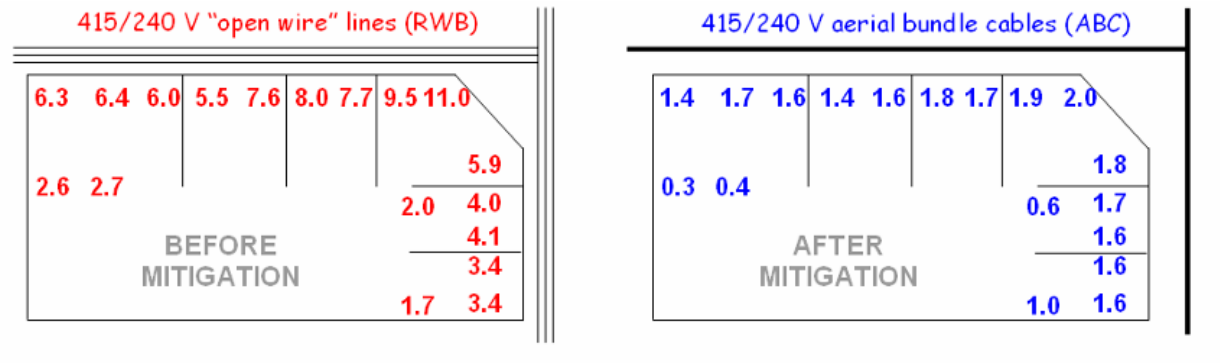

Figure 6.1.5 Case study 5: measured MFD (in microtesla) on the second floor office areas adjacent to external open wire 415/240 V lines, before mitigation (left); measurements after mitigation by replacing the open-wire lines by aerial bundled cables (right).

6.1.5 Case study 5: Ground current in water pipe

Installation:

This case study involves house wiring in which a large current loop was formed by the active conductor located above the ceiling and the water pipe located on ground acting as a neutral conductor.

Modification:

Rewiring the house to ensure the neutral current returns via the neutral conductor.

Results:

Field reductions ranging from 10 to 20 fold were achieved in different areas of the residence. A summary of the measurements before and after rewiring are given in Figure 6.1.6.

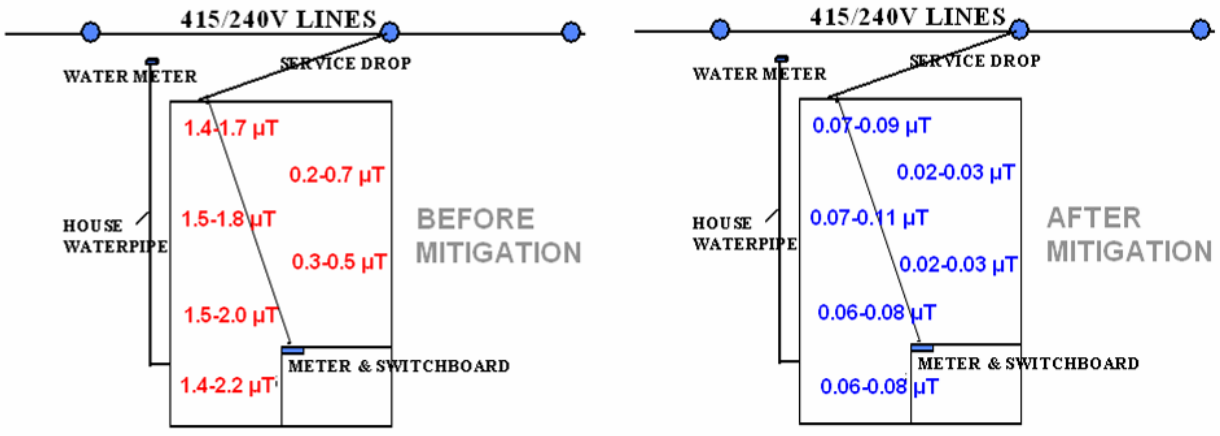

Figure 6.1.6 Case study 5: measured MFD (in microtesla) in a house with water pipe ground current, before (left) and after field mitigation (right) which was achieved by elimination of the water pipe ground current.

6.2 Power cables in Belgium

Several experiences with aluminium shielding and passive loops have been applied to underground cables in Belgium. These experiences are partly discussed in chapter 5.3. The present section describes with more details some of the techniques applied.

6.2.1 H shaped shielding for underground cables[29]

The shielding design presented in Figure 6.2.26 is an illustration of the technique described in section 5.3.4.3. It has been incorporated in the construction of a 6 km section of 150 kV double circuit underground cable link which is 30 km long. Each circuit is constructed from three 2000 mm^2 XLPE cables laid in a flat formation 20 cm above the bottom of a the 150 cm deep cable trench. The horizontal separation distance between the centres of the three cables is 25 cm. The horizontal separation distance between the centres of each cable circuit is nominally about 2 m, but in some locations it is as wide as 5 m.

The phase sequence in both circuits is the same, RST-RST, despite the fact that the low reactance configuration, RST-TSR, would result in a faster field reduction with distance. This has been done because of the low reactance arrangement results in a much higher magnetic field in the space between the two circuits, approaching 100 µT at the ground level.

The screen is built with a large number of 200 cm × 80 cm aluminium plates of 3 mm thickness. The vertical plates are installed to line up both sides of the trench for the entire 6 km length of the cable section. The distance between the vertical plates on either side of the cable circuit is 100 cm. The horizontal plates are installed at 40 cm above the bottom of the trench.

The vertical plates are installed with a small overlap and welded together in argon atmosphere,, starting from the top, over 2/3 of the width of the vertical plates (i.e. the lowest parts of the plates are not welded together).

At both ends of any shielded area, the two vertical walls, formed from welded aluminium plates, were electrically connected together by U-shaped aluminium sections of the same thickness and width as all other plates. This ensures the necessary electrical linkage between the two aluminium walls installed on either side of the cable circuit (see dotted lines on Figure 6.2.26).

In relation to the width of the shielding, it has been shown experimentally that when the distance between the two walls is 100 cm, it results in better shielding effectiveness than when the walls are at 80 cm distance from each other. However, an increase of the width of the horizontal plates to 100 cm resulted in a decrease of the shielding factor above the cables (where the field is the highest).

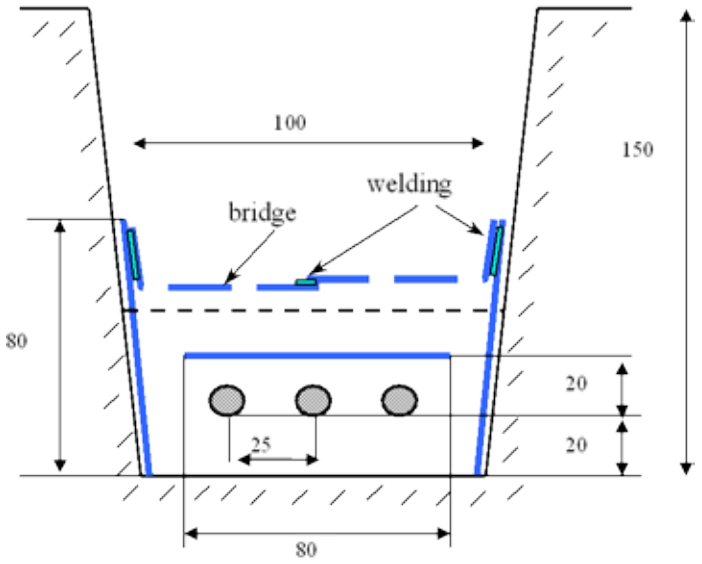

Figure 6.2.26 Practical layout for a H shape shielding.

[29] Source: J.Hoeffelman – Elia - Belgium

Figure 6.2.27 Sight of the vertical and horizontal plates before refilling the trench.

Figure 6.2.28 shows the measured magnetic field above the double circuit cable installation with and without the H-shaped shielding structure described here.

Although the distance between both circuits is not exactly the same in the shielded and unshielded sections, the figure shows that the achieved shielding factor is about 10 in the area directly above the cables and at lateral distances from the cables. If the cable phases were arranged in low reactance configuration, RST-TSR, the shielding factor would have been larger above the cables but lower at lateral distances from them.

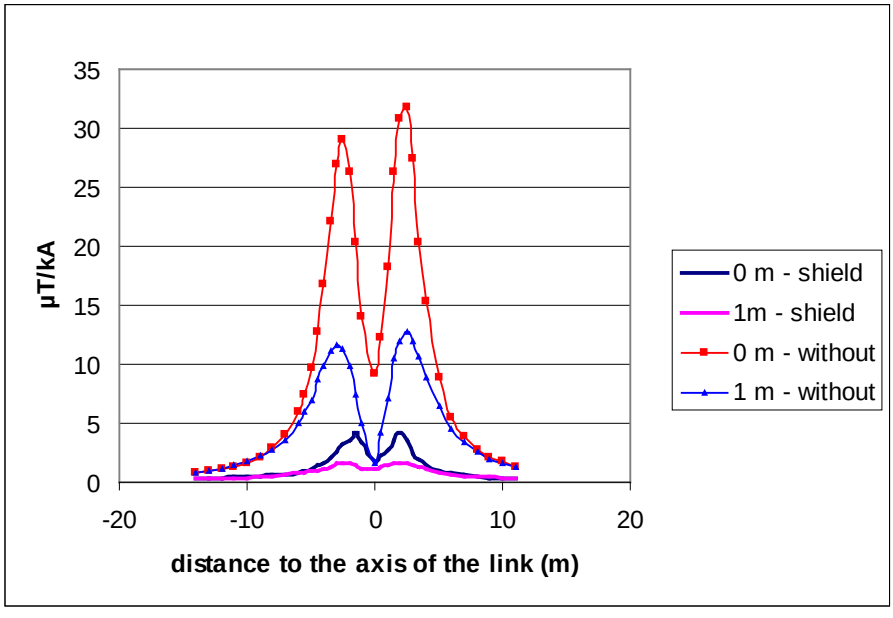

Figure 6.2.28 Measurement results with and without shielding at two different heights above ground.

6.2.2 Passive loop for road crossing

In the project described in 6.2.1, the passive loop technique has been applied to cross some streets and roads. The purpose was not to reduce the field everywhere but to achieve a specific target in terms of the maximum field level in the houses located in the vicinity. The passive loop technique, although less efficient than the shielding technique was easier to apply and less "invasive". It was considered particularly interesting here due to the presence of a double link with an RST-RST configuration and the use of tubes to cross the roads.

Indeed, calculations have shown that putting a passive loop of 300 mm^2 Cu in close vicinity of the external cables of the double circuit could lead to a shielding factor close to 6 at some distance of the link. Practically this was achieved by pulling inside the external tubes two insulated conductors of 150 mm^2 connected to each other at both sides of the road in order to form a double uncompensated loop. This is shown in Figure 6.2.29 where the double aluminium shielding (blue lines) is interrupted and prolonged by the passive loop (red line).

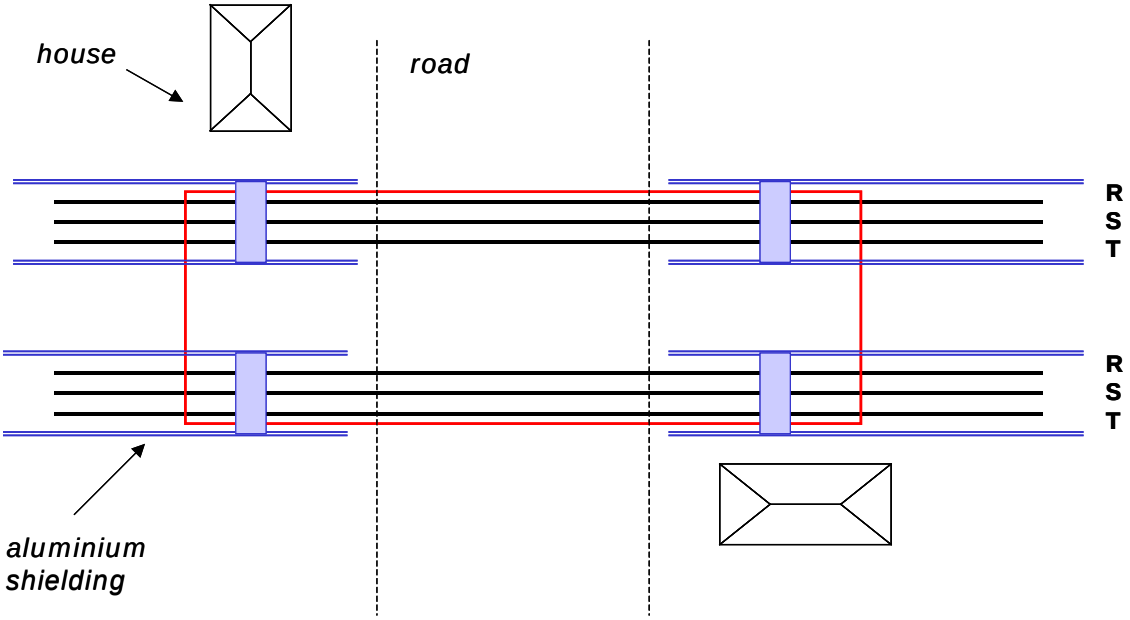

Figure 6.2.29 Passive loop layout for double circuit link.

The exact layout of the power cables and the loops is shown in Figure 6.2.30, whereas Figure 6.2.31 presents a picture of the construction site with some aluminium plates of the H shaped shielding removed.

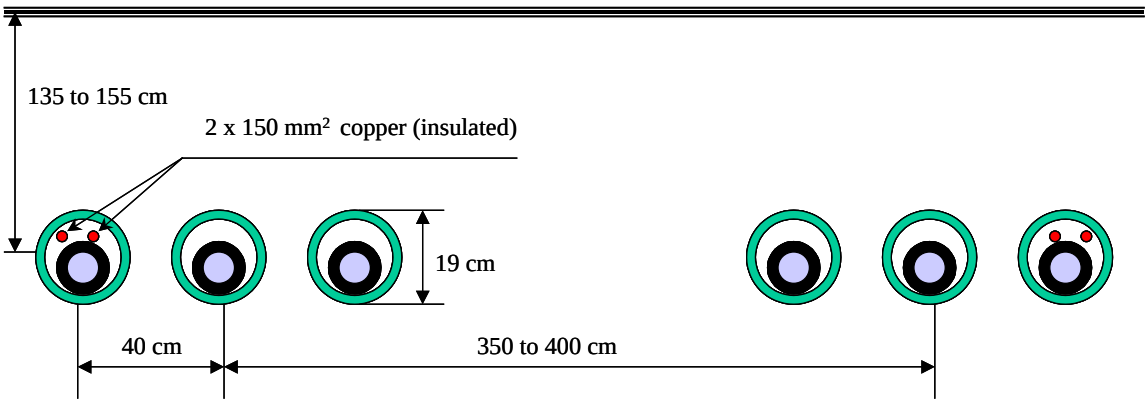

Figure 6.2.30 Layout of the power cables, the PE tubes and the loops.

The efficiency of the loop is shown in Figure **6.2.32**.

Although the ratio of the field level before and after installation of the double loop is limited to 5 at about 12 meter from the axis of the link, the actual shielding factor is higher because the field level before the installation of the loops is already positively influenced by the presence of the aluminium shielding at both sides of the road.

In the absence of this aluminium screen, the shielding factor would have been about 6 at more than 15 m from the axis of the link, very close to the calculated value. This is shown by the dotted line on the graphic.

The impact of the passive loop on the ampacity of the link is very limited: with a maximum of 1300 A in the cable (rated current) the total current in the double loop is about 300 A and the calculated temperature increase of the external power cable less than 6 °C.

Figure 6.2.31 Passive loop at the output of the tube.

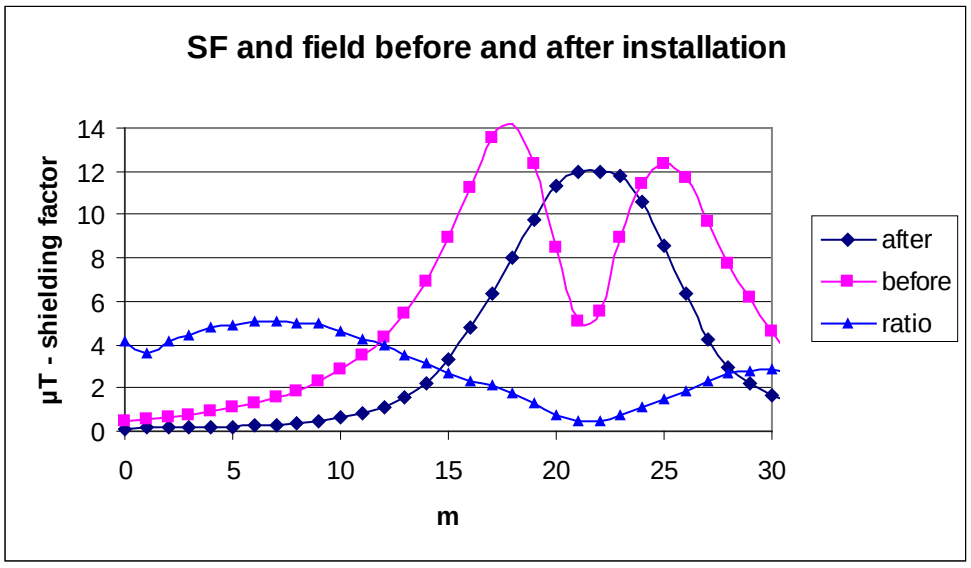

Figure 6.2.32 Shielding factor and field level before and after installation of the loop.

6.2.3 References

[27] A. Gille, V. Beghin, G. Geerts, J. Hoeffelman, D. Liémans, K. Van Gucht - Double 150 kV link, 32 km long, in Belgium: Design and construction - CIGRE report B1-305 – Paris, 2004 session.

[2] A method for applying a magnetic shielding along an AC power line - European - patent application EP 1598911 A1.

6.3 Magnetic Field Mitigation at the Gothenburg City Library

An implementation example of mitigation techniques for the magnetic fields originating from a secondary substation is presented, which is in the cellar of a public library (Göteborgs stadsbibliotek). These premises, shown in Figure 6.3.1 (left), are located in the centre of the city of Gothenburg and are surrounded by other public and urban buildings. At the time of the study, about 190 persons were working in the building and around 3,000 visited it each day [1]. A preliminary survey of the magnetic fields in the library indicated high values on the floor above the substation. Evidence of image distortion in computer monitors [2] and care for concerned workers and persons frequenting the reading room of this library initiated the mitigation study [3], which was carried out in cooperation between the utility firm who owned the substation (Göteborg Energi) and academia (Chalmers University of Technology).

6.3.1 Specifications and field measurements

The electricity supply to the library and neighbouring buildings is a secondary 10/0.4 kV substation (comprising two 800 kVA, 3-phase, transformers) as it is described by Figure 6.3.1 (right). The ceiling of the substation room is 3.5 m over the cellar floor level.

Figure 6.3.1 The City Library located in a central area of Gothenburg (left). The secondary substation is located in the cellar of the building (Right). T1 and T2 are connected by cables to high voltage (HV) and to low voltage (LV) switchboards Swb-T1 and Swb-T2 respectively.

The field magnitude in and around the substation and more particularly in the reading room were measured extensively (Figure 6.3.2). The following was observed:

(i) Fields up to 4μT were measured in the region just above the substation, indicating that these fields may well originate from the substation components.
(ii) Surprisingly, even higher values (up to 7μT) were also registered in extended areas of the reading room (under which there were no substation parts) following a diagonal path along the floor.

Fields produced by some of the substation components could explain observation (i). The field values over the low-voltage parts (LV Swb-T1, LV Swb-T2) were due to the field originating at the busbars situated inside the switchboards. Cables passing near the ceiling of the substation also contributed to the measured field. This was verified by additional measurements of the fields outside the building in areas adjacent to that side of the substation. The observation (ii) demanded another explanation and required further analysis. A stray current (current that escapes from an intended electric circuit) was suggested as the most probable cause of the field values described in (ii).

The cables producing the main values of the magnetic field in the reading room were found in the space between the ceiling of the cellar and the floor of the reading room. The cables were connected to a switchboard and running diagonally, at the predicted locations. The value of this current (averaged 12 A) was also in agreement with the estimations. Measurements of the field at extended regions showed the penetration of the magnetic field, due to stray currents, in other areas of the building.

A magnetic field logger was installed at the reception desk in the reading room. It was situated 10 cm over the floor. The purpose was to detect 24-hours variations on the magnetic field. The average magnetic field during the day was observed to increase about 2 μT with respect to the night values. Short-time variability (order of seconds and minutes) was also observed showing a correlation with the currents of various loads at the library.

6.3.2 Mitigation strategy

Before the initiation of this study, relocation of the substation was under consideration as a first option. Since the majority of the substation components were about 25 years old, a renovation was also planned. The first option was too expensive. Therefore the second option was chosen in combination with component replacement (renovation) and field mitigation operations. It was also decided to mitigate at the sources rather that at the affected areas, i.e. each component was studied and its field emission minimized.

6.3.3 Mitigation techniques applied

Conductive shielding was used to mitigate the emission of new replacement transformers. The field from the busbars was also reduced using conductive shielding. Field reduction from cables was obtained by conductor management, i.e. optimal phase cancellation. Stray currents were treated separately with ferromagnetic "field absorbers".

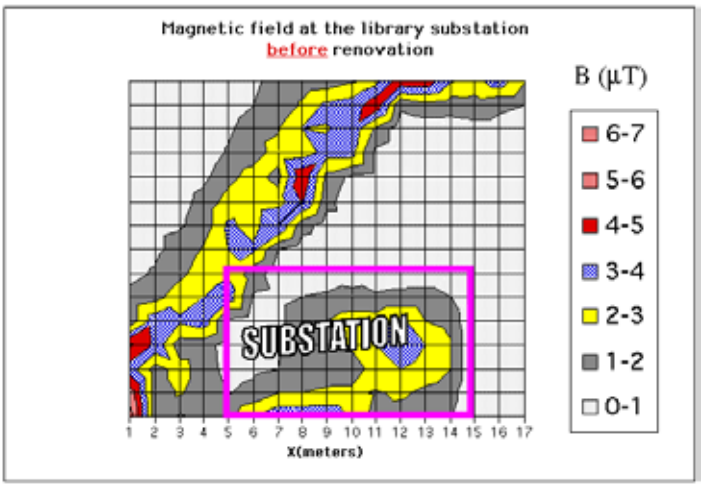

Figure 6.3.2 Magnetic field at the reading room of the Gothenburg city library, one floor above the substation.

6.3.4 Assessment methods used to achieve mitigation

The modification of the various parts of the substation (transformers, busbars, switchboard, and cable-arrangement) implied the choice of low field emission components. For this purpose several experiments were performed (at a large experimental facility of the utility) evaluating the 50 Hz magnetic field emission of various substation parts. The field from a shielded (5mm-aluminum cover) transformer was compared with an unshielded one. Besides the shielding, and even though produced by two different manufacturers, they have very similar characteristics, e.g. both are dry type, three-phase, same size, 800 kVA. As a realistic arrangement, a connection to a switchboard (containing 2m-bus bars, made of Al covered by Cu) was added. The cables were arranged in bundles of different phases, in order to yield the lowest field emission. The shielded transformers showed an averaged decrease in magnetic field emission of 6 times in the area of interest. For the analysis of the shielding of the field from busbars, finite elements were used to simulate the effect of various geometries and materials for shielding plates. The most efficient was 5mm aluminium plates parallel to the plane of the busbar's system [4]. The minimization of magnetic field emission from the numerous cables was obtained by simple rules and computations of phase cancellation and distance management.

6.3.5 Implementation of the techniques

Taking advantage of renovation procedures in which the substation was disconnected, various modifications were implemented, not only by installing new substation components, but also by altering their geometrical disposition in the room of the substation. The main modifications were:

- The unshielded transformers were replaced by new low emission transformers with an aluminium cover (Figure 6.3.3 left).
- A shield of aluminium (5mm thick) was welded to the back of the low voltage switchboard. Additionally a 5mm welded aluminium shield lined the wall at the back of the low-voltage switchboards (Figure 6.3.3 centre).
- Cable connections between components were positioned under the floor.
- A modern high voltage switchboard with low magnetic field emission characteristics replaced the previous one.

The last part consisted of reducing the field due to stray currents. There are two methods to achieve this; one is to install a five conductors system; the other is to install magnetic field reducers of ferromagnetic laminates. The first solution is very costly thus the second option was adopted. Figure 6.3.3 (right) shows one of the ferromagnetic cores that we installed at the location originating the stray currents. The devices are placed surrounding the cable and forming a booster transformer, thus forcing the net current in the cable to be reduced.

Figure 6.3.3 Some of the measures taken to mitigate the field from the substation under the City Library.

6.3.6 Mitigation results

After the modification of the substation a series of measurements were again performed in the same area. The contour plot of these values is shown in Figure 6.3.4-(left). Most of the values registered in the region right above the substation were well under 1 μT and had an average value of 0.5 μT. In the same figure it can be observed that the values of the field due to stray currents, though still high, have an appreciable different distribution than before the renovation. This is due to the fact that stray currents have a broad variation in time. The result after installing the reducers is shown in Figure 6.3.4-(right). Not only the large extended area shows drastic field reduction, but also the average field on the particular area above the substation has diminished.

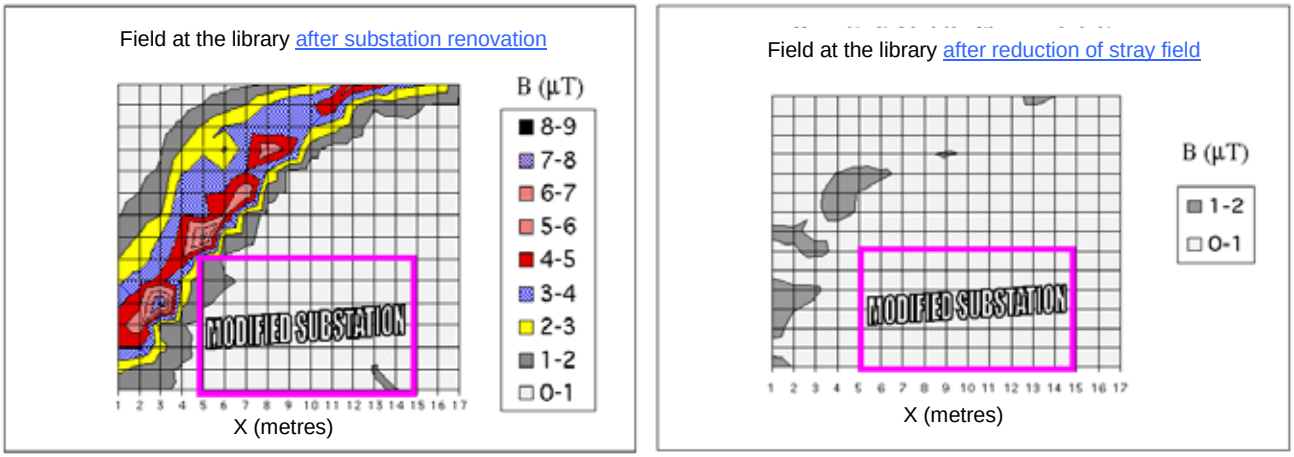

Figure 6.3.4 Magnetic field at the library after renovation operations (left) and after applying booster transformers (right).

6.3.7 Remarks and conclusions

The example presented shows the application of various techniques to a problem in which more than one source is involved. The resulting field pattern is a complex one. Moreover, this case had a major additional complication due to the remarkable extended influence of stray currents. The aim of reaching an averaged sub-microtesla level on the floor above the substation (reading room) was achieved. 1μT is just a technical level of what can be achieved in a cost-effectively approach. If one takes into account that a former alternative was to relocate the substation, which represented a difficult and costly option (the cost of the relocation alone was estimated in 2M SEK~200,000 € in 1999), the decision to modify the substation produced significant cost reductions to the utility as their initial requirement of removing the station from the premises was dropped.

6.3.8 References

[1] Göteborgs stadsbibliotek, Årsredovisning 1999, booklet.

[2] M. Sandström, K. Hansson Mild, and A Berglund, Abstract book work with display units, Tech. Univ. Berlin, Sept. 1992, pp. C5-7.

[3] Swedish Building Board, Krav och råd, Byggnads- styrelsens tekniska standard, Stockholm, 1992-11.

[4] E. Salinas, A. Bondeson, J. Daalder and Y. Hamnerius, Proceedings of CIRED'2001, 16th Conference on Electricity Distribution, IEE Conference Publication No 482, Technical Theme 2, Paper 2.5, Amsterdam, 2001.

6.4 Interference with computer monitors[30]

Cathode Ray Tube (CRT) computer monitors can be disturbed by power frequency magnetic fields with flux density level around 1 μT. Although the problem is becoming less acute with the emergence of flat screen monitors (LCD, TFT, plasma), it is worth recalling some classical mitigation methods that have been applied to solve the problem.

6.4.1 Mitigation by modifying the scan frequency

The visual interference is mainly due to the jitter of the picture that appears with a frequency equal to the difference between the power frequency of the field and the vertical scan frequency of the CRT. The annoyance can practically disappear when this jitter is at zero frequency, i.e. when the scan frequency is identical to the power frequency (this is the case for a classical television screen) or when the jitter frequency is high enough for leading to a beat frequency that is no more noticeable by the eyes (above 20 Hz). Hence, one way to solve the interference problem is either to increase the vertical scan frequency, or to synchronise it with the power frequency. Increasing the scan frequency is only a solution when the amplitude of the jitter is low. Otherwise it can lead to an increase of the eyes' fatigue.

6.4.2 Mitigation by shielding

Magnetic shields for monitors usually take on the form of an external box in which the monitor is placed (easy installation), however, these may also be manufactured to fit the shape of the cathode ray tubes inside the outer enclosure of the monitors.

Most commercially available shields are made of high permeability materials (e.g. mu-metal), however, combinations of high permeability and high conductivity materials can also be used as a trade-off between cost and shielding effectiveness as can be seen in the following illustrative example:

Combined material shields were manufactured at approximately 30% of the cost of imported mu-metal shields in South Africa [1, 2]. The shield comprised layers of (high permeability) Silicon Steel (Si-Fe, 95% also known in trade as M5-30 transformer steel) and layers of (high conductivity) aluminium supporting the Silicon Steel on the outside of the shield (See Figure 6.4.1 below).

Two models were commercialised [2] with the following specifications:

Shield A			
Trade Name	MAGNA IMPRES (MI)*		
Shielding Factor	17		dB
Maximum field level	7		μT
Model	MI14S	MI17S	
Fits monitor size	14	17	inch
Mass	11	15	kg

Shield B			
Trade Name	MAGNA OPUS (MO)		
Shielding Factor	30		dB
Maximum field level	45		μT
Model	MO14S	MO17S	
Fits monitor size	14	17	inch
Mass	~ 30	~ 36	kg

The shield comprises a four-sided enclosure, which made both manufacturing and installation easy. With only four sides, the shield has to be positioned so that the elliptically rotating magnetic field falls perpendicular to the sides of the shield.

Approximately 120 shields have been installed in various locations with successful elimination of interference. The shield is illustrated in the figure below:

Figure 6.4.1 Magnetic field shield with a 14-inches monitor inside.

6.4.3 References

[1] Pretorius, P H, Passive Shielding: A Solution to Magnetic Field Interference with Computer Monitors, IEEE South Africa – SAIEE Joint Energy Chapter, Workshop on EMC: DC to Visible Light, Johannesburg, South Africa, October 1996.

[2] The Shielding of Objects, Republic of South Africa Patent Application 98-1894, 5 March 1998.

[30] Source: P. Pretorius – South Africa

6.5 Shielding of underground cables using ferromagnetic pipes in Genoa (Italy)

This example reports the implementation of a mitigation technique for a three-phase system of underground cables. The technique is based on the use of ferromagnetic shields with tubular geometry. As a result very effective shielding factors of up to two orders of magnitude were obtained [1], [2].

6.5.1 Specifications

The methodology was applied to HV underground cables in Italy. Some of the circuits of these systems cross central and populated areas of cities such as Genoa and Trieste. The present report is the work made in the city of Genoa where about 2 km of circuit of 150 kV 1x1000 mm2 XLPE cable were shielded with this technology.

6.5.2 Technique and materials

The applied technique consists of enclosing the three cables inside a tubular “closed section” shield of a relatively good ferromagnetic material (Figure 6.5.1). The effect of this operation is the trapping of the magnetic flux lines inside the magnetic circuit, preventing propagation to the outside region. The ferromagnetic pipes were realized with low carbon steel, with an external diameter of 508 mm and a thickness of 9.5 mm: the laying depth was between 1.6 and 1.0 meters, according to interference with existing services.

Figure 6.5.1 Disposition of cables within the shielding pipe.

The pipes are protected with a 5 mm thick polyethylene sheath, to prevent corrosion. The extremities of each tube, 8 meters long, were spherically bickered to follow small changes in the path direction and for a perfect welding (Figure 6.5.2). The overlapping zone was protected with a special primer and a polyethylene sheath.

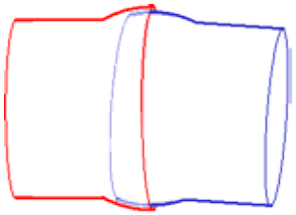

Figure 6.5.2 Spherical bickering of the shielding pipes.

6.5.3 Implementation of the technique

Three plastic pipes, external diameter 160 mm, were pulled inside the shielding tube and blocked with cement injected from an extremity. The trench was backfilled and each cable was pulled in when a section of the entire link was prepared.

6.5.4 Results and observations

The measured magnetic field at 1 meter above ground was found to be always below 0.2 microtesla on the axis of the link, with a current of 800 A. This corresponds to shielding factors larger than 50.

It was not possible to use the ferromagnetic pipes in the main curves, due to mechanical pulling problems (Figure 6.5.3). In these cases, copper plates, 3 mm thick and 1 m wide, were installed, below and above the cables: a higher field value was accepted for these sections.

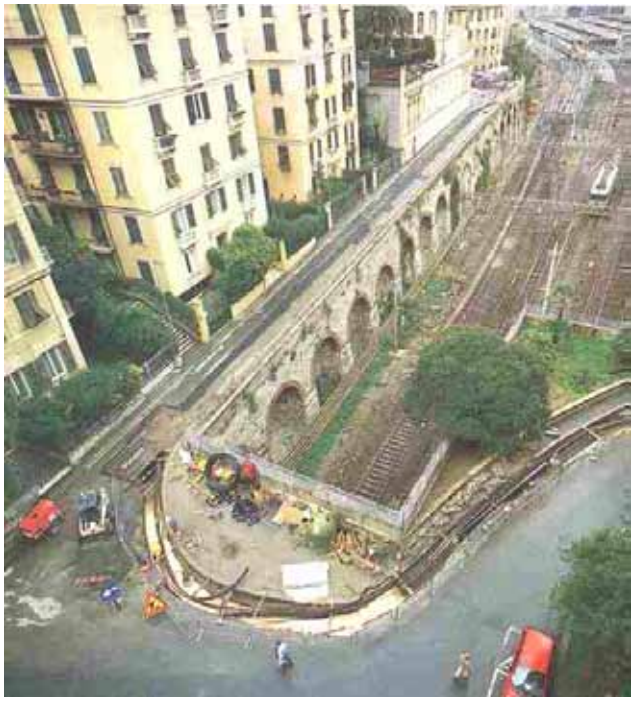

Figure 6.5.3 Aerial view during the pipe installation in Genoa.

In spite of its effectiveness, the pipe system has demonstrated some difficulties in the laying operations and in the successive pull-in of the cables, mainly for very tortuous paths. These two are the main reasons for the subsequent introduction of the raceway system, combining the closed perimeter shielding efficiency with an open shape and the absence of welding.

6.5.5 References

[1] P. Argaut, J. Y. Daurelle, F. Protal, K. Savina and C.A. Wallaert. Shielding technique to reduce magnetic fields from buried cables, JICABLE, A10.5, pp. 331-338, 1999.

[2] R. Conti, F. Donazzi, P. Maioli, R. Rendina, E.A. Sena. Some Italian experiences in the utilization oh HV underground cable systems to solve local problems due to magnetic field and other environmental issues, Cigré 2006 session , paper C4 -303.

6.6 Shielding of underground cables in Naples (Italy) using a ferromagnetic raceway

Several advantages are presented of a mitigation technique for underground cables using a ferromagnetic shielding enclosure with raceway shape.

6.6.1 Specifications

The underground cables between the towns of Lettere and Castellammare, near Naples (Italy), follow a complex and tortuous path. This is a consequence of the existence of numerous underground crossing services within a structure of very narrow streets of medieval villages. The 3-phase cable link to be shielded is 5km long, 132 kV, 1x1000 mm^2 XLPE. The cable has an external diameter of 103 mm. The nominal rating of the currents is 860 A per phase.

6.6.2 Mitigation technique and materials

In view of the special characteristics of the path, the shield design posed several challenges and the ferromagnetic raceway revealed to be the best solution. The raceways are light, easy to install and are designed in such a way that the cables automatically assume the trefoil configuration. The particular shape allow the raceways to follow the small curves of the trench and lateral and vertical variations of direction; for large curves, special shaped elements are used.

The raceway has a base width of 220 mm, a height of 210 mm: the cover is 350 mm wide (Figure 6.6.1). The dimensions of the raceway are adapted to the diameter of the cables, so that any high voltage connection can be shielded. Each section of the raceway has a conical shape so that it can be partially overlapped to the next one, to form a continuous shield, in such a way that any welding is avoided.

The ferromagnetic raceway is composed of different elements: the base, the cover and the closing clips, curved elements and a special box for joint bay. It is constructed with high permeability ferromagnetic steel, galvanised to avoid corrosion problems.

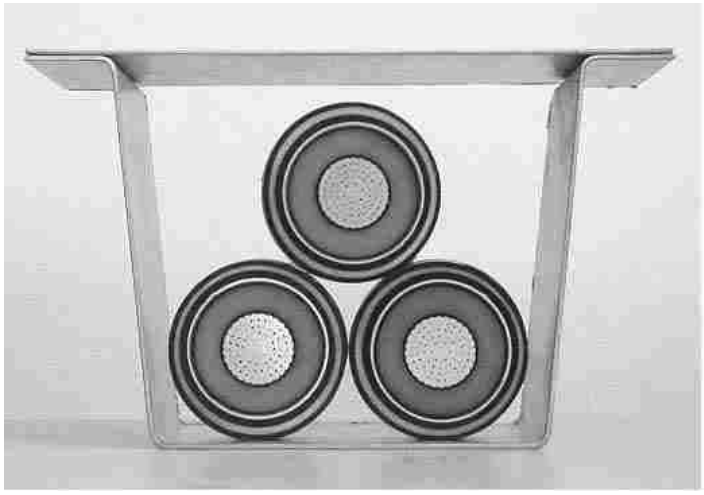

Figure 6.6.1 Photo of the cables lying within the shielding raceway.

6.6.3 Implementation

The bottom of the trench is prepared with a bed of compacted sand and the bases of the raceway are installed, with an overlapping of about 200 mm. Then the rollers are placed on the top of the bases, as can be seen in Figure 6.6.2. The cable is pulled with a simple operation and deposited into the raceway simply by lifting the roller. The same operation is repeated for the other two cables. Subsequently, the raceway is filled with cement mortar and closed with the cover, which is finally fixed by the clips. For the joint bay a metallic box is installed, made of the same

special steel, of rectangular shape, containing the three joints; the box is successively closed with a flat cover which is welded. In order to obtain an effective shielding, the raceway must be installed for some meters longer than the strictly length that has to be shielded because the unshielded field tends to diffuse towards the shielded zone.

Figure 6.6.2 Implementation of the raceway technique in Naples.

6.6.4 Results and conclusions

It was possible to reduce the peak value of the external magnetic field at 1 meter above ground below 0.2 microtesla, at the nominal rating current of 860 A per phase. The effective shielding factor was greater than 18. Other methods based on open-section shields, such as a sheet of ferromagnetic material placed above the cables, will yield only 6-7 attenuation factors [2] at a similar location. On the other hand closed-section conduits made of ferromagnetic materials can provide even larger attenuation factors (e.g. over 20), yet the implementation of this technique presented some hindrances (section 6.5).

Some clear advantages of the raceway shielding technique are: It is light and of simple design; when lying down, the cables automatically assume the trefoil configuration; and, due to the inexpensive materials used, the method is cost-effective.

6.6.5 References

[1] P. Argaut, J. Y. Daurelle, F. Protal, K. Savina and C.A. Wallaert, Shielding technique to reduce magnetic fields from buried cables, JICABLE, A10.5, pp. 331-338, 1999.

[2] Paolo Maioli, Sergio Belli, Fabrizio Donazzi, Method for shielding the magnetic field generated by an electrical power transmission line and electrical power transmission line so shielded, Patent, International Publication Number: WO 2005-013450 A1. Date: 10 Feb, 2005.

6.7 Field mitigation for 3-phase cables with locally flat-configuration using passive loops in the city of Vienna

This example describes the implementation of a passive-loop technique to reduce the magnetic field emission produced by a three-phase system of cables in a location where the system, which has otherwise a triangular disposition, adopts a flat configuration. The technique and the loop geometry were proven to be suitable for this case, which was implemented in the city of Vienna, since the requirements on the shielding factors were not high.

6.7.1 Specification

The arrangement is a 400 kV of underground cables carrying a nominal current of 1500A per phase. The system consist on a open trefoil configuration has been designed and installed with an interaxis of 270 mm at a laying depth of 2.7 m. The field is limited to values below 15 µT. However, locally, the three joints are disposed in an open flat configuration with an inter-axis separation of 300 mm, at a distance of 250 mm from the floor of the chamber (Figure 6.7.1). This local system produces at the ground level a magnetic field of 22 µT. Prescriptions by local authorities demand values of the magnetic field below 15 µT. This, fortunately, represents a shielding factor not higher than 2.

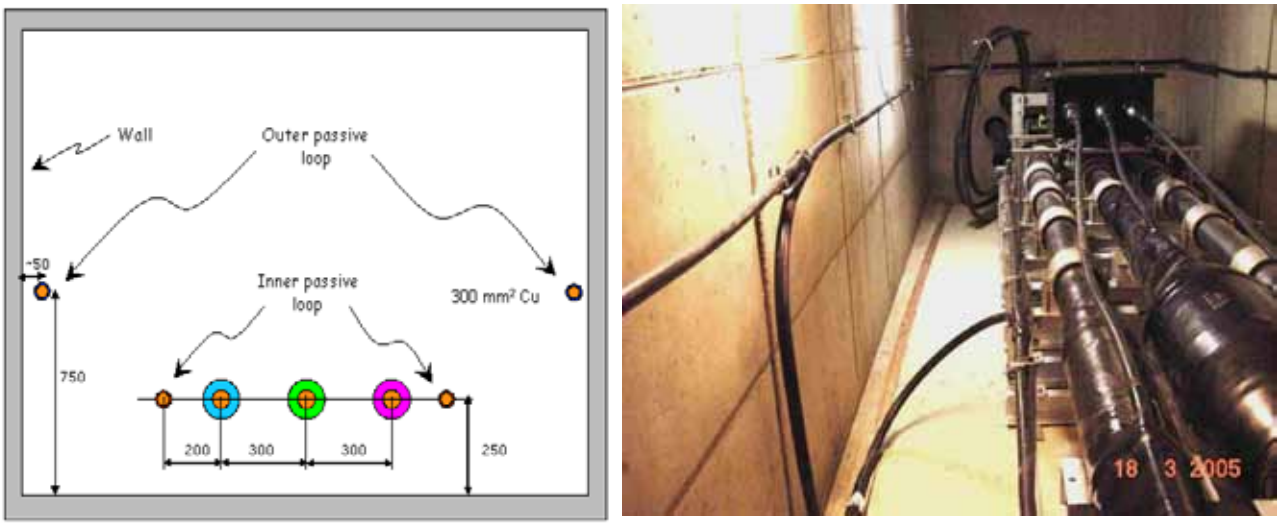

Figure 6.7.1 Left: schematic cross section of the three-phase system and the passive loops inside the joint chamber. Right: **t**he passive loops inside the joint chamber.

6.7.2 Mitigation technique and its implementation

To achieve the desired reduction of the field at the specified locations, a passive loop technique was proposed and designed. The solution consists of two passive loops consisting of flexible copper cables symmetrically arranged near the joints and on the walls of the chamber (Figure 6.7.2). A safety margin was introduced to consider schematic modelling and installation uncertainties.

The inner loop was disposed laterally to the external phase of the three 400 kV cables. The elevation is the same as that of the cables, with a constant inter-axial separation distance of 200 mm from the outer cable. At the extremities, where the cables recover the triangular disposition, the inner loop is parallel to the most external cable, always at the same distance and passes across the three cables, to be connected to the other side: the geometry is the same on both sides of the chamber. To implement the inner loop, 25 m of 0.6/1kV 1x300 insulated copper cable have been used, for a shielded length of 12 metres. The error in positioning (either vertical or horizontal) was less than 10 mm.

The outer loop was fixed on the walls of the chamber, with a spacer to maintain a separation of 50 mm for air circulation. The elevation from the floor is 750 mm and is constant for all the perimeter of the chamber. For practical purposes the same kind of cable was installed for both loops. A less stringent precision of ± 30 mm has been prescribed for the positioning of this loop. The outer loop is isolated from the inner loop and both are grounded. The junctions are protected by heat shrinking sheaths.

6.7.3 Results and observations

The measured results showed that the mitigation technique performed fine, achieving field values lower than the requested limit. This is displayed in Figure 6.7.3 where the field is reported for a full current of 1500 A. The peak value of the field along the joint chamber is below 11 μT. The shielding factor is 2, with respect to the unshielded value of the magnetic field in that zone. In the inner loop a current of 337 A was measured, while in the outer 86 A were observed.

The first applications of passive cable techniques started in Vienna in 2005, to reduce the magnetic field of the joint chambers of a 5.2 km 400kV double circuit [1]. The technique used is not difficult to implement. Since it does not involve shielding materials, its final mitigation results can be predicted rather accurately. Experimental methods can also be applied for the same purpose. Mitigation via passive loops is often a relatively low-cost task. In general, using a reduced number of loops, the technique would not produce great shielding factors (e.g. in comparison with ferromagnetic enclosures). Therefore they should be used in cases where the demands in field attenuation are not high. Yet, extensions to a large number of loops optimally located are possible [2], as they will yield larger attenuation factors.

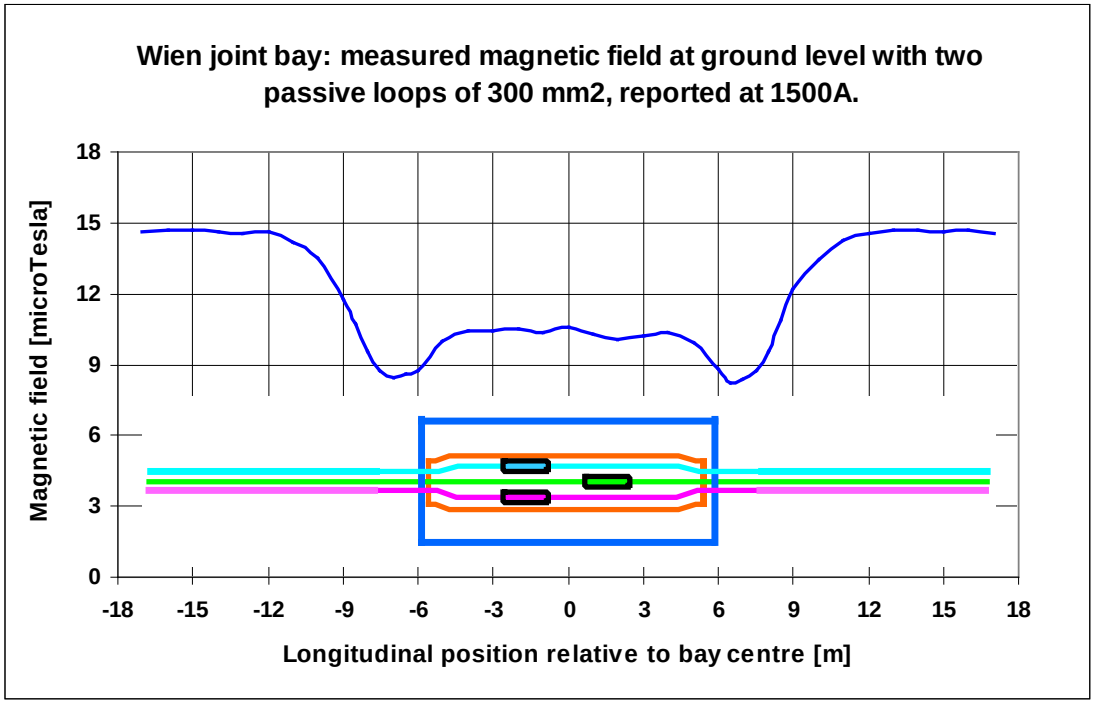

Figure 6.7.3 Modulus of the magnetic field measured along the joint chamber with passive shielding loops.

6.7.4 References

[1] J. Vavra, M. Wanda 400kV Vienna: the Vienna 400 kV North input. - CIGRE Conference paper, B1-101, 2006.

[2] Paolo Maioli, Ernesto Zaccone - Passive loops technique for electromagnetic fields mitigation: Applications and theoretical considerations - 7th International Conference on Power Insulated Cables, JICABLE 07, 2007.

6.8 Numerical modelling for the Ringhals substation (Sweden)

The Ringhals substation case study shows an example of numerical simulations to obtain the best alternative for mitigating the magnetic field originating from a relatively long system of busbars inside this indoors secondary substation. The example includes realistic issues and restrictions, such as the busbars metal surrounding inside the switchboard, which were unavoidable. The final result was a design that fulfilled the suggested requirements for the magnetic field values in the region of interest.

6.8.1 Background

Ringhals is the largest Swedish nuclear power plant and is located in Gothenburg. One of its electrical MV/LV secondary substations is located below an office which is the region of interest. Due to the nature of these premises, any type of emission that could potentially affect workers' health is given special attention to. For this reason it was decided to mitigate the magnetic field from this substation; the requirement being that at 1m above the floor the maximum field should be under 0.5 μT, while its average should be not more than 0.2 μT.

6.8.2 Specifications

The substation contains a 50 Hz, 3-phase system of busbars. The length of the system is 9.86m. The distance from the upper bar (R) to the next floor level is 1.61 m. The value of the current is unknown. However, at 1m above the floor above, i.e. at (x, y) = (1.15m, 4.60m), a preliminary measurement gave a magnetic field value of 2.0 μT.

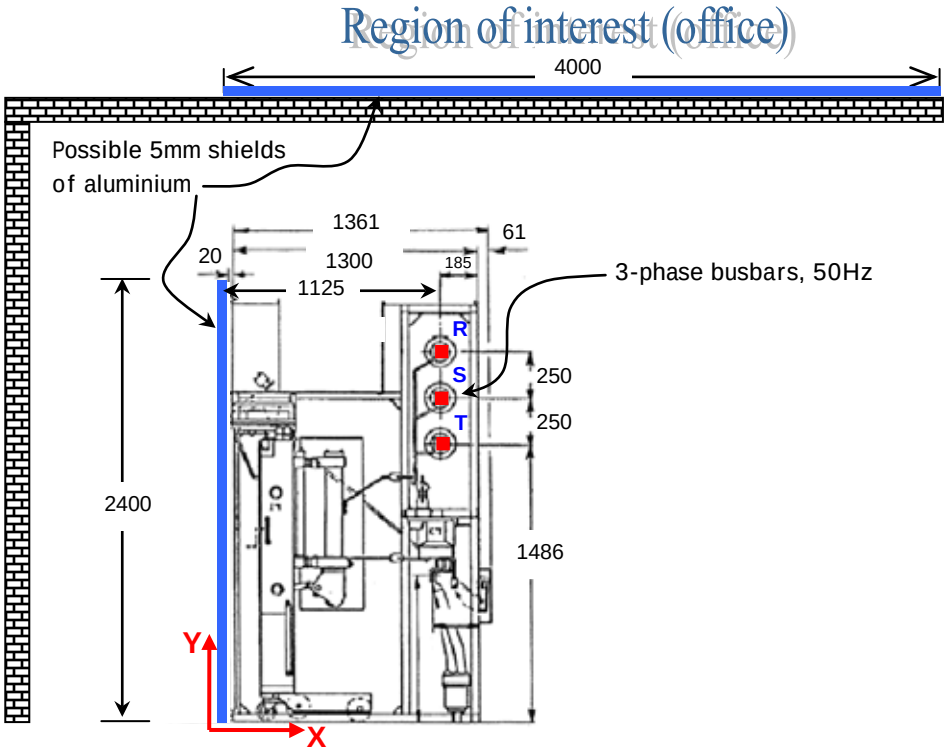

Figure 6.8.1 Cross section of a 10 metres long busbars system surrounded by a complex metal environment. The possible locations of the shielding are also shown.

6.8.3 Mitigation technique

As a result of the long length of the busbars system compared with its inter-bar separation, it is satisfactory to approach this case as a 2D problem. Passive shielding using conductive (aluminium) shields was chosen as the mitigation technique. Since the field mitigation was not applied at the design stage of the substation, but after it had been in operation for some time, several restrictions were present which made it difficult to make an optimal design. The possible shielding plates could be located in only a few places; one at the back of the switchboard and a second one on the floor of the storey above. One of the resulting hindrances is the large distance from busbar to shield, which diminishes the eddy currents' effectiveness. The influence of the complex distribution of the metal around the busbars is twofold. On the one hand it would transform the problem to 3D, harder to solve; on the other

hand, as the busbars' surrounding is composed mainly of ferromagnetic enclosures, it helps mitigate the field. The proposed procedure is to first determine the *effective current* that results from the modification of the actual current due to the inclusion of the mitigation by the busbars surrounding. Then to use this effective current and consider three cases, namely mitigation due to vertical shield alone, mitigation due to horizontal shield alone, and the combination of both of them.

6.8.4 Results of numerical simulations

The numerical simulations were made using the FEM program Multiphysics (from COMSOL). The *effective current* (I_{eff}) that produced the 2 μT field value at the point (1.15m, 4.60m) was computed to be 188A. This value served to compute the three mentioned cases of which the results are shown in Figure 6.8.2.

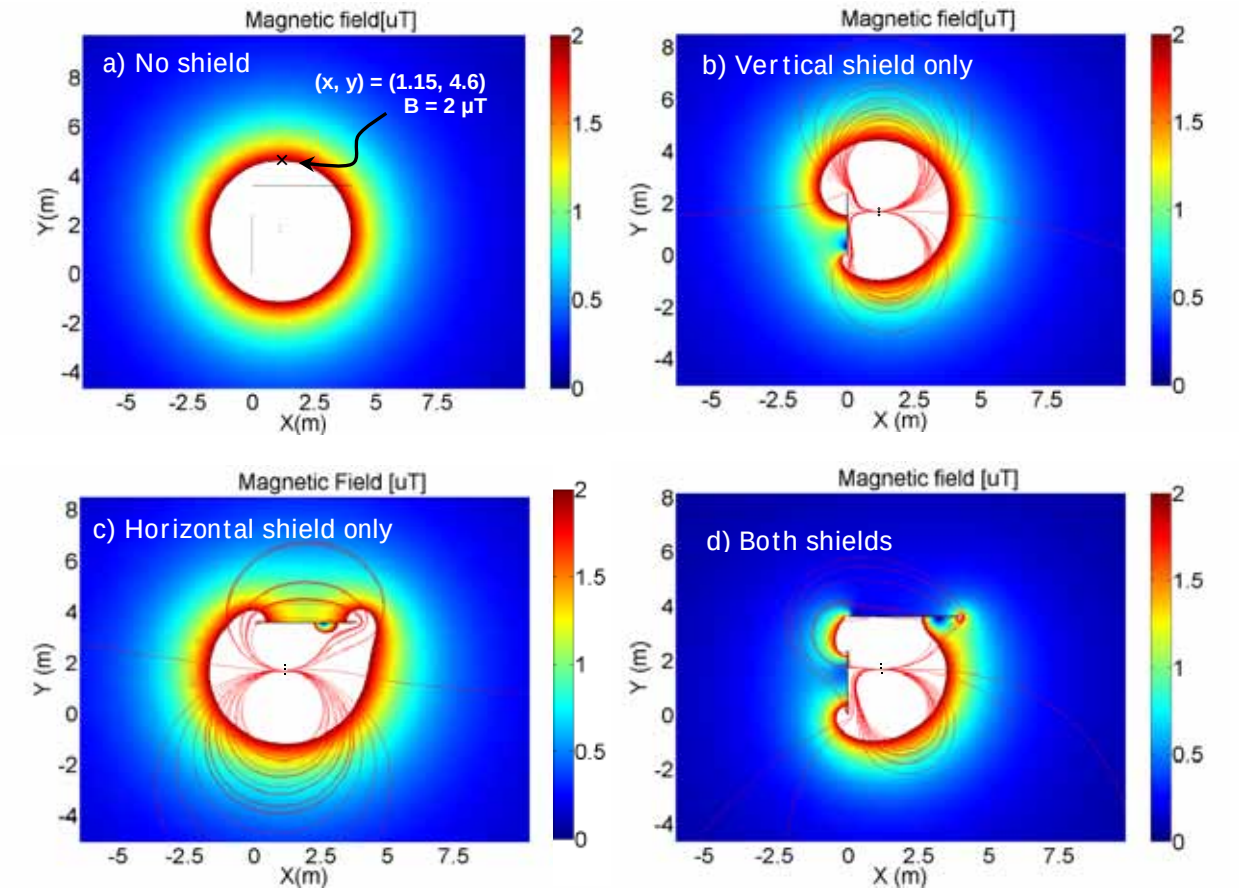

Figure 6.8.2 Results of the numerical simulations for the magnetic field originated from a busbars system. The current that is used in b), c) and d) is resulting from a) and its value was computed to be 133 A. In the last case both shields are joined at the edges.

As it can be observed, the placement of the vertical shield (Figure 6.8.2-b) does not affect the region of interest much. On the other hand, the horizontal shield (Figure 6.8.2-c) affects significantly the field in the same region. Therefore this was tried as an improved alternative (Figure 6.8.2-d) to use both plates; moreover they are joined at the edges. This is shown in Figure 6.8.3. This additional connection creates a conductive loop for electrons to run from plate to plate. In this way additional currents are produced, which helps mitigating the magnetic field.

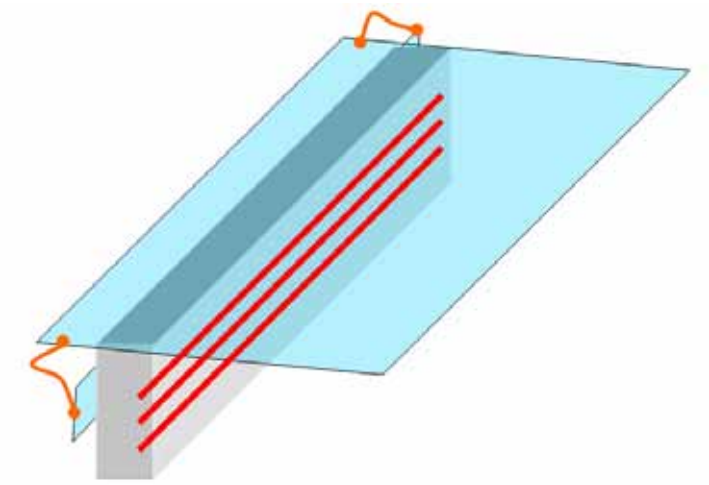

Figure 6.8.3 A schematic 3D-view of the shielding showing the connections to join the vertical and horizontal plates creating a continuity that helps to mitigate the field.

A comparison between the cases a) to d) is shown in Figure 6.8.4. The curve for the vertical shielding shows a little reduction only. The two hills for the horizontal case are due to the field penetration by the edges of the plates. A remaining of this effect is shown in the joint case, much less reduced.

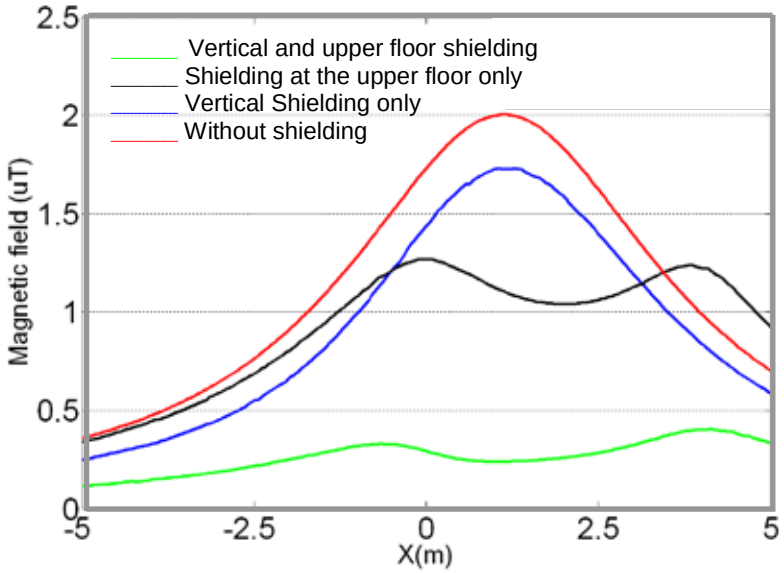

Figure 6.8.4 Comparative diagram showing the magnetic filed values along the line at 1m above the floor over the substation.

6.8.5 Conclusion

Numerical results pointed out that the best option for solving this mitigation case is the usage of both horizontal and vertical shields. In the simulation it was assumed that physical continuity exists at both ends between both shields. Therefore, it was recommended to implement case c) with continuity at the edges of the plates using good conductors (copper cables) and good joints. In the combined case, the resulting magnetic fields are lower than 0.5 μT while the average is about 0.2 μT. These results fulfilled the requirements imposed on the magnetic field at these premises.

6.9 Castiglione Project: a case of active shielding of an overhead line in Italy

The Castiglione Project [1] is the first Italian application of magnetic field active shielding applied to HV transmission lines in Italy. The scope of this project was the reduction of the magnetic field in an area of children activity below 0.2 μT requested by the local administration.

6.9.1 Description of the Project

The state of the site before the work is shown in Figure 6.9.1, where, for the sake of clarity, towers are represented on a different scale than the line and the environment. The area to be protected is highlighted in a shaded square. Tower 36 near this area is a tension tower in an angle position while tower 37 is an aligned suspension one; in both of them conductors are disposed in triangle.

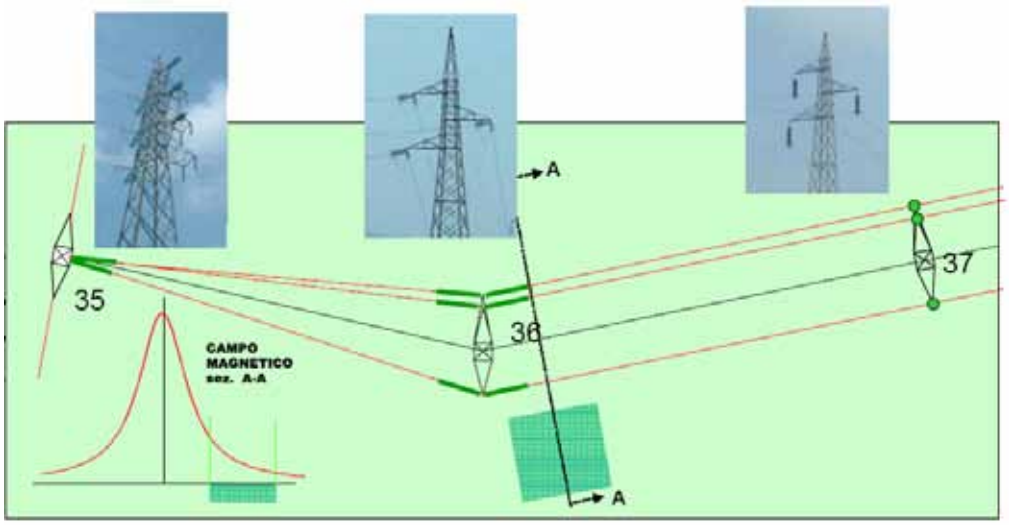

Figure 6.9.1 State of the site before mitigation.

Tower 35 is a double circuit derivation tower; the conductors are therefore disposed in vertical arrangement. The arrangement chosen for the active shielding implies the modification of tower 36 head in such a way that the conductors result in a vertical arrangement (Figure 6.9.2). Due to the line angle the conductors can be supported by sub horizontal suspension strings reducing the conductor-conductor distance; due to the direction of the angle the conductors become more distant from the sensible area. This line transformation implies the following advantages:

- The new conductor geometry reduces in itself the magnetic field
- The vertical conductor arrangement produces a quasi pulsating field (linearly polarized) which can be mitigated efficiently by a single loop in the same vertical plane of the conductors
- The new conductor geometry does not increase the mechanical stresses on the tower body and foundation, avoiding any structural modification

The screen conductors, in Alumoweld®[31], are installed over and below line conductors; the upper screen conductor deserves ground wire function. The current in the screen conductors is held at 40 % of the line current in order to obtain the maximum screening effect; this current is injected by a current generator, a regulated static device fed by the local distribution network.

The current generator control is based on a microprocessor device which receives a sinusoidal signal via radio as an input, generated by a current transformer installed on a line conductor. The control system elaborates the signal and acts on the current generator in order to adjust the current (amplitude and phase) at a pre-determined value which minimizes the magnetic field. The control system is highly reliable as requested by the application; nevertheless any failure is detected and transmitted to the line operator. All these devices are installed in a cabin below tower 36 (Figure 6.9.3).

[31] Alloy that combines excellent conductivity, light weight and good resistance to corrosion, with strength comparable to that of steel.

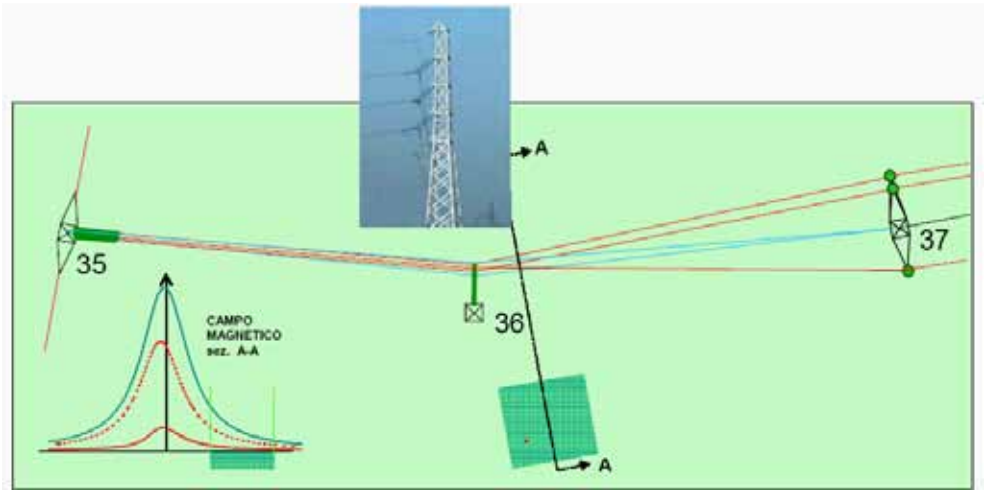

Figure 6.9.2 State of the site after works.

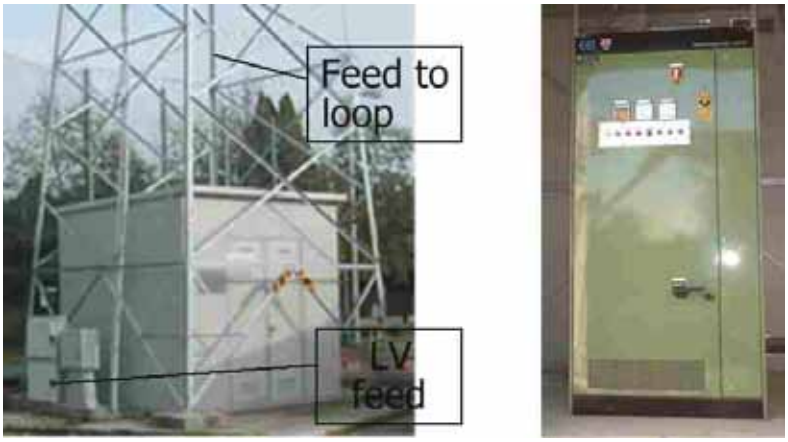

Figure 6.9.3 Cabin containing loop feeding devices (left) and, inside, regulated current generator (right).

6.9.2 Mitigation effect

The relative magnetic induction in the A-A section versus the distance from the line axis is shown in figure 6.9.4 in a logarithmic scale. Field reduction in the sensible area achieved with the entire project is 8 times: 2 times due to the new conductor geometry and 4 times due to the screening effect.

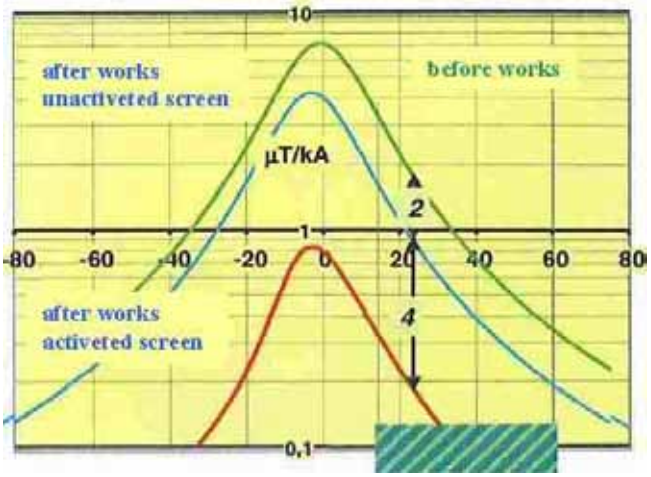

Figure 6.9.4 Magnetic induction in µT per kA of the line current versus distance from the line axis in meters.

6.9.3 Operation experience

The mitigation system is in continuous operation since December 2004: an interruption of the service an august night due to a LV network thunderstorm failure was limited to a 12 hours period; Figure 6.9.5 shows the line current and induction registration for the first 7000 hours of operation (induction is measured at 15 meters from the line axis). Registrations are reported in temporal sequence and in terms of duration; the induction measurement seems to be discontinuous due to the sensibility of the digital registration limited at 0.01 μT.

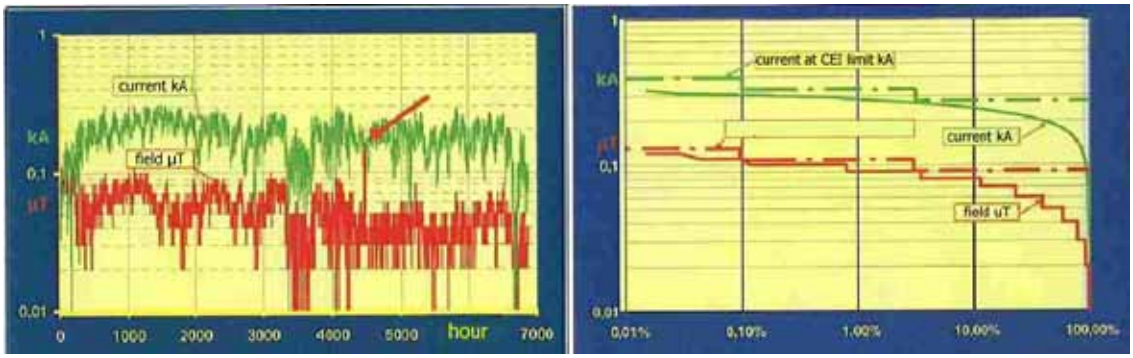

Figure 6.9.5 Registration of line current and magnetic induction; left: temporal sequence; right: duration.

6.9.4 Engineering

This project was developed by Zerotesla, a service company that studies, designs, constructs and assists magnetic field mitigation projects mainly based on active shielding.

6.9.5 References

[1] "Schermo attivo per ridurre il campo magnetico di un elettrodotto", Zerotesla Newsletter, Nº 1, Nov. 2004.

6.10 Traction Systems

Electrical traction is one of the most widespread applications of electricity. Thus it seems useful to give some comments on its corresponding networks and the magnetic fields emitted by these systems. First a brief overview is given of the types of traction systems. Then, in view of this guide, attention is given to AC railways as they are a relevant source of ELF magnetic fields to which travellers and people leaving in their vicinity are exposed. It is also briefly described how these fields are generated and how their magnitude is linked to the different possible feeding systems. Mitigation of these fields as a result of implementation of booster and auto transformer systems or by conductor management are given as examples.

6.10.1 Types of railway supply systems and their typical magnetic field emission

Traction systems can be classified in two categories, namely DC and AC. With respect to the supply voltage, these systems can also be classified as low voltage and high voltage. A simplified list of the most frequent electrical traction systems is presented in Table 6.10-1. The table also contains information concerning the magnetic field levels evaluated at 10 m from the nearest track and at 1 m above the rail level has been collected and reported in the European standard EN 50121-2. These results show that DC traction systems give rise to magnetic field levels in the same range as the magnitude of the Earth's magnetic field (Chapter 1) and very far below the limits suggested by ICNIRP (40.000 µT). On the other hand, AC traction systems can be treated in a similar manner as the other sources in this guide (e.g. power lines, substations, underground cables). Therefore, some of the mitigation techniques developed for the power electric network can be used in AC traction systems. The worldwide classification of electrified long-distance traction lines are plotted in Table 6.10.2.

Table 6.10.1 Simplified classification of traction systems and related magnetic fields for traction systems according to EN 50121-2 (2000).

Type	Voltage (kV)	Frequent applications	Frequency (Hz)	Magnetic field (µT)	Reference conditions
DC ***Low Voltage:*** 0.5kV-3kV	0.75-1.2 Conductor rail	Subways	0	**46**	Ic = 4kA, 50% return current in rails
	0.6-0.75 Catenary	Tramways	0	**15**	Ic = 1kA , 50% return current in rails
	1.5 Catenary	Railways	0	**111**	Ic = 8kA, 50% No aerial wire
	3.0 Catenary	Railways	0	**28**	Ic = 3kA, aerial wire
AC ***High Voltage:*** 15kV-25kV	15	Medium or high speed systems	**16.7**	**40**	Ic = 2kA, No aerial wire
	25		**50**	**16**	Ic = 1.5kA, with feeder wire autotransformer

Table 6.10.2 Worldwide classification of electrified long-distance traction lines (end of 1997).

Supply type	Approximate length (km)	Usage (%)
DC 1.5 kV	20 000	11
DC 3 kV	70 000	38
AC 15 kV, **16.7 Hz**	33 000	18
AC 25 kV, **50Hz**	60 000	33
Total	183 000	100

Concerning voltage levels and frequencies, railway systems still differ today in European countries, (see Figure 6.10.1 and Table 6.10-3). Recently, with the aim of improving traction capabilities, the following modifications have been implemented in various countries:

- DC feeding is replaced by AC 50 Hz, 25kV or 2x25 kV systems for high speed train (e.g. TGV) and for high density traffic (e.g. Netherlands)
- booster transformer (BT) system is replaced by auto transformer (2x15kV or 2x25kV, AT) for heavy freight train traffic (e.g. Sweden iron ore transport) and for high speed train traffic.

6.10.2 Arrangement, current schemes and B field of AC traction supply systems

In case of AC traction supply systems, the traction current is transmitted through the overhead line system to the train and then injected by the traction units on the rails. A significant portion of this injected current penetrates into the earth and returns to the feeding point through the earth. The earth return portion of the current creates with the overhead line a large loop (in km range). This loop current can cause, by inductive coupling, significant longitudinal voltages into the metallic structures (telecom lines, pipe-lines, low voltage overhead lines etc.) installed in the vicinity of the traction lines. In many cases, to mitigate this induction problem, the so called special feeding systems are used instead of the simple feeding systems. The different feeding systems are different regarding the magnetic field generation. This is shortly reviewed hereunder for the three most frequently used AC feeding arrangements [5].

Table 6.10.3 Electric characteristics of the main railway network in Europe.

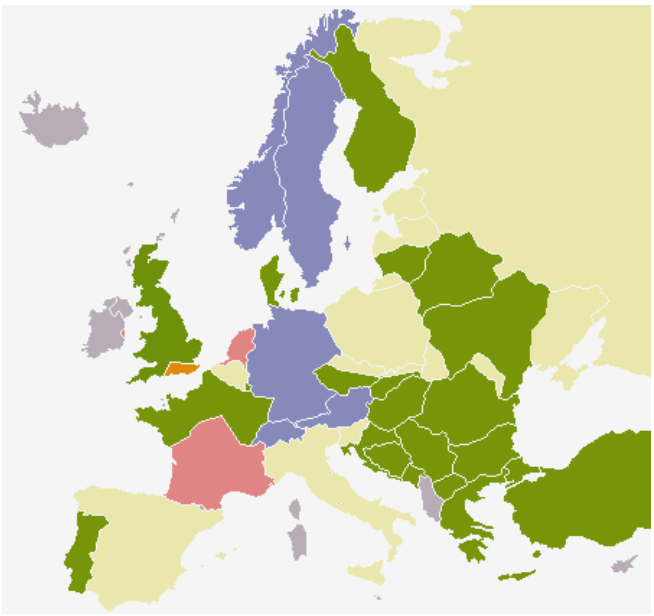

Figure 6.10.1 Supply types of the main railway network in Europe.

Country	Network specifications
Austria	***15kV – 16.2/3Hz***
Belgium	3kV DC ***25kV - 50Hz***
Denmark	***25kV - 50Hz***
France	1500V DC ***25 kV and 2x25kV - 50Hz***
Finland	***25 kV and 2x25 kV – 50 Hz***
Germany	***15kV -16,2/3Hz***
Holland	1500V DC ***2x25 kV 50 Hz***
Hungary	***25 kV and 2x25 kV – 50 Hz***
Ireland	***25kV -50Hz***
Italy	3kV DC ***2x25kV - 50Hz***
Norway	***15kV [2] – 16.2/3Hz***
United Kingdom	***25 kV -50Hz***
Poland	3kV DC
Portugal	***25kV -50Hz***
Spain	3kV DC ***25 kV and 2x25kV -50Hz***
Sweden	***15kV [1] and 2x15 kV – 16.2/3Hz***
Switzerland	***15kV – 16.2/3Hz***

Notes:
(1) Booster transformer system with return conductor
(2) Booster transformer system typically with rail return.

The ***simple feeding system with rail return*** *(RR)* is showed in Figure 6.10.2-a. In this system the locomotive current is taken from the contact wire and returns to the feeding source through the rail and the earth.

The profiles vs. the lateral distance of the magnetic flux density *B* are plotted at 1.5 m above the railhead for 3 train locations in Figure 6.10.3-a. The magnitude of the *B* field rapidly decreases with the lateral distance in the ±5m zone. This is the zone which is essentially excited by the current loop formed by the overhead conductors and the rail. For higher lateral distances the *B* magnitude is much lower and the rate of change is also quite low. In this high distance zone *B* is essentially excited by the current loop formed by the overhead conductors and the earth. Regarding the effect of the distance between observation plane and train location, it can be stated that: in the zone of small lateral distances *B* is higher for closer trains and in the zone of high lateral distances B is higher for distant trains. This results from the above mentioned excitation phenomena and the change in the current share between the rail and the earth due to end effects, i.e. the closer is the train, the higher is the rail current and the smaller the earth current portion will be.

It is worth mentioning also that, in case of multi-train operation the currents of the trains travelling in the supply fed section are superposed and the total traction current flowing through the observation cross section generates the magnetic field at the observation place.

One of the special feeding is the ***booster transformer (BT) system***. In this case the primary winding of each booster transformer is connected in series to the catenary while the secondary winding of each booster transformer is connected in series to the specially provided return conductor (RC) to ensure that a high proportion of the return current will flow through the RC instead of the rail and the earth (Figure 6.10.2-*b*. The catenary (CL) to return conductor (RC) loop is a small sized balanced type loop.

In case of multi-train operation the overhead conductors-to-rail currents, which are the source of extensive *B* field, are added only for the trains which are running the same BT-bond line section. The probability of presence of more trains in a BT to bond section is quite limited due to the short section length. The currents of the trains which are outside the observation section are added in the CL-RC current loop, which is a balanced type narrow loop causing limited excitation.

The arrangement of an ***autotransformer (AT) system*** is presented in Figure 6.10.2-*c*. This system is fed between the contact line (C) and the inverted (or negative) feeder (P) with a voltage which is twice the normal contact line voltage. The ATs are connected across the contact line and the inverted feeder and their mid-points are connected to the rail (R); thus, the difference of potential between contact line and rail is, as required, the normal contact line voltage. The current distribution in AT system is also shown in Figure 6.10.2-*c* as per unit (p.u.) values of the train current.

The current taken by the train is divided half-by-half between the two neighboring ATs (see loop currents marked by solid lines) when the train is around the middle of the AT section. Each current portion is circulating in the AT – contact line – train – rail – AT midpoint loop. In fact, the conditions in the "*trained AT section*" are similar to the one of the simple feeding system, i.e. it works with rail (plus earth) return.

The ATs terminating a trained section are transforming the above mentioned 1U level loop currents to currents circulating in the 2U level balanced type contact line – negative feeder loops marked by doted lines in Figure 6.10.2-*c*. The magnitude of each balanced 2U level current is half of the converted 1U level current magnitude.

The B field outside the trained section is excited essentially by the balanced C-P loop current, which is a narrow loop and the current magnitude in is only half of the traction current taken by the trains.

More comprehensive information is given in Figure 6.10.3-*b* showing the variation of the *B* field with the train location in the observation place at 12.5 km from the supply section, assuming the following train locations:

- inside the trained section at the km 13.0, close to the observation place;
- outside the trained section at the km 20.5, behind the next AT;
- outside the trained section at the km 30.5, behind the next but one AT.

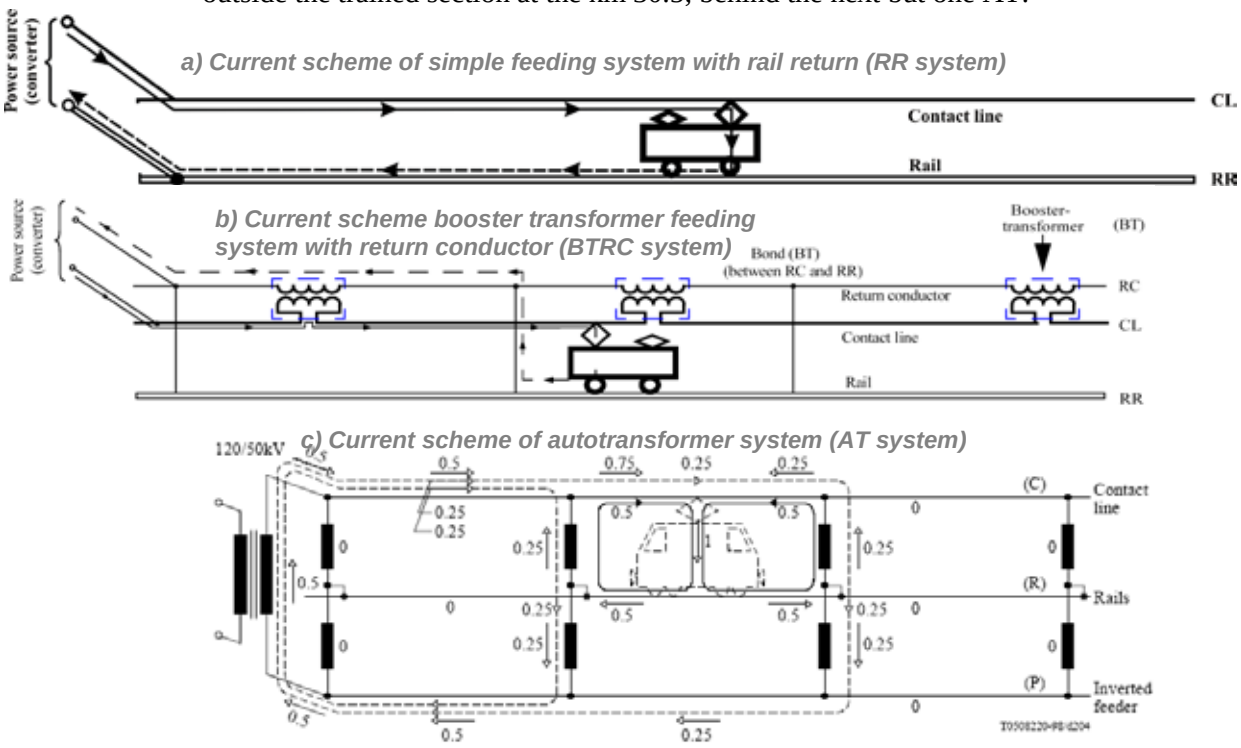

Figure 6.10.2 Arrangement and current schemes for the different AC traction feeding systems.

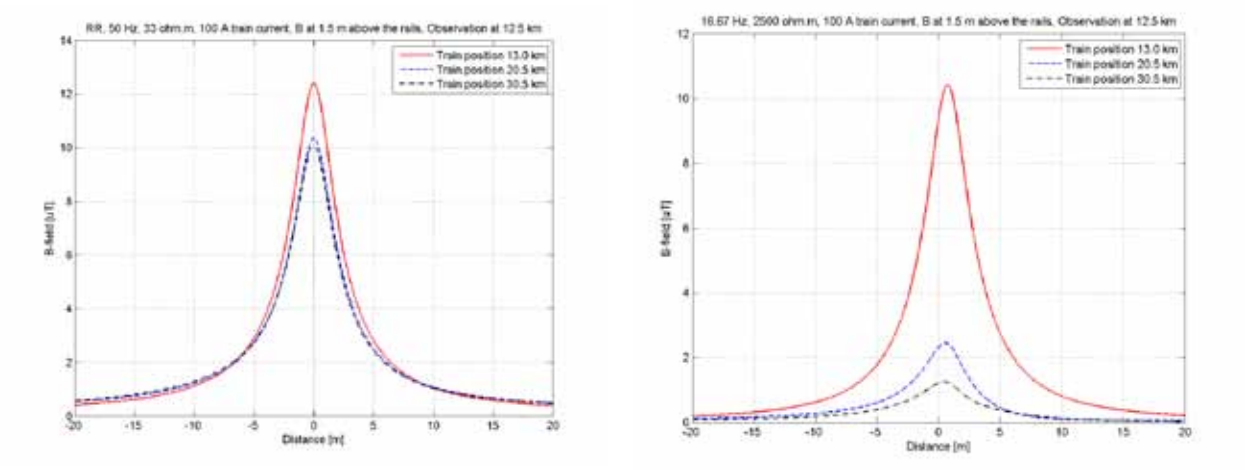

a) Simple feeding system *b) Autotransformer feeding system*

Figure 6.10.3 Lateral profile of the magnetic field density at 1.5 m above the railhead of a single-track line for 3 train distances (observation place at 12.4 km from the feeding point, traction current: 100 A).

6.10.3 Remarks on field mitigation by transformer systems

The use of the special feeding systems, i.e. the booster transformer and the autotransformer systems, originally aimed at the reduction of the induction effect from the traction line to other metallic lines. In addition to the just mentioned advantage, these especial feeding systems mitigate the magnetic field emission in the following manners:

- *The overhead conductors to rail and to earth current loops, which can excite extensive B field in the surroundings of the traction line, are limited to the short trained section, i.e. the train to the nearest bond section in case of BT system and the train to the neighbouring ATs sections in case of AT system. Consequently the duration of the higher level B field generated by the current circulating in the overhead conductors to rail and to earth current loops is limited to that short time during which the train is passing through that trained section where the observation place is. Fig 6.10.4 shows the measured B field, produced by a 25kV-50Hz High Speed railway line equipped with AT, versus time, during the train transit in the trained section. The observation point is placed at about 11.1m from the track axis and at 0.6m from the soil. More information can be found in [4]. This does not apply to the B field inside the railway coaches caused by the current taken by the engine of the train itself, because this B field is moving together with the train.*

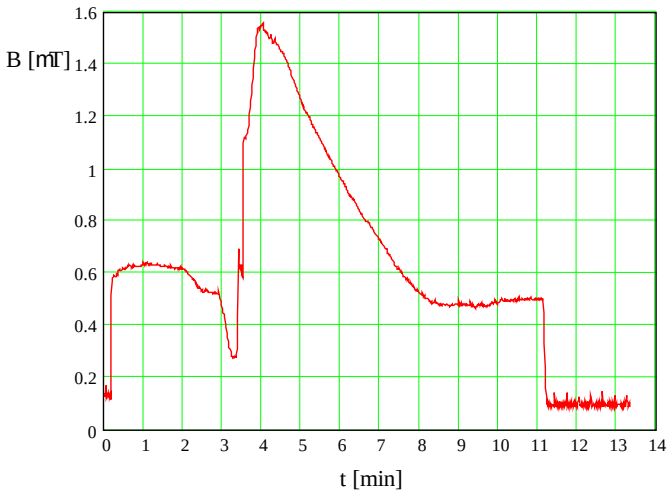

Figure 6.10.4 Measured magnetic flux density field versus time produced by a 25kV-50Hz High Speed railway line; the distance from the line axis 11m.

Ø *In case of multi-train operation the currents in the overhead conductors to rail and to earth loops are summed up only for those trains which are taking the current in the same trained section. The number of these trains is very limited due to the short lengths. The currents of trains running in different trained sections are superposed in the transformed wire-to-wire loop (contact line-return conductor for BT and positive-negative feeder conductors for AT). These balanced type loops are generating smaller B field due to their smaller size. In addition the current magnitude in the loop of the positive-negative feeder conductors is half the magnitude of the traction current, due to the transformation on double voltage level.*

6.10.4 Case study (Italy) of the magnetic field from a typical 2x25 kV AC system

Italy has been chosen here as example for AC Traction systems. The Italian high-speed railway system is mainly composed of three parts:

- railway lines (the AC contact line at 25 kV, the railway tracks and the feeders)
- electrical substation (called SSE) for the transformation of the electric energy from a three phase 132kV system to a one phase 50 kV (or two phases 2x25 kV)
- overhead lines at 132 kV dedicated to the supply of the railway system

The supply voltage of 25 kV is obtained from a 132kV/50kV power transformer. The two voltages +25 kV and -25 kV are derived between the terminals of the secondary winding and its central point. The central point is connected to the rail, while the other two terminals are connected respectively to the contact line and to the feeder, as shown in Fig. 6.10.5 For the second railway line, parallel to the one considered, the two potentials +25 and -25 kV are inversely connected to the feeder and to the contact line. The feeders, through the autotransformers connected between the rails and the feeders, allow reducing the current in the rails and, consequently, the part of the current that naturally tends to flow through the ground, producing effects like corrosion or electromagnetic interferences. For example in the Italian high speed system the distance between two subsequent SSEs is about 50 km while the distance between two subsequent boosters is about 12 km.

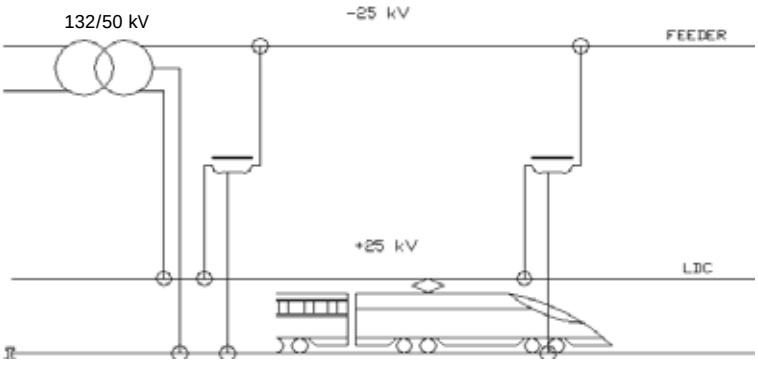

Figure 6.10.5 Principle scheme of a SSE.

The one-phase 25 kV traction transformers connected to the line-to-line conductors of the AC high voltage system generates unbalanced currents on the three phases 132 kV side. This effect is reduced by connecting the transformers suitably selected line-to-line voltages in the subsequent SSEs (as shown in Figure 6.10.6). Assuming typical train traffic on the two parallel railway lines, it is possible to assess, for making the magnetic field analysis, a set of balanced three phase currents.

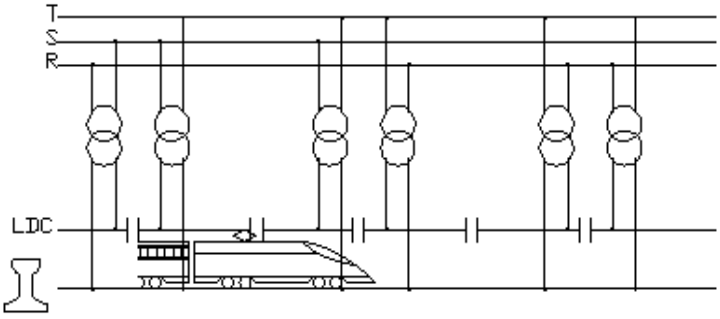

Figure 6.10.6 Reducing unbalance in the three phase system caused by the traction power.

A simplified scheme of the conductor layout of double-track railway line is reported in Figure 6.10.7, where: 1,2,5,6 are the railway tracks; 3, 7 are the 25 kV AC contact lines and 4, 8 are the negative feeder conductors.

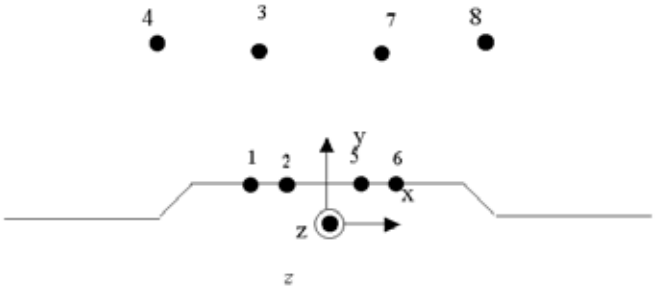

Figure 6.10.7 Conductor layout of the 25kV AC.

The line current value depends on the number of trains which are present on the railway track. An indicative set of current values is reported in Table 6.10.4.

Table 6.10.4 Current values assumed for the railway conductors

Conductor	**Current**
Contact line (3;7)	250 A
Feeder (4;8)	-150 A
Rail (1-2; 5-6)	-50 A (for each track rail)

To support the energy requirements of the 25 kV AC railway system a dedicated high voltage line is usually built near the railway track. In Italian installations the voltage is 132 kV. Different pylon solutions can be adopted: standard and compact tower (Figure 6.10.8). Here, the case of two transmission lines (on the same tower), one dedicated to the supply of the existing 3kV DC substation and the other for the supply of the 25 kV AC railway system is presented. The current amplitudes are assumed to be of respectively 140 and 280 A without any phase transposition.

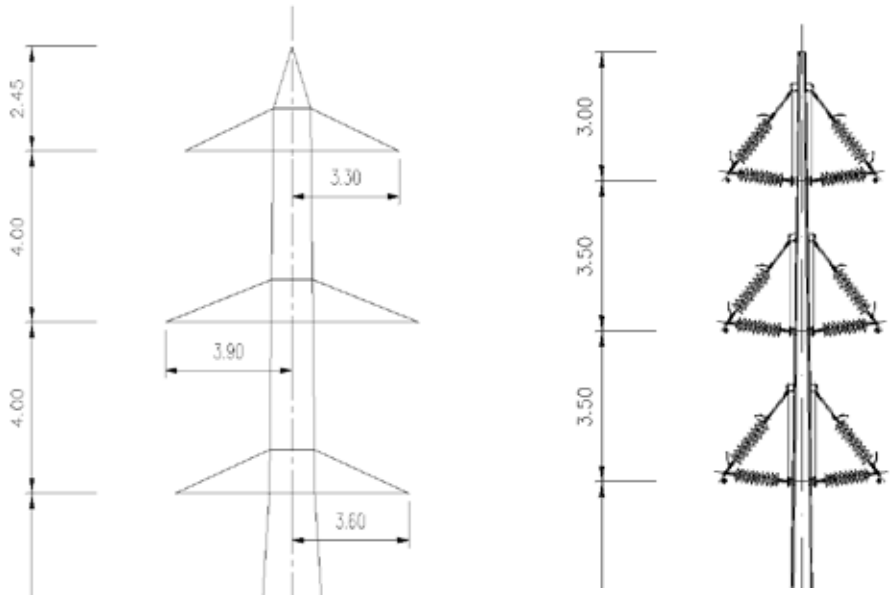

Figure 6.10.8 Standard and compact pylon for the 132kV three phase line; both start at the same height.

The magnetic flux density distribution due to the railway system is reported in Figure 6.10.9. It is possible to observe that, at 10-20 m distance from the line centre, the field levels are very low.

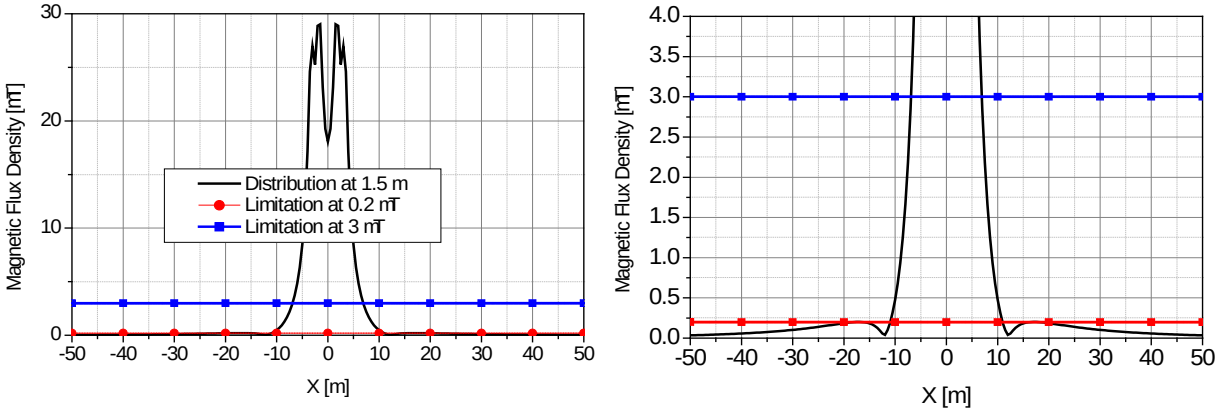

Figure 6.10.9 Magnetic flux density distribution at 1.5 m from the rail level, double track line; currents in the conductors are according to Table 6.10.4.

The 3 μT contour plot of the magnetic flux densities produced by the 132 kV lines are represented in Figure 6.10.10 for both the normal and compact layout.

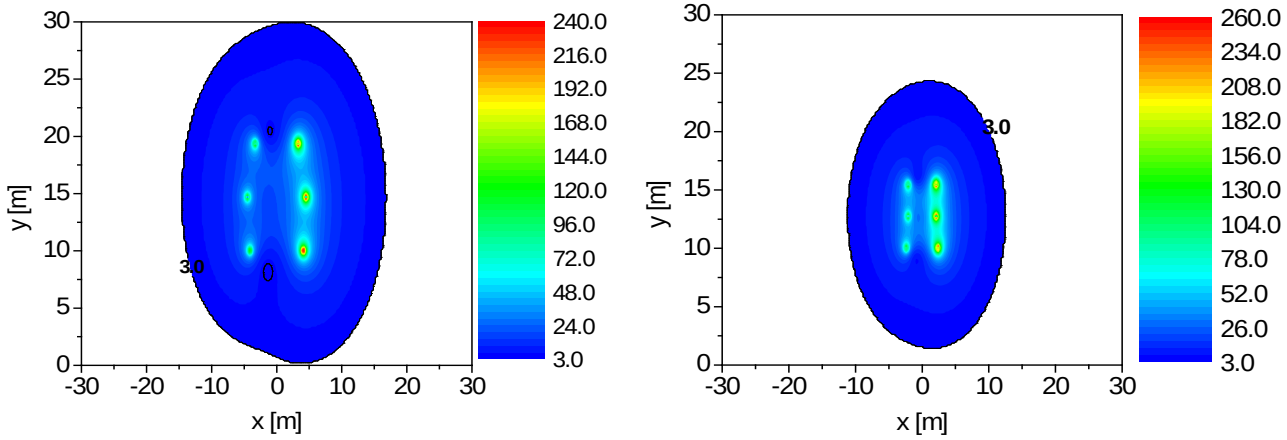

Figure 6.10.10 Magnetic flux density colored map on the plane normal to the lines left: normal layout, right: compact layout.

Finally, the possibility of applying cost-effective shielding techniques using a combination of thin plates and ribbons to mitigate the magnetic field in specific areas of interest (e.g. large buildings), affected by the passage of AC powered trains, has been explored in paper [6].

6.10.5 References

[13] O. Bottauscio, G. Farina, **"**A model for the design and control of urban electric traction systems", in: *Applications of Advanced Technologies in Transportation Engineering*, Y.J. Stephandes, F. Filippi (eds.), 1995, pp. 39-43.

[14] O. Bottauscio, A. Canova, G. Crotti, G. Farina, L. Rege and M. Tartaglia, "Analysis of magnetic field generated by tramway networks", Proc. of IX Int. IGTE Symp. Sept. 2000, pp. 252-257.

[15] Krahenbuhl, L., Muller, D., "Thin layers in electrical engineering. Example of shell models in analysing eddy-currents by boundary and finite element methods", *IEEE Trans. on Magn.*, 1993, **29** (2), pp. 1450-1455.

[16] G. Lucca, M. Moro, A. Pagani and L. Zucchelli, "Measurements of Magnetic Field Produced by the 25kV-50Hz Italian High Speed Railway Line", *Proceedings of International Symposium on Power Electronics, Electrical Drives, Automation and Motion SPEEDAM 2006*, Taormina, Italy, May 23rd-26th , 2006.

[17] G. Varju, "Magnetic field investigation, Comparison of AT-, BT-, and ATBT systems", *Technical Report for the Swedish Railways (Banverket)*, by the Budapest University of Technology and Economics, Department of Electric Power Engineering, Budapest, June 2005.

[18] E. Salinas, J. Atalaya, Y. Hamnerius, C.J. Solano, D. Gonzales, C. Contreras, C. Leon, M. A. Sumari, S. Dimitriou and M. Rezinkina, *"A new Technique for reducing Extremely Low Frequency Magnetic Field Emissions affecting Large Building structures"*, The Environmentalist, Springer Netherlands, vol. 27, no. 4, pp 571-576, Oct. 2007.

6.11 Mitigation of EMF emission from 132kV cables and cable joint pit[32]

A new configuration of a dual cable circuit which results in low magnetic field emission is proposed for installation in one common trench. It is demonstrated that this arrangement of cables allows keeping the magnetic field emission from the trench low even when one circuit is out of service. In addition, an innovative method of application of passive conductors is introduced for reduction of magnetic field at the cable joining pit. Calculations and magnetic field profiles are presented across the cable trench and across the joining pit to demonstrate the effectiveness of the proposed mitigation measures.

6.11.1 Six cables in one common trench

Previously[33] it was determined that for the dual circuit 132kV sub-transmission cables the most optimal arrangement of cables in terms of the magnetic field emission, was a double stack arrangement of six cables in one common trench. In this arrangement each group of three cables is in the horizontal flat configuration with one group laid directly above the other but with reversed sequence of phases.

Due to high cancellation effectiveness such arrangement of cables resulted in very low level of magnetic field emission, even if the cables are spaced apart. However, one cause of concern with such arrangement is a possible outage of one circuit with the remaining circuit carrying twice the load current.
The magnetic field emission from the remaining in service circuit will be much greater for the horizontal flat arrangement of the cables as compared to the arrangement where the cables are installed in trefoil or triangular configuration.

To limit the level of magnetic field emission during an outage of one circuit it is suggested to arrange the cables of each circuit in a triangular formation. When both circuits are in service and operating in parallel then the two triangular groupings of cables in each circuit can be viewed as a double stack arrangement of two sets of three cables in horizontal flat arrangement. Each flat set of three cables has a reversed sequence of phase in respect to the other set (see Figure 6.11.1).

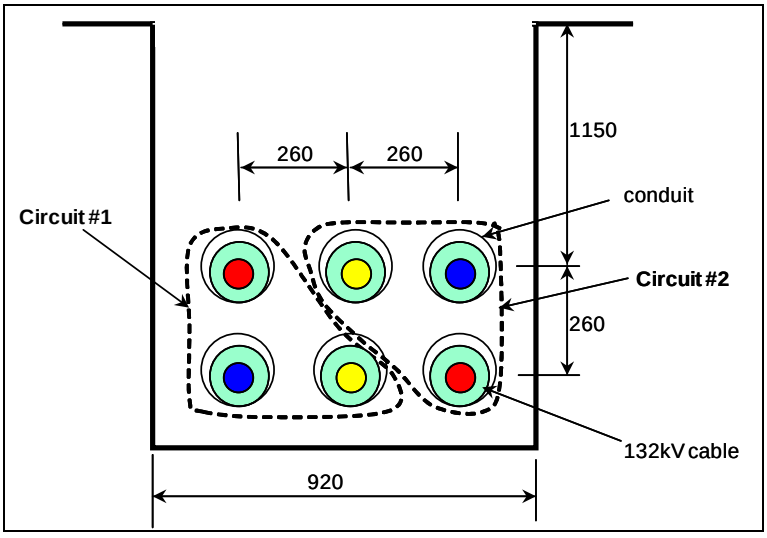

Figure 6.11.1 Two 132kV cable circuits made of single core cables in triangular formation.

The magnetic field profiles for the cables installed in the trench as shown in Figure 6.11.1 are presented in the graphical form in Figure 6.11.2.

The magnetic field profiles were calculated at 1m above the ground for the following three service conditions:

a. Both circuits are in service and each circuit is loaded with 100 MVA
b. Circuit #1 is out of service while circuit #2 is loaded with 100 MVA
c. Circuit #2 is out of service while circuit #1 is loaded with 100 MVA.

In comparison, a graph of the magnetic field profile for the flat configuration of cables with circuit #1 is out of service is also presented in Figure 6.11.2 (graph Cct #2 o/serv (flat)).

[32] Garry Melik, Magshield Products (Aust.) International Pty. Ltd. (www.magshield.com.au)
[33] Report *EMF from proposed 132kV cable*, Part 1.

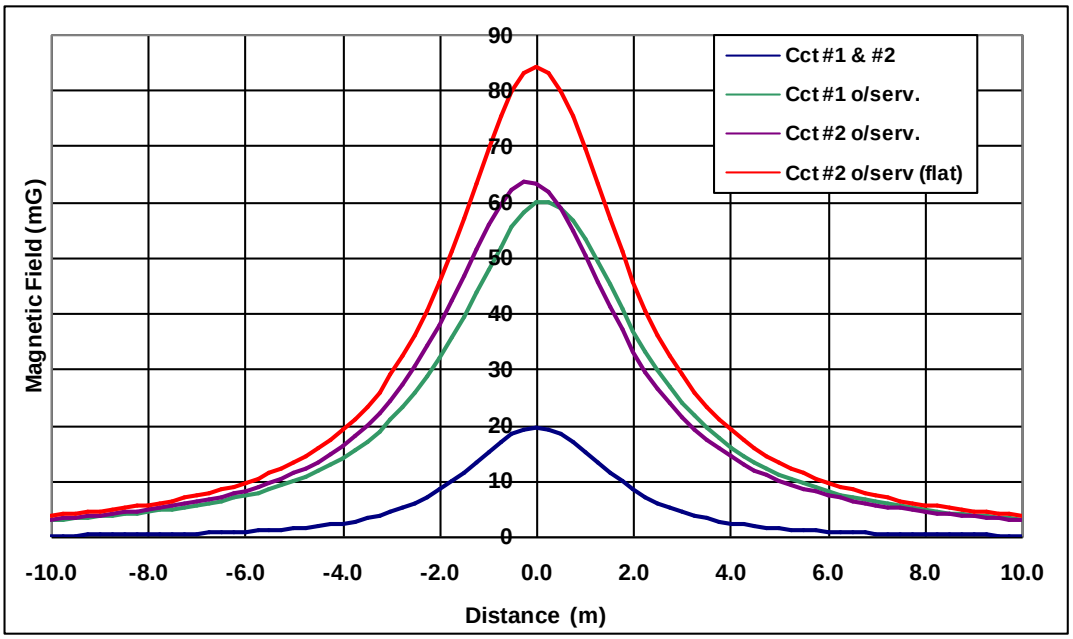

Figure 6.11.2 Magnetic field profiles calculated across cable trench at 1m above ground.

As can be seen from the graphs, the magnetic field emission across the trench when both circuits are in service is very small as compared to the two cases when either circuit is out of service.

As can also be seen from the graphs, the magnetic field emission from the cable trench, when the cables are in a triangular formation and one circuit is out of service, is smaller than when the cables are in the horizontal formation.

6.11.2 Magnetic field emission from cable joining pit

At some regular intervals (approximately every 1km of the cable length) the 132kV cables are jointed together for extension of length. The joining of cables resulted in wider spacing between the adjacent single core cables. The larger the distance between the cables, the larger the magnetic field emitted by them.

Based on the size of the cables, the minimum spacing between the cables buried in the joining pit is 500mm.

The magnetic field profiles calculated at the height of 1m above the ground across the cable joining pit for the three service conditions (a, b & c) as specified in the previous section are presented in Figure 6.11.3.

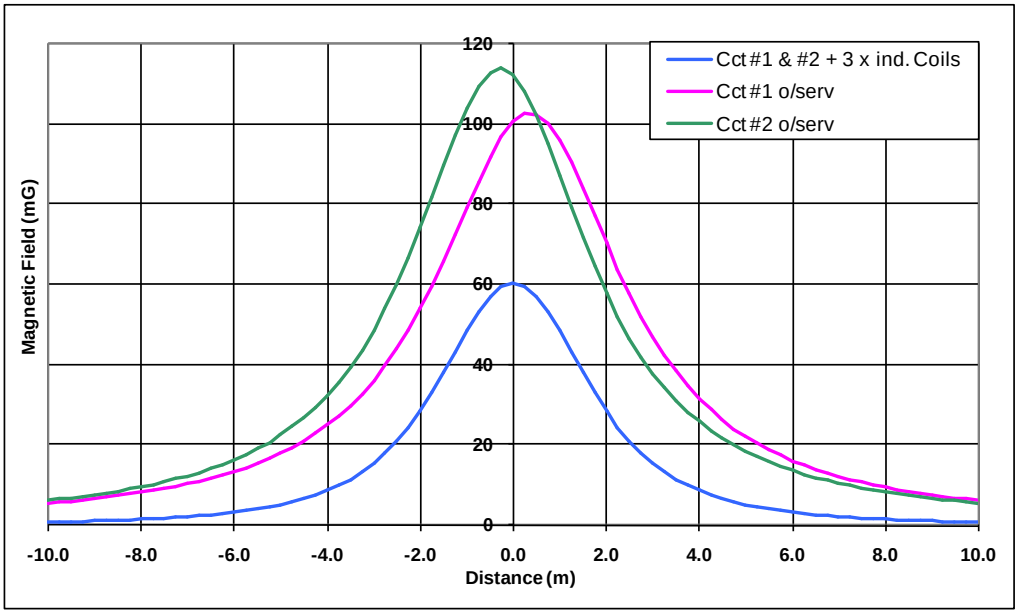

Figure 6.11.3 Magnetic field profiles calculated across the cable joining pit at the height of 1m above the ground.

As can be seen from the graphs in Figure 6.11.3, the magnetic field emission from the cables in the joining pit is much smaller when both circuits are in service as compared to the two cases where either circuit is out of service.

6.11.3 Magnetic field mitigation by induction loops

The calculations showed that the magnetic field is higher that the 4 mG target value aimed to be achieved at a distance 5 m from the centre of the cable joining pit.

To control the magnetic field emission from the cable joining pit it is proposed to place three passive induction loops in the cable joining pit. The loops that can be made from XLPE insulated copper cables with large cross-sectional area.

The three induction loops can be installed in the cable joining pit such that they would carry no induced current during the system normal condition when both cable circuits are in service and loaded equally. However, the loops will carry induced current if either of the 132kV circuit is out of service.

If either of the circuit is out of service, the remaining circuit will induce current in all three induction loops. The current in each loop will produce its magnetic field that will counteract the magnetic field emitted by the 132kV cable circuit resulting in much lower magnetic field emission from the joining pit.

Figure 6.11.4 shows a cross-section view of the cable joining pit with six 132kV cables in the two-tear formation spaced at 500 mm distance, both in the vertical and the horizontal directions. The proposed three induction coils are also shown on the drawing in Figure 6.11.4. As can be seen the plains of the two coils are crossing and are at an angle to the horizontal plain, while the third coil (the middle coil) is in the vertical plain and also crossing the plains of the two other coils. The length of each coil extends for the entire length of the cable joining pit.

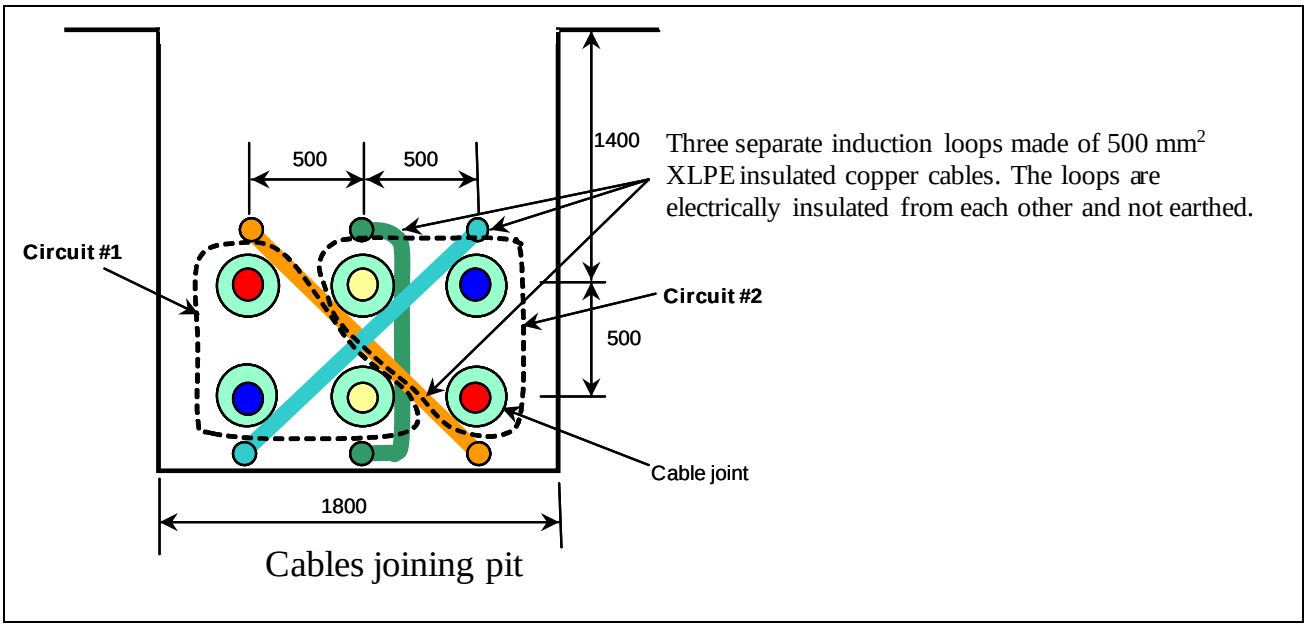

Figure 6.11.4 Two 132kV cable circuits in triangular formation with three induction loops.

The small coloured circles shown directly above or below each 132kV cable represent one 500 mm^2 XLPE insulated copper cable that runs for the length of the cable joining pit. At both ends the cables are joined together. The joining of the cables at both ends is represented by coloured lines that connect the same colour circles.

The resultant magnetic field profile when one circuit is out of service while the remaining circuit is still loaded with 100 MVA load is shown in Figure 6.11.5.

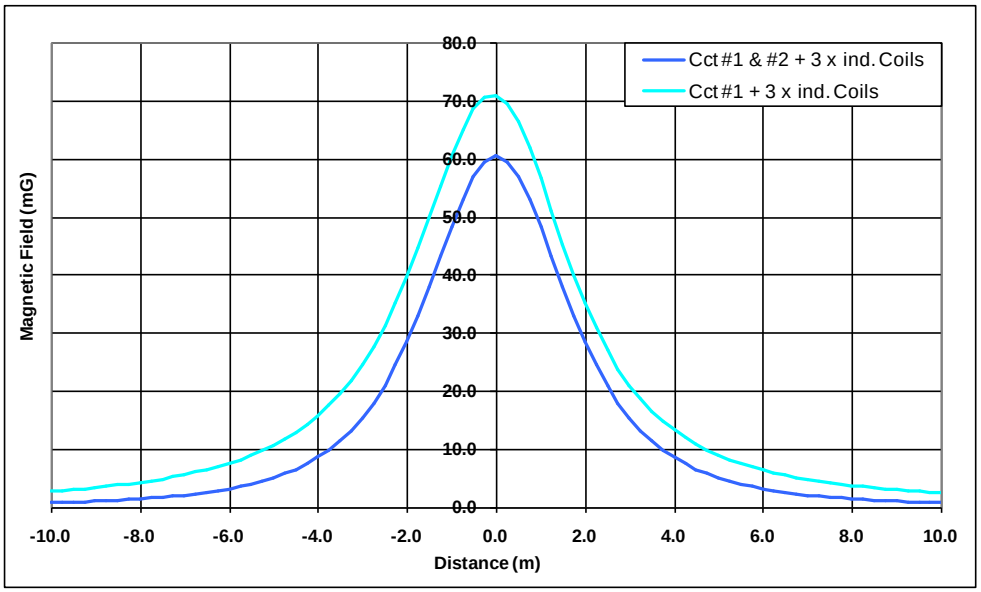

Figure 6.11.5 Magnetic field profiles calculated across the cable joining pit with induction loops at the height of 1m above the ground.

As can be seen from the graphs in Fig.6.11.5 when one circuit is out of service, the three induction coils collectively suppress the magnetic field emission from the cables in the joining pit to the level which is only 20% higher that the magnetic field level across the joining pit during the normal operation of the two cable circuits with the same load current.

6.11.4 Conclusions and Recommendations

This stage of the study of the magnetic field emission from 132kV cables of the dual circuit sub-transmission supply resulted in the following outcomes:

- The two-tier configuration of six cables in one common trench results in low magnetic field emission from the cables trench during the system normal operation.
- If the cables in the two-tier formation are arranged such that each circuit is constructed from the cables in a triangular formation (see Figure 6.11.1), the level of magnetic field emission is relatively small if either of the two circuits is out of service.
- When the cables are spaced at greater distances apart in the cable joining pit they generally emit higher magnetic field as compared to the cables in the trench. However, the level of the magnetic field emission substantially increases if one circuit is out of service. To effectively manage this condition it is proposed to install three induction coils in the cable joining pit as shown in Figure 6.11.4.

As a result of the above three recommended mitigation measures, the level of the magnetic field emission from the cable trench and from the cable joining pit is substantially reduced even if one circuit is out of service.

6.12 High Magnetic Coupling (HMC) passive loops

The system presented here is particularly useful for the mitigation of the low frequency magnetic field produced by power cable lines and cables connected to transformers. The basic idea lies in the use of standard passive loops (discrete shields) with enhanced magnetic coupling between the inductive loop and the source - high magnetic coupling (HMC), through application of ferromagnetic cores.

The passive loop principle is based on the Faraday's induction law: the alternating magnetic flux produced by a source creates an induced current in the loop which produces a magnetic field that compensates the original field. In the standard passive loop the magnetic coupling occurs through the air, while in the HMC passive loops the ferromagnetic cores enhances the electromagnetic coupling between the source and the passive loop. A simple arrangement comprising a 3-phase cable and a passive loop is presented in Figure 6.12.1. Without the ferromagnetic cores the coupling coefficient between the source (phase cable) and the shield conductors is equal to one.

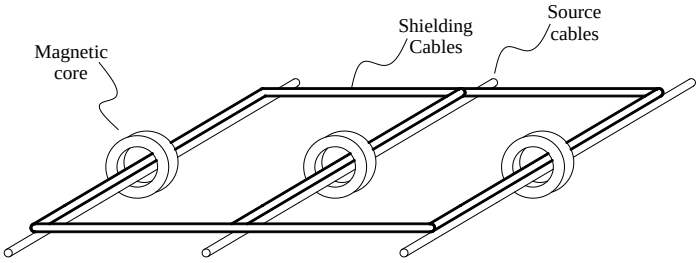

Figure 6.12.1 HMC passive loop with unitary coupling coefficient.

With the ferromagnetic cores it is possible to induce, in the conductors of the passive loops, the electric currents with the opposite phase angle in respect to the current in the source. While in the standard passive loop configuration the phase displacement, between the current in the source and the current in the loop, is usually at 90° electrical angle to each other with the use of compensating capacitor. The HMC allows the best utilisation of properties of all materials: conductive material of the loops and the ferromagnetic material of the cores. Of course, the ferromagnetic cores have to be carefully designed, as demonstrated in the patent [1], in order to avoid the magnetic saturation. The patent [1] includes description of the systems with different topologies for the HMC passive loops particularly applicable to the power cables and power transformers. It also explores the application of different ferromagnetic core shapes.

In the simple case presented in Figure 6.12.1, the maximum shielding factor is obtained when the distance between the source and the shield cables is minimal. The thermal condition should be carefully analyzed because the induced current in the conductors of the passive loop will be of the same order of magnitude as the current in the source conductors. If the thermal emission is high, then the different configurations can be considered, where the conductors of the passive loops are placed at some distance away from the conductor of the source. The electromagnetic coupling between the passive loop and the source can be enhanced by various methods as shown in Figures 6.12.2 and 6.12.3. In this case, the optimal displacement of the loop conductors must to be found by using numerical or analytical procedures [2].

Some applications of the HMC system are presented in the following pages.

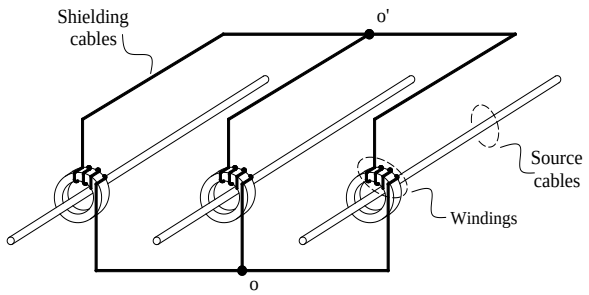

Figure 6.12.2 HMC with enhanced coupling.

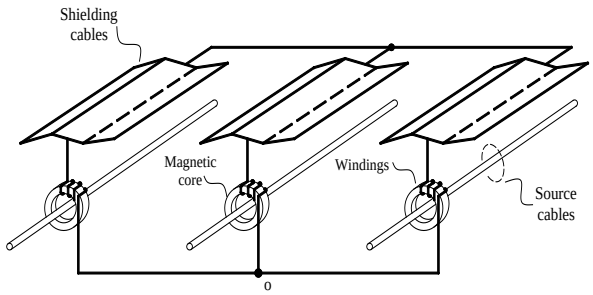

Figure 6.12.3 HMC with enhanced coupling and phase splitting.

6.12.1 Single phase cable power line

A single phase line with a passive shielding loop is presented in Figure 6.12.4. The *l* long section of the line conductors are spaced from each-other at the distance of i_0. The optimal displacement of the shielding loop can be found for the magnetic field at the height, *h*, above the wires of the power line. In addition, the appropriate value of the shielding current has to be determined [2]. The value of the shielding current can be increased by increasing the number of turns of the shield wire around the ferromagnetic core. This later option involves introduction of the transformer ratio $K_{SH}=N_1/N_2$ which links I_S with I_{SH}: $I_{SH}= I_S / K_{sh}$.

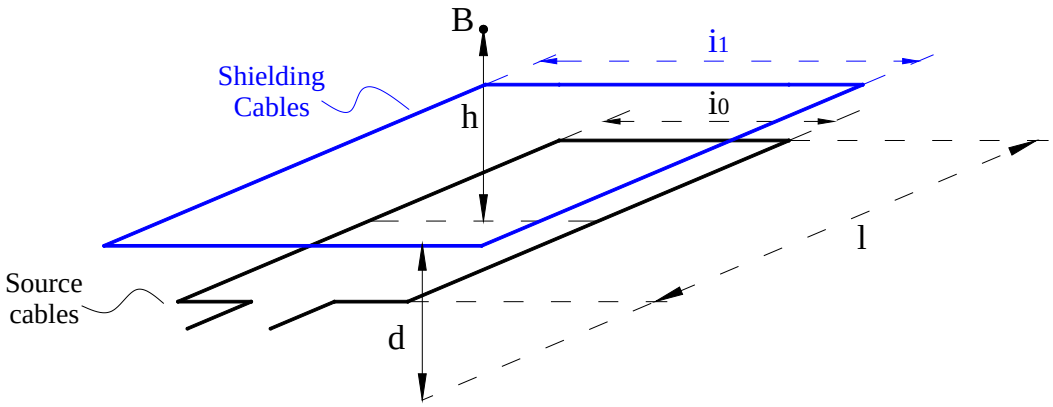

Figure 6.12.4 Single phase test line.

Experimental measurements have been performed on a test line with the following parameters:

- i_0 = 0.5 m
- l = 3.5 m
- h = 1.35 m (measurement point for the magnetic flux density)

An optimization procedure leads to the following result: d = 0.14 m, i_1 = 1.18 m and K_{SH} = 3.

Table 6.12.1 shows that the maximum magnetic field reduction factor happens to be when K_{SH} is set to 3. The last two rows in the Table 6.12.1 show that the shield is self-regulating, i.e. a reduction of the source current linearly reduces the current in the shield (see Figure 6.12.5). This means that the magnetic field reduction factor has a constant value for different load currents in the line and is completely defined by the displacement (d, Dx, i_1) and the design (K_{SH}) of the shielding loop.

Table 6.12.1 Single phase line: experimental results

K_{SH}	I_s [A]	I_{SH} [A]	B [uT]	F_{rid}
4	100	25.6	2.5	2.01
5	106	21.4	3.45	1.46
3	100	33.9	1.43	3.52
3	50.6	17.1	0.72	3.49

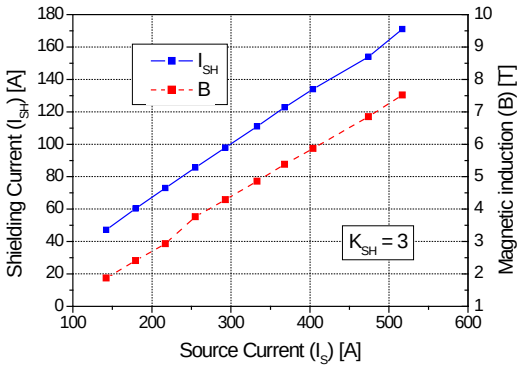

Figure 6.12. 5 Self regulation of the shield for current source variation.

6.12.2 Three phase power cable line

Experimental measurements concerning the solution with a unity coupling factor have been performed on a three phase (Figure 6.12.6) test line with the following parameters:

- i_0 = 0.5 m
- l = 3.5 m
- h = 1.35 m (measurement point for the magnetic field density)

Table 6.12.2 shows the performance of the HMC passive loop. The induced current in the wires of the shielding loop are of similar magnitude as the current in the source and the shielding factor is almost constant for different

values of the source currents. As can be seen from the table, the shielding factor changes from 20 to 17 when current in the source increases from approximately 19 A to 100 A.

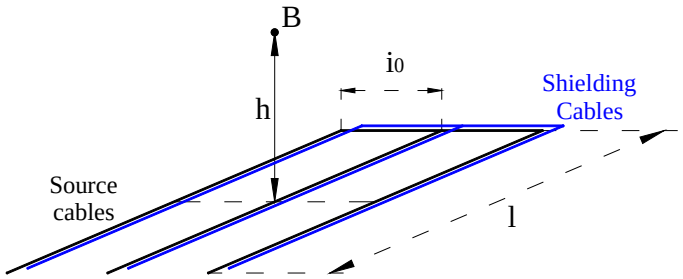

Figure 6.12.6 Three phase test line.

Table 6.12.2 Three-phase line: experimental results.

	I_1 [A]	I_2 [A]	I_3 [A]	I_{sh1} [A]	I_{sh2} [A]	I_{sh3} [A]	B [muT]	F_{rid}
No shield	18.8	18.1	18.8	---	---	---	1.94	---
With shield	18.9	18.4	19	18.1	17.7	18.2	0.111	20.05
No shield	106.6	114	112.5	---	---	---	9.48	---
With shield	102.5	112	110.6	99.5	109.1	107.4	0.555	17.08

6.12.3 Three phase power cable line in the jointing zone

Figures 6.12.7 and 6.12.8 show a typical jointing zone layout of a three-phase power line. The line is composed of the three high voltage cables with the conductor cross section of 1600 mm^2.
Simulations have been carried out in order to evaluate the performances of the HMC passive loop installed on the jointing zone (blue rectangle in Figure 6.12.7).

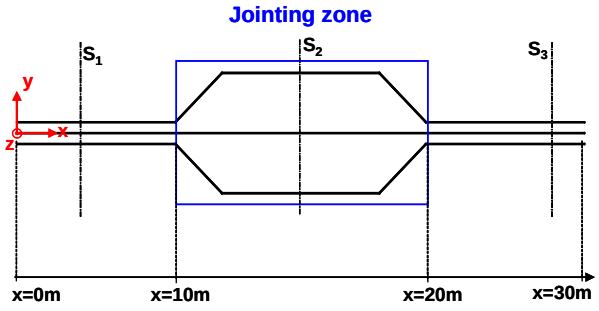

Figure 6.12.7 Jointing zone.

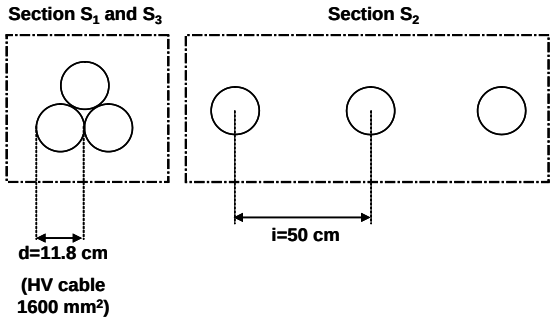

Figure 6.12.8 Jointing zone section.

At first, the magnetic flux density of the line without any shield has been evaluated on a reference plane parallel to the power line at the height z = 1.5 m (Figure 6.12.10). The HMC shielding solution has been simulated in two different configurations:

- **Configuration 1**: each phase of the shield is composed by a conductor identical to the source cable, Figure.6.12.11;
- **Configuration 2**: each phase of the shield is split into two conductors of smaller size (1000 mm^2) than the source cables (see Figure 6.12.13). Hence, the shielding current is equally divided between the two conductors which constitute the shielding phase.

The result obtained using the HMC passive loop in **Configuration 1** is shown in Figure 6.12.12,. Above the jointing zone the magnetic flux density is reduced to the same degree as if the cables of the source were in trefoil formation.

The result obtained using the HMC passive loop in **Configuration 2** is shown in Figure 6.12.14. The magnetic flux density above the jointing zone is significantly reduced as compared to **Configuration 1**.

Figure 6.12.15 shows the graphs of the magnetic flux density at height of 1.5 m above the cables of the power line across a section at x = 17.4 m (see Figure 6.12.7). The graphs were plotted for two shielding **Configurations** and compared with the graph with no shield. Figure 6.12.15 shows that the shielding factor for **Configuration 1** is 7.3 and is 88.4 for **Configuration 2**.

Figure 6.12.9 Power line without shield.

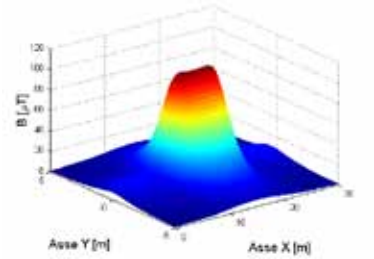

Figure 6.12.10 Power line magnetic flux density.*

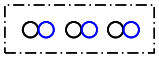

Figure 6.12.11 Shielding configuration 1.

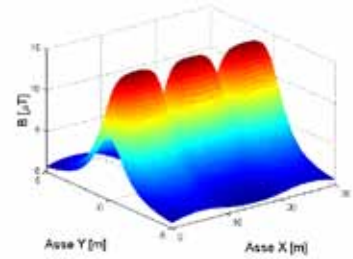

Figure 6.12.12 Magnetic flux density with shielding configuration 1.*

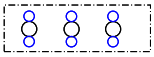

Figure 6.12.13 Shielding configuration 2.

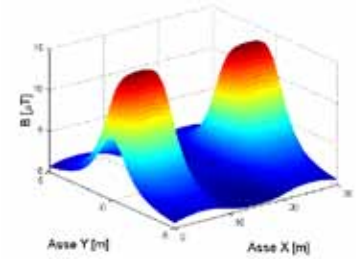

Figure 6.12.14 Magnetic flux density with shielding configuration 2.*

* Magnetic flux density is evaluated on a plane parallel to the power line at height z = 1.5 m

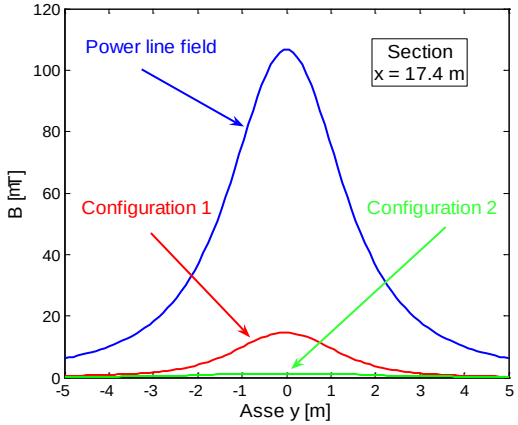

Figure 6.12.15 Magnetic flux density at 1.5 m above the cables of the power line across a section at x = 17.4 m (see Figure 6.12.7).

6.12.4 Other developments and applications

The application of the HMC passive loops can be easily extended to the cable connected to substation transformers, particularly for LV connections.

6.12.5 References

[1] Canova A.and Giaccone L., "Sistema di schermatura passiva di tipo magliato e conduttivo ad elevato accoppiamento magnetico", *Italian patent application* TO2008A000176.

[2] Canova A.and Giaccone L., "Optimal design of *High Magnetic Coupling Passive Loop* for power lines field mitigation" – to be published in the *Proceedings of the 10th workshop on Optimization and Inverse Problems in Electromagnetism*, OIPE 2008.